Vitor Manuel Guerra Vaz da Silva

Mestre em Engenharia Electrotécnica e Computadores

Reconfigurable Photonic Logic Architecture

Dissertação para obtenção do Grau de Doutor em
Engenharia Electrotécnica e de Computadores

Orientador: Prof. Doutora Maria Manuela de Almeida Carvalho Vieira,
Professora Associada Convidada, UNL-FCT

Co-orientador: Prof. Doutor Manuel Martins Barata,
Professor Coordenador, ISEL

Júri:

Presidente: Prof. Doutor Paulo da Costa Luís da Fonseca Pinto

Arguentes: Prof. Doutor Adolfo Sanchez Steiger Garção
Prof. Doutor João Manuel de Almeida Serra

Vogais: Prof. Doutor Carlos Alberto Caridade Monteiro e Couto
Prof. Doutora Maria Manuela de Almeida Carvalho Vieira
Prof. Doutor Rui Manuel Leitão Santos Tavares

FACULDADE DE CIÊNCIAS E TECNOLOGIA
UNIVERSIDADE NOVA DE LISBOA

Dezembro, 2015

Dedicado aos meus alunos

A ideia de fazer uma tese de doutoramento surgiu nos finais de 2004, e foram diversas as áreas em que ao longo de anos fui procurando, desde a Inteligência Artificial, Pedagogia, Robótica, Bio engenharia, e Electrónica. Agradeço assim a todos os que directamente ou indirectamente durante esse período me proporcionaram momentos de aprendizagem, de decisão e de companhia.

Aos meus orientadores Manuela Vieira e Manuel Barata, que foram meus professores no Bacharelato do ISEL, e deram-me a oportunidade de fazer esta tese.

Ao ISEL, que me acolheu como docente e à FCT-UNL cujo protocolo com o ISEL financiou o programa doutoral.

Ao grupo GIAMOS/ISEL detentor do sensor estudado nesta tese, pelo trabalho fundamental desenvolvido previamente e pelo acolhimento como membro.

Ao CTS/UNINOVA pelo acolhimento deste projecto e pela participação como membro durante o programa doutoral.

Aos colegas do ISEL, Manuela, Barata, Paula Louro, Miguel Fernandes, Alessandro, Frazão, Yuri, João Costa, Maçarico, Isabel Rodrigues, Dora, Paula Graça, Carvalhinho, Valentim, e muitos outros, com quem partilhei almoços e conversas que muito contribuíram quer para descontrair como para projectar ideias.

Aos colegas do ISR/IST, António Pascoal, Sebastião, Rufino, Pedro Aguiar, João Botelho, Carlos Silvestre e Paulo Oliveira, pelas boas oportunidades de trabalho na robótica submarina.

Aos colegas da USNA/FM-UL, Isabel Rocha, Mário de Oliveira, Carlos Neves, Vera Geraldes, Cristiano, Nataniel, Gabriela, Ana, Sérgio, pelos conhecimentos de fisiologia e do sistema nervoso autónomo.

Ao IMM, pelos cursos e actividades que proporcionaram.

Ao José Reis e Luís Silva (ANFEI/SIEMENS), ATEC, por me terem colocado de novo na área da formação.

À Gustave Eiffel, Pedro Rodrigues, Pedro Braz, J Pires e Mário Direito.

À UCP, Tito, Barata Marques, Rui Pires, Cecília e Pedro Encarnação.

Aos amigos, GJA, Ai Que Canseira, Andanças, Tradballs, Evoé, ASAUR, Irish, Mercês, Matias, Ana, Marisa, Filipa, Maria Ventania, Virgínia, Pedro, Vanda, Francisco, José Marques, Eusébio Roque, Lourenço, Celina Piedade, Mestre Li Naiguang e muitos outros.

Aos meus pais Zé e Lai pelo excelente começo de vida que me proporcionaram.

À família mais chegada, Tina, Tiago, Ricardo, Baptista, Carlos e Zezinha.

À Patrícia pelos sítios lindos que temos partilhado.

Um obrigado também a todos os que de um modo gratuito colocam os seus recursos e conhecimentos disponíveis na Internet.

Este trabalho teve o apoio da FCT (CTS-FCT/UNL financiamento anual) através do programa de fundos do PIDDAC, e PTDC/EEA-ELC/111854/2009, e PTDC/EEA-ELC/120539/2010.

Abstract

The amorphous silicon photo-sensor studied in this thesis, is a double pin structure (p(a-SiC:H)-i'(a-SiC:H)-n(a-SiC:H)-p(a-SiC:H)-i(a-Si:H)-n(a-Si:H)) sandwiched between two transparent contacts deposited over transparent glass thus with the possibility of illumination on both sides, responding to wavelengths from the ultra-violet, visible to the near infrared range. The frontal illumination surface, glass side, is used for light signal inputs. Both surfaces are used for optical bias, which changes the dynamic characteristics of the photo-sensor resulting in different outputs for the same input. Experimental studies were made with the photo-sensor to evaluate its applicability in multiplexing and demultiplexing several data communication channels. The digital light signal was defined to implement simple logical operations like the NOT, AND, OR, and complex like the XOR, MAJ, full-adder and memory effect. A programmable pattern emission system was built and also those for the validation and recovery of the obtained signals. This photo-sensor has applications in optical communications with several wavelengths, as a wavelength detector and to execute directly logical operations over digital light input signals.

Keywords: amorphous silicon, a-Si:H, a-SiC:H, pin, photosensor, optoelectronics, multiplexer, demultiplexer, logic function, memory, digital light signal.

Resumo

O foto-sensor de silício amorfo estudado nesta tese, é uma estrutura pin dupla (p(a-SiC:H)-i'(a-SiC:H)-n(a-SiC:H)-p(a-SiC:H)-i(a-Si:H)-n(a-Si:H)) entre dois contactos transparentes depositado sobre vidro transparente e por isso com a possibilidade de ser iluminado por ambas as extremidades, respondendo a comprimentos de onda desde o ultra-violeta, visível ao infra-vermelho próximo. A superfície de iluminação frontal, a do vidro, é usada como entrada de sinais luminosos. As duas superfícies são iluminadas para polarização óptica, alterando as características dinâmicas do foto-sensor, manifestando resultados diferentes para a mesma entrada. Foram realizados estudos experimentais sobre o foto-sensor no sentido de avaliar a sua aplicabilidade em comunicação multiplexada e desmultiplexada com vários canais de entrada. Foi definido o sinal digital luminoso (*digital light signal*) para poder efectuar as operações lógicas simples NOT, AND, OR, e complexas XOR, MAJ, somador e efeito de memória. Foi construído um sistema de emissão de padrões luminosos, e o de recuperação e validação dos sinais obtidos. Este foto-sensor tem aplicação em comunicações ópticas em vários comprimentos de onda, como detector de comprimentos de onda, e para realizar operações lógicas directamente sobre sinais digitais luminosos de entrada.

Palavras-chave: silício amorfo, a-Si:H, a-SiC:H, pin, fotosensor, memória, optoelectrónica, multiplexer, demultiplexer, função lógica, sinal digital de luz.

Contents

Figure List

Table List

Table of Abbreviations

(g)	Gas
(s)	Solid
11/9	99.9999999%
5/9	99.999%
6/9	99.9999%
$70Li_2S\text{-}30P_2S_5$	Glass ceramic
ac	Alternate current
AM 1.5	Standard solar spectrum illumination $1000Wm^{-2}$
AMLCD	Active Matrix Liquid Cristal Display
AND	Logic conjunction
ASCA-2D	Device simulation program
a-Si	Amorphous Silicon
a-Si:H	Hidrogenated Amorphous Silicon
a-SiC	Amorphous Silicon Carbide
a-SiC:H	Hidrogenated Amorphous Silicon Carbide
a-SiGe:H	Hidrogenated Amorphous Silicon Germanium
B	Blue wavelength 470 nm

B_2H_6	Diborane
C	Carbon
C	Cyan wavelength 460 nm
CCD	Charge Coupled Device
CMOS	Complementary metal oxide semiconductor
CO	Carbon Oxide
c-Si	Crystalline Silicon
CTS	Centre of Technology and Systems
dc	Direct current
DEMUX	Demultiplexer
DNA	Deoxyribonucleic acid
DTL	Diode Transistor Logic
eV	Electron Volt
G	Green wavelength 524 nm
GIAMOS	Grupo de Investigação Aplicada à Microelectrónica, Opto-electrónica e Semiconductores
HIT	Heterojunction with Intrinsic Thin layer
$HSiCl_3$	Trichlorosilane
Hz	Hertz
i	Intrinsic
I	Infra-red wavelength 700 nm
ICL	Irreversible Capacity Loss
IIT	Image Intensifier Tube
IR	Infra-red
ISEL	Instituto Superior de Engenharia de Lisboa
ITO	Indium Tin Oxide (In_2O_3:Sn) (TCO)
I-V	Current-voltage

L	Lime wavelength 565 nm
LCD	Liquid Crystal Display
LED	Light Emitting Diode
Li	Lithium
$Li_{22}Si_5$	Lithium Silicon Alloy
$Li_{4.2}Si$	Lithium Silicon Alloy
$Li_4Ti_5O_{12}$	LTO
LTO	Lithium Tin Oxide ($Li_4Ti_5O_{12}$)
M	Magenta wavelength 640 nm
MAJ	Majoring function
MGS	Metallurgical Grade Silicon
MIN	Minoring function
MUX	Multiplexer
n	Negative
N	Navy wavelength 430 nm
NC12	Sensor similar to the NC5 with intermediate TCO contact
NC5	Sensor p'inpin under study in this thesis
nip	Negative-Intrinsic-Positive
NIR	Near Infra-red
NOT	Logical inverse function
n-p	Negative-Positive
NRZ	Non Return to Zero
O	Orange wavelength 605 nm
OR	Logical disjunction function
p	Positive
PECVD	Plasma Enhanced Chemical Vapour Deposition

PH_3	Phosphine
pi'npin	Double pin
pin	Positive-Intrinsic-Negative
p-n	Positive-Negative
p-Si	Polycrystalline Silicon
R	Red wavelength 626 nm
RF	Radio Frequency
RGB	Red, Green, and Blue colours
RTL	Resistor Transistor Logic
sccm	Standard Cubic Centimetre per Minute
sc-Si	Single crystal Silicon
Si	Silicon
SiC	Silicon Carbide
$SiCl_4$	Silicon tetrachloride
SiH_4	Silane
SiO_2	Silica
TCO	Transparent Conductive Oxide (ZnO:Al)
TFT	Thin-Film Transistors
TTL	Transistor Transistor Logic
U	Ultra-violet wavelength 390 nm
UNL	Universidade Nova de Lisboa
UV	Ultra-violet
V	Violet wavelength 400 nm
VCE	Voltage between the Collector and Emitter
VIS	Visible
WDM	Wavelength-Division Multiplexing

XOR	Logical exclusion function
ZnO:Al	TCO
μc-Si:H	Microcrystalline Hydrogenated Silicon

Table of Symbols

Symbol	Units	Description
E	eV	Energy
E_C	eV	Bottom edge of the conduction band
E_F	eV	Energy of the Fermi level
E_g	eV	Energy gap
E_{op}	eV	Optical gap
E_V	eV	Top edge of the valence band
h	Js	Planck's constant (6.626069×10^{-34})
I_{ph}	A	Photocurrent
k	eVK^{-1}	Boltzmann constant (8.617332×10^{-5})
P_{opt}	W	Optical power
T	K	Absolute temperature
V	V	Applied voltage
λ	nm	Wavelength

Preface

Previous research around the pi'npin device, a photo sensor that can be illuminated by both sides with ultra violet illumination and also by several different channels in the visible range that impinge on the sensor's front surface, has arose several questions that span the proposed work.

- How many channels in the visible light range can be transmitted by WDM with a a-SiC:H/a-Si:H sensor selecting the desired channel with visible light?
- What wavelengths ranges are best suited for the de-multiplexing function?
- Which are the logical functions that can be translated by this sensor?
- How to build complex logical functions with the device.
- How to de-multiplex light channels using light selectors with one sensor.
- How to build a memory due to charges stored by light.

The answer to these questions, that is the purpose of this work, began with the following approach:

Light shining on one of the surfaces, the selector, can be used to distinguish between two signals with different wavelengths. For n different selecting frequencies there would be 2^n different signals to be identified. Value of n is

then limited by the bandwidth of each channel. By changing the wavelength of the selector the output changes due to the non linear gain of the device which will reduce the maximum number of distinguishable channels. This limitation can be overcome and the number of identifiable channels may increase if the output of the selecting wavelengths are combined with an algorithm and signal modulation.

The non linearity of the device introduces a significant influence of the previous signal over the present one thus producing a non deterministic output. This non deterministic output subjected to digital filtering, clustering techniques and or algorithmically eventually can be successfully classified.

The identifiable complex functions must be from the use of only one sensor. The study of the output is necessary to identify the functions and define the domain of the input signals.

The distribution of this doctoral thesis spreads through eight chapters.

Chapter 1 – The pi'npin device; is a short review of amorphous silicon and some of its current application areas. The pin junction is shown in other similar uses as the one that is proposed here and has been used with the GIAMOS working group for almost a decade.

Chapter 2 – Experimental Setup; shows how to connect the p'inpin device and how to make several measurements. Each different experiment has dedicated equipment and procedures that have to be followed. This chapter is necessary if another working group wants to work with an equivalent pi'npn device and compare results.

Chapter 3 – Sensor Operation; is a continuation of the characterization of the pi'npin device and shows the fundamental aspects that are used in the subsequent chapters. This chapter also projects working paths for future research topics with the pi'npin device.

Chapter 4 – Multiplexer; is one of the main applications of the pi'npin device. The use of two and three channels has been previously referenced, and in this chapter four, five and n channels are explained and studied. This chapter also helps answering a couple of research questions.

Chapter 5 – Logic Functions; represents a whole new topic regarding the pi'npin device. Two milestones, the digital light signal and the NOT logical function prepare the lane that supports all other logical functions, like the AND, OR, XOR and MAJ. A rather complex logical function, the half-adder and the full-adder are also presented. This chapter also helps answering a couple of research questions.

Chapter 6 – Memory function; is a topic that imposed itself during the experimental results. Observation of the behaviour of the pi'npin device output indicated that a memory of past illumination influenced the present output values, predicting a hidden memory function. A new research question was introduced among the existing ones, and the experimental setup was redesigned to account for the study of the memory function. The results are presented in this section and an application that resembles a Set-Reset flip-flop is shown.

Chapter 7 – Validation; shows how the results that up to this point have been almost exclusively classified by a human observer are now classified by a program. Different classifiers can be used and compared. The number and percentage of errors, and also the type of errors (false and positive) can be studied. This chapter allows the recovery of the multiplexed channels and of the logic function output.

Chapter 8 – Conclusion; and discussion of the results. Here all research questions are discussed and answered. Future trends are also presented.

1

1 The pi'npin device

Silicon has been of great importance to humanity. First applications were based on natural occurrences of silicon like silex, a variety of quartz, very hard and tailored to make tools, weapons and pottery. Glass made of silicate can be dated to 12000 B.C. Although Silicon is the second most abundant element on earth, after oxygen, it does not occur as a free element in nature, but combined with oxygen forming oxides and silicates [1]. The first known free form of silicon was prepared by Berzelius, Jöns Jacob, in 1823, a Swedish chemist which is the founder of modern chemistry. He chlorinated silicate/silica forming silicon tetrachloride with which he passed over heated potassium. The first known crystalline silicon was made by accident in 1854, when Saint-Claire Deville, a French chemist, was working in aluminium electrolysis. Moisan, French chemist and awarded with the Nobel Prize in Chemistry 1906, produced in 1895 silicon and silicon rich alloys in an electric arc furnace [2]. In 1896 G. Acheson discovered by chance silicon carbide (SiC), also known as carborundum, during an experiment in which he was trying to synthesise diamonds [3]. Presently the electric furnace consists essentially of a vessel filled with quartz and carbon materials. Silicon is freed by the carbothermic reduction of silica SiO_2 with carbon electrodes producing Silicon ($Si_{(s)}$) and carbon oxide ($2CO_{(g)}$) at temperatures between 1900 and 2100^{o}C in the inner zone of the furnace. On the outer zone, where temperature drops below 1900^{o}C, $SiO_{(g)}$ and $CO_{(g)}$ coming from the inner zone react with free carbon and consequently silicon carbide $SiC_{(s)}$ and condensation products are formed [4]. Depending on

the quality of the raw materials used and the operational strategy and skills, the silicon yield as metallurgical silicon ranges from 80 to 90%, the balance resulting in silica fume. This metallurgical grade silicon (MGS) has 1 to 3% impurities, depending on the quality and quantity of the raw material [4], which is unsuitable for the demands of high-tech industries, thus the next step is conversion to chlorine compounds such as trichlorosilane ($HSiCl_3$) and silicon tetrachloride ($SiCl_4$) and purification via distillation. Silicon tetrachloride is a primary ingredient in producing the pure glass cores of optical fibres. For microchips and solar cells, trichlorosilane is converted into a valuable commodity known as polysilicon, which is extremely pure silicon with impurity levels in the parts per billion. This polysilicon is used in the production of silicon wafers, thin discs of pure silicon. These silicon wafers form the base onto which microchips, certain solar cells, and other semiconductor devices are fabricated [5]. There are ten global industrial sectors considered in the silicon production chain, those producing quartz/silica, coal, charcoal, silicon metal, chlorosilane compounds (intermediate chemicals used in purifying silicon), polysilicon, semiconductor devices (microchips), solar cells, and optical fibre. A diagram of the sectors, squares, and their relationships, arrows, appears in Figure 1-1 [5].

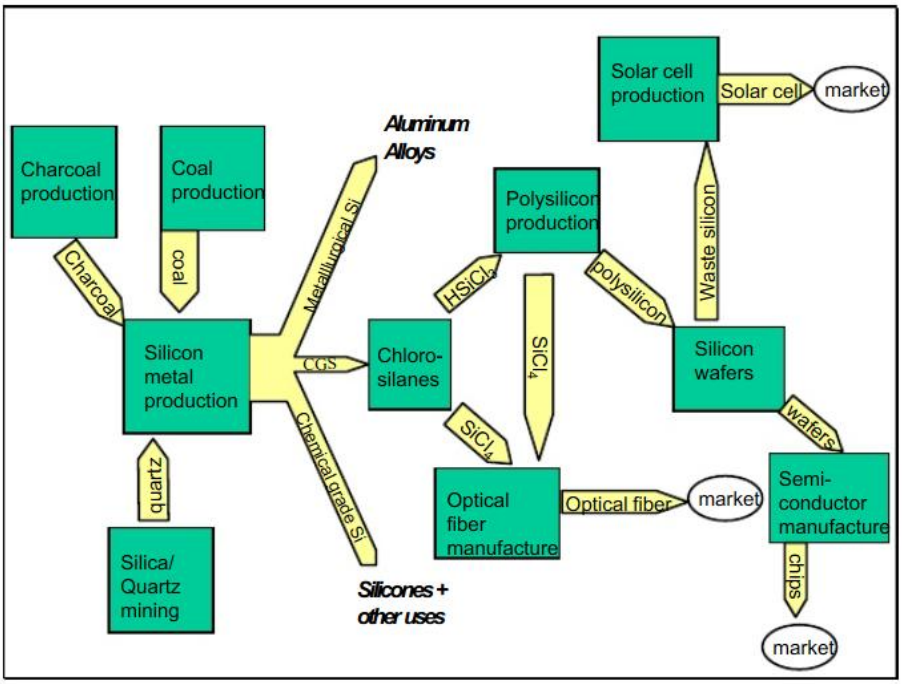

Figure 1-1 - The production chain for high-purity silicon and its use in semiconductors, solar cells, and optical fibres.

Polysilicon, a term used to refer to extremely pure polycrystalline silicon, is a key precursor in the production of semiconductors; the primary ingredient in producing silicon wafers. Polycrystalline refers to the fact that the material is divided into domains in which the atomic alignment is the same. This is in contrast with a monocrystalline substance, in which atoms are aligned throughout the entire object, or an amorphous substance like glass that has no long-range arrangement of atoms. The purity of electronics grade polysilicon is known as 11/9 (eleven nine), denoting that metallic impurities are in the parts per billion level. Polysilicon is also a major feedstock for solar cell production, though the purity requirements are far less stringent, 5/9 or 6/9 is apparently acceptable. Nearly all silicon for solar cell production is supplied from the scrap silicon from the semiconductor industry that arises from production of polysilicon and ingots of single crystal silicon. Polysilicon is the purest substance among materials produced on an industrial scale [5].

1.1 Amorphous Si

The research on amorphous semiconductors in the 1950s and 1960s was focused on the chalcogenides, i.e. materials containing group VI elements (sulfur, selenium and tellurium). These glasses are formed by cooling from the melt, their structure being similar to oxide glasses. Of particular interest was the relation between disorder of the structure and the electronic properties. Amorphous silicon (and germanium) was prepared in those days by thermal evaporation or sputtering. This unhydrogenated material was highly defective, which inhibited its use as a useful semiconductor. Research on incorporating hydrogen as a passivating element was pursued by introducing hydrogen in the sputtering system, which indeed improved the electronic properties [6].

In 1965 it was discovered that deposition of amorphous silicon employing glow discharge as the deposition technique yielded a material with much more useful electronic properties. The deposition occurs on a moderately heated substrate (200-300^{o}C) through reactions of gas radicals with the substrate. At that time the infrared absorption bands of silicon-hydrogen bonds were

observed, but they were not recognized as such. Some years later, Fritsche and co-workers in Chicago confirmed that a-Si produced from a glow discharge of SiH_4 contains hydrogen. Spear and co-workers in Dundee succeeded in improving the electrical properties, and finally, in 1975, a boost in research activities occurred when it was shown that a-Si:H could be n- or p-type doped by introducing phosphine (PH_3) or diborane (B_2H_6) in the plasma [6].

Amorphous silicon is presently used in devices typically deposited by plasma-enhanced chemical vapour deposition (PECVD) from silane (SiH_4) at ~300ºC. Although a-Si has no long range order like a crystal, in device-grade a-Si most silicon atoms still have bonds to four neighbouring silicon atoms as represented in Figure 1-2 [7].

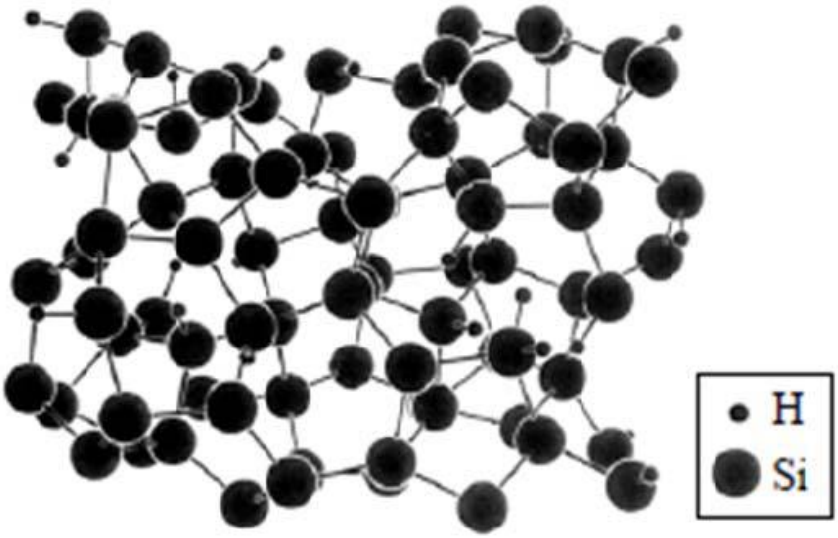

Figure 1-2 - Structure of hydrogenated amorphous silicon.

Surprisingly, these bonds have a bond length and an angle between bonds close to those in crystalline silicon, despite the lack of long range order. About 10% of the silicon orbitals do not form bonds with other silicon atoms, but nearly all of these form bonds to atomic hydrogen. Because the material contains on the order of ~10% hydrogen, it is often referred to as "hydrogenated amorphous silicon" a-Si:H [7]. As the hydrogen dilution is increased, the transition from amorphous to microcrystalline phase takes place; recent work has shown that the best amorphous silicon alloy is grown at a dilution just below the edge of amorphous to the microcrystalline (μc) transition (μc-Si:H) [8].

1.2 a-Si:H Applications

The main use of hydrogenated amorphous silicon has been its role as the switch to control pixel addressing in Active Matrix Liquid Crystal Displays (AMLCD). The glass substrate combined with the TFT's (Thin Film Transistor) and row and column metal lines is known as the "backplane" of the display. Due to its relative process complexity compared to that of the liquid crystal, the backplane is a dominant component of the cost of displays [9].

Future products such as flexible displays, wearable electronics embedded with sensors, and unbreakable "electronic sensor wallpaper" requires that the glass substrates be replaced with plastic or even metal foil substrates. For cost reasons, it is desirable that the TFT's be fabricated directly on the thin foils, in contrast to first fabricated on rigid substrates and then transferred to flexible substrates. As long as the substrates are thin, the strain induced in the TFT's when the structured are cylindrically deformed (e.g. rolled) is small. Because the TFT's can withstand a strain on the order of ~0.5% before mechanical failure, radii of a few mm can be achieved [7].

Another application of amorphous silicon is in energy production. Single crystal silicon (sc-Si), polycrystalline silicon (p-Si), and amorphous silicon (a-Si) can all be used to make solar cells, with fabrication cost and device photoconversion efficiencies decreasing as one moves from single-crystal to amorphous materials [8]. Solar cells made from p-n junctions in a-Si:H and a-SiGe:H have been in production for some time, but their power efficiency has been limited to the 7% range. On the other hand, crystalline silicon (c-Si) solar cells can reach efficiencies of ~25%, but require high temperature diffusion steps, which could be a major cost component [7,9]. Amorphous silicon is one of the most developed thin film technologies to-date, and offers interesting possibilities in further development through the use of "microcrystalline" silicon which seeks to combine the stable high efficiencies of crystalline Si technology with the simpler and cheaper large area deposition technology of amorphous silicon [8]. By 2005, the approach of using c-Si/a-Si heterojunctions has created hybrid Heterojunction with Intrinsic Thin layer (HIT) a-Si:H/c-Si solar cells with efficiencies of ~21.5% [7, 10]. To improve the solar cell efficiency other structures have been researched. The pin device consists of a three-layer stack,

with an intrinsic (i-type) layer between a n-type layer and p-type layer. This geometry results in an electric field between the p- and n-type regions that stretches across the resistive intrinsic region. Each photon absorbed in the intrinsic layer generates an electron-hole pair that is then separated by the electric field. Amorphous silicon pin device with a photoconversion efficiency of 13% has been reported [8]. In Figure 1-3 there are two types of solar cells, pin and nip. Since a-Si:H holes have limited mobility relative to that of electrons, the devices are designed so that light enters through the p-layer to enable efficient hole collection [8]. This structure, also called a tandem or stacked cell, can achieve relatively higher total conversion efficiencies by capturing a larger portion of the solar spectrum. Different semiconductor materials, suited for different spectral ranges, are arranged atop each other; the higher bandgap material is on the top surface, absorbing high-energy photons, while allowing lower-energy photons to be absorbed by the lower bandgap materials underneath. These selective absorption processes continue through to the final cell possessing the smallest bandgap. Such cells have achieved efficiencies of about 40% but are of course more costly to make than single junction devices [8].

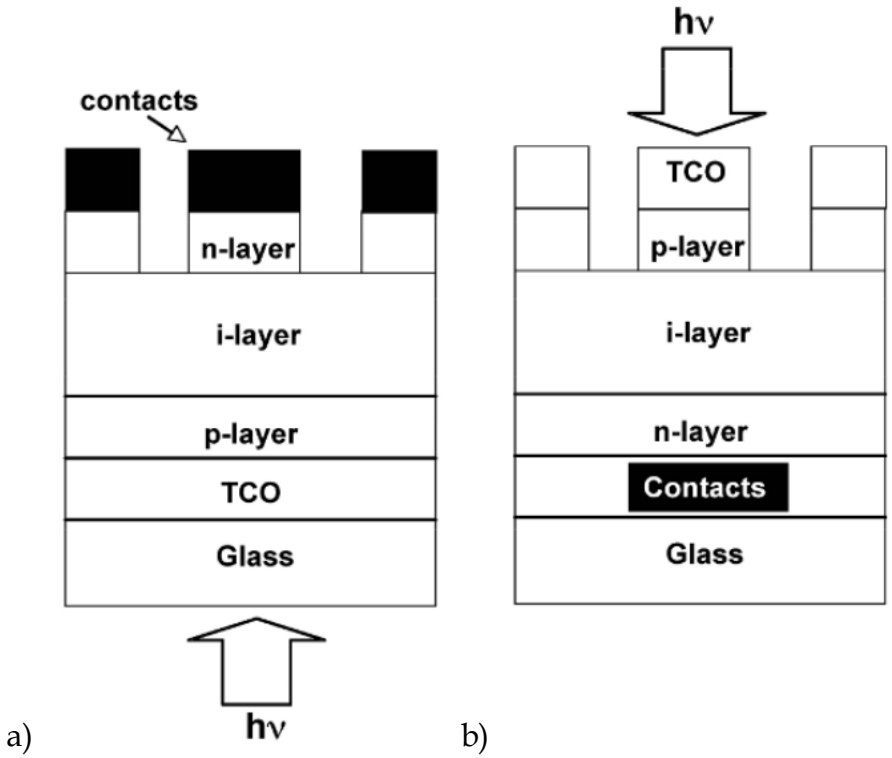

Figure 1-3 – Device structure of a) pin and b) nip solar cells.

A rather different application for the pin structure is hydrogen production [11,12]. Hydrogen is primarily used in the chemical industry, but in the near future it will become a significant fuel. There are many processes for hydrogen production. Fuel processing of methane is the most common hydrogen production method in commercial use in these first decades of the XXI century. Hydrogen can also be produced from ethanol, biodiesel, gasoline, or methane, making it a universal fuel. Infrastructures to develop and store hydrogen have been built, and besides using the hydrogen from these processes as energy directly in fuel cells, the hydrogen rich streams can be used for the production of gasoline, methanol, ethanol, and other high value chemicals [13]. A fuel cell by definition is an electrical cell, which unlike storage cells can be continuously fed with a fuel so that the electrical power output is sustained indefinitely. They convert hydrogen, or hydrogen-containing fuels, directly into electrical energy plus heat through the electrochemical reaction of hydrogen and oxygen into water. The process is that of electrolysis in reverse [14]. There has been a great deal of research in splitting water to make hydrogen and oxygen; in fact its commercial uses date back to the 1890s. Water splitting can be divided into three categories: electrolysis, thermolysis, and photoelectrolysis. While electrolysis uses an electrical current passing through two electrodes to break water into hydrogen and oxygen, thermolysis where heat alone is used to decompose water to hydrogen and oxygen, and the photoelectrolysis process that uses sunlight to directly decompose water into hydrogen and oxygen, and uses semiconductor materials similar to those used in photovoltaics [13]. At present, more than 90% of photovoltaic activities are concentrated on classical crystallized silicon solar cells. Only 7.8% are related to thin layer solar cells, which include the not yet satisfactorily stable amorphous silicon solar cells [15] and also cells made from other materials, which, however, include rare and toxic elements like cadmium, tellurium, indium, and gallium [16].

Applications of amorphous silicon in energy storage are also possible. Elemental lithium is the most favourable material for negative electrodes in Li-ion batteries in terms of electrode potential and specific energy. However, potential safety problems and loss of capacity upon cycling has been an impediment to using lithium as a practical negative electrode (anode) in rechargeable lithium batteries. Present commercial rechargeable lithium cells

use carbon materials for negative electrodes because lithium can be reversibly inserted into them. Since the carbons suffer irreversible capacity loss (ICL) on the first cycle, various alternative materials such as lithium alloys and metal oxides have been extensively studied. Some have larger charge capacities than graphite but cycle-life is still unsatisfactory [17]. Using amorphous silicon as anode yielded results from cycling tests that were performed for the Li|electrolyte|a-Si cell, in which data shows that the discharge capacity of a-Si is as high as 4 Ah g^{-1}, the highest capacity reported (2003), and indicate that each silicon atom can uptake as many as 4.2 Li atoms ($Li_{4.2}Si$) at room temperature reversibly, which approaches the theoretical capacity limit of $Li_{22}Si_5$. After 20 cycles, however, the capacity reduces rapidly. This decline in performance can be overcome and the durability extended to more than 400 cycles changing the lower limit of the voltage window from 0 to 0.2 V, and with this condition the discharge capacity is about 400 mAh g^{-1} [17, 18]. Most interesting is the use of a solid state electrolyte instead of a liquid electrolyte which has disadvantages of liquid leakage, narrow range of operation temperature and explosion upon heating [19]. A schematic diagram is shown in Figure 1-4 for an all solid-state lithium battery constructed employing $Li_{4.4}Si$ (0.06 g) as a negative electrode and $70Li_2S$-$30P_2S_5$ (0.1 g) as a solid electrolyte. The cathode (0.06 g) consists of a mixture of $Li_4Ti_5O_{12}$ (LTO) (40 wt %), the solid state electrolyte (40 wt %) and Denka black (20 wt %). The Denka black (high purified carbon) is used as a conductive agent (0.22 Ω cm).

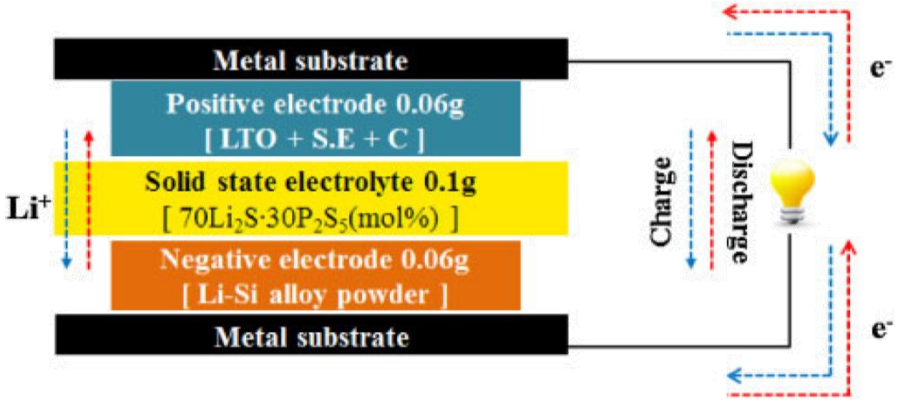

Figure 1-4 - Schematic diagram of solid electrolyte cell consisting of Li-Si alloy ($Li_{22}Si_5$) as anode, LTO ($Li_4Ti_5O_{12}$) as cathode and $70Li_2S$-$30P_2S_5$ as solid electrolyte.

Lithium silicide (Li_xSi) is known as a narrow band gap electronic conductor (Eg = 0.057 eV, T < 450 K), with a reported electrical resistivity in the range 1.5 - 4 x 10^{-4} Ω cm at 300K which is lower than that of Denka black [19].

X-ray imaging sensors have become practical through the emergence of large-area, amorphous silicon thin-film transistor and photodiode technologies [20]. X-ray imaging has been used in many ways, including high resolution imaging using film, real-time video imaging using image intensifier tubes (IITs), and digital imaging for digital subtraction angiography and computer-aided tomography. Additional uses of digital x-ray imaging include bone mineral densitometry, portal imaging for radiotherapy, and many areas of materials monitoring which use x-rays for non-destructive testing. In many of these applications, a large-area flat-panel imager based on a-Si thin-film transistor technology [21] is an attractive component due to its light weight and small form-factor, high photosensitivity, and lack of image distortion that is present in IITs [20]. In contrast to conventional area detectors such as imaging plates (IPs) and charge-coupled devices (CCDs) used in X-ray scattering studies, mostly at moderate X-ray energies (20 keV), the a-Si detector is optimized for the detection of high X-ray energies (80 keV) owing to its originally intended applications in medical imaging. Furthermore, it has a large active area, improved effective detector resolution, and is capable of virtually continuous data accumulation with fast readout (up to 7.5 or 30 Hz) [22].

There are several fields of application for amorphous silicon in integrated optics namely waveguides, filters and tapper-structures shown in Figure 1-5, which enables back-end electronic-photonic integration [23].

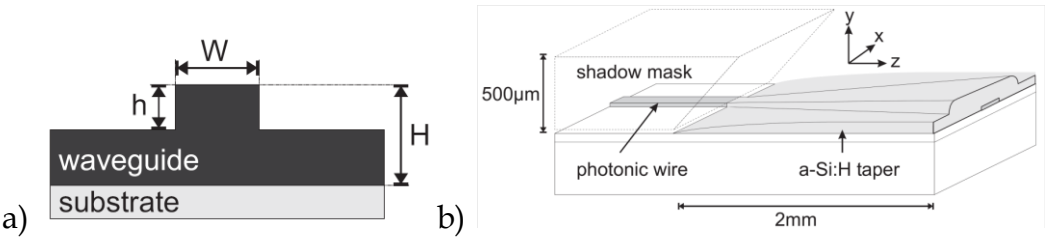

Figure 1-5 – a) Characteristic waveguide dimensions b) Schematic representation of the taper concept.

Three different waveguide designs use the structure presented in Figure 1-5a), Multimode strip waveguides (e.g.: W=4 µm and h=H=2.5 µm) with a

relatively low influence of scattering on propagation losses due to a large cross section which also facilitates efficient butt or end-fire coupling. Monomode strip waveguides (e.g.: W=0.5 μm and h=H=220 nm) also called "photonic wires", allows for the lowest curvature losses, and hence highest integration densities can be achieved. Efficient in- and out-coupling is challenging and requires special taper structures represented in Figure 1-5b). This type of design is state of the art in silicon photonics. Monomode rib waveguides (e.g.: W=1.1 μm and h=380 nm, H=1.3 μm) have efficient coupling without taper structures [23].

The traditional way of identifying the colour of visible light, such as colour vidicon, is to use three band pass filters to extract three fundamental components (red, green, and blue) of the incident light. This method becomes difficult when the detectors are small in size and closely spaced as in the case of a line sensor. Another way is to construct detectors which could simulate the response of the human eyes to the light [25]. There are two classes of photosensitive cells in the eyes called rods and cones which are responsible for the vision. The rod is only active at dim light for sensing the brightness of objects, and the cone is responsible for sensing the colours at normal light intensity. The cone can be divided into three types and each contains a different visual pigment. The response of each type of pigments has peak responses at ~450 (blue), ~530 (green), and 550-600 nm (red), respectively. Therefore, to fully reproduce the colour sensation of eyes, it is necessary to design three detectors which could simulate the responses of these three visual pigments [25, 28].

The three-colour structure of Figure 1-6 is an enhancement of the two-colour detector [29], with improvements in its performance by adding different intrinsic layers [25]. The basic idea is to use different voltage polarities to select one of the two back-to-back pin junctions to collect the incident photons. When the collector to emitter bias $V_{CE} > 0$ V, the collector junction (bottom piin heterojunction) which mainly absorbs the blue light is reverse biased and the photoresponse shows a peak in blue.

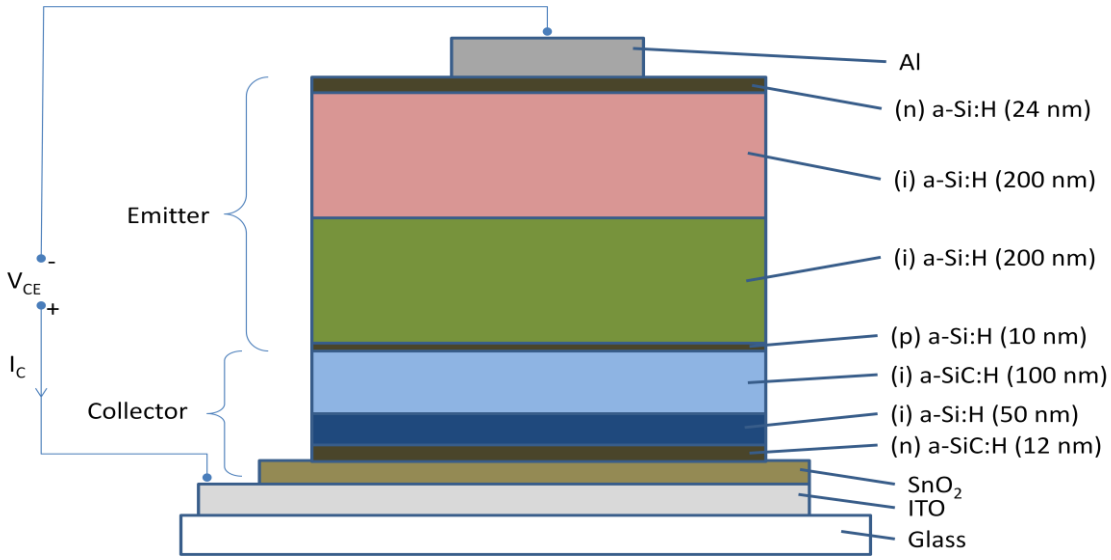

Figure 1-6 – Schematic diagram of the device structure.

The purpose of inserting a 50 nm intrinsic a-Si:H in the collector junction is to absorb more blue photons in the collector and less in the emitter. This improves the rejection ratio in the 450-480 nm region when the detector is biased at 2 and -2 V, respectively. On the other hand, when V_{CE} < 0 V, the photoresponse is determined by the emitter junction which is now reverse biased and mainly absorbs red and green light. In order to further separate the green from red, the emitter junction is designed to consist of two a-Si:H layers which are deposited at different conditions. The first layer should be deposited with a higher donor-type gap state density than the second layer; i.e., at equilibrium, the Fermi level is closer to Ec. Then, at small bias, only the first layer is depleted and the response will peak at the green region. In addition, the optical gap of the first layer (1.84 eV) is slightly higher than that of the second layer (1.74 eV) which provides a discontinuity at the valence band mobility edge and helps to retard the collection of photogenerated carriers in the second layer under small reverse bias. As the bias is increased to deplete the first layer, the depletion region rapidly extends into the second layer and the response should shift to the longer wavelength. The usage of different gap state density is better than that just using one uniform a-Si:H layer in which a large voltage is needed to change the collection region [25]. Summarizing, the device has three different responsivities which can be selected by changing V_{CE} from -2 to 2 V. The peaks of the three responses are 480, 530, and 575 nm at V_{CE}= 2.0, -0.2, and -

2.0 V, respectively, close to the response of three types of cone cells in the eyes [25].

1.3 The pi'npin heterostructures

The pi'npin device that is the basis of the work presented in this thesis is the result of the continuous research made on the GIAMOS (Grupo de Investigação Aplicada à Microelectrónica, Optoelectrónica e Semiconductores) working group [30]–[33]. The working group belongs to the Instituto Superior de Engenharia de Lisboa (ISEL) and is part of the Centre of Technology and Systems (CTS) of the Universidade Nova de Lisboa (UNL) [34].

1.3.1 Device configuration and sample preparation

The pi'npin device (p(a-SiC:H)-i'(a-SiC:H)-n(a-SiC:H)-p(a-SiC:H)-i(a-Si:H)-n(a-SiC:H)) was produced by PECVD as displayed in Figure 1-7.

The thickness (200 nm) and the optical gap (2.1 eV) of the a-SiC:H intrinsic layer (i') is optimized for blue collection and red transmittance. The thickness (1000 nm) of the a-Si:H i-layer was adjusted to achieve full absorption in the green and high collection in the red spectral ranges. As a result, both front and back diodes act as optical filters confining, respectively, the blue and the red optical carriers, while the green carriers are absorbed across both [33, 35].

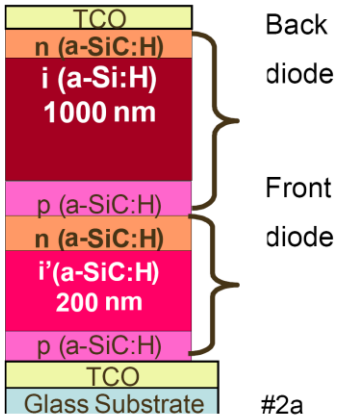

Figure 1-7 - Sensor configuration (referred as #2a or NC5).

The deposition conditions of the i and i' intrinsic layers were kept constant. They present good properties with conductivities between 10^{-11} and 10^{-9} $\Omega^{-1}cm^{-1}$

and photosensitivity gain higher than 10^4 under AM1.5 illumination (100 $mWcm^{-2}$). To decrease the lateral currents which are crucial for device operation [28, 30], low doping levels were used and methane was added during the deposition process. The doped layers (20 nm thick) have high resistivity (>10^7 Ωcm) and optical gaps around 2.1 eV. Transparent contacts have been deposited on the front and back surfaces to allow the light to enter and leave from both sides. The back contact defines the active area of the sensor (1x1 cm^2). The front and back contacts are based on ZnO:Al, a transparent conductive oxide (TCO), and have an average transmission around 80% from 425 nm to 700 nm and a resistivity around $9x10^{-4}$ Ωcm [37].

Table 1-1 - Deposition conditions of the a-Si:H and a-SiC:H films.

Type	RF Power (W)	Pressure (mTorr)	Gas flow(sccm)			
			SiH_4	1%TMB+99%H_2	2%PH_3+98%H_2	CH_4
p (a-SiC:H)	4	600	10	25	–	15
i (a-SiC:H)	4	500	10	–	–	15
n (a-SiC:H)	4	500	10	–	5	15
i' (a-SiC:H)	2	400	20	–	–	–

The film layers were deposited using a parallel-plate PECVD reactor. Deposition conditions such as the RF power, partial pressure and gas flow rates are shown in Table 1-1. The substrate temperature was held at 260°C [38].

The sensor displayed in Figure 1-7 is referred to as either #2a or NC5.

1.3.2 Light Filtering

The characterization of the devices was performed through the analysis of the photocurrent dependence on the applied voltage and spectral response under different optical and electrical bias conditions. The responsivity was obtained by normalizing the photocurrent to the incident flux. To suppress the DC components all the measurements were performed using the lock-in technique. Figure 1-8a) displays the spectral photocurrent of the sensor under different applied bias (+3V < V < -10 V). In Figure 1-8b) the spectral photocurrent, under different electrical bias is displayed for the front, p-i' (a-SiC:H)-n, and the back p-i (a-Si:H)-n, photodiodes [37].

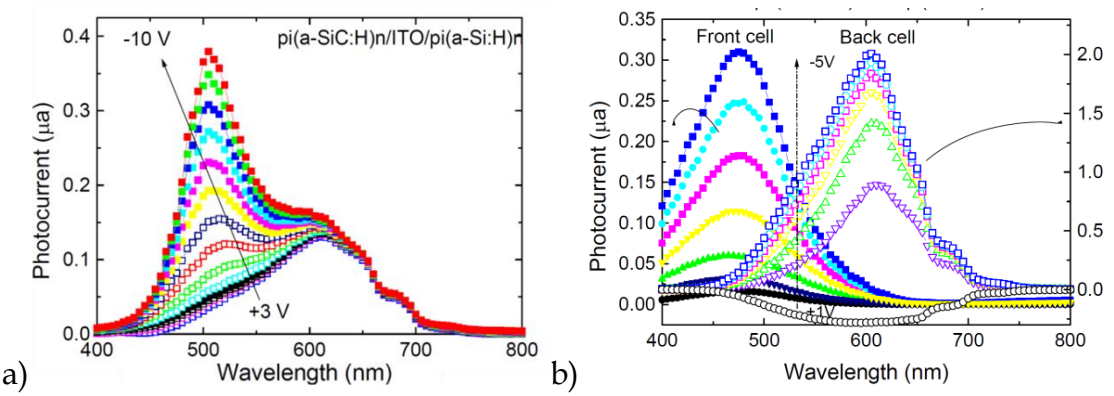

Figure 1-8 -(a) pi'npin spectral photocurrent under different applied voltages, (b) Front, p-i'(a-SiC:H)-n, and back, p-i (a-Si:H)-n spectral photocurrents under different applied bias.

Results confirm that the front and back photodiodes act, separately, as optical filters. The front diode, based on a-SiC:H heterostructure, cuts the wavelengths higher than 550 nm while the back one, based on a-Si:H, cuts the ones lower than 500 nm. Each diode, separately, presents the typical responses of a single pin cell with intrinsic layers based on a-SiC:H or a-Si:H materials, respectively. Since the current across the device has to remain the same, in the stacked configuration, it is clearly observed the influence of both front and back diodes modulated by its serial connection through the internal n-p junction [37].

1.3.3 Current – Voltage Characteristics

The typical I-V characteristics in dark and under red, blue and red&blue irradiation are displayed in Figure 1-9 [39].

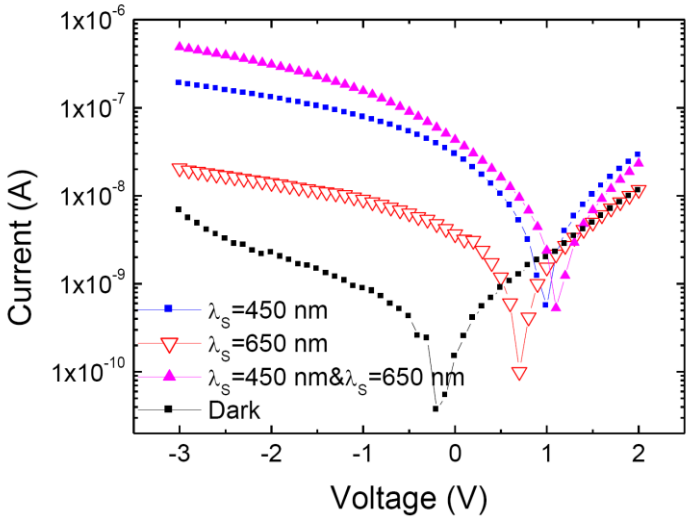

Figure 1-9 - I-V characteristics in dark and under red, blue and red&blue irradiation.

Results show that the shapes of the I-V characteristics are controlled by the background light and by the applied voltage [39].

1.3.4 Numerical Simulation

A device simulation program ASCA-2D [30] was used to analyze the potential profiles in the pi'npin structure of Figure 1-7. Typical values of band tail and gap state parameters for amorphous materials were used. The doping level was adjusted in order to obtain approximately the same conductivity of the layers as in the tested samples. In the films the optical band gaps were chosen in compliance with the obtained experimental values (Table 1-1). Band discontinuities were equally distributed over the valence and conduction band offsets ($\Delta E_v = \Delta E_c = 0.15$ eV) [39].

The photogeneration/recombination profiles used in the simulation are depicted in Figure 1-10 for a tandem p-i(a-SiC:H)-n/p-i(a-Si:H)-n -cell having, respectively, 200 nm and 1000 nm thick absorbers [39].

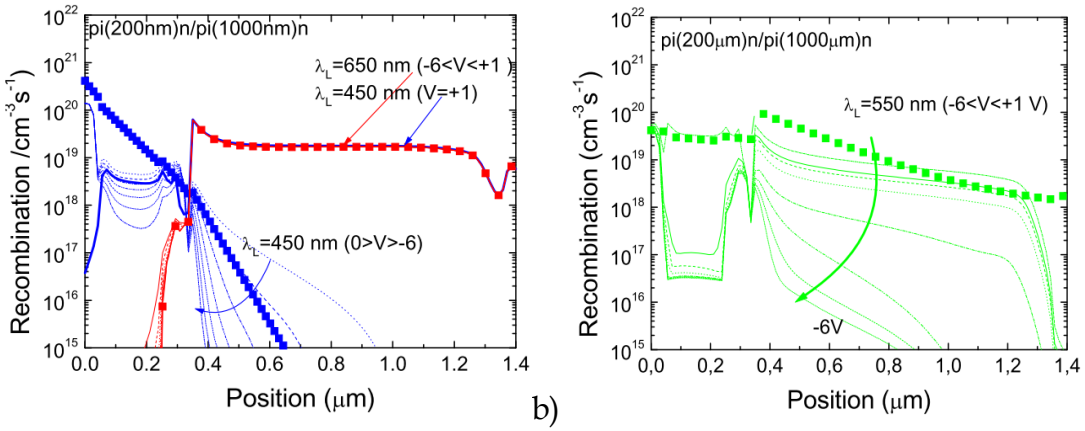

Figure 1-10 - Numerical simulation under different applied voltages and background light: generation (solid lines)/recombination (dash lines) rates a) 450 and 650 nm b) 550 nm.

The thickness of the front diode and its optical gap was optimized for high conversion efficiency in the blue/green light and transparency of the red photons coming from the glass side. In the a-SiC:H and a-Si:H absorbers an optical band gap of 2.1 eV and 1.8 eV and a thickness of 200 nm and 1000 nm were, respectively, chosen in compliance with the obtained experimental values. The doping level was adjusted in order to obtain approximately the same conductivity of the layers as in the tested samples [40].

1.3.5 Electrical Field Profiles

The simulated electric field profile of the pi'npin structure shown in Figure 1-7 under different optical bias wavelengths and for different values of the external electrical bias is presented in Figure 1-11a), b) and c). In Figure 1-11 d) the electric field profile under thermo-dynamical equilibrium is displayed [41].

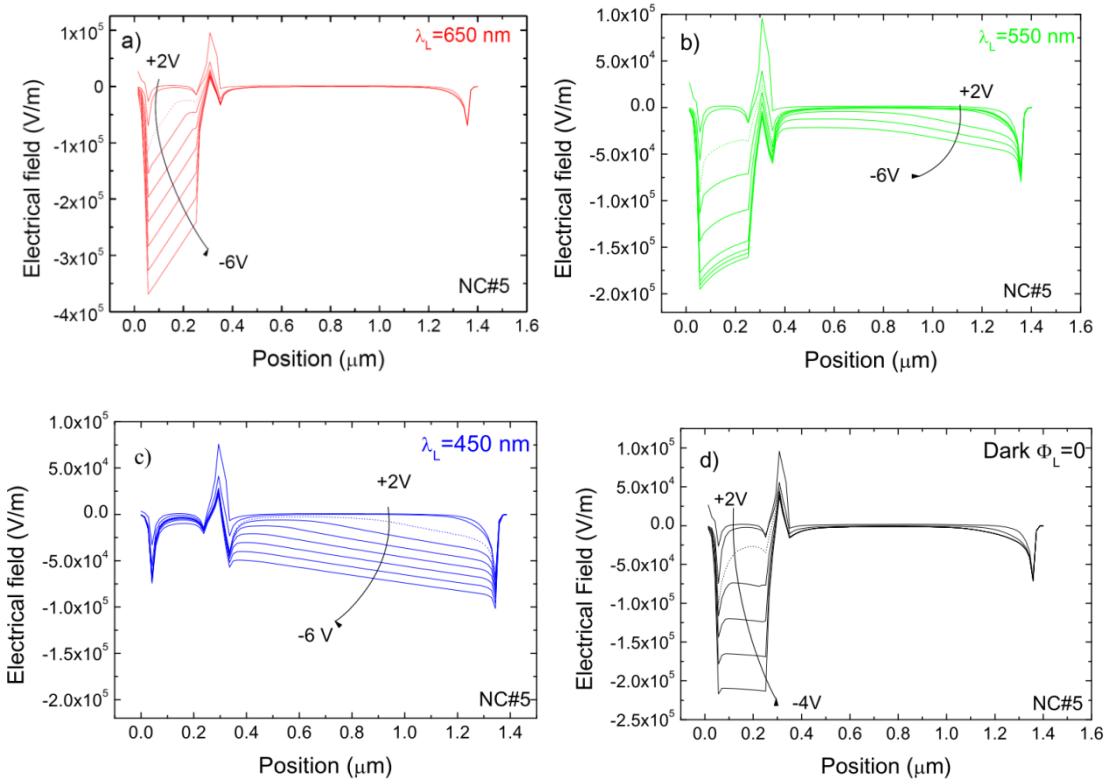

Figure 1-11 - Electric field profile within the pi'npin structure for different values of the external electrical bias and for different wavelengths of impinging light: a) 650 nm; b) 550 nm; c) 450 nm d) thermo-dynamical equilibrium (dark).

Simulated results show that the shallow penetration of the blue photons into the front diode, the deep penetration of the red photons into the back absorber or the decay of the green absorption across both, controls the internal electrical field. The balance between the electrical field adjustments due to the non uniform absorption throughout the structures depends on the generation/recombination ratio profiles at each applied voltage (Figure 1-10) [41]

When an external electrical bias (forward or reverse) is applied, it mainly influences the field distribution within the less photo excited sub-cell. When

compared with the electric field profile under thermo-dynamical equilibrium conditions, the field under illumination is lowered in the most absorbing cell, while the less absorbing one reacts by assuming a reverse bias configuration. Consequently, opposite behaviour is observed under red and blue background light while under green light condition the redistribution of the field profile is balanced between the two sub-cells [41].

1.3.6 Potential Profile

Figure 1-12 shows the simulated potential profiles at different applied voltages in dark (dash line) and under red (straight line), green (cross +) and blue (cross x) irradiation [42].

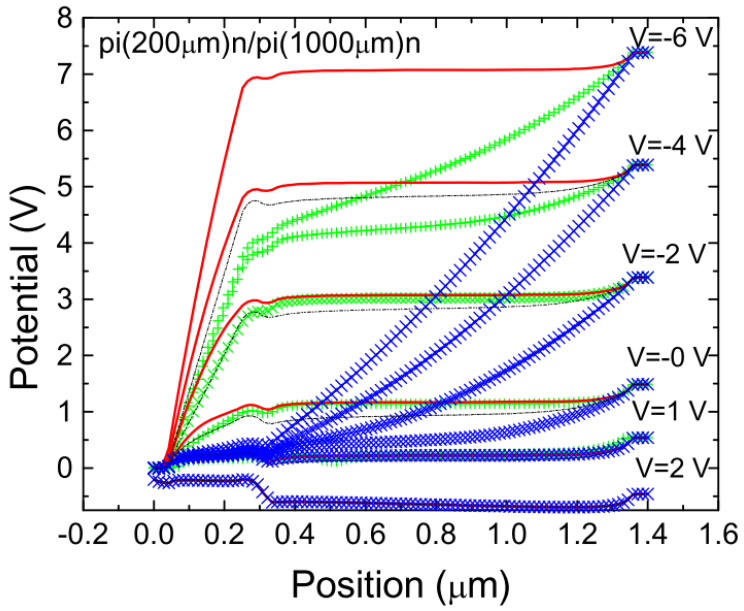

Figure 1-12 - Simulated potential profile under different applied voltages in dark and under red (λ_L= 650 nm) green (λ_L = 550 nm) and blue (λ_L = 450 nm) irradiation.

Results show that the application of an external electrical bias interferes mainly with the less absorbing cell. In the blue range as the reverse bias increases the potential drop across the non irradiated diode increases while in the front it remains almost negligible. In the red range the potential drop occurs across de front diode where no carriers are generated and remains negligible at the absorbing region. Due to the non uniform absorption across the back diode (Figure 1-11), under green irradiation, the potential drop is distributed across

both diodes and balanced between the blue (in the back diode) and the red (in the front diode) behaviours [38].

1.3.7 Self-bias effect in pi'npin structures

Taking into account the geometry of the structure, both the front and the back diodes are optically and electrically in series. The incident light traverses through the sequence and is absorbed accordingly to its wavelength. As the diodes are electrically in series, both must ensure that each supplies the same current:

$$I_1^{pin} = I_2^{pin} = I \qquad V = V_1 + V_2 \tag{1.1}$$

$$I_1^{pin} = I_{01}\left[exp\left(\frac{V_1}{\eta V_T}\right) - 1\right] - I_{ph1} \qquad I_2^{pin} = I_{02}\left[exp\left(\frac{V_2}{\eta V_T}\right) - 1\right] - I_{ph2} \tag{1.2}$$

Where V_1 and V_2 are the voltage drop across each diode and V the external voltage. $I_{0,1,2}$ and $I_{ph,1,2}$ are, respectively, the leakage and the photo currents, V_T the thermal voltage and η the ideality factor [42]. The ideality factor depends on the fabrication process and compounds used, and in this case it is considered equal in both pin1 and pin2.

Neglecting the series resistance and assuming: $I_1=I_{01}+I_{ph1}$ and $I_2=I_{02}+I_{ph2}$ the current across the structure will be given by:

$$I = \frac{1}{2}\left(-(I_1 + I_2) + \sqrt{(I_1 - I_2)^2 + 4I_{01}I_{02}exp\left(\frac{V}{\eta V_T}\right)}\right) \tag{1.3}$$

$$V = \eta V_t\, ln\left(\frac{(I+I_1)(I+I_2)}{I_{01}I_{02}}\right) \qquad V_1 = \eta V_t\, ln\left(\frac{I+I_1}{I_{01}}\right) \qquad V_2 = V - V_1 \tag{1.4}$$

In Figure 1-13 is displayed the trend of potential across the front (V_1) and back (V_2) diodes as a function of the applied voltage (V) and for different photocurrent values. The η, I_{01} and I_{02} parameters were obtained in compliance with the experimental I-V characteristics ($I_{01} < I_{02}$) shown in Figure 1-9 [42].

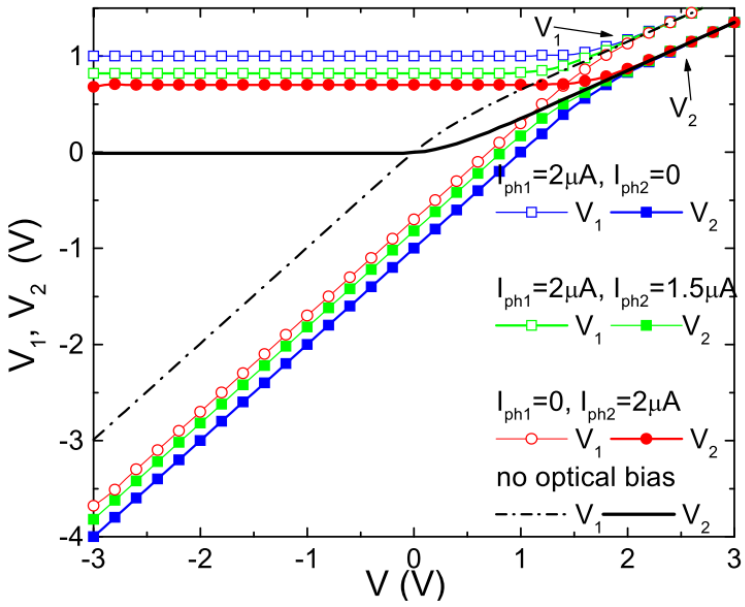

Figure 1-13 - Potential drop across front (V_1) and back (V_2) diodes as a function of the applied voltage (V) and for different photocurrent values.

Data shows that the potential across each diode depends on the level of irradiation of both front and back diodes. Opposite behaviours are observed under red ($I_{ph1}=0$, $I_{ph2}\neq0$, Figure 1-11a) and blue ($I_{ph1}\neq0$, $I_{ph2}=0$, Figure 1-11c) background light. Under green ($I_{ph1}\neq0$, $I_{ph2}\neq0$, Figure 1-11b) the trend depends on the I_{ph1}/I_{ph2} ratio, it approaches the blue trend if $I_{ph1}>I_{ph2}$, the red if $I_{ph1}<I_{ph2}$ and is the same as in dark if both photocurrent are balanced. Any diode whose current ($I^{pin}_{2,1}$) is below the other would have to reduce its net current (Equation 1.2) and consequently voltage (Equation 1.4) in order to try to hold up. This diode may even have to reverse bias itself in its efforts to get in line with the other. This effect is called the self reverse bias effect [42].

1.3.8 Selective Wavelength Discrimination

Figure 1-14 displays the spectral photocurrent under negative (-10 V) and positive (+3 V) external bias and their differences (symbol), and the dotted lines are the multi peak curve fit at -10 V [41].

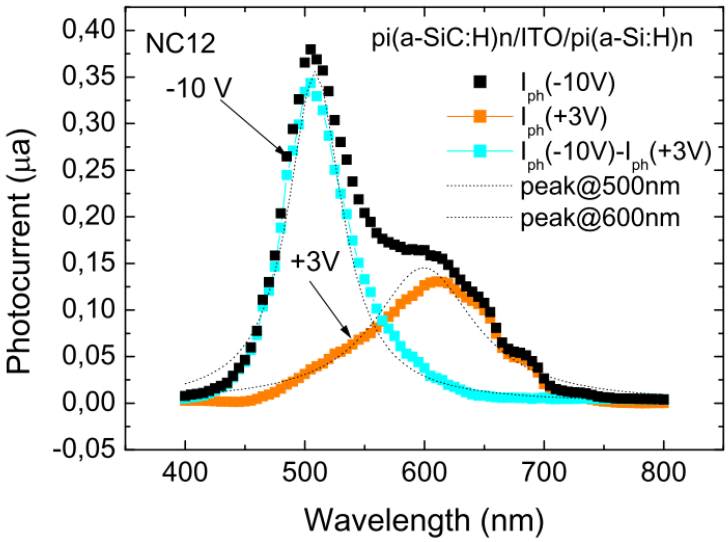

Figure 1-14 – Spectral response of the pi'npin device under negative and positive bias.

Under negative bias the contribution of both front and back diodes (dotted lines) is clear. Two peaks centred, respectively at 500 nm and 600 nm are observed. Under positive bias, the response around 500 nm disappears while the one around 600 nm remains constant as expected from Figure 1-8a). So, under forward bias the device becomes sensitive to the red region and under reverse bias to the blue one working as a selective optical device in the visible range [41].

1.3.9 Self Bias Amplification under Uniform Irradiation

Three monochromatic pulsed lights (input channels): red (R: 626 nm), green (G: 524 nm) and blue (B: 470 nm) illuminated separately the pi'npin device. Steady state red, green and blue optical bias was superimposed separately and the photocurrent generated measured at -8 V and +1 V. In Figure 1-15 the signal is displayed for each monochromatic input channel.

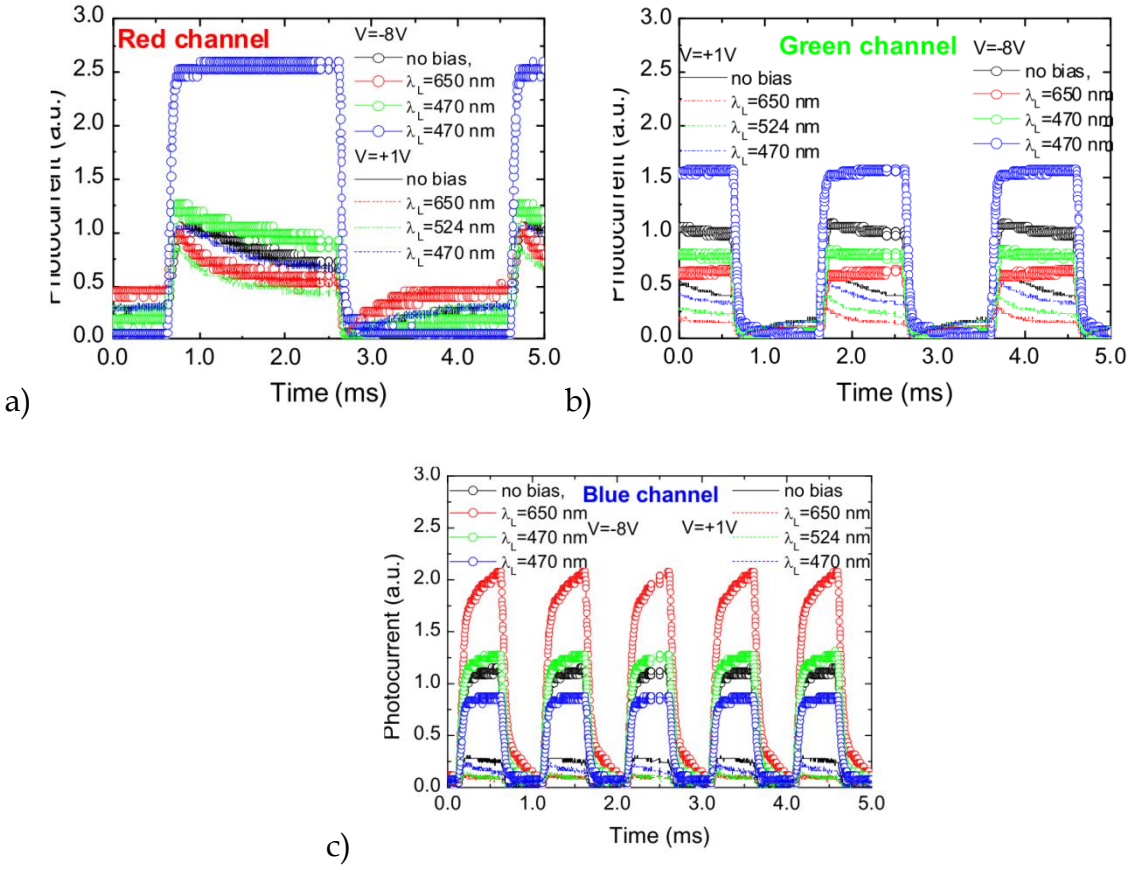

Figure 1-15 - Input red (a) green (b) and blue (c) channel signals under negative and positive bias without and with red, green and blue steady state irradiation for the pi'npin device.

When an optical bias is applied it mainly enhances the field distribution within the less photo excited sub-cell: the back under blue irradiation and the front under red steady bias (see Figure 1-11). Experimental results confirm that blue steady state optical bias amplifies the red channel and that the red light amplifies the blue channel. So, the reinforcement of the electric field under blue irradiation and negative bias increases the collection of the carriers generated by the red channel and decrease the blue one. Under red optical bias an opposite behaviour is observed. The green bias absorption is balanced in both front and back cells. The green channel collection is reduced while the red and blue collections are almost insensitive to the green irradiation. This effect can be used either to amplify the red or blue channels or to tune the green one since the others remain almost constant [43].

When an external electrical bias (positive or negative) is applied to a double pin structure, its main influence is in the field distribution within the

less photo excited sub-cell. The front cell, under red irradiation, the back cell, under blue light, and both, under green steady state illumination, in comparison with thermodynamic equilibrium conditions (dark), results in the following: the electric field under illumination is lowered in the most absorbing cell (self forward bias effect) while the less absorbing reacts by assuming a reverse bias configuration (self reverse bias effect) [39].

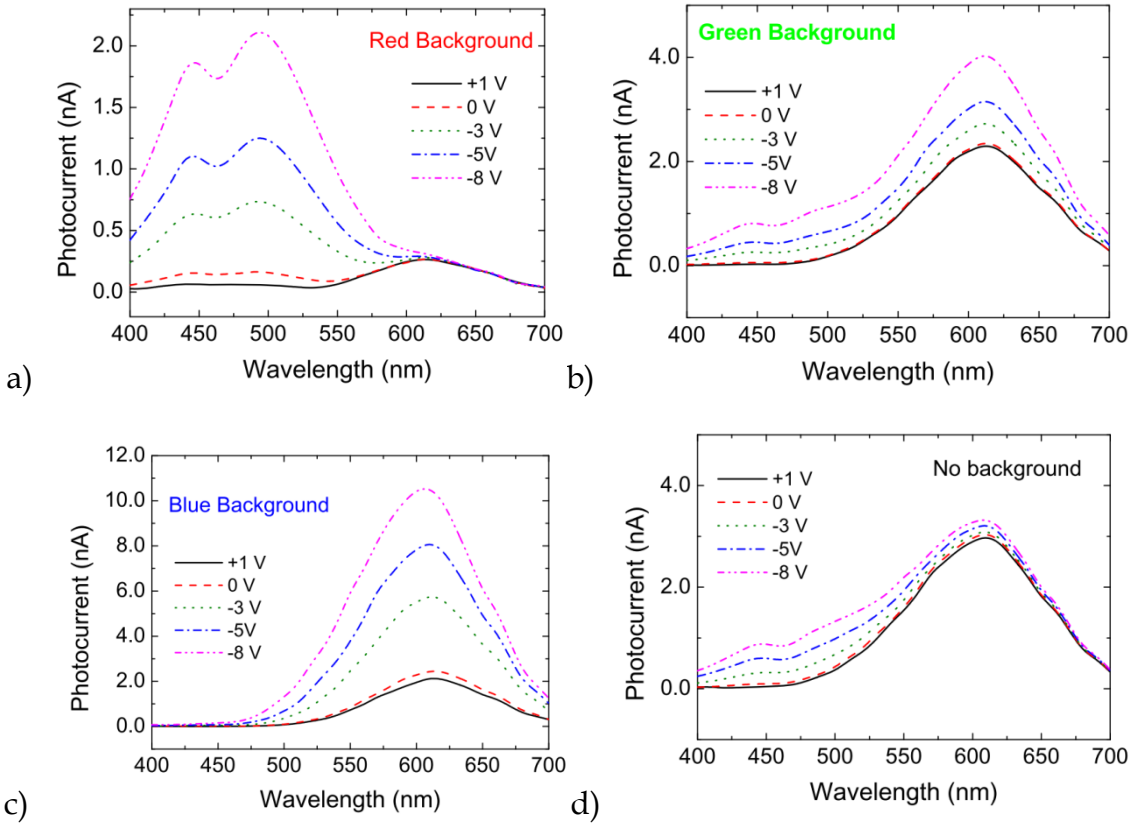

Figure 1-16 - Spectral photocurrent under reverse and forward bias measured without and with (λ_L) background illumination.

In Figure 1-16 the spectral photocurrent at different applied voltages is displayed under red (a), green (b) and blue (c) background irradiations and without it (d). Results confirm that a self biasing effect occurs under unbalanced photo generation. As the applied voltages changes from positive to negative the blue background enhances the spectral sensitivity in the long wavelength range. The red bias has an opposite behaviour since the spectral sensitivity is only increased in the short wavelength range. Under green background the spectral photocurrent increases with the applied voltage everywhere. In Figure 1-17 the ratio between the spectral photocurrents @ +1 V and -8 V, under red, green and blue steady state illumination and without it (dark), are plotted [44].

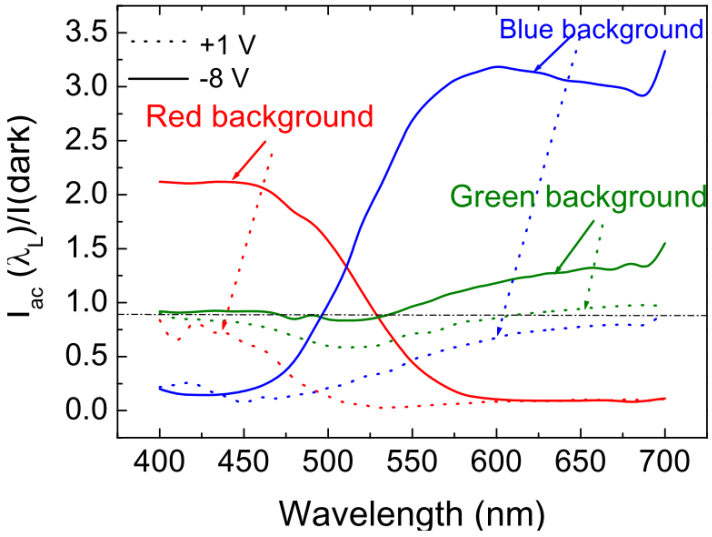

Figure 1-17 - Ratio between the photocurrents under red, green and blue steady state front illumination and without it (no background).

As expected the blue background enhances the light-to-dark sensitivity in the long wavelength range and quenches it in the short wavelength range. The red bias has an opposite behaviour; it reduces the ratio in the red/green wavelength range and amplifies it in the blue one. The sensor is a wavelength current-controlled device that makes use of changes in the wavelength of the optical bias to control the power delivered to a load, acting as an optical amplifier. Its gain, defined as the ratio between the photocurrent with and without a specific background, depends on the background wavelength that controls the electrical field profile across the device (Figure 1-11). If the electrical field increases locally (self optical amplification) the collection is enhanced and the gain is higher than one. If the field is reduced (self optical quench) the collection is reduced and the gain is lower than one. This optical nonlinearity makes the transducer attractive for optical communications [45].

1.3.10 Voltage Controlled Wavelength Discrimination

Monochromatic pulsed beams together or in one single polychromatic beam (mixture of different wavelength) impinge in the pi'npin device and are absorbed, according to their wavelength (Figure 1-10, Figure 1-11). By reading out, under appropriate electrical bias conditions, the photocurrent generated by the incoming photons, the input information is electrically multiplexed or demultiplexed [43].

To increase the capacity of transmission over one strand fibre, wavelength division multiplexing (WDM) is used. This technique transmits multiple optical signal channels (multiplex) in a single optical fibre using different wavelengths (colours) for each channel, and restores on the receiving side each individual channel (demultiplex) [46].

In the multiplexing mode the device faces the modulated light incoming together (monochromatic input channels). The combined effect of the input signals is converted to an electrical signal, via the device, keeping the input information (wavelength, intensity and modulation frequency) [43].

Figure 1-18 displays the photocurrent signal obtained with the WDM device under single and combined modulated light bias: red (R: 626 nm), green (G: 524 nm) and blue (B: 470 nm) from the glass side. The generated photocurrent is measured under negative (-8 V; solid arrow) and positive (+1 V; dotted arrow) bias to readout the combined spectra. The light modulation frequency of each channel was chosen to be multiple of the others to ensure a synchronous relation of ON-OFF states along each cycle. For each independent wavelength, the output optical powers were adjusted to give different signal magnitudes at -8 V (solid arrows). The correspondent photocurrent signals at +1 V are also displayed (dotted arrows). The reference level was assumed when all the input channels were OFF.

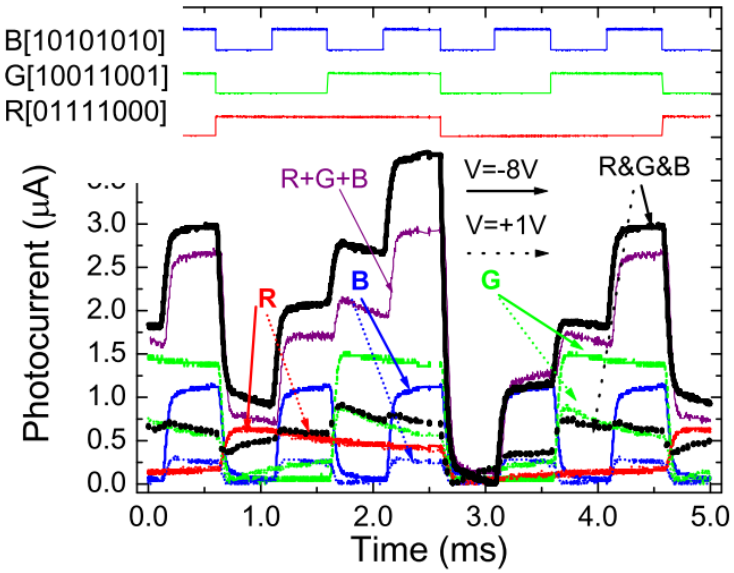

Figure 1-18 - Single (R, G and B) and combined (R&G&B) signals under -8 V (solid arrows) and +1 V (dotted arrows).

The output multiplexed signal, obtained from the combination of the three optical sources, depends on both the applied voltage and on the ON-OFF state of each input optical channel. Under negative bias, the multiplexed signal presents eight separate levels. The highest level appears when all the channels are ON and the lowest if they are OFF. Furthermore, the levels ascribed to the mixture of three or two input channels are higher than the ones due to the presence of only one (R, G and B). Optical nonlinearity was detected; the sum of the input channels (R+B+G) is lower than the correspondent multiplexed signals (R&G&B). This optical amplification, mainly on the ON-ON states, suggests capacitive charging currents due to the time-varying nature of the incident lights. Under positive bias the levels were reduced to one half, since the blue component of the combined spectra falls into the dark level, the red remains constant and the green component decreases [43].

In Figure 1-19 the multiplexed signals are shown, under reverse and forward bias, obtained with two RGB bit sequences and the same bit rate (2000 bps) [43].

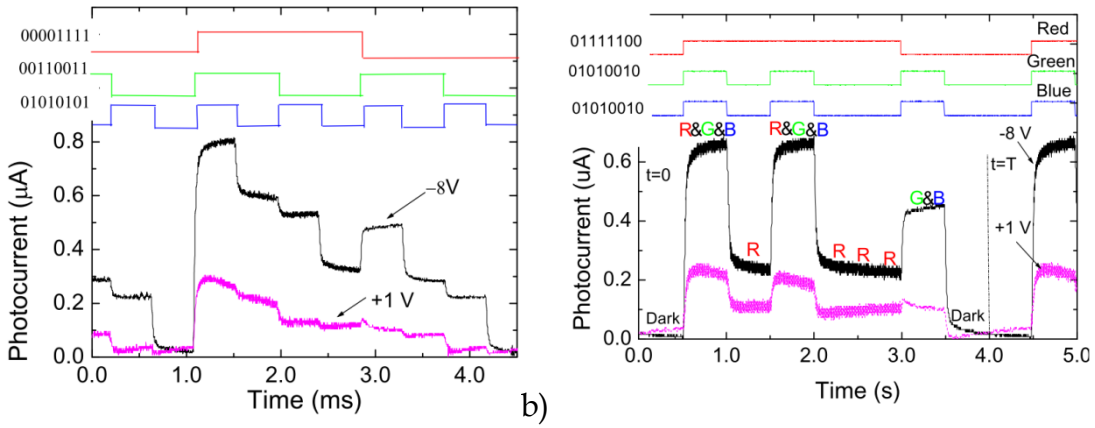

Figure 1-19 - Multiplexed signals under negative and positive bias using two different bit sequences: a) R [00111100], G [01010010], B[00110011] and b) R [01111100], G [01010010], B[01010010]. On the top, there are the optical signals used to transmit the information to guide the eyes onto the different ON-OFF states.

In the bit sequence of Figure 1-19a) there is a synchronous relation of ON-OFF states along each cycle. The photocurrent under reverse bias, exhibits the expected eight different levels that correspond each to different optical bias states. As the electrical bias goes from reverse to forward the signal amplitude decreases and the levels of the threshold photocurrent associated to each optical

state become closer and less defined showing the extinction of the photocurrent caused by the short wavelength optical signals. This mechanism can be used for the identification of the input channels using the photocurrent signal obtained under forward and reverse signals and comparing the magnitude of the variation in each optical state. In the input sequence of Figure 1-19b) the blue and the green channels transmit the same information, and thus the thresholds assigned to the single green or blue channel ON (G or B) and their combination with the red (R&G, R&B) do not appear in the multiplexed signal that contains only four photocurrent levels: R&G&B, G&B, R and Dark even under negative bias [43].

1.3.11 Signal Recovery

In the demultiplexing mode a polychromatic modulated light beam is projected onto the device and the readout performed by shifting between forward and reverse bias. Figure 1-20 displays, under reverse and forward bias, the multiplexed signals due to the simultaneous transmission of three independent bit sequences, each one assigned to one of the RGB colour channels.

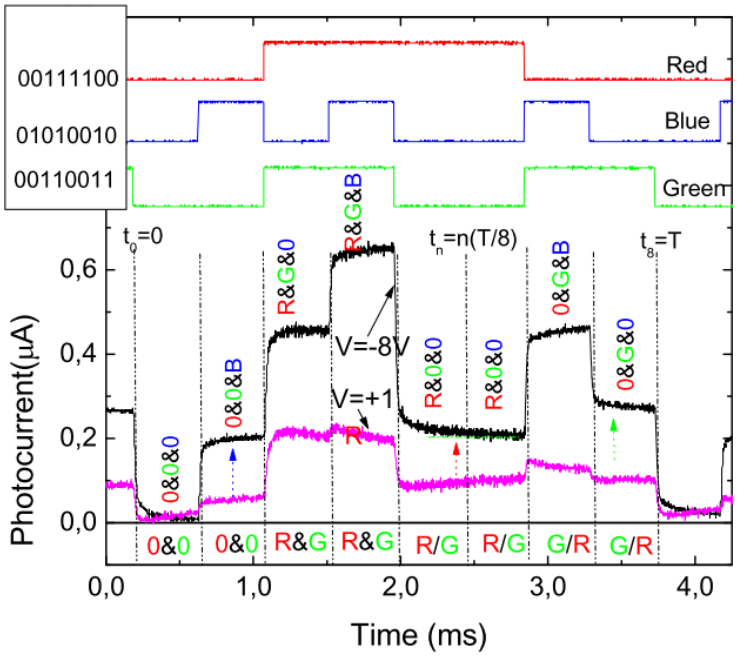

Figure 1-20- Multiplexed signals under negative and positive electrical bias. On the top, there are the optical signals used to transmit the information to guide the eyes onto the different ON-OFF states. The bit sequence for the demultiplexed signal is shown for comparison.

At the top of the Figure 1-20 the optical signals used to transmit the information are displayed to guide the eyes onto the different ON-OFF states. The bit sequence obtained for the demultiplexed signal is also shown for comparison [41].

To recover the transmitted information (8 bit per wavelength channel) the multiplexed signal, during a complete cycle (0<t<T), was divided into eight time slots, each corresponding to one bit where the independent optical signals can be ON (1) or OFF (0). As, under forward bias, the WDM device has no sensitivity to the blue channel, the red and green transmitted information can be identified from the multiplexed signal at +1 V. The highest level corresponds to both channels ON (R&G: R=1, G=1), and the lowest to the OFF-OFF stage (R=0; G=0). The two levels in-between are related with the presence of only one channel ON, the red (R=1, G=0) or the green (R=0, G=1) (see horizontal labels in Figure 1-20). To distinguish between these two situations and to decode the blue channel, the correspondent sub-levels, under reverse bias, have to be analyzed. From Figure 1-15, Figure 1-16 and Figure 1-17 it is possible to observe that the green channel is more sensitive to changes on the applied voltage than the red, and that the blue only appears under reverse bias. So, the highest increase at -8 V corresponds to the blue channel ON (B=1), the lowest to the ON stage of the red channel (R=1) and the intermediate one to the ON stage of the green (G=1). Using this simple algorithm the independent red, green and blue bit sequences can be decoded as: R[00111100], G[00110011] and B[01010010] [39].

To validate the ability of this device to multiplex and demultiplex optical signals, the multiplexed signals, in Figure 1-18, were analyzed, in a time window between 0.7 ms and 4.2 ms, resulting in the bit sequences: B[10101010], G[10011001] R[01111000], which are in agreement with the signals acquired for the independent channels. A demultiplexing algorithm was implemented in Matlab that receives as input the measured photocurrent and derives the sequence of bits that originated it. The algorithm makes use of the variation of the photocurrent instead of its absolute intensity to minimize errors caused by the signal attenuation. A single linkage clustering method is applied to find automatically eight different clusters based on the measured current levels in both forward and reverse bias. This calibration procedure is performed for a short calibration sequence. Each cluster is naturally bound to correspond to one

of the known eight possible combinations of red, green and blue bits. Following this procedure the sequence of transmitted bits can be recovered in real time by sampling the photocurrent at the selected bit rate and finding for each sample the cluster with the closest current levels. In Figure 1-21 is an example of the output obtained for two different sequences at 4000 bps [47].

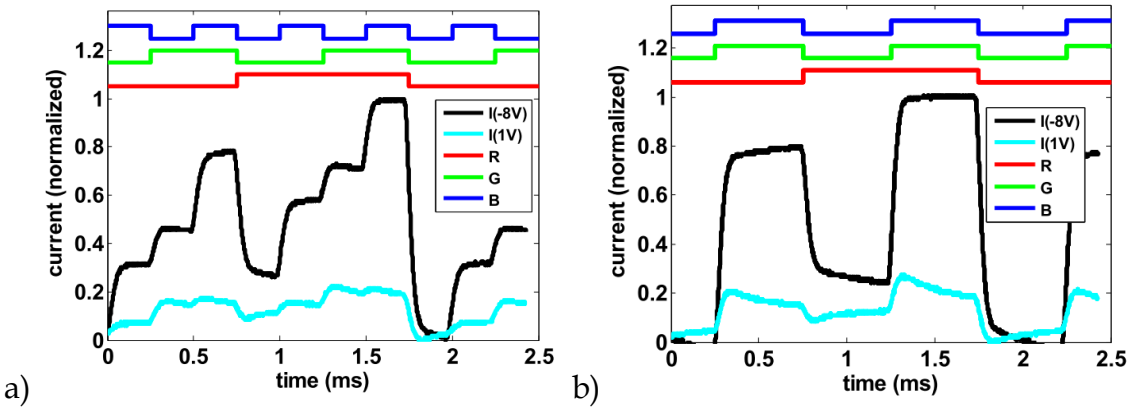

Figure 1-21 - A snapshot of the output from the Matlab routine used to demultiplex the transmitted sequence of bits two sequences a) and b). The sequence of red, green and blue bits (shown at the top) was derived from the measured currents.

Output data of the demultiplexing algorithm shows that the derived sequences are R [00011100], G [011001100] and B [10101010] for the multiplexed signal of Figure 1-21a) and R [00011100], G [011001100] and B [011001100] for Figure 1-21b). Both results were found to be in exact agreement with the original sequences of bits that were transmitted [47].

1.3.12 Optical Bias Controlled Wavelength Discrimination

A chromatic time dependent wavelength combination (4000 bps) of R (λ_R=624 nm), G (λ_G=526 nm) and B (λ_B=470 nm) pulsed input channels with different bit sequences, was used to generate a multiplexed signal in the device. The output photocurrents under negative voltages with (colour lines) and without (dark lines) background lights are displayed in Figure 1-22a). The bit sequences are shown at the top of the figure. Results show that, even under transient input signals (the input channels), the background wavelength controls the output signal as in Figure 1-15 and Figure 1-16. This nonlinearity is due to the transient asymmetrical light penetration of the input channels across

the device together with the modification on the electrical field profile due to the optical bias (Figure 1-11) [39].

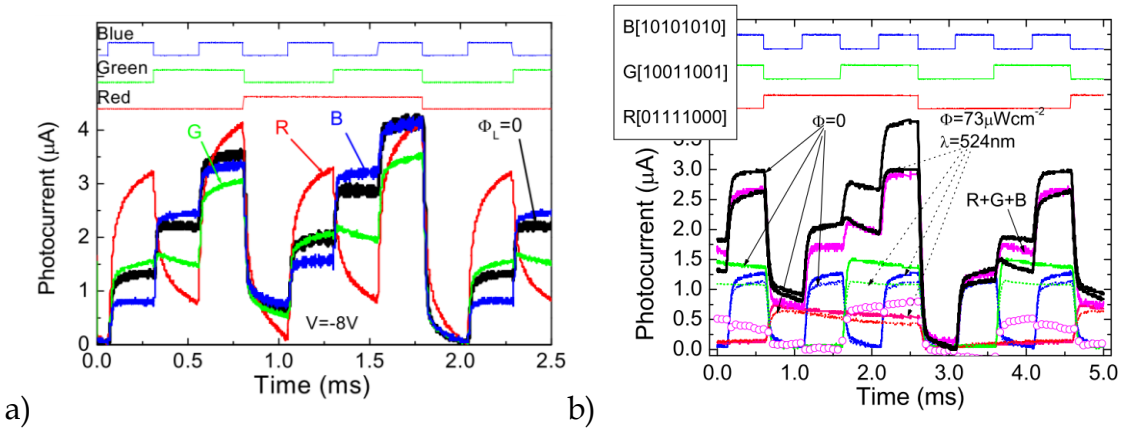

Figure 1-22 – a) Multiplexed signals @-8V; without (black line) and with (colour lines) different R G B steady state optical bias. b) Single and combined signals @ -8 V; without (solid arrows) and with (dotted arrows) green optical bias.

In Figure 1-22b), the input and the multiplexed channels, without or with green bias, are displayed at -8 V. The bit rate sequence is shown at the top of the figure to guide the eyes. The sum of the individual channel without optical bias (R+G+B) is also shown. Results show that the presence of the optical bias reduces significantly the amplitude of green channel. The sum of the input colour channels shows that when the green channel is ON no amplification occurs. This suggests that the green channel can be tuned by making the difference between the multiplexed signal without and with green irradiation (symbols in the figure) [44].

Taking into account Figure 1-11, under green light irradiation the electric field decreases on both sub-cells. So, some of the carriers generated by the green channel, also in both sub-cells, recombine and the collection decreases. When the red or blue channels are ON, the generation occurs only in one sub- cell. The electrical field, in the presence of the red and blue channels, lowers, respectively, in the back and front photodiodes (most absorbing cells), while the correspondent front and back photodiodes (less absorbing cells) reacts by assuming a reverse bias configuration compensating the effect of the green optical bias. This self bias effect explains the slightly increase on the red and blue collection under green optical bias. This nonlinearity provides the possibility for selectively removing and adding wavelength and can be used to

boost signal power after multiplexing or before demultiplexing which usually introduce optical loss into the system [44].

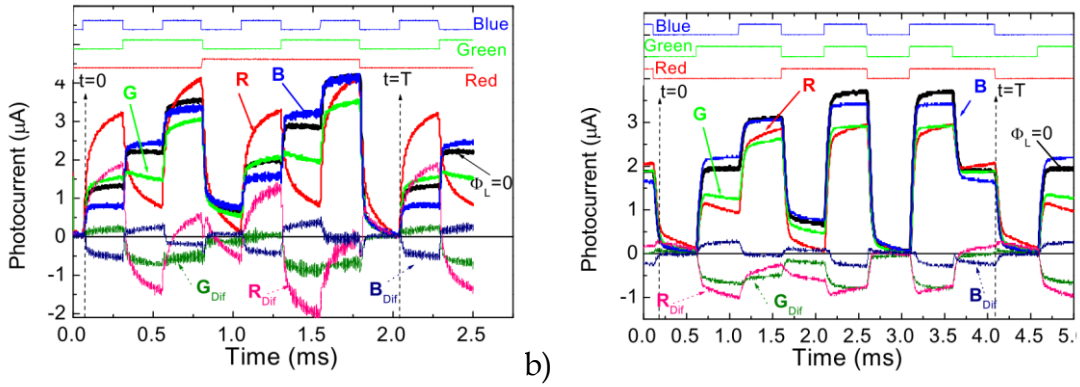

Figure 1-23 - Multiplexed signals @-8V (solid lines); without (ΦL=0) and with (R, G, B) optical bias. The bit sequences are shown at the top of the figures.

In Figure 1-23 a chromatic time dependent wavelength combination: a) 4000 bps; b) 2000 bps of R (λ_R=624 nm), G (λ_G=526 nm) and B (λ_B=470 nm) pulsed input channels with different bit sequences, was used to generate a multiplexed signal. The output photocurrents, under negative (-8 V) voltage with (colour lines) and without (dark lines) background and their differences (dotted lines; R_{Dif} , G_{Dif} and R_{Dif}) are displayed. The bit sequences are shown at the top of the figure. Results show that the device combines the demultiplexing operation with the simultaneous photodetection and self amplification of the signal. When a polychromatic combination of different pulsed channels impinges on the device, under steady state additional optical bias, the output signal has a strong nonlinear dependence on the light absorption profile in a mode that induces a nonlinear wavelength bias dependent gain. This gain depends on the background wavelength (Figure 1-17) that controls the output signal. The red background enhances the sensitivity in the short wavelength range (blue channel) and quenches it in the short wavelength range (red/green channels). The blue background as an opposite and the green one only interferes with its own colour channel [44].

To recover the information (8 bit per wavelength channel), as in section 1.3.11, the multiplexed signal, during a complete cycle (T), was divided into eight time slots, each corresponding to one bit where the independent optical signals can be ON (1) or OFF (0). Taking into account the sublevels without optical bias (Φ_L=0) and the differences between the signal with and without R,

G and B backgrounds, the different thresholds are compared. Under green irradiation the green channel is immediately decoded (negative difference). The blue channel information is obtained from the difference under red background light and the red channel is obtained by comparing the multiplexed signals under red and green irradiations. Using this simple algorithm the independent red, green and blue bit sequences were decoded as: B[10101010], G[01001101] and R[00001111] in Figure 1-23a) and B[00101011], G[01101010] and R[00011011] in Figure 1-23b). A good agreement was achieved [39].

1.3.13 Influence of Optical Signal Intensity

The identification of the different input channels requires a previous calibration of the transmission signal in order to know the response of the WDM device to each individual channel as the signal attenuation along the transmission medium causes a reduction of the optical intensity at the reception end (WDM device). In order to analyze the influence of this effect the multiplexed signal was acquired with input signals of different optical intensities at -8 V and +1 V. Measurements were made with different levels of increasing optical power to a maximum 140 μWcm^{-2}. Figure 1-24 displays the output photocurrent density variation with the optical bias measured for each optical channel (R: 626 nm, G: 524 nm and B: 470 nm) at -8 V and +1 V [48].

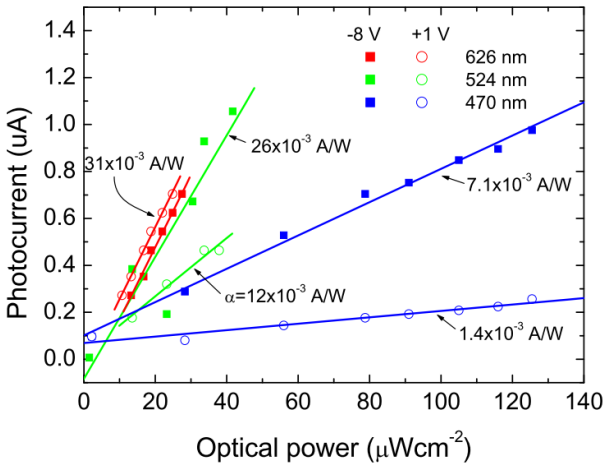

Figure 1-24- Photocurrent density variation with the optical bias measured for each optical channel (R: 626 nm, G: 524 nm and B: 470 nm) at -8 V (solid symbols) and + 1 V (open symbols). The solid lines correspond to linear fits of the experimental data. Slopes (α) of each plot are also displayed.

Results show that under red illumination the multiplexed signal magnitude, under the same intensity conditions, is almost independent on the applied bias. Its magnitude increases with the optical power intensity, exhibiting a linear behaviour with a growth rate around $31x10^{-3}$ A/W. Under green and blue light the dependence of the photocurrent magnitude is strongly dependent on the polarity of the applied bias as already demonstrated before. It increases with the optical intensity of each channel either for reverse and forward bias and the growth rate depends on the applied voltage, being higher at reverse bias. Under blue light (470 nm) the slope rate is 5 times higher at reverse than under forward bias, while under green illumination (524 nm) this ratio is only of a factor of 2. This is due to the strong reduction of the device sensitivity for the shorter wavelengths under forward bias [48].

1.4 Summary

Silicon although common around the world and identified as sand beach does not really occur as a free element in nature, but combined forming silicates the majority of them being oxides.

Silicon is produced in an electric arc furnace where quartz and carbon materials form silicon in the centre and silicon carbide close to the vessel depending on the temperature being above or below 1900ºC respectively. The quality of the Silicon determines if it can be used for electronics or any other use. Polysilicon, pure polycrystalline silicon, is the prime ingredient in semiconductors and solar cells.

At lower temperatures, 300ºC, amorphous silicon is formed by deposition of Silane. Without a long range order structure, electronic properties are improved by Hydrogen that form bonds with 10% of those silicon orbitals that do not bond with other silicon atoms.

Amorphous silicon has many applications, and the one that is of particular interest for this study is its use as a photosensitive material.

The pin structures are junctions formed by depositions of amorphous silicon doped with group III elements (p), with a layer of intrinsic amorphous silicon (i) and another layer of amorphous silicon doped with group V elements

(n). This pin structure can be deposited over another pin structure forming a tandem structure. The width of each layer can be different which results in different responses to electrical or photonic inputs.

The pi'npin device used in this study was tailored to have optimal response in the blue and red ranges of the visible spectrum.

The GIAMOS working group has provided studies of the p'inpin structure that show its light filtering properties when biased from +3 V to -10 V.

The electrical bias influences the wavelength discrimination of the filter. With electrical bias and also using an optical bias the wavelength discrimination of the filter changes.

The filtering properties were used with a combined set of wavelengths showing that a multiplex signal is obtained.

Using different voltage and optical bias, the signals were recovered.

The photocurrent varies linearly with the intensity of the input optical power.

1.5 References

[1] Lee P . Hunt, "Silicon precursors: their manufacture and properties," in *Handbook Of Semiconductor Silicon Technology*, Online 200., 1991, p. 204.

[2] "The Nobel Prize in Chemistry 1906." [Online]. Available: http://www.nobelprize.org/nobel_prizes/chemistry/laureates/1906/.

[3] S. Sömiya and Y. Inomata, Eds., *Silicon Carbide Ceramics – 1*. Dordrecht: Springer Netherlands, 1991.

[4] A. Ciftja, T. A. Engh, and M. Tangstad, "Refining and Recycling of Silicon: A Review," 2008.

[5] E. Williams, *Global Production Chains and Sustainability. The case of high-purity silicon and its applications in IT and renewable energy*. United Nations University, Institute of Advanced Studies, 2000.

[6] W. G. J. H. M. van Sark, "Methods of deposition of hydrogenated amorphous silicon for device applications," *Thin Film. Nanostructures*, vol. 30, no. C, pp. 1–215, 2002.

[7] J. C. Sturm, Y. Huang, L. Han, T. Liu, B. Hekmatshoar, K. Cherenack, E. Lausecker, and S. Wagner, "Amorphous silicon: The other silicon," *Ulis 2011 Ultim. Integr. Silicon*, pp. 1–4, 2011.

[8] C. Grimes and O. Varghese, *Light, water, hydrogen: the solar generation of hydrogen by water photoelectrolysis*. Springer, 2008.

[9] Y. Kuo, "Thin Film Transistor Technology—Past, Present, and Future," *Electrochem. Soc. Interface*, no. 22, pp. 55–61, 2013.

[10] M. Taguchi, A. Terakawa, E. Maruyama, and M. Tanaka, "Obtaining a higher voc in HIT cells," *Prog. Photovoltaics Res. Appl.*, vol. 13, no. 6, pp. 481–488, 2005.

[11] Y. Sakai, S. Sugahara, M. Matsumura, Y. Nakato, and H. Tsubomura, "Photoelectrochemical water splitting by tandem type and heterojunction amorphous silicon electrodes," *Canadian Journal of Chemistry*, vol. 66, no. 8. pp. 1853–1856, 1988.

[12] G. H. Lin, M. Kapur, R. C. Kainthla, and J. O. Bockris, "One step method to produce hydrogen by a triple stack amorphous silicon solar cell," *Appl. Phys. Lett.*, vol. 55, no. 4, p. 386, 1989.

[13] J. D. Holladay, J. Hu, D. L. King, and Y. Wang, "An overview of hydrogen production technologies," *Catal. Today*, vol. 139, no. 4, pp. 244–260, Jan. 2009.

[14] B. Cook, "Introduction to fuel cells and hydrogen technology," *Eng. Sci. Educ. J.*, vol. 11, no. 6, pp. 205–216, Dec. 2002.

[15] G. H. Lin, M. Z. He, and J. O. M. Bockris, "An amorphous silicon alloy stable under solar illumination," *J. Appl. Phys.*, vol. 73, no. 3, pp. 1449–1454, 1993.

[16] H. TRIBUTSCH, "Photovoltaic hydrogen generation," *Int. J. Hydrogen Energy*, vol. 33, no. 21, pp. 5911–5930, Nov. 2008.

[17] H. Jung, "Amorphous silicon anode for lithium-ion rechargeable batteries," *J. Power Sources*, vol. 115, no. 2, pp. 346–351, Apr. 2003.

[18] S. Bourderau, T. Brousse, and D. . Schleich, "Amorphous silicon as a possible anode material for Li-ion batteries," *J. Power Sources*, vol. 81–82, pp. 233–236, Sep. 1999.

[19] H. W. Park, J.-H. Song, H. Choi, J. S. Jin, and H.-T. Lim, "Anode performance of lithium–silicon alloy prepared by mechanical alloying for use in all-solid-state lithium secondary batteries," *Jpn. J. Appl. Phys.*, vol. 53, no. 8S3, pp. 08NK02–1–6, Aug. 2014.

[20] R. L. Weisfield, "Amorphous Silicon TFT X-ray Image Sensors," *Hand, The*, pp. 1998–2001, 1998.

[21] W. S. Wong, S. E. Ready, J. P. Lu, and R. A. Street, "Hydrogenated amorphous silicon thin-film transistor arrays fabricated by digital lithography," *Ieee Electron Device Lett.*, vol. 24, no. 9, pp. 577–579, 2003.

[22] P. J. Chupas, K. W. Chapman, and P. L. Lee, "Applications of an amorphous silicon-based area detector for high-resolution, high-sensitivity and fast time-resolved pair distribution function measurements," *J. Appl. Crystallogr.*, vol. 40, no. 3, pp. 463–470, 2007.

[23] A. Harke, "Amorphous Silicon for the Application in Integrated Optics," Technischen Universität Hamburg-Harburg, 2010.

[24] G. De Cesare, D. Caputo, A. Nascetti, C. Guiducci, and B. Riccò, "Hydrogenated amorphous silicon ultraviolet sensor for deoxyribonucleic acid analysis," *Appl. Phys. Lett.*, vol. 88, no. 8, 2006.

[25] H.-K. Tsai and S.-C. Lee, "Amorphous SiC/Si three-color detector," *Appl. Phys. Lett.*, vol. 52, no. 4, p. 275, 1988.

[26] H. O. Kang, Z. Zhiguo, S. K. Jeon, H. Jung, H. R. Kim, D. H. Kwon, J. H. Lee, S. W. Kang, and S. H. Kong, "Fabrication and performance analysis of an amorphous silicon-based thermal IR detector," in *2010 IEEE 5th International Conference on Nano/Micro Engineered and Molecular Systems, NEMS 2010*, 2010, pp. 696–699.

[27] "hypochromic effect." [Online]. Available: http://medical-dictionary.thefreedictionary.com/hypochromic+effect.

[28] Y. K. Fang, S. B. Hwang, Y. W. Chen, and L. C. Kuo, "A vertical-type a-Si:H back-to-back Schottky diode for high-speed colour image sensor," *IEEE Electron Device Lett.*, vol. 12, no. 4, pp. 172–174, Apr. 1991.

[29] K. C. Chang, Y. K. Fang, and S. C. Jwo, "The amorphous Si/SiC heterojunction color-sensitive phototransistor," *IEEE Electron Device Lett.*, vol. 8, no. 2, pp. 64–65, Feb. 1987.

[30] A. Fantoni, M. Vieira, and R. Martins, "Simulation of hydrogenated amorphous and microcrystalline silicon optoelectronic devices," *Math. Comput. Simul.*, vol. 49, no. 4–5, pp. 381–401, Sep. 1999.

[31] M. Vieira, A. Fantoni, M. Fernandes, P. Louro, and I. Rodrigues, "Stacked n-i-p-n-i-p Heterojunctions for Image Recognition," *MRS Proc.*, vol. 762, p. A18.13, 2003.

[32] M. Fernandes, Y. Vygranenko, P. Louro, and M. Vieira, "Non-pixeled amorphous silicon-based image sensors," in *Physica E: Low-Dimensional Systems and Nanostructures*, 2003, vol. 16, no. 3–4, pp. 563–567.

[33] "GIAMOS." [Online]. Available: https://www.isel.pt/investigacao/grupos/giamos. [Accessed: 25-May-2015].

[34] "CTS - Centre of Technology and Systems." [Online]. Available: http://cts.uninova.pt/. [Accessed: 25-May-2015].

[35] P. Louro, M. Vieira, Y. Vygranenko, M. Fernandes, and A. Garção, "Optical Readout in Pinpi'n and Pini'p Imagers: A Comparison," *MRS Proc.*, vol. 989, pp. 0989–A12–04, Feb. 2011.

[36] P. Louro, Y. Vygranenko, J. Martins, M. Fernandes, and M. Vieira, "Colour sensitive devices based on double p-i-n-i-p stacked photodiodes," *Thin Solid Films*, vol. 515, pp. 7526–7529, 2007.

[37] M. Vieira, M. A. Vieira, P. Louro, J. Costa, M. Fernandes, A. Fantoni, and M. Barata, "Multilayer architectures based on a-SiC:H material: tunable wavelength filters in optical processing devices.," *J. Nanosci. Nanotechnol.*, vol. 11, no. 6, pp. 5299–5304, 2011.

[38] M. A. Vieira, "Three Transducers for One Photodetector: essays for optical communications," FCT-UNL Universidade Nova de Lisboa, 2012.

[39] M. A. Vieira, M. Vieira, J. Costa, P. Louro, M. Fernandes, and A. Fantoni, "Double Pin Photodiodes with Two Optical Gate Connections for Light Triggering.," *Sensors & Transducers*, vol. 10, no. Special issue, pp. 96–120, 2011.

[40] M. Vieira, A. Fantoni, P. Louro, M. Fernandes, R. Schwarz, G. Lavareda, and C. N. Carvalho, "Self-biasing effect in colour sensitive photodiodes based on double p-i-n a-SiC:H heterojunctions," *Vacuum*, vol. 82, no. 12, pp. 1512–1516, Aug. 2008.

[41] P. Louro, M. Vieira, M. A. Vieira, S. Amaral, J. Costa, and M. Fernandes, "Optical demultiplexer device operating in the visible spectrum," *Procedia Eng.*, vol. 5, pp. 657–660, 2010.

[42] M. Vieira, P. Louro, M. Fernandes, M. A. Vieira, Q. Torre, and M. Caparica, "Three Transducers Embedded into One Single SiC Photodetector : LSP Direct Image Sensor , Optical Amplifier and Demux Device," in *Advances in Photodiodes*, vol. March Ch19, G. F. D. Betta, Ed. Intech, 2011, pp. 403–426.

[43] M. Fernandes, M. Vieira, A. M. Vieira, and P. Louro, "Effect of the Optical Bias on the a-Si:H Optical Demultiplexer Device," in *SensorDevices*, 2011, pp. 118–122.

[44] P. Louro, M. A. Vieira, S. Amaral, M. Fernandes, J. Costa, and M. Vieira, "Integrated demultiplexer and photodetector for short range transmission in the visible range," *Phys. status solidi*, vol. 8, no. 3, pp. 919–923, Mar. 2011.

[45] M. Vieira, P. Louro, M. A. Vieira, J. Costa, and M. Fernandes, "Direct color sensor, optical amplifier and demux device integrated on a single monolithic SiC photodetector," *Procedia Eng.*, vol. 5, pp. 232–235, Jan. 2010.

[46] M. Bass, J. M. Enoch, E. W. Stryland, and W. L. Wolfe, *Handbook of Optics - Vol 1.* .

[47] M. Vieira, P. Louro, M. Fernandes, M. A. Vieira, A. Fantoni, and M. Barata, "Large area double p-i-n heterostructure for signal multiplexing and demultiplexing in the visible range," *Thin Solid Films*, vol. 517, no. 23, pp. 6435–6439, 2009.

[48] P. Louro, M. Vieira, M. A. Vieira, M. Fernandes, and J. Costa, "Use of a-SiC:H Photodiodes in Optical Communications Applications," 2011.

2

2 Experimental Setup

The characterization of electronic components is necessary to ensure the expected behaviour when used in different applications. During research it is also necessary to characterize parts or the whole device not only to study but also to determine further experiments and search for other solutions. The experimental setup is composed by all equipment necessary to conduct an experiment. It is necessary to define also the procedures and their sequence in order to replicate the experiments and ensure that the results are the same. The whole description must also be clear so that it may be replicated by other research groups and providing them with similar results.

The study of the pi'npin sensor requires different experimental setups that focus on the output signals that lead to the parameters that are expected to be read, namely the output current of each input wavelength, the transmittance of each wavelength, and the output current with modulated input wavelengths.

The pi'npin device needs to be electrically polarized. Unless there is an experiment to study the influence of the electrical polarization the bias setting should be otherwise equal to -8 V. This bias value was considered as the most adequate for the pi'npin device to operate. The electrical connection of the pi'npin is shown in Figure 2-1.

The -8 V setting is maintained by very precise equipment, the Lock-in Amplifier (SR830) [1]. This is so because the Lock-in can be used for other biasing settings if needed for some specific experiments.

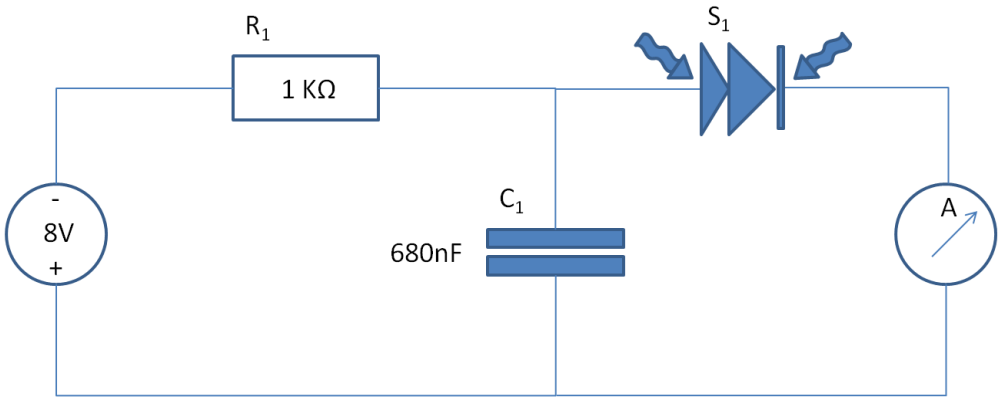

Figure 2-1 – Electrical connection of the pi'npin device.

The electrical connection to the pi'npin device is shown in Figure 2-1. The voltage power supply maintains a fixed tension of -8 V. The pi'npin has high impedance when inversely biased. The output current is measured by the ammeter shown in the figure. The C_1 capacitor is needed to ensure that the DC bias does not change when the output current changes due to the illumination of the pi'npin device by a light signal. The dynamic current change and its voltage will be accounted for by the R_1 resistor. The R_1 value is much lower than the pi'npin impedance.

The circuit has a low pass filter, where the cut-off frequency is given by $fc = 1/2\pi R_1 C_1 = 234$ Hz. The input light signals used in this work have frequencies from 3000 to 12000 Hz which are tenfold higher than the cut-off frequency [2].

This electrical connection is maintained in the following Sections: 2.2 Spectrum Analysis and 2.3 Timeline measurements.

2.1 Transmittance Analysis

The study of the sensor's transmittance is achieved by varying wavelengths on both sides of the sensor and reading the interference patterns. The setup is presented in Figure 2-2.

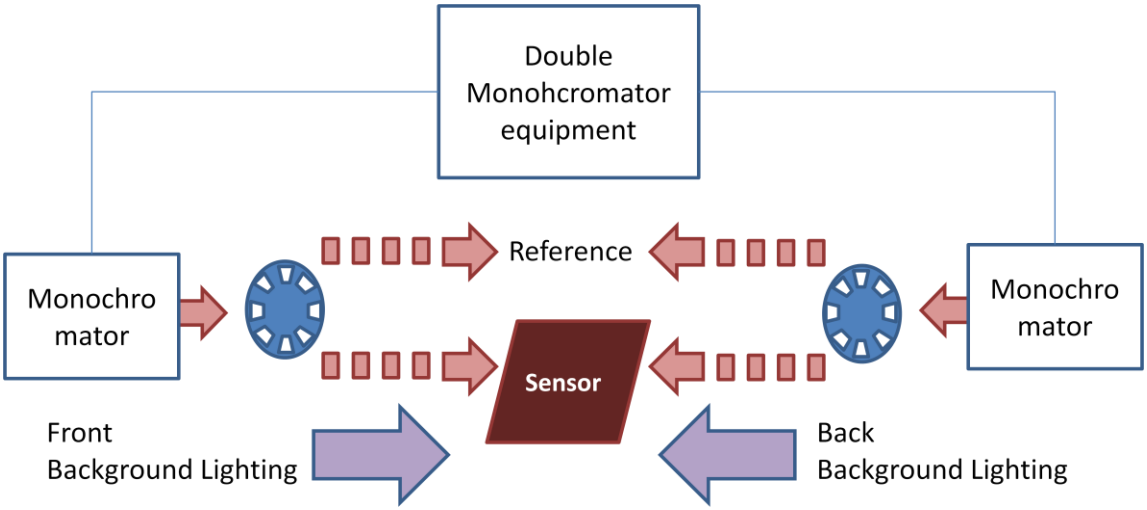

Figure 2-2 – Transmittance analysis setup.

The setup to analyse the transmittance of the sensor is presented in Figure 2-2. The double monochromator equipment is a Shimadzu UV-2501PC [3]. The interference patterns are influenced by the sensor deposited layers. By setting either back or front background lighting this setup allows the reading of variations in the transmittance of the sensor´s layers.

The front and back LED's are of the same wavelength 390 nm and they were light up with several currents supplied by two programmable current sources, equipment Keithley 2400 and Keithly 6430 [4, 5].

The wavelengths used to scan the sensor spanned from the ultra violet, visible and near infrared ranges.

The Shimadzu UV-2501PC is connected to a computer with a graphical user interface. The results are exported and stored in a file by the equipment and in a format that is read by Origin[1] [6] or other programs that import files in comma separated value format (.csv) [7].

In Figure 2-3 there is an example of the transmittance of the p'inpin and its individual components.

[1] Origin is a Data Analysis and Graphing Software tool made by OriginLab, it is the software that is used to produce the graphs and to fit deconvoluted curves.

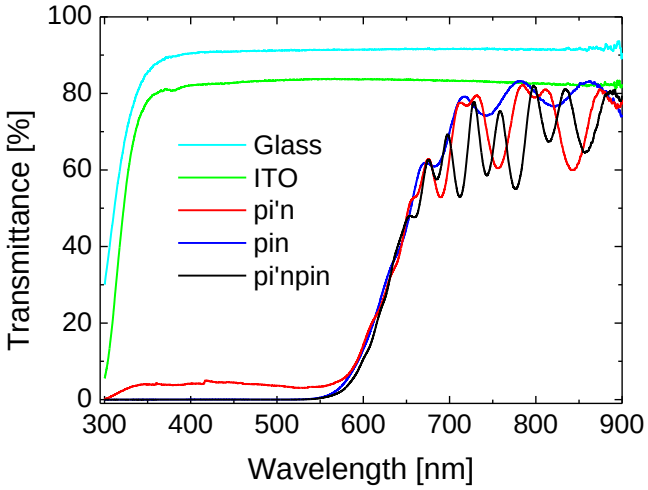

Figure 2-3 – Transmittance of the p'inpin and its components

The different transmittance readings of the components that build up the p'inpin, and shown in Figure 2-3, was possible due to the fact that the deposition of the sensor on the glass was such that there is a set of the ITO, front pin (p'in) and back pin (pin) that overlap to build the complete sensor and there are parts that do not overlap. These non overlapping parts were used for the readings. The thickness of the layers and their absorbance at each wavelength influences the number of fringes and their length allows the calculation of the optical gap.

2.2 Spectrum Analysis

The study of the output of the sensor with varying wavelength of the input produces a spectrum graph. The setup used is presented in Figure 2-4.

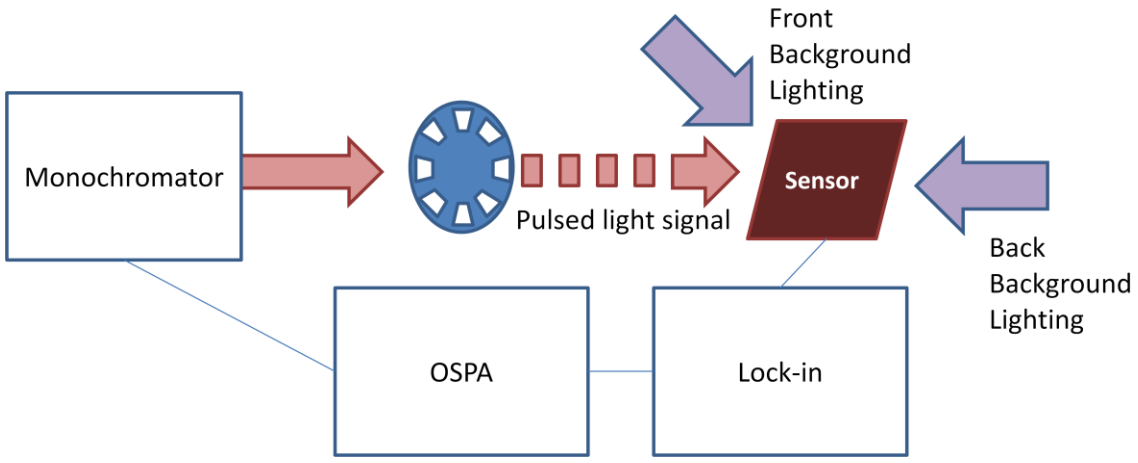

Figure 2-4 – Spectrum analysis setup.

The spectrum experimental setup is shown in Figure 2-4. The light beam that exits the monochromator (TRIAX 180) [8] is chopped by the chopper (SR540) [9] into a pulsed signal that impinges onto the front side of the sensor. The OSPA (Optoelectronic Semiconductor Parameter Analysis) program synchronizes the monochromator wavelength selection with the Lock-in Amplifier (SR830) reading of the sensor's output. For each experiment the chopper angular velocity is maintained constant.

Readings are made with the monochromator wavelength stepping 1 nm or 10 nm at every 2 seconds. The angular velocity of the chopper is such that the light beam is chopped from 500 Hz to 3500 Hz.

Depending on the experiment, Dark readings are made without any background lighting, Front readings have front background lighting and the Back readings have the background lighting at the back of the sensor. An example is shown in Figure 2-5.

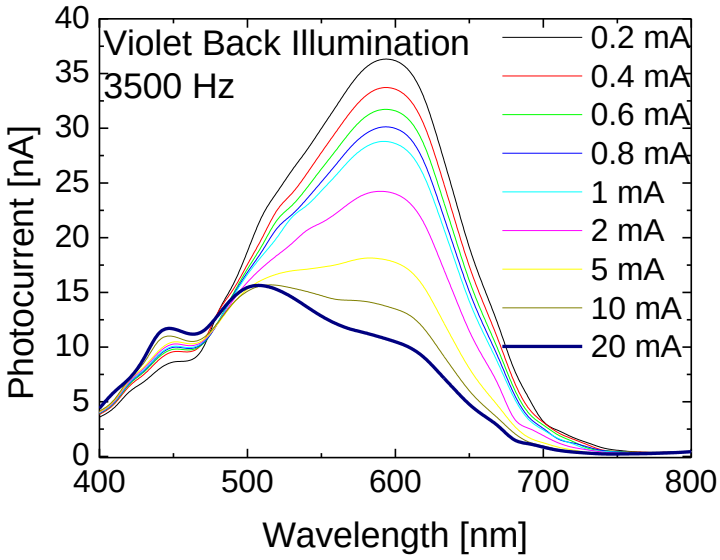

Figure 2-5 – Spectral response for violet back illumination with different intensities.

The example of Figure 2-5 shows the grouping of all readings for each individual current set to the violet back illumination LED, with a chopper frequency of 3500 Hz.

Front and Back lighting of the background is made with two independent programmable current sources, Keithley 2400 and Keithly 6430.

The OSPA software was developed by our working group [10]. This application runs in a desktop computer and communicates with the monochromator TRIAX and a Lock-in-Amplifier by an IEEE488 instrumentation bus [11]. It configures both instruments with parameters set by the user, including electric bias, wavelength range, scanning speed and slot dimension. The scanning process assures that there is synchronization between the wavelength set in the monochromator and the reading made by the Lock-in-amplifier throughout the selected wavelength. The captured data of each complete scan is stored directly into an Origin window.

2.3 Timeline measurements

The most general case of the experimental setup is to gather data from time measurement which is presented in Figure 2-6.

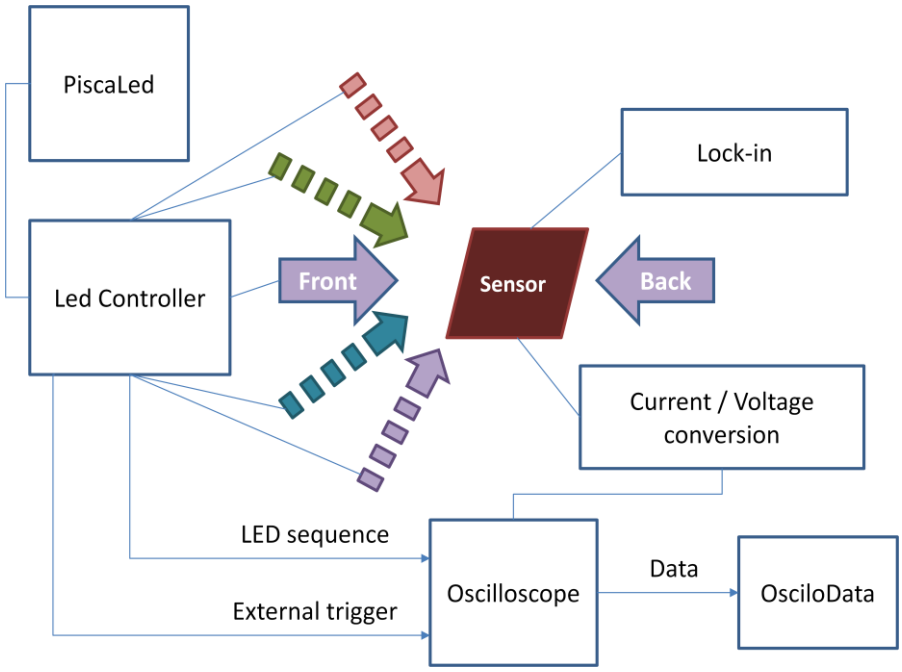

Figure 2-6 – Timeline measurements.

The PiscaLed [11, 12] software, explained in the next section, is controlled by the user that chooses the light intensity and time sequences of the LED's, and programs the Led Controller accordingly. The sensor has a constant electrical bias of -8 V (see sensor electrical circuit) generated by the Lock-In (SR830) programmable power source output.

The output of the sensor is an electrical current signal that is converted into voltage to be displayed in the oscilloscope. This conversion is made by the current to voltage converter SR570 (Low-noise Current Preamplifier) [14] which is setup without filters and with a sensitivity of 2 μA/V; except were stated otherwise, this sensitivity is adjusted whenever saturation of the SR570 occurs. Other values of sensitivity used are 1 μA/V, 5 μA/V and 10 μA/V.

The 4-channel digital storage oscilloscope (Tektronics TDS 2024B 200MHz, 2GS/s) [15] displays the converted sensor's output and the LED signals which are replicated by the LED Controller. The oscilloscope is connected through an USB link for configuration and data recording, to the same computer were the PiscaLed is running. The OpenChoice software that communicates with the oscilloscope allows the writing of the display into the clipboard memory which is then read by the OsciloData software which normalizes the signals and makes them available, by the clipboard, to the Origin software.

OpenChoice is a program supplied by Tektronics and that communicates with their oscilloscopes through USB connections.

The OsciloData software was developed by our working group, this application written in Java works with the contents of the clipboard using it as an interface between two applications. It is used to prepare data read out by the oscilloscope to be entered into an Origin worksheet

An external trigger generated by the LED Controller is used to synchronize the oscilloscope, as shown in Figure 2-6.

There are 16 light channels available on the PiscaLed and LED Controller, 4 of which available for the oscilloscope to display the selected LEDs, 2 channels are for the Back and Front background lighting and the remaining 10 channels are available to choose from different LED wavelengths.

All the LEDs and sensor are maintained inside a wooden box that inhibits outside light from reaching the sensor. The interior of the box is covered by black non reflecting material. Between the wood and the non reflecting material is an aluminium foil that converts the whole box into a Faraday cage. The box aluminium foil is connected to the optical bench and grounded.

Several configuration files can be stored and retrieved for experimental purposes by the PiscaLed.

The LED Controller composed by a microcontroller (NXP LPC 1768) [16] connected to a led driver (HexaLed) [13]. The microcontroller is powered by the USB power supply through which it communicates with the PiscaLed. An additional power supply (Velleman PS613, DC power supply 0-30V, 2.5A) [17] is used as a +5V source to the HexaLed that drives all LED currents. Two different examples are shown in Figure 2-7 and Figure 2-8.

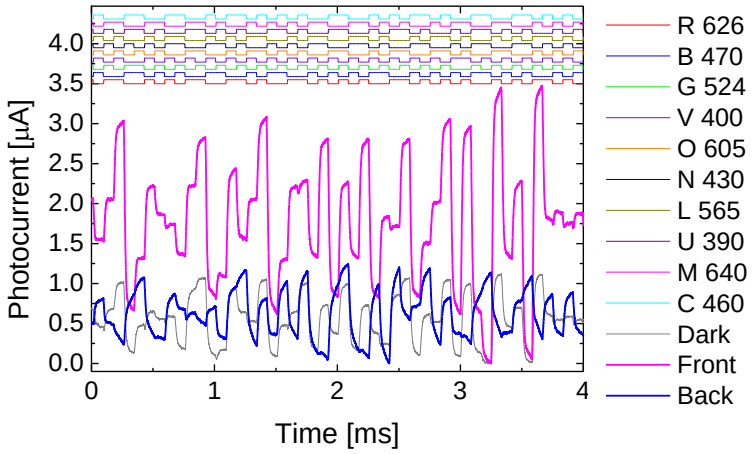

Figure 2-7 – A Ten channel (5 digital light signals) input with Dark, Front and Back responses.

Ten channels that hold five different digital light signals with random data illuminate the pi'npin device, continually, repeating the same pattern cyclically, are shown in Figure 2-7. Readings are then made for the Dark signal and Front and Back illumination signals. All readings are then grouped and stored. This is the Continuous mode which is different from the Impulse mode shown in Figure 2-8.

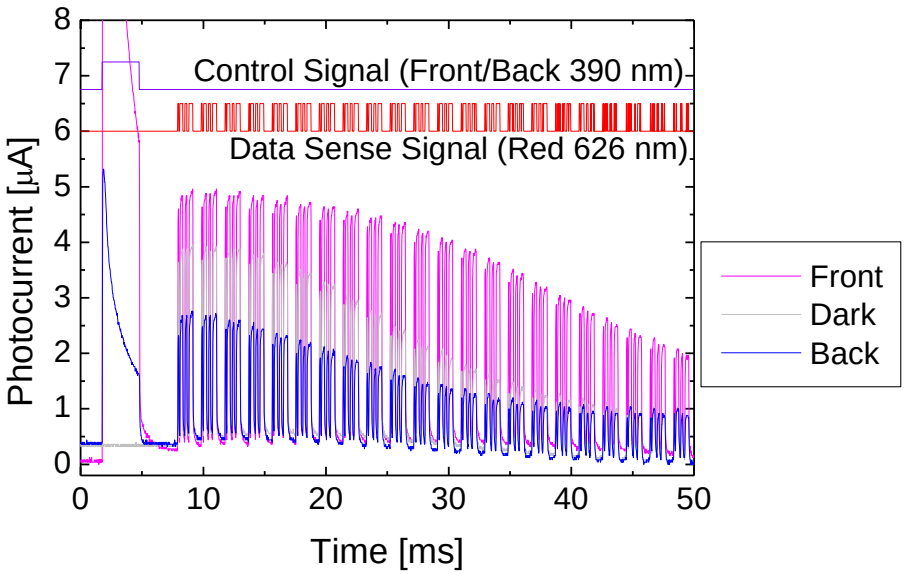

Figure 2-8 – Single Control impulse (Front/Back) followed by continuous Data Sense pattern.

In the Impulse mode, the entire sequence is run only once, as shown in Figure 2-8. The Control signal (which is either a Front or Back illumination of the background) occurs for 3 ms followed by a Dark time of 3 ms. Then a sequence of Red impulses, illuminating the front side of the device, is repeated at 0.5 ms intervals. A time lapse of 2 minutes is held before each impulse experiment to allow the same initial conditions.

This same setup is used for other specific experiments namely: static readings and FRET samples [18–21]. In case of the FRET samples, the setup has to be set into a horizontal position to allow the microscope lamella to be inserted between the light sources and the Front side of the sensor.

2.4 Signal Generator

The data signals applied to the LEDs that constitute the data channels are controlled by the same software that controls the lighting LEDs of the front and back surfaces of the device. That software is called PiscaLed. The PiscaLed communicates with a program that is on a microcontroller platform mbed NXP LPC1768 which in turn communicates with the HexaLed LED driver.

2.4.1 PiscaLed

PiscaLed is a java programe that controls 16 LEDs with selectable fixed individual currents, and with several synchronous configurable sequenced on-off patterns [12].

Each LED pattern can be selected from one of the shown in Figure 2-9.

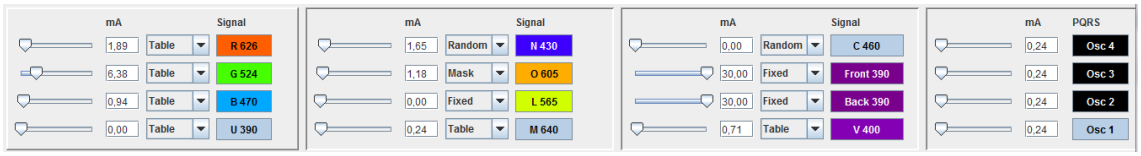

Figure 2-9 – All LEDs with their individual configurations. LEDs are ordered 0-15 from top to bottom, and left to right.

Each LED can be programmed with one of the possible selections: "*Table*", "*Random*", "*Fixed*" and "*Mask*".

The "*Table*" option uses the table settings shown down in the text. "*Random*" option uses random values {0, 1} for each bit. "*Fixed*" holds a steady state optical flux, used for optical bias. "*Mask*" is the logical AND between the table and the random values; the table values are used as a mask where the bits set as 1 will have random values {0, 1} while the bits set as 0 in the table will remain as 0.

The table used for each LED is presented in Figure 2-10.

The buttons on the left hand side are automatic settings that change all 16 channels of the PiscaLed. At any moment, clicking in a single cell of the table toggles its value {0, 1}. The buttons on the middle are used for transformation among columns; channels.

Figure 2-10 – A detail of the "*Table*" table options with automatic and manual settings.

The detail of Figure 2-10 shows some of the 32 rows that can be set for all 16 LEDs. Every time a reference to the table "*Table*" is made in the PiscaLed it refers to the settings shown in this figure.

The "*Table*" settings are used for the most part of the experiments shown in this thesis when digital signals are used as input light data channels.

Another option that is used for communications and is not limited to the 32 table patterns is the "*Communications*" option shown in Figure 2-11.

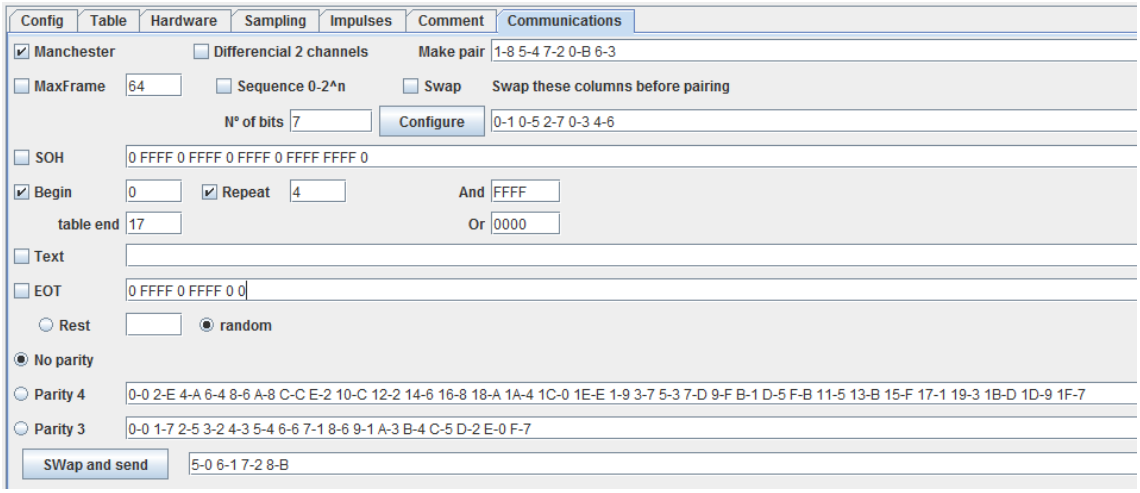

Figure 2-11 – Settings for a maximum bit data frame with Manchester coding.

PiscaLed can also transmit frames with a variable number of bits of 0 to 1024 by selecting the options of the "*Communications*" tab shown in Figure 2-11. Of these options the most important is the possibility of adding a Start of Header (SOH) that are the first bits to be sent, and used in the experiments as a preamble in which all data signals are set to 1 (FFFF) and then to 0 (0000). The setting of each LED is still subject to the option selected and shown in Figure 2-9. If a LED is not selected, as is the case of the Magenta (M 640) and Cyan (C 460) in the figure, they will not light up even if their table value or SOH has bits set to 1.

This communications option allows the inclusion of the table patterns total or partially and in the chosen number of times.

The maximum frame is of 1024 bits unless a shorter length is chosen. If necessary the padding of the frame can be random or with a fixed value to fill in missing values to complete the desired frame length.

The maximum value of 1024 was chosen according to the available memory in the microcontroller.

This frame is continually sent to the LEDs, but it can also be used for impulse measurements by configuring the "*Impulses*" tab shown in Figure 2-12.

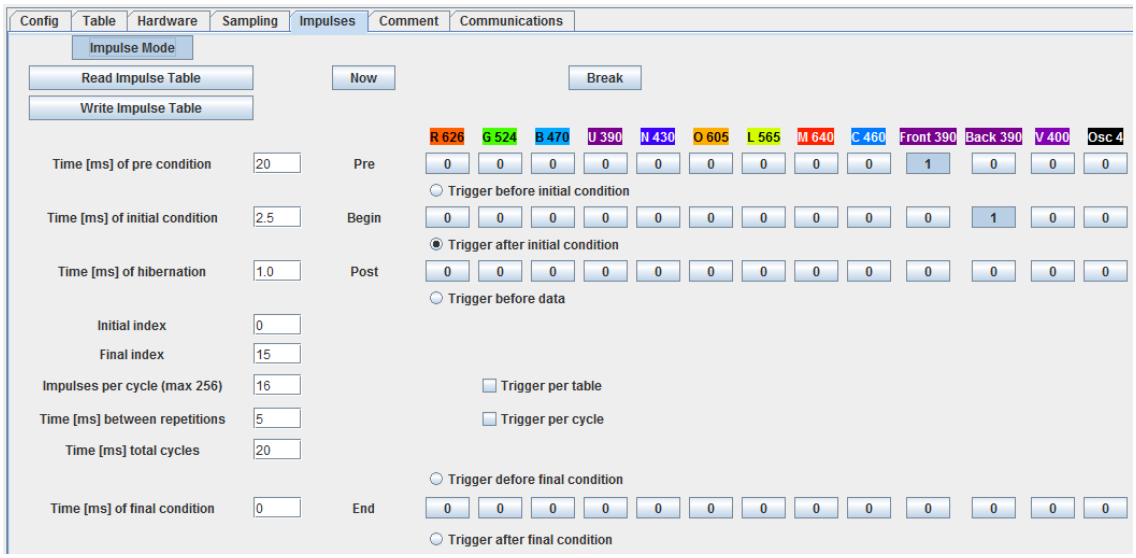

Figure 2-12 – The "Impulses" tab for quasi static impulse measurements.

When in "*Impulse Mode*" the bit timing is maintained by the defined configuration (usually 12000 bps) but the four rows shown in Figure 2-12 can set the LEDs to be *on* or *off* for a configured timing in milliseconds. A table or

frame sequence can be included between rows three and four. The total time of the whole table or frame can be defined and also the time between repetitions.

The PiscaLed system also allows acquisition of analogue samples for a single input channel. This is configured in the "*Sampling*" tab shown in Figure 2-13.

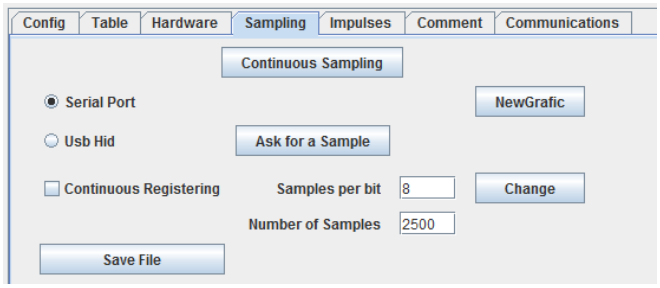

Figure 2-13 – Configuration setup of the "*Sampling*" tab.

The sampling option shown in Figure 2-13 uses an analogue input of the microcontroller and a trigger input for synchronization purposes. The data can be sent to the computer through a serial USB (Universal Serial Bus) port or a faster HID (Human Interface Device) port. All samples can be written to a file. This sampling option was not used to acquire data presented in this thesis due to several factors: the analogue input would require a dedicated electronic circuit that maintains the signal to be sampled within well defined limits; the sampling should be made at the reception, for example in the analysis program IndicaLed, and not by the emitter which is the main purpose of the PiscaLed; the sampling and emission interfere with each other due to differences in their triggers and frequency generators. Both input ports have been tested and work well, to be in future trends added to the IndicaLed [22].

The general use of PiscaLed setup divides the 16 LEDs into three groups: 10 data channels, 2 background lighting front and back, and 4 PQRS outputs that have the same data as the data channels from which they are selected. The PQRS outputs are usually connected to the 4 channel oscilloscope for the acquisition of the selected digital channels. This type of use can be seen by the labels of the LEDs in Figure 2-9. For more information please refer to the Users [12] and Technical Manual [13] of the PiscaLed.

Shown in Figure 2-14 is the block diagram of PiscaLed connections to other equipment.

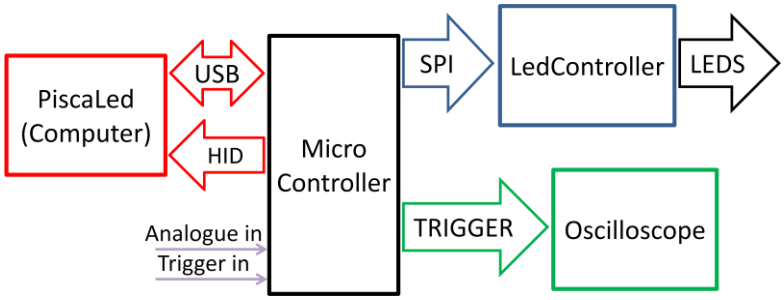

Figure 2-14 – Block diagram of the connections of PiscaLed and required equipment.

The PiscaLed runs in a computer that is connected by a USB serial connection to the microcontroller as shown in Figure 2-14. An optional HID connection is used if required by the sampling option which uses the Analogue input and a trigger input for synchronization purposes. The microcontroller connects to the LedController by a SPI (Serial Peripheral Interface) Bus. The LedController drives the current to the LEDs. The microcontroller is also connected to the Oscilloscope's external trigger through one of two possible triggers: a frame trigger and a table trigger.

2.4.2 LedController

The LedController is named HexaLed and is a printed circuit board (PCB) that drives 16 LEDs with the TLC5922 LED driver [23]. It is controlled by a program [13] on a mbed NXP LPC1768 microcontroller [16] shown in Figure 2-15.

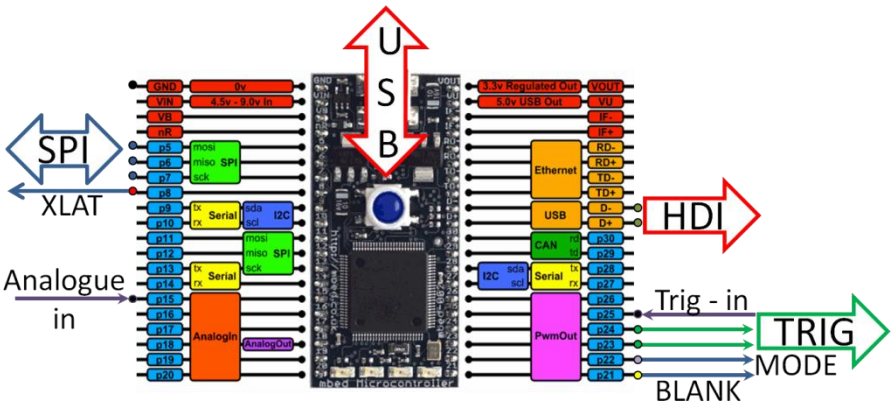

Figure 2-15 – Microcontroller pinout labelled with signals and connections to other equipment.

The connections shown in Figure 2-15 are equivalent in name and colour to the ones shown in Figure 2-14. These connections are physical cables whose signals are controlled by the ModLed [13] software loaded into the microcontroller. The LedController integrated circuit is shown in Figure 2-16.

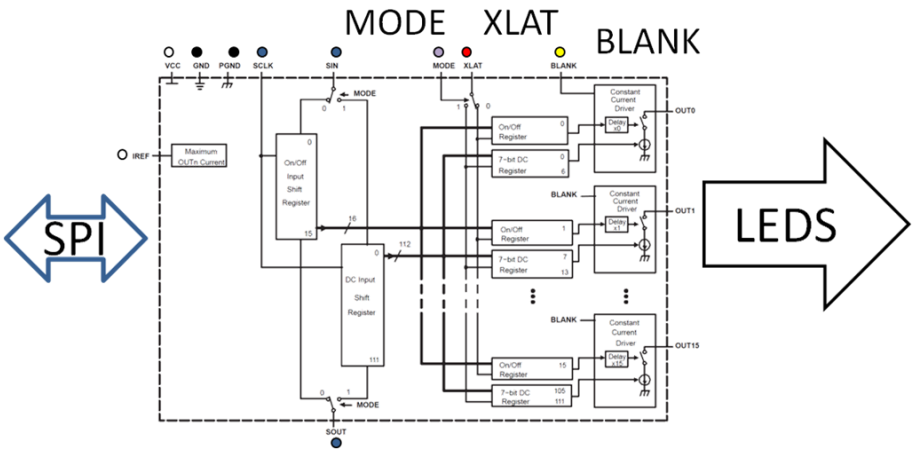

Figure 2-16 – LedController with signals and connections to the microcontroller of Figure 2-15.

Each LED current and on/off state is set through the SPI connection from the microcontroller as shown in Figure 2-15 and Figure 2-16. The MODE signal sets either the current or the state. The XLAT signal updates all outputs (LEDs) with their new values and the BLANK signal works as a power switch. The update action of the XLAT introduces a 20 ns delay wave throughout the outputs 0-15 ensured by the graduated delay circuits between outputs [23].

2.5 Signal Analysis

Several programs were developed to analyse the data and algorithms that are now in three frequently used: Descodifica, Papagaio, IndicaLed.

The Descodifica program was written in R and is used to analyse the data that is gathered in the Origin tables [24].

The Papagaio program, written in Java, is used when configuring the LEDs current so that the eye diagram is sufficiently open to allow for signal recovery [25].

The IndicaLed program, written in Java, will be discussed in Chapter 7, it is used to classify the output of the pi'npin device allowing the recovery of all input channels that were used in the PiscaLed [12, 22].

2.5.1 Descodifica

The Descodifica program is used to analyse the output values from the pi'npin device. The input values of each channel that illuminated the pi'npin is also fed into the program. The user interface is shown in Figure 2-17.

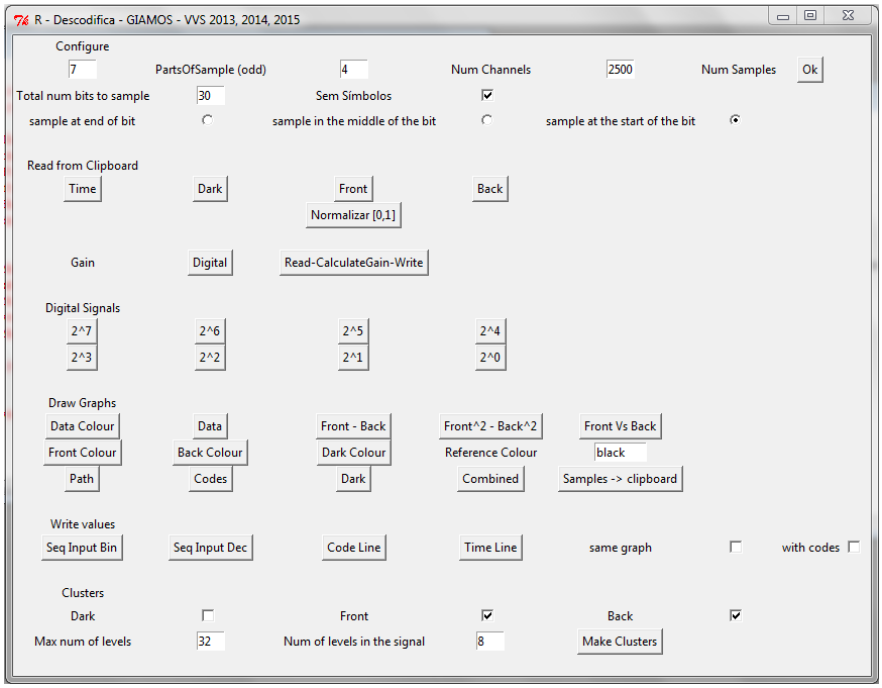

Figure 2-17 – Descodifica program.

The user interface of the Descodifica program, written in R, is shown in Figure 2-17. This program is used as a tool to understand the behaviour of the pi'npin device. Several R commands can be given on the command line console, namely those that have statistical meanings. An example of one of the graphics that can be produced with this software is shown in Figure 2-18.

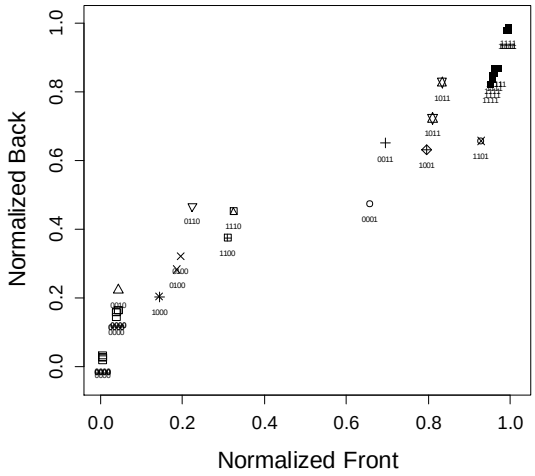

Figure 2-18 – Sample points and their respective code

Shown in Figure 2-18 is the result of a 4 channel input with 32 bits of random data. The code of each bit according to the digital input data is shown.

2.5.2 Papagaio

The Papagaio program uses the data that has previously been stored in the Origin graphs. It uses the digital data channels values input into the pi'npin, the front and back signal. The dark signal can also be included but it is not used in the current version.

As an example the pi'npin device was subjected to five digital data channels as shown in Figure 2-19.

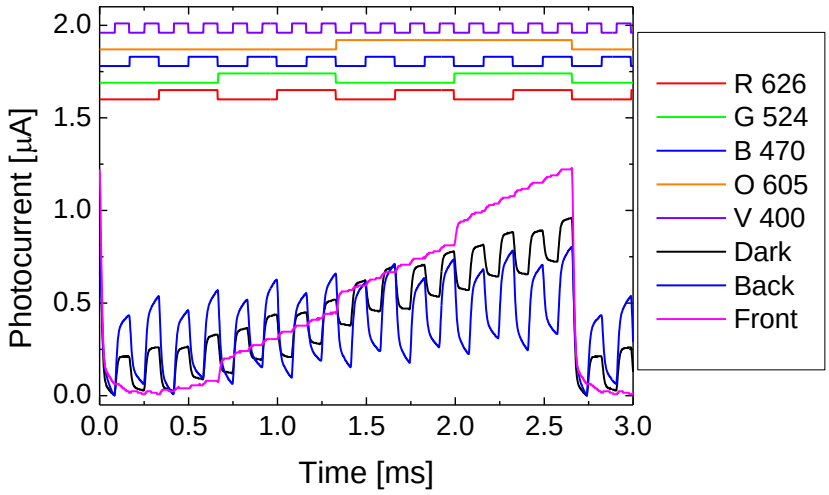

Figure 2-19 – Values from an experiment stored in Origin.

The values presented in Figure 2-19 in graphical form are inserted into the Papagaio program by using the system clipboard as an auxiliary memory, by copying column by column from the Origin tables into the respective button selection of Figure 2-20.

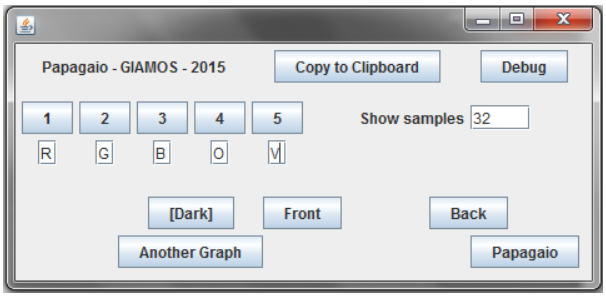

Figure 2-20 – Papagaio program's user interface

Shown in Figure 2-20 is the setting of the Papagaio program. After setting the digital channels 1 to 5 and the Front and Back output of the pi'npin, the number of visible samples can be chosen, and in this case set to 32. If for example a random frame had 512 bits and 50 was the selected number of samples, then only the first 50 samples would be marked and shown.

Using all data from Figure 2-19, and selecting the first 32 samples to be shown which includes all 2^5 combinations the result would be the one shown in Figure 2-21.

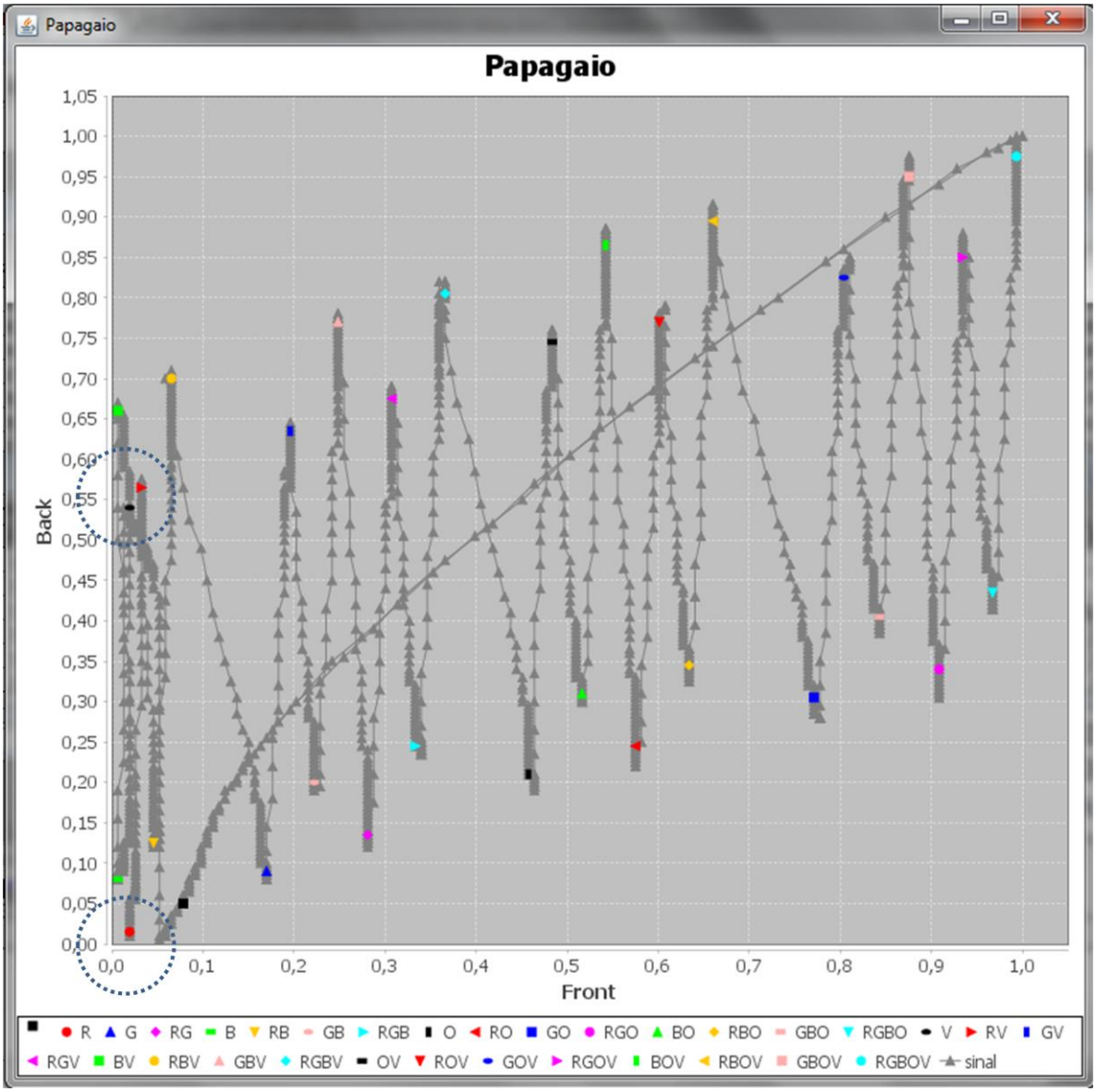

Figure 2-21 – Example of a 5 channel multiplexer eye diagram for the frame shown in Figure 2-19.

Observing Figure 2-21 the samples RV and V are very close together, and both away from the R sample, see marked areas. A better response could be found if the R LED current value is changed (increased), or instead changing the V LED current value (decrease). By changing one value, the whole response changes, this due to the cross gains among different wavelengths.

The Papagaio program has a debug window that can be used to better understand the input signals and for debugging purposes, this is shown in Figure 2-22.

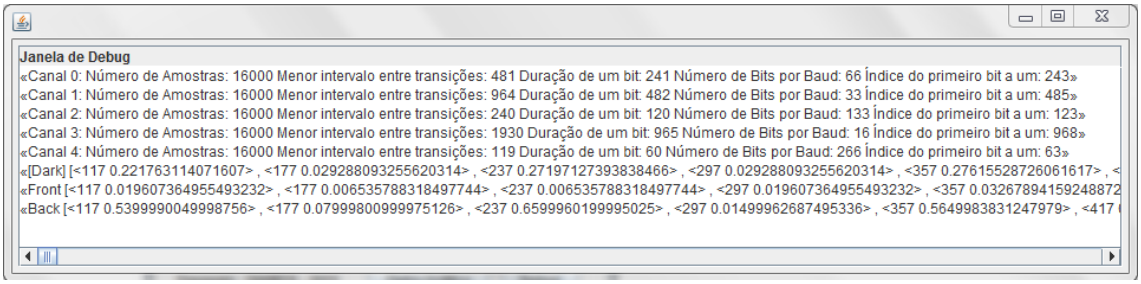

Figure 2-22 – Debug output window of the Papagaio program.

Although errors can be easily found with the debug output of Figure 2-22, the output result of the sampling can be copied into the clipboard by clicking in "*Copy to Clipboard*" and the tabled data can be stored into the Origin program. The samples include among other data, the front and back value, and a colour code that indicates the sample classified against the digital channels input data. The result is shown as an Origin graph in Figure 2-23.

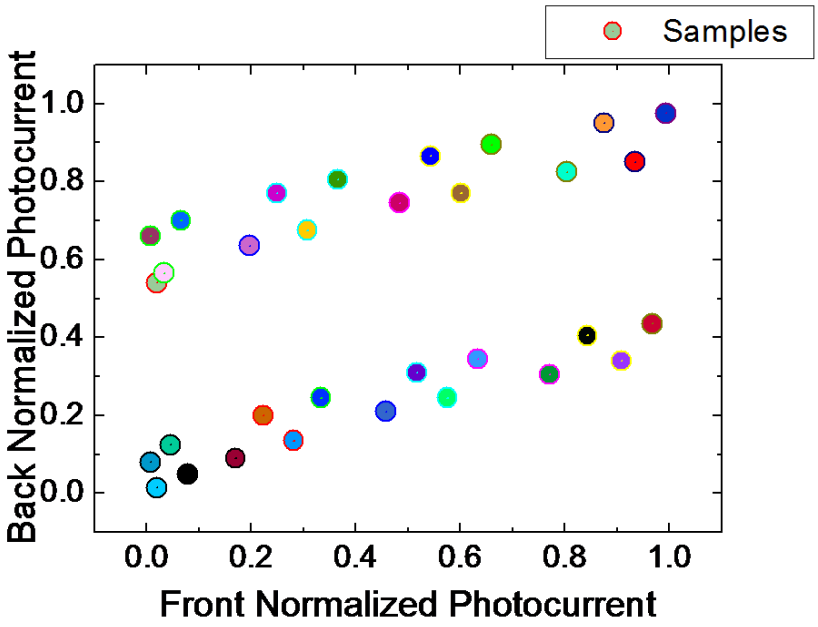

Figure 2-23 – Sampled data visualized in the Origin program.

The sampled data shown in Figure 2-23 is the same as that shown in Figure 2-21. The colours were chosen by the Papagaio program. The two RV and V sample positions can be seen almost overlapping.

The Papagaio program is used mainly for the LED current configuration, helping especially when the number of channels is higher than four.

2.6 Summary

The most common setup is the one explained in section 2.3 - Timeline measurements. The setup in use by the current experiment is always checked up before prior use, even after any interruption during which the setup might have been interfered with. It has been noted that electromagnetic noise has a slight increase during the afternoons, mainly due to the surrounding laboratories, so that experiments are usually scheduled for the mornings. Figure 2-24 shows the Timeline measurements' setup.

Figure 2-24 – The Timeline measurements setup showing some of the equipment used.

In Figure 2-24 the PiscaLed software can be seen on the computers display at the right hand side. At the centre of the figure are the Lock-in and low-noise current preamplifier. The Tektronics oscilloscope can be seen at the left hand side. The wooden box is the support of the Faraday cage built with aluminium foil and has the inside covered with black cardboard to reduce reflections. Inside the box are the pi'npin sensor and all active LEDs that can be selected for each experiment. Close to the wooden box and behind it are the power supply and the microcontroller with the led driver. The aluminium foil is connected to ground as is the optical table. The leads that connect to the LEDs pass under the wooden box that has no bottom side. The box can be opened by its' lid as it can

be seen by the hinges on the wooden box. Coaxial cables connect the pi'npin sensor to the equipment.

Other equipment has not been referenced because of its' seldom use, like the Thorlabs' compact spectrometer CCS200/M with a reading range from 200 to 1000 nm [26]. All LED's have been measured to ensure that they are single wavelength.

During the time this work was done, the Tektronics TDS 2024B four channel oscilloscope was changed by the Keithley InfiniiVision MSO-X 3034A 350MHz 4 GSa/s oscilloscope [27]. This new oscilloscope could not communicate with the OpenChoice software which in turn also invalidated the OsciloData software which made the data bridge between the oscilloscope and the Origin graph program. The OsciloData had to be updated and is now communicating directly to the oscilloscope using GPIB commands over the USB connection. This new OsciloData plus OpenChoice functionality software is now called the ClipBoardVisa [28].

Like the ClipBoardVisa, other software like the PiscaLed is also periodically changed due to experiment requirements which result from the incremental study of the pi'npin device and its behaviour.

A hardware setup that needs some attention is the pi'npin structure which is shown in Figure 2-25.

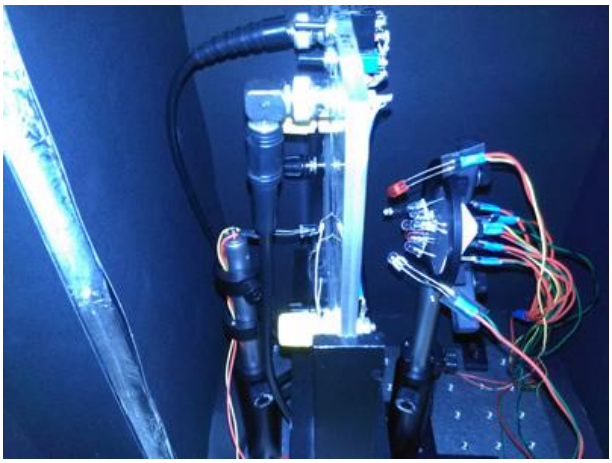

Figure 2-25 – The pi'npin sensor support and illuminating LEDs.

The pi'npin structure and LEDs can be seen inside the above mentioned wooden box in Figure 2-25. The picture shows the aluminium around the lid's

hinges and the black cardboard that is glued over the aluminium. The missing bottom side of the box allows the optical table to be seen. The pi'npin is perpendicular to the plane of the page with the back surface facing the left hand side where the ultra violet back LED can be seen, positioned as close to the sensor as possible. The right hand side of the image shows all signal LEDs. There are 10 signal LEDs that can be used simultaneously and one ultra violet led which is used for the front illumination. This front led cannot be seen because it is overlapped by the other LEDs that are showing. Both back and front ultra-violet LEDs are set perpendicular to the pi'npin and in its' dead centre. As can be observed by the image this LED structure is not very stable. As a future trend for continuing research with this kind of setup, is the project and implementation of a 3D printed structure that can hold all front LED´s secure in place and contained in the same solid angle that covers the whole of the surface's front area. The same structure could be used at the back of the pi'npin sensor, with the back LED occupying the position that the front LED has on the other structure. This would allow for different experiments in which light signals are also impinging at the back surface of the device. As an advice, these 3D structures should be easy to replace allowing different LED combinations easy to swap. The electrical connection of the LEDs to the LED driver can also be improved on a newer design update.

2.7 References

[1] Stanford Research Systems, "Lock-in Amplifier (SR830)." [Online]. Available: https://www.ece.cmu.edu/~mems/resources/HH1212/SR830m.pdf. [Accessed: 22-May-2015].

[2] Millman, *Microelctronics*. Mcgraw Hill.

[3] S. Corporation, "Shimadzu UV-2501PC." [Online]. Available: http://www.bioeng.nus.edu.sg/people/PI/trau/Lab_manuals/UV-VIS Spectrophotometer/UV-2401-2501PC_IM_UsersSystemGuide_RevCocr.pdf. [Accessed: 22-May-2015].

[4] Keithley, "Keithley 2400." [Online]. Available: http://research.physics.illinois.edu/bezryadin/labprotocol/Keithley2400Manual.pdf. [Accessed: 22-May-2015].

[5] Keithly, "Keithly 6430." [Online]. Available: https://mm.ece.ubc.ca/mediawiki/images/0/07/K6430Manual.pdf. [Accessed: 22-May-2015].

[6] OriginLab, "Origin." [Online]. Available: http://www.originlab.com/. [Accessed: 22-May-2015].

[7] "RFC4180 - Common Format and MIME Type for Comma-Separated Values (CSV) Files," *Network Working Group*. [Online]. Available: https://tools.ietf.org/html/rfc4180. [Accessed: 22-May-2015].

[8] Horiba, "TRIAX 180." [Online]. Available: http://sites.fas.harvard.edu/~phys191r/Bench_Notes/A8/Spectrometer.pdf. [Accessed: 22-May-2015].

[9] Stanford Research Systems, "SR540 - OPTICAL CHOPPER." [Online]. Available: http://www.thinksrs.com/downloads/PDFs/Manuals/SR540m.pdf. [Accessed: 22-May-2015].

[10] Y. Vygranenko and M. Fernandes, "OSPA," *GIAMOS - ISEL - Inst. Super. Eng. Lisboa*, p. 6, 2012.

[11] "GPIB - General Purpose Interface Bus." [Online]. Available: http://www.hit.bme.hu/~papay/edu/GPIB/tutor.htm. [Accessed: 22-May-2015].

[12] V. Silva, "PiscaLed - User's Manual," *GIAMOS - ISEL - Inst. Super. Eng. Lisboa*, 2013.

[13] V. Silva, "PiscaLed - Technical Manual," *GIAMOS - ISEL - Inst. Super. Eng. Lisboa*, 2013.

[14] Stanford Research Systems, "SR570." [Online]. Available: http://www.thinksrs.com/downloads/PDFs/Manuals/SR570m.pdf. [Accessed: 22-May-2015].

[15] Tektronics, "Tektronics TDS 2024B Osciloscope." [Online]. Available: http://www.physics.rutgers.edu/ugrad/389/scope-TDS 2000 Manual.pdf. [Accessed: 22-May-2015].

[16] mbed, "mbed LPC1768." [Online]. Available: https://developer.mbed.org/platforms/mbed-LPC1768/. [Accessed: 22-May-2015].

[17] Velleman, "Velleman PS613." [Online]. Available: http://www.designnotes.com/downloads/PS603U_PS613U_Manual.pdf. [Accessed: 22-May-2015].

[18] P. Louro, M. Vieira, M. a. Vieira, V. Silva, and J. Costa, "Characterization of a monolithic device for detection of FRET signals," *MRS Proc.*, vol. 1426, pp. mrss12–1426–a20–02, Jul. 2012.

[19] P. Louro, V. Silva, M. A. Vieira, A. Karmali, and M. Vieira, "Use of a-SiC:H Semiconductor-Based Transducer for Glucose Sensing through FRET Analysis," in *Springer Berlin Heidelberg*, 2013, pp. 631 – 638.

[20] P. Louro, M. Vieira, J. Costa, V. Silva, J. Patriarca, and A. Karmali, "Detection of FRET signals with a wavelength sensitive device based on a-SiC:H," *Appl. Surf. Sci.*, vol. 275, pp. 49–53, Jun. 2013.

[21] P. Louro, V. Silva, M. a. Vieira, and M. Vieira, "Detection of Change in Fluorescence Between Reactive Cyan and the Yellow Fluorophores Using a-SiC:H Multilayer Transducers," *Plasmonics*, vol. 8, no. 1, pp. 139–142, Sep. 2013.

[22] V. Silva, "IndicaLed," *GIAMOS - ISEL - Inst. Super. Eng. Lisboa*, p. 29, 2015.

[23] Texas Instruments, "TLC5922 - Led Driver."

[24] V. Silva, "Descodifica," *GIAMOS - ISEL - Inst. Super. Eng. Lisboa*, p. 5, 2013.

[25] V. Silva, "Papagaio," *GIAMOS - ISEL - Inst. Super. Eng. Lisboa*, p. 6, 2015.

[26] Thorlabs, “CCS200 - Spectrometer.” [Online]. Available: https://www.thorlabs.com/thorcat/18100/CCS200-Manual.pdf. [Accessed: 22-May-2015].

[27] Agilent, “Keithley InfiniiVision MSO-X 3034A oscilloscope.” [Online]. Available: http://web.mit.edu/6.115/www/document/agilent_mso-x_manual.pdf. [Accessed: 22-May-2015].

[28] V. Silva, “ClipBoardVisa,” *GIAMOS - ISEL - Inst. Super. Eng. Lisboa*, p. 12, 2015.

3

3 Sensor Operation

The sensor is a two stacked pin structures (p(a-SiC:H)- i'(a-SiC:H)-n(a-SiC:H)-p(a-SiC:H)-i(a-Si:H)-n(a-Si:H)) sandwiched between two transparent contacts one at each end. The thicknesses and optical gap of the i'- (200 nm; 2.1 eV) and i- (1000 nm; 1.8 eV) layers are optimized for light absorption in the blue and red ranges [1]. Based in silicon carbon technology [2] this structure can be seen in Figure 3-1, where the wavelength arrows indicate the absorption depths during operation and λ_V(400 nm), λ_B(470 nm), λ_G(524 nm), λ_R(626 nm) the digital light signals within the visible spectrum.

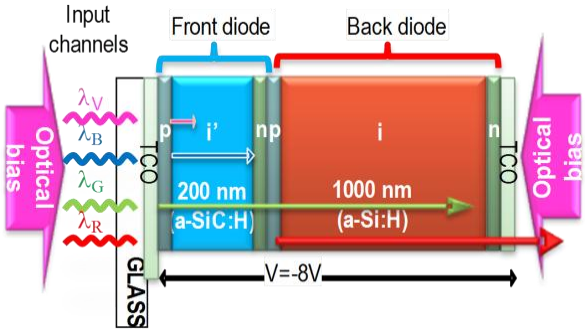

Figure 3-1 - Device structure and operation.

The experimental setup use LEDs as light sources in two different ways: as digital signals and as background lighting. The digital signals are impinged on the front side of the sensor. The background lighting is either at the back or at the front side. The intensity of the signal sources is very low compared to the background intensity. The spectra of the LEDS are shown in Figure 3-2.

Different wavelength signal sources are used: violet (400 nm), blue (470 nm), green (524 nm) and red (626 nm).

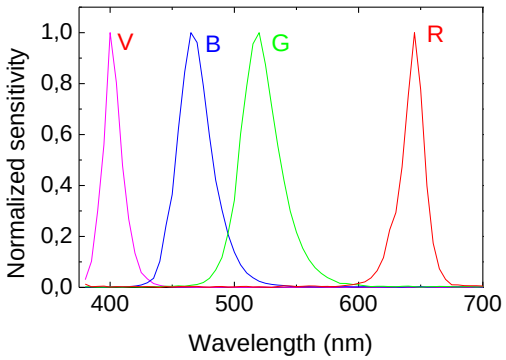

Figure 3-2 - Spectra of the input channels with commercial LEDs.

For background lighting the same type of LEDs are used and lighting is applied in a continuous and steady flux. When the background side changes the digital signals are sampled after transient influence has diminished.

3.1 Background Transmittance effect

The light tuneable filter is realized by using a double pi'n/pin a-SiC:H photodetector presented in Figure 3-1. Optoelectronic characterization was performed through spectral response and transmittance measurements without and with steady state applied optical bias. The optical bias (φ; background) was superimposed using near-ultraviolet LEDs (350 nm-400 nm). Currents between 1 mA and 30 mA were used to drive the LEDs in order to change the light flux background.

Monochromatic (infrared, red, green, blue and violet; $\lambda_{IR,R,G,B,V}$;) pulsed communication channels (input channels) are combined together, each one with a specific bit sequence and absorbed accordingly to their wavelengths (see coloured arrow magnitudes in Figure 3-1). The combined optical signal (multiplexed signal; MUX) is analyzed by reading out the generated photocurrent under negative applied voltage (-8 V), without and with near ultraviolet background ($350 < \lambda < 400$ nm) and different intensities, applied either from front (λ_F) or back (λ_B) sides. The device operates within the visible range using as input colour channels the square wave modulated low power light supplied by near-infrared/red (NIR/ R: 880-626 nm), green (G: 524 nm),

blue (B: 470 nm) and violet (V: 400 nm) LEDs. In Figure 3-3a) the transmittances from the front and back diodes are plotted as well as the transmittance of the complete device without any background light.

In Figure 3-3b) the transmittance is displayed under different 390 nm background intensities.

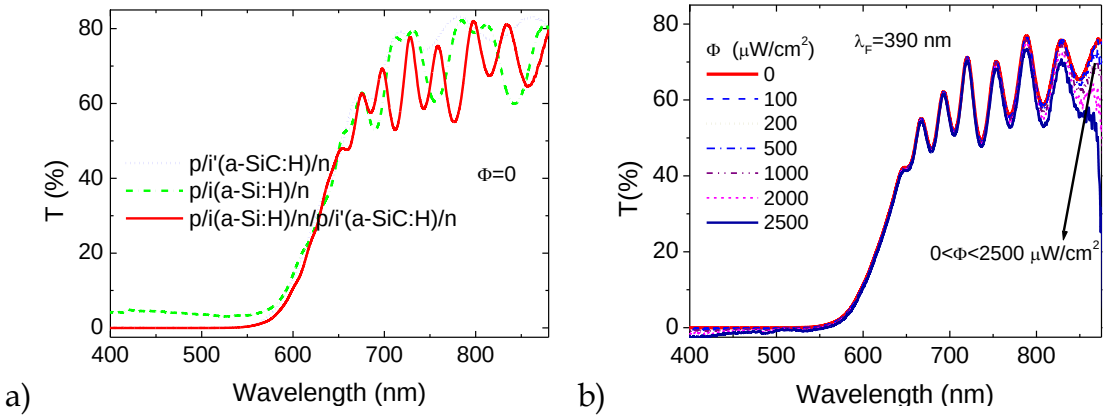

Figure 3-3 - Transmittances from: a) front, back and whole device; b) the pi'npin structure under front irradiation with 390 nm irradiation and different intensities.

The transmittance presented in Figure 3-3 was measured with a double monochromator which allows for the interference patterns of both light sources impinging on the pi'npin to be registered. The transmittance experimental setup is described in detail in Chapter 2.

Results confirm the influence of the thickness of each front and back diode on the transmittance of the whole device (Figure 3-3a). It is interesting to notice that under front light irradiation the transmittance decreases in the infrared range (Figure 3-3b) as the background intensity increases leading to an infrared absorption window[3].

3.2 Noise Margin

For its operation the pi'npin sensor is inverse electrically biased and illuminated by light. The output is an electrical signal and as such it is subject to noise. The pi'npin output is connected to a current to voltage converter and the output of that converter is connected to an oscilloscope for visualization and sampling and shown in Figure 3-4.

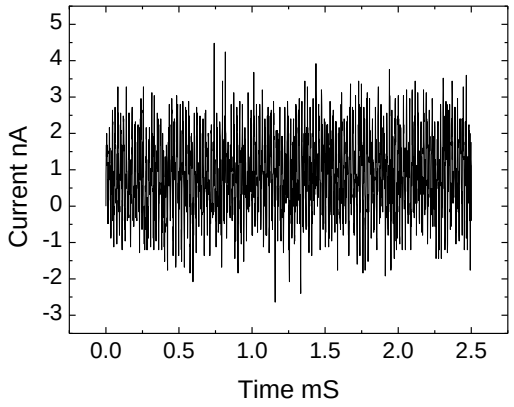

Figure 3-4 - Dark current

Figure 3-4 shows the electrical output of the sensor when it is not subjected to any illumination. This is defined as the dark current. The value is very low and identifies the noise margin of 8 nA, so any electrical output signal will have an error of ± 4 nA.

The sensor biased at -8.00 V and with no light shining in either of its surfaces presents a noise current which is depicted in Figure 3-4 with a mean value of 0.89 nA. The values were registered with a low-noise current preamplifier (SRS-SR570). Static power consumption is 7.15 nW. The low values are due to the reverse polarization of the two pi'npin junctions.

3.3 Self Bias Amplification under Uniform Irradiation

The spectral photocurrent of Figure 3-5 was obtained by the Spectrum Analysis Setup explained in detail in Chapter 2. The background illumination is set on the front surface of the device.

The sensor is electrically biased with -8 V as this voltage is the one that induces the highest spectral photocurrents within the experimented values.

3.3.1 Spectral Sensitivity

The spectral sensitivity was analyzed by applying different wavelengths optical bias from the back and front sides of the device (see Figure 3-1). Under front irradiation, in Figure 3-5 it is displayed the spectral photocurrent for different frequencies without (a) and under violet (b), blue (c), green (d) and red

(e) light bias control at -8 V applied voltage and different frequencies (250 Hz-3500 Hz) [4].

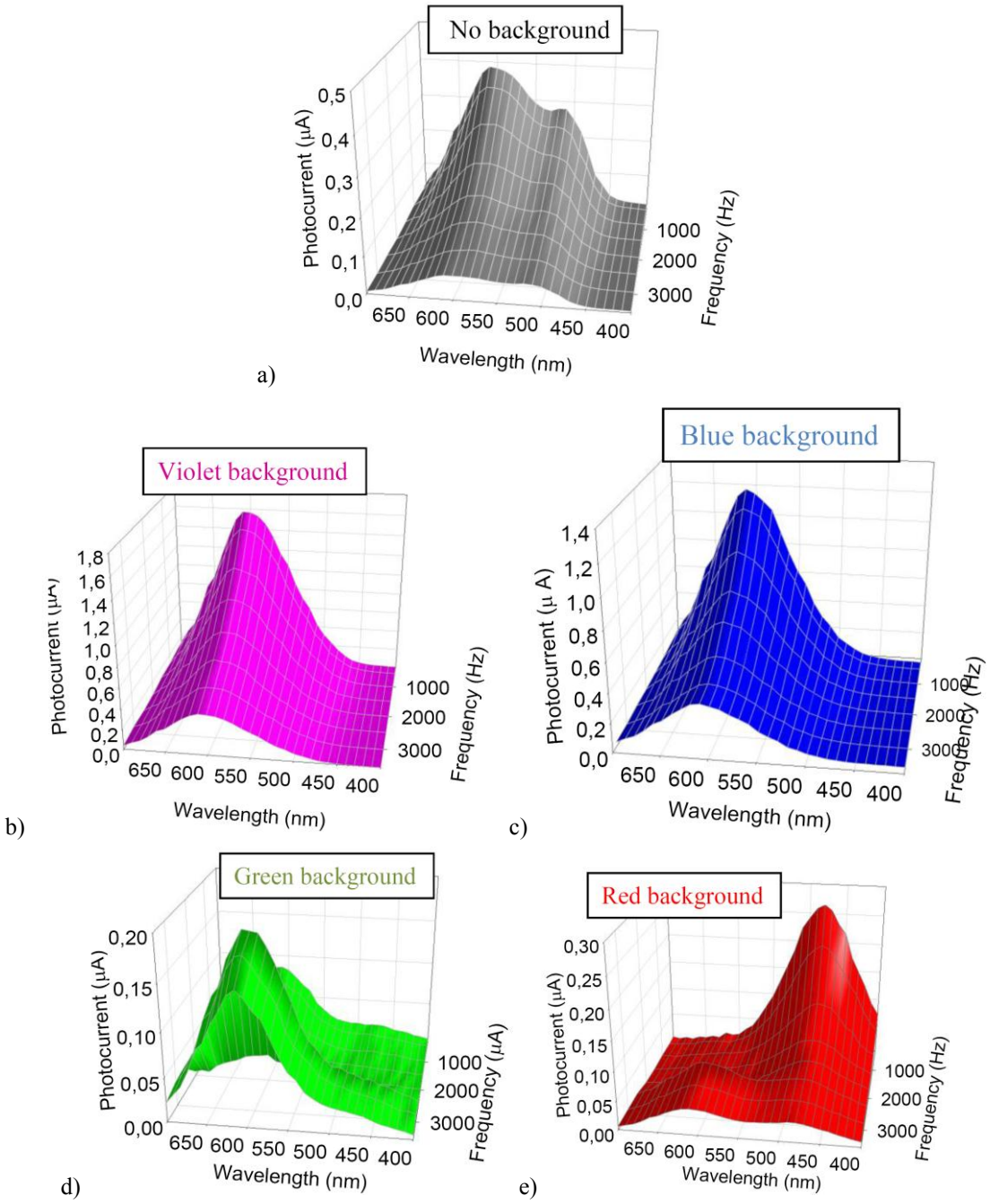

Figure 3-5 - Spectral photocurrent without (a) and under violet (b), blue (c), green (d) and red (e) bias control applied from the front side.

Results show that the spectral response depends strongly on the bias control wavelength and frequency. As the bias control wavelength increases the spectral sensitivity shifts to the low wavelength spectral regions and decreases with the frequency, suggesting a capacitive effect across the device [4].

3.3.2 Front and back optical bias control

Displayed in Figure 3-6 there is the spectral photocurrent at 3500 Hz, under red, green, blue and violet background irradiations (colour symbols) and without it (black symbols) applied from the front (a) and back (b) diodes. For comparison the spectral photocurrent (right axis) for the front, pi'n and the back, pin, photodiodes (dash lines) are superimposed.

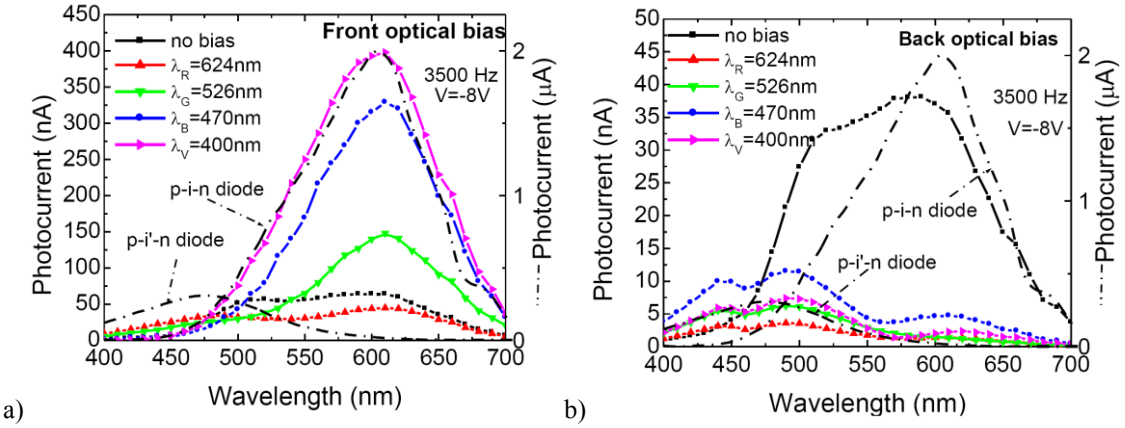

Figure 3-6 - Spectral photocurrent under red, green, blue and violet background irradiations (colour symbols) and without it (black symbols) applied from the front (a) and back (b) diodes.

Results show that the spectral sensitivity, under steady state irradiation, depends on its wavelength and on the impinging side.

Under front irradiation, the back diode photo-response is tuned and the sensitivity strongly increases for wavelengths higher than 500 nm when compared with its value without optical bias. Here, as the background wavelength decreases the spectral response increases [4].

Under back irradiation the front diode photo-response is selected. The sensitivity strongly increases in the short wavelengths range and collapse in the long wavelength region.

3.3.3 Light filtering effects

In Figure 3-7, at 3500 Hz, it is displayed the ratio between the photocurrent under different optical bias and without it (gain) under front (symbols) and back (lines) irradiations: red (α^R), green (α^G), blue (α^B) and violet (α^V).

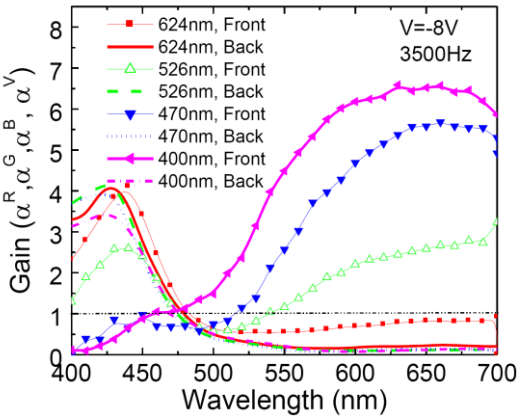

Figure 3-7 - Gain under front (symbols) and back (lines) irradiations: red (α^R), green(α^G), blue (α^B), violet (α^V).

Results confirm that under controlled wavelength backgrounds it is possible to fine-tune the spectral sensitivity of the device. Its sensitivity is strongly enhanced ($\alpha > 1$) in a specific wavelength range and quenched ($\alpha < 1$) in the others, tuning or suppressing a specific band.

Under back irradiation (lines) the gain does not depend on the wavelength of the background. The spectral sensitivity in the low wavelength range is enhanced and the device acts, always, as a short-pass filter.

Under front irradiation (symbols) the filter properties of the device depend on the background wavelength. Under red irradiation (Figure 3-5e) the gain is high in the short wavelengths range acting the device as a short-pass filter. Under violet (Figure 3-5b) and blue (Figure 3-5c) irradiations the transfer function presents an enhanced gain in the long wavelength range acting as a long-pass filter. Under front green background (Figure 3-5d) the device, for frequencies higher than 2000 Hz, is a band-rejection active filter that works to screen out wavelengths that are within the medium range (475-550 nm), giving easy passage at all wavelengths below and above.

The sensor is a wavelength current-controlled device [5] that makes use of changes in the wavelength and impinging side of the optical bias to control the power delivered to the load. Self optical bias amplification or quenching under uniform irradiation is achieved. By using background lights with complementary light penetration depths across the pi'npin device and changing the irradiation side, it is possible to control the spectral response and to filter a specific wavelength band.

3.3.4 Transfer function characteristics

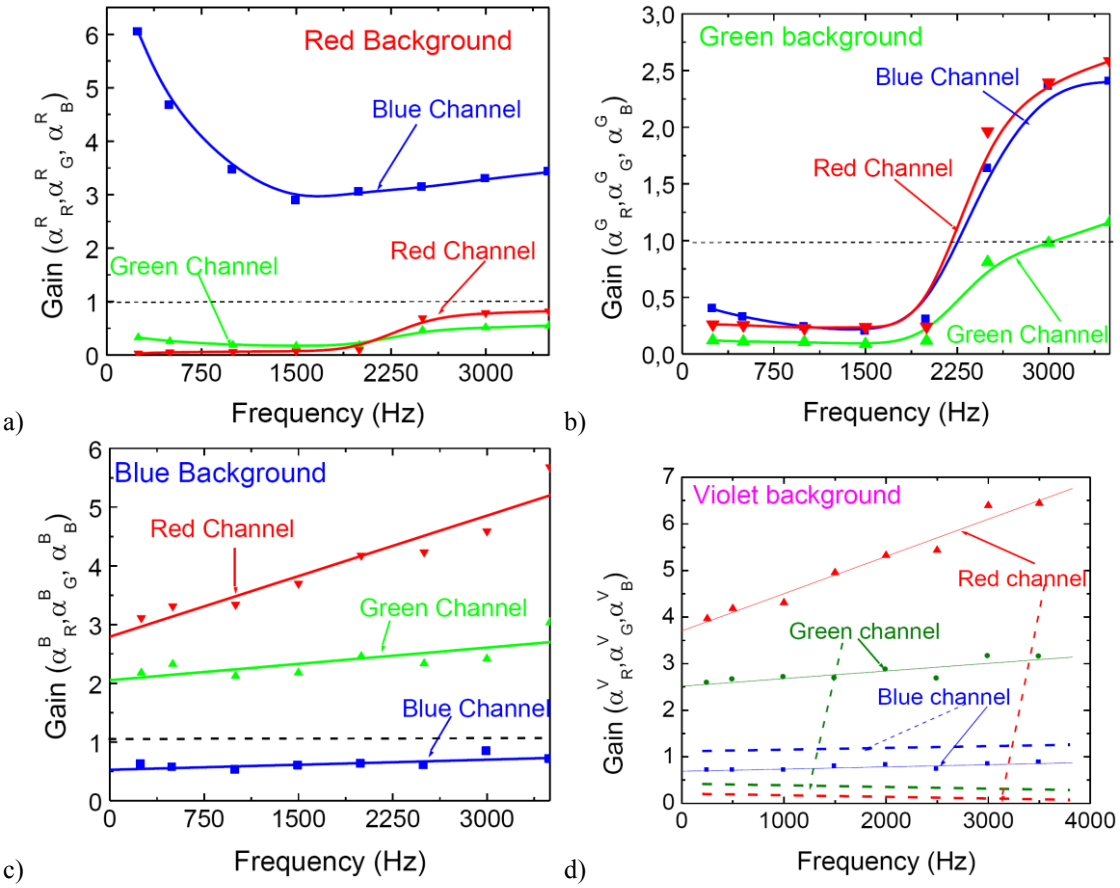

Figure 3-8 - Spectral gain as a function of the frequency at 624 nm (red channel), at 526 nm (green channel) and at 470 nm (blue channel) under red (α^R), green (α^G) , blue (α^B) and violet (α^V) backgrounds from the front side (symbols) and back (lines) sides, as a function of the frequency.

Figure 3-8 shows the ratio between the spectral response with and without light bias control (gain) as a function of the frequency under red (α^R), green (α^G), blue (α^B) and violet (α^V) backgrounds at 624 nm (α^R, red channel), at 526 nm (α^G, green channel) and at 470 nm (α^B, blue channel). In the figure the symbols are ascribed to the front irradiation and the lines to the back one.

As expected from Figure 3-5 under red and green light control two frequency regimes can be considered. One, for frequencies lower than 2000 Hz, were either under red and green backgrounds the green and the red channel gains are very low (<< 1) and the blue gain is strongly enhanced (>> 1) under red background or reduced (< 1) under green irradiations. The other regime, for frequencies higher than 2000 Hz, the gain increases with the frequency, gradually under red and quickly under green steady state illumination.

Under blue and violet irradiation, the gain increases slowly with the frequency being higher than one for the red and green channels and lower for the blue one, resulting in an amplification of the green and red spectral channels. Back violet irradiation slightly amplifies the blue channel and quenches all the others.

Consequently, under red irradiation the transfer function has higher gain at short wavelengths (blue channel), than at longer wavelengths acting as a short-pass filter whatever the frequency. Under green background, the manipulation of amplitude is achieved by changing the frequency of the modulated lights. At high frequencies the device is a band-stop active filter that screens out the green channel, giving easy passage to the blue and red channels. In the low frequency regime all the amplitudes are quenched. Under blue and violet steady state optical bias the device behaves as a long-pass active filter that transmits and enhances the red and green channels while blocking the blue one. Back irradiation only amplifies the blue channel, quenching the others, whatever the background wavelength [4].

3.3.5 Sensor Sensitivity

Photocurrent results are presented in Figure 3-9.

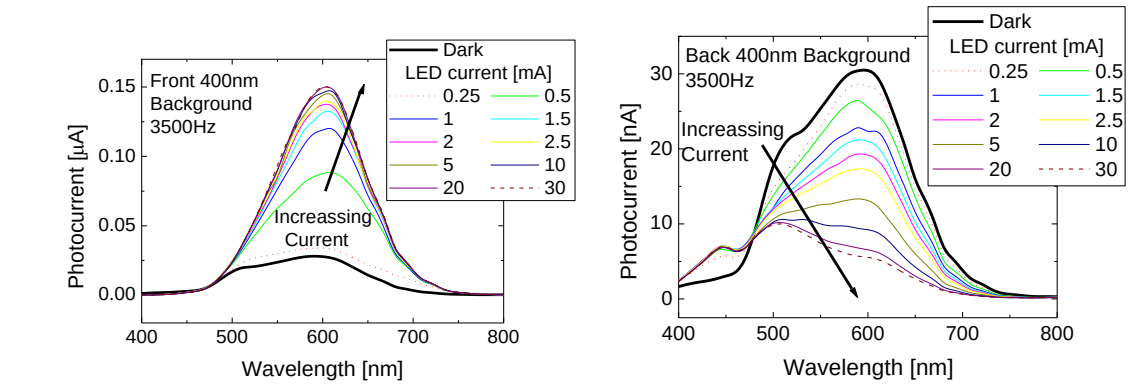

a) b)

Figure 3-9 - Photocurrent with a) front and b) back lighting of the background.

The experimental results of Figure 3-9a) show the photocurrent's increase in the 470 to 700 nm bandwidth. There is a significant increase just by the presence of the violet light; the fivefold increase from no LED current to 0.5 mA is outstanding when compared to the increase from 0 to 30 mA. In Figure

3-9b) the thick black curve is the same of the previous figure and represents the dark level. With increasing LED current the photocurrent in the 470-700 nm bandwidths gradually decreases and there is an almost fixed increase of the photocurrent in the 400-470 nm bandwidths. The photocurrent gain is shown in Figure 3-10.

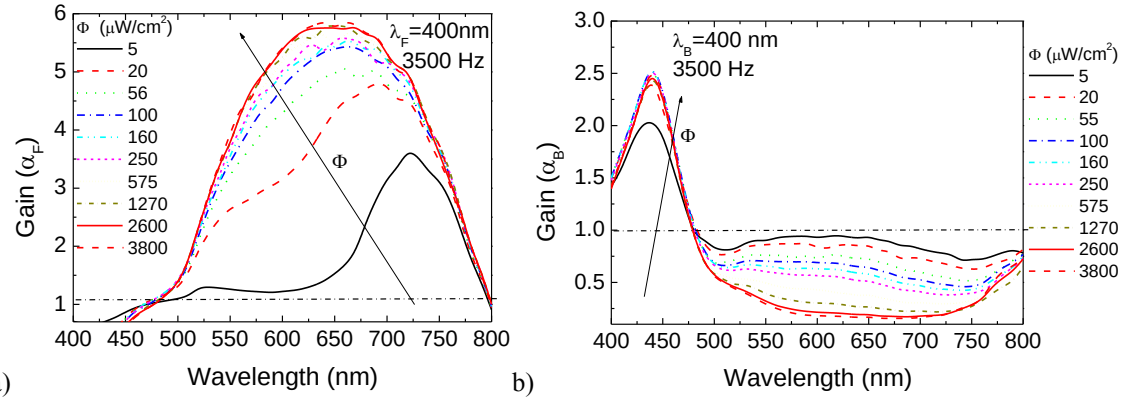

Figure 3-10 - Photocurrent gain when background light is at the a) front and b) back surfaces.

The spectral gain shown in Figure 3-10a), with front background, reduces the short wavelengths (< 470 nm) and increases the long wavelengths (> 470 nm). This behaviour is that of a selective filter centred in 650 nm. The opposite happens when the background lighting is at the back side, Figure 3-10b), the short wavelengths increase while the long wavelengths decrease. This is also a selective filter centred in 440 nm. Thus the sensor can act as a selective filter, where the gain of the short and long pass wavelengths is controlled by optical bias at either one of the sides. The gains of both filters suffer almost no changes with LED currents above 10 mA. Normalizing the photocurrent gains shown in Figure 3-10 and plotting them in the same graph yields Figure 3-11.

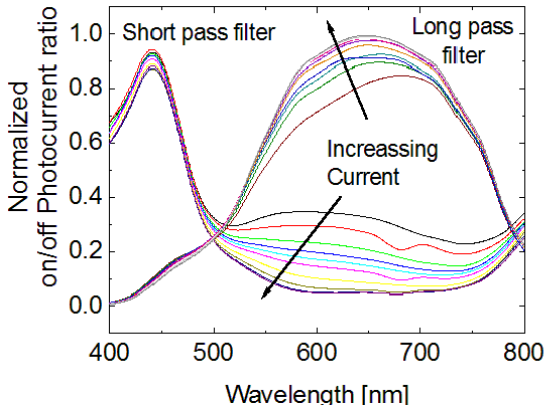

Figure 3-11 - Short and long pass filters.

Setting both filters in the same graph, Figure 3-11, each one normalized to its highest level, enables a view of the two filters and the eye figure assures the effectiveness of the filtering capabilities of the sensor. A notch filter around 500 nm is also perceived.

These experimental results were made with the front LED positioned at 6.5 cm from the sensor and the back LED at 2.5 cm as described in Chapter 2.

The spectral sensitivity was tested through spectral response measurements [6] without and under 350 nm and 400 nm front and back backgrounds of variable intensities. In Figure 3-12 the spectral gain (α), defined as the ratio between the spectral photocurrent with and without applied optical bias, is displayed under near-UV (λ=350 nm; Figure 3-12a) and Figure 3-12b) and violet (λ=400 nm; Figure 3-10a) and Figure 3-10b) illuminations. In Figure 3-12a) the light was applied from the front (λ_F) and in Figure 3-12b) the irradiation occurs from the back side (λ_B) while in Figure 3-10a) and Figure 3-10b) visible violet light was used from front and back sides, respectively. The background intensity (φ) was changed between 5 μWcm^{-2} and 3800 μWcm^{-2}.

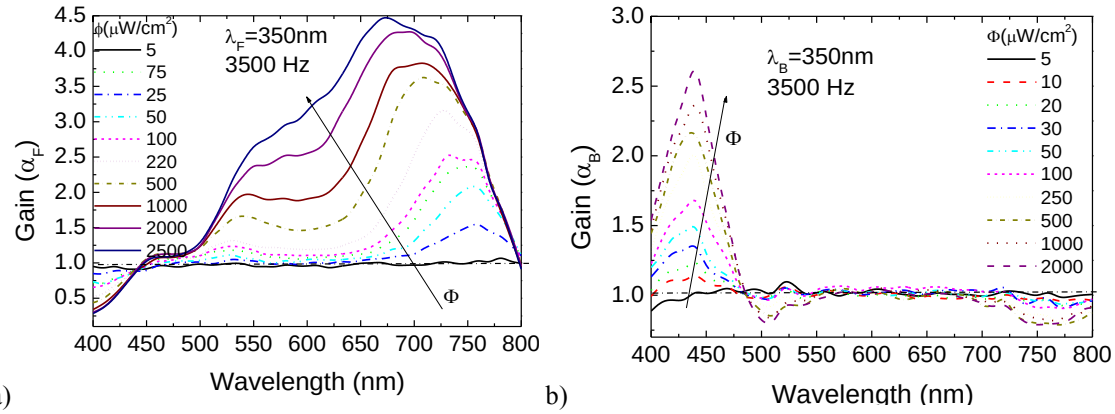

Figure 3-12- Front (λ_F, left) and back (λ_B, right) spectral gains ($\alpha_{F,B}$) under λ=350 nm irradiation.

Results show that the optical gains have opposite behaviours under front and back irradiations. Under 350 nm front irradiation (Figure 3-12a) and low flux, the gain is high in the infrared region, presents a well-defined peak at 750 nm and strongly quenches in the visible range. As the power intensity increases the peak shifts to the visible range and can be deconvoluted into two peaks, one in the red range that slightly increases with the power density of the background and another in the green range that strongly increases with the intensity of the UV radiation. In the blue range the gain is much lower. This

shows the controlled high-pass filtering properties of the device under different background intensities. Under back bias (Figure 3-12b) the gain in the blue/violet range has a maximum near 420 nm that quickly increases with the intensity. Besides, it strongly lowers for wavelengths higher than 450 nm, acting as a short-pass filter. Thus, back irradiation, tunes the violet/blue region of the visible spectrum whatever the flux intensity, while front irradiation, depending on the background intensity, selects the infrared or the visible spectral ranges. Here, low fluxes select the near infrared region and cuts the visible one, the reddish part of the spectrum is selected at medium fluxes, and high fluxes tune the red/green ranges with different gains. Under visible violet front and back backgrounds (Figure 3-12c and Figure 3-12d) the behaviour is similar, however under front irradiation the spectral sensitivity quickly increases and saturates at low fluxes when compared with the near-UV irradiation. Under back light the visible range is strongly quenched as the flux intensity increases [3].

Numerical simulation

To understand the light filtering properties of the device, a device simulation program ASCA-2D was used to analyze the spectral sensitivity in the device [7]. The generation rate is calculated following a Urbach-Tauc-Lorentz model [8] for the absorption coefficients. The input parameters were obtained based on the experimental results of the front and back diodes [1].

In Figure 3-13 the simulated spectral sensitivity of the front (pin1) and back (pin2) diodes (lines) are compared with the normalized experimental sensitivity of the individual front and back diodes (symbols).

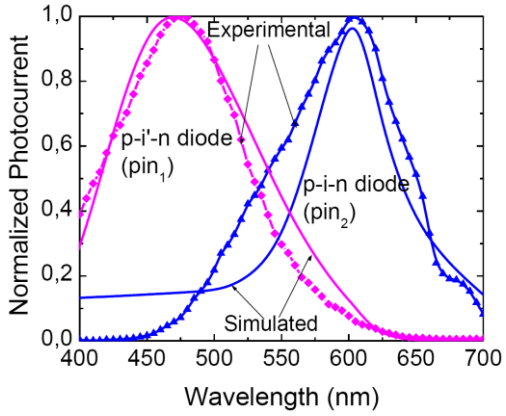

Figure 3-13 - Comparison between simulated (lines) and experimental (symbols) normalized front (pi'n) and back (pin) diodes.

A good fit between simulated and experimental results was achieved for the individual optimized diodes. As a result, both front and back pin structures act separately as optical filters confining, respectively, the blue and the red optical carriers to their active absorption areas.

Based on the optimized input parameters for the absorption coefficients, Figure 3-14 reports the simulated generation/recombination rate profiles across the whole device, under front and back violet optical bias.

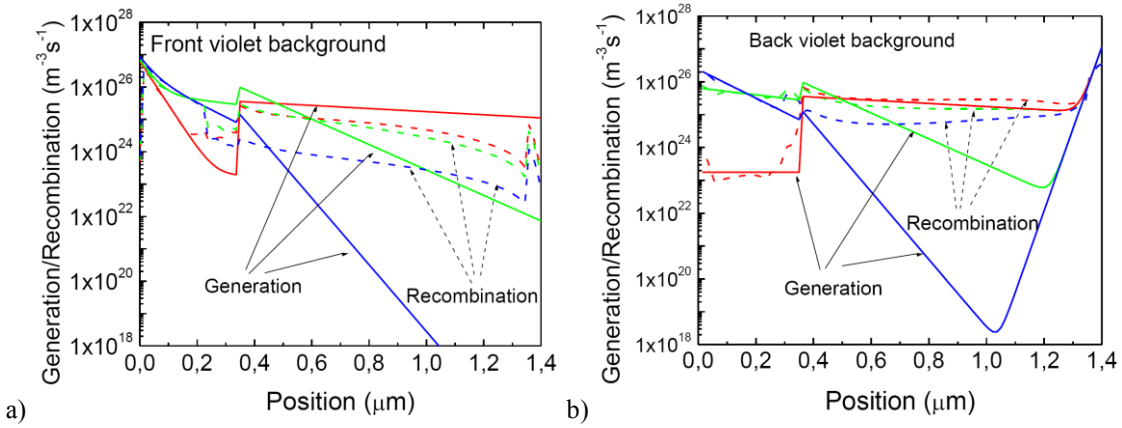

Figure 3-14 - Generation/Recombination rate profiles of the device under: a) front and b) back steady state violet illumination.

Results show that the depth of light penetration within the device depends on both the wavelength of the input channels and background side. If the background is a short wavelength radiation (violet), the photogeneration profile is strongly influenced by the choice of the device side for light incidence. When compared with the absence of background light, under front irradiation the generation in the front diode increases mainly for the long wavelengths channels (green and red) due to the contribution of the background light that generates carriers exclusively in the front diode. Under back irradiation, the generation in the back photodiode increases for short/medium wavelengths due to the light penetration depth of the violet light across the bottom of the a-Si:H intrinsic layer [4, 9].

In Figure 3-15 the simulated electric field profile, under front and back violet background without channels (OFF) or with the red, green and blue channels ON (ON) are displayed.

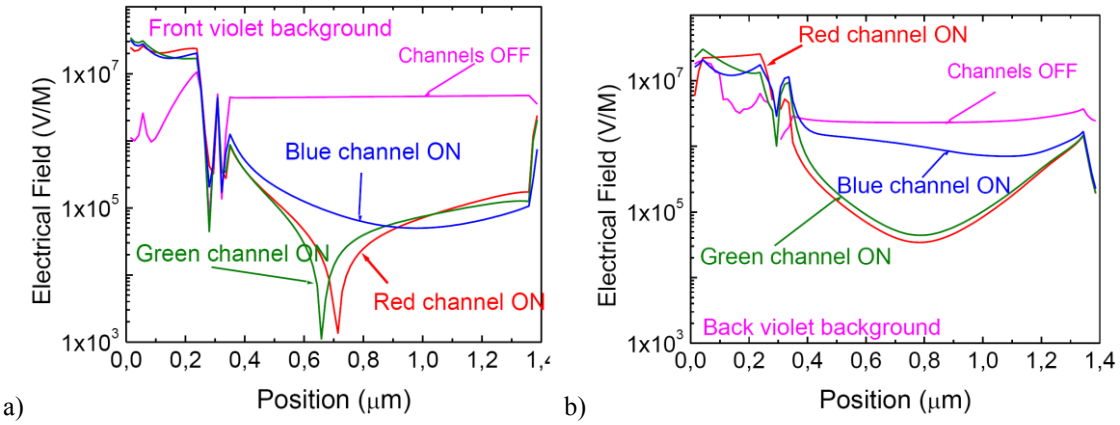

Figure 3-15 - Simulated electric field profile under front (a) and back (b) violet background without (OFF) or with the red, the green and the blue channels ON (ON)

As expected the electric distribution across the device depends on the irradiation side and on the on/off state of the channels. The small absorption depth of the violet photons across the front (a) or the back (b) diodes changes the electric field profile in opposite ways due to an increase of the trapped charge at the internal interface [4].

3.4 Optical bias controlled filters using violet background

3.4.1 Spectral response

Illuminating the device with violet light and different intensities, either at the back or at the front side, changes the spectral photocurrent changes as pictured in Figure 3-16. For comparison both graphics show the spectral photocurrent without applied optical bias (dark). When violet irradiation is applied from the front side (Figure 3-16a) or from the back (Figure 3-16b) the spectral response changes significantly. A peak fit adjustment to the data was performed (lines) with peaks centred on 630 nm (solid), 520 nm (dash) and 430 nm (dot).

Results show that under increased intensity and front violet irradiation the peak centred at 630 nm (red range) strongly increases whereas the blue part of the spectrum is negligible. Illuminating the back side of the device it quenches the 630 nm peak intensity and increases the blue range mainly at the three marked positions. So, front illumination and high intensity enhances the

reddish part of the spectrum while under back illumination the main enhancement occurs in the violet-blue region. A trade-off between the background intensity and the enhancement or quenching of the different spectral regions has to be taken into account [10].

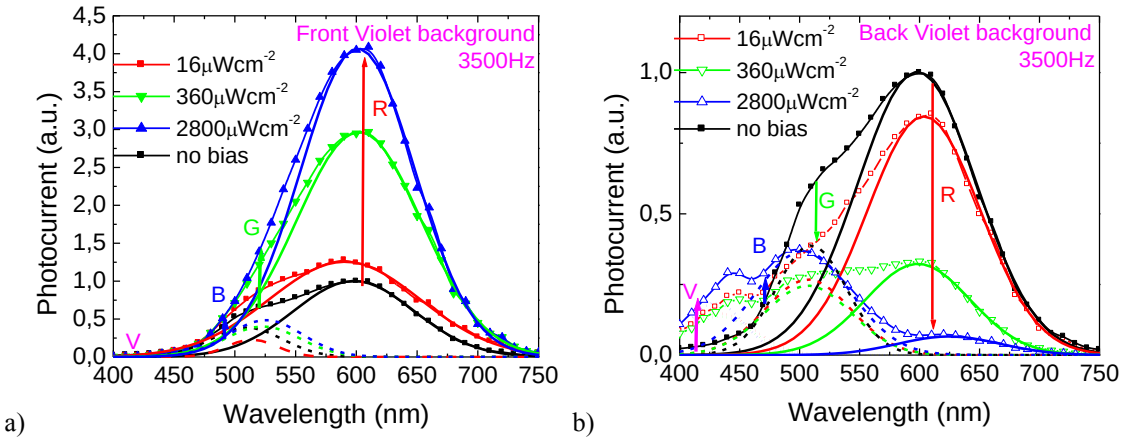

Figure 3-16 - Normalized spectral photocurrent under front (a) and back (b) violet irradiations with different intensities.

Plotting the ratio between the spectral responses with and without optical bias (2300 μWcm^{-2}) either from the front or back gives the spectral gain (α^V) presented in Figure 3-17. As expected from Figure 3-16 under back bias, the gain is high at short wavelengths and lowers strongly at wavelengths higher than 500 nm, acting as a short-pass filter. Under violet front light the device works as a long-pass filter for wavelengths higher than 550 nm, blocking shorter wavelengths.

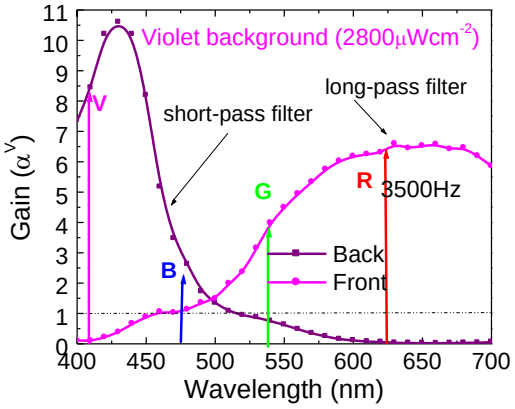

Figure 3-17 - Normalized spectral photocurrent under front (a) and back (b) violet irradiations.

Results show that by combining the irradiation sides the short-, and long- spectral region can be sequentially tuned. The medium region can only be tuned by using both active filters.

3.4.2 Optical gain

In Figure 3-18 the spectral gain (α^V), defined as the ratio between the spectral photocurrents under violet illumination and without it, is plotted. The background intensity was changed between 2300 μWcm^{-2} and 16 μWcm^{-2}. Results show that under back bias the gain is high at short wavelengths and strongly lowers for wavelengths higher than 500 nm, acting as a short-pass filter. Under violet front light the device works as a long-pass filter for wavelengths higher than 500 nm, blocking the shorter wavelengths. So, by switching the irradiation side the short-, and long- spectral region can be sequentially tuned. The medium region (475 -530 nm) can only be tuned by using both active filters. A trade-off between the background side and intensity has to be established. Under front illumination the reddish part of the spectrum is enhanced with the intensity while under back illumination the main enhancement occurs at the violet-blue region [10].

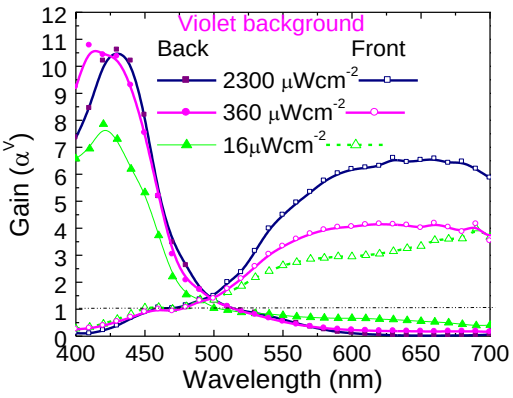

Figure 3-18 - Spectral gain (α^V) under front and back bias.

Four monochromatic pulsed lights separately (red, green, blue and violet input channels) or combined (multiplexed signal) illuminated the device at 12000 bps, as shown in Figure 3-19.

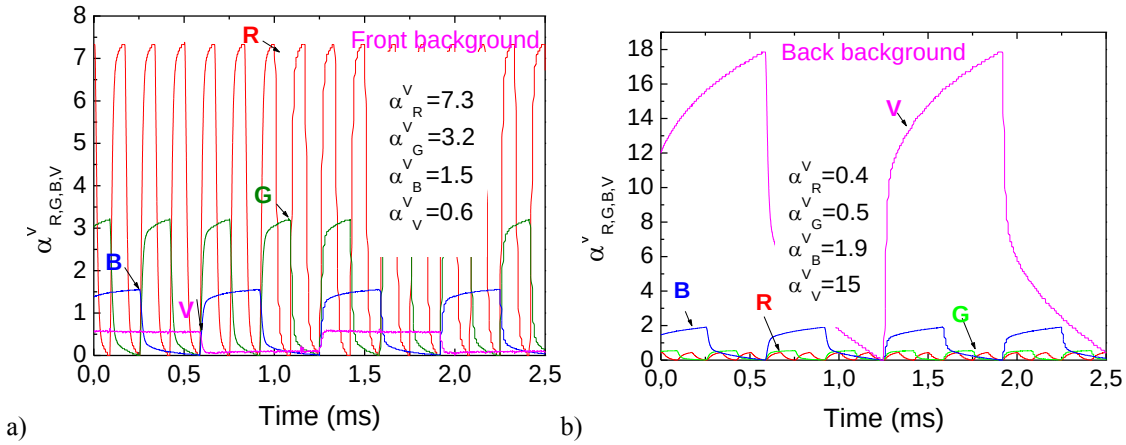

Figure 3-19 - Normalized red, green, blue and violet transient signals at -8V with violet (400 nm) steady state optical bias applied from the front (a) and from the back (b) sides.

Steady state violet bias was superimposed separately from the front (a) and the back (b) sides and the photocurrent was measured. In Figure 3-19, the transient signals were normalized to their values without background and, for each individual channel, the mean values of the optical gains added. Results show that, even under transient conditions and using commercial LED the background side alters, in a different way, the signal magnitude of the input channels. This nonlinearity provides the possibility for selective removal or addition of wavelengths. As expected from Figure 3-18, under front irradiation it enhances mainly the spectral sensitivity in the medium-long wavelength ranges (α^V_R=7.3, α^V_G=3.2). Violet radiation is absorbed at the top of the front diode (Figure 3-1), increasing the electric field at the back diode [2] where the red and part of the green incoming photons are absorbed. Under back irradiation the electric field increases mainly near the front p-n interface where the violet and part of the blue incoming channels generate most of the photocarriers (α^V_V=15, α^V_B=1.9). So, by switching between front to back irradiation the photonic function is modified from a long- to a short-pass filter alternately selecting the red or the violet channels [10]. This switching can be visualised in Figure 3-20. On this experiment the data channels are the red (626 nm), green (524 nm) and blue (470 nm) wavelengths. These three channels are always transmitting the binary sequence 000 to 111, corresponding to the RGB bit order. The 000 to 111 sequence is continuously repeated, and every 256 times, there is a 1 ms in which all RGB LEDs are switched off; this blanking is necessary due to the configurations of the PiscaLed that allows the whole pattern to be constructed.

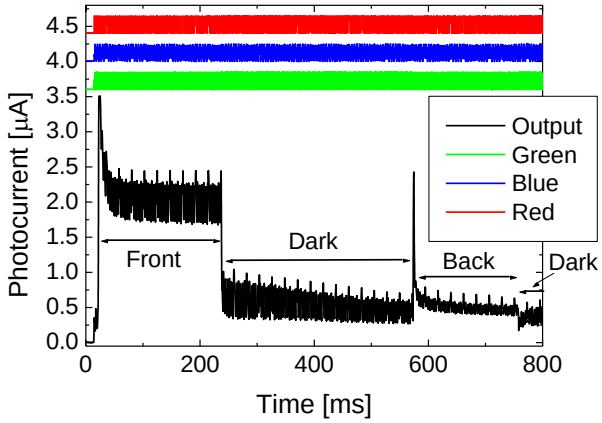

Figure 3-20 - Sensor output with a front to dark to back to front background illumination.

While the data channel pattern is shinning upon the front surface of the device, the background lighting also performs a pattern, that begins with no illumination, and then the front surface is illuminated with ultra-violet light, follows a dark period without illumination, then the back surface is illuminated, after which a dark period ends the experiment. The whole experiment shown in Figure 3-20 (0-800 ms) is shown in specific ranges in time of the front (100-105 ms) , dark (400-405 ms) and back (700-705 ms) periods, in Figure 3-21.

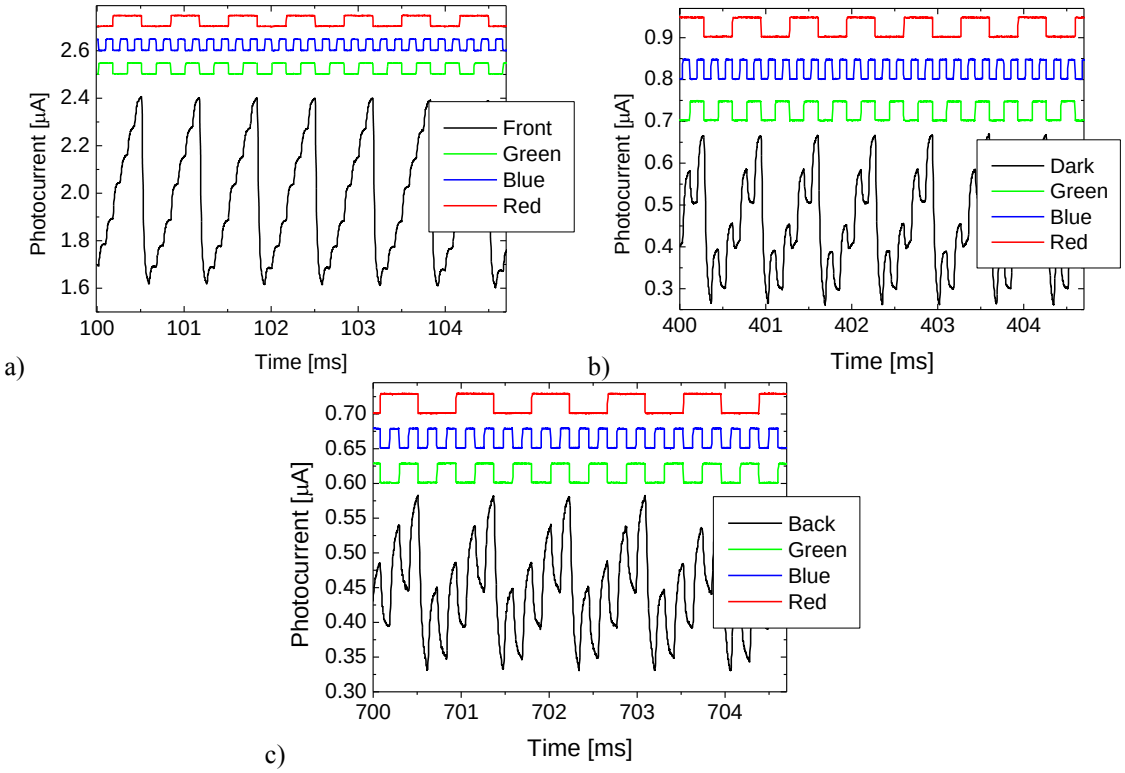

Figure 3-21 - Detail of the a) front, b) dark and c) back periods of Figure 3-20.

The differences between the three graphs of Figure 3-21, are resultant of the photonic function. The red channel is clearer in Figure 3-21a) and the blue channel is identified by Figure 3-21b). The interaction of the three channels is presented in Figure 3-21c).

3.5 Photonic active filters

3.5.1 Self-bias amplification

To analyze the device under information-modulated wave and uniform irradiation, three monochromatic pulsed lights separately (red, green and blue input channels) or their combination (MUX signal) illuminated the device. Steady state red (652 μWcm^{-2}), green (515 μWcm^{-2}), blue (680 μWcm^{-2}) and violet (2800 μWcm^{-2}) optical bias was superimposed separately from the front (pi'n = pin1) and the back (pin = pin2) sides and the photocurrent measured at -8 V.

In Figure 3-22a), the transient signals under front and back violet irradiations are plotted. In Figure 3-22b) the signals are displayed under red and blue front backgrounds.

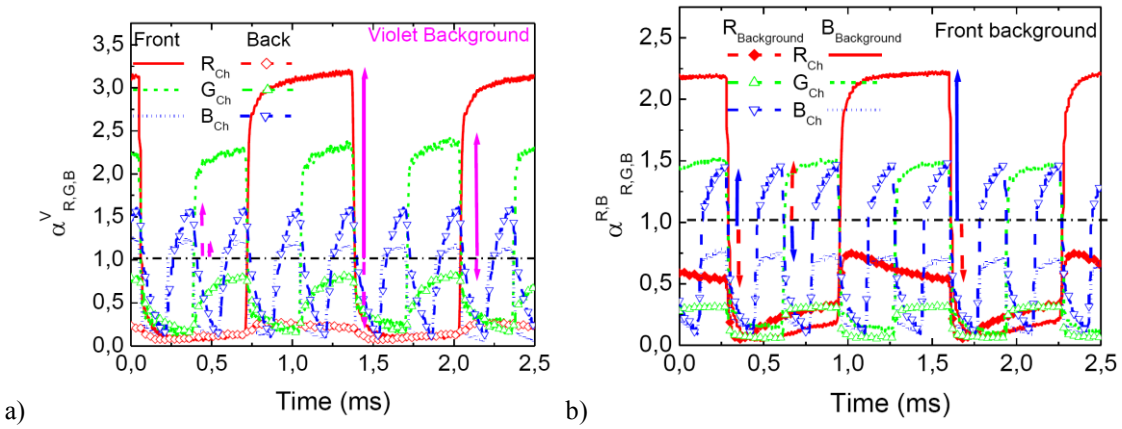

a) b)

Figure 3-22 - Red (R_{Ch}), green (G_{Ch}) and blue (B_{Ch}) channel signals under: a) violet background from the back and front sides; b) front red and blue irradiations.

As expected from Figure 3-5 and Figure 3-7, even under transient condition, the device acts as an active bias controlled optical filter. Under front short wavelength irradiation (blue or violet) the magnitude of the red and green channels are amplified and the blue reduced (see solid arrows). Under red

optical bias (dash arrows in Figure 3-22b) an opposite behaviour is achieved. The green and red channels are amplified and the blue quenched. Violet back irradiation (dash arrows in Figure 3-22a) cuts the red channel and slightly influences the magnitude of the green and blue ones.

In Table 3-1 the gains (α), for the red, green, and blue input channels are presented. Here, the superscripts are related to the background wavelength (R, G, B, V) and the subscripts ($_{Rpin1,2}$, $_{Gpin1,2}$, $_{Bpin1,2}$) to the channel colour and irradiation side[4, 7].

Results show that, even under transient conditions, the effect of the background wavelength and impinging side presents the same nonlinear dependence as in Figure 3-7. The morphology of filter results from the interaction of the electric field under applied optical bias (red, green, blue, violet) and the transient electric field induced by the input channels (red, green, blue and violet). This interaction results in electric field lines that guide the photocarriers generated by the input channels.

Table 3-1 - Gains ($\alpha^{R,G,B,V}{}_{R,G,B,pin1,2}$) at the input red, green, and blue channels wavelengths.

Channels	α^R	α^G	α^B	α^V
$\alpha_{R,pin1}$	0,83	1,01	2,84	3,09
$\alpha_{R,pin2}$	0,14	0,19	0,19	0,19
$\alpha_{G,pin1}$	0,92	1,03	1,64	2,21
$\alpha_{G,pin2}$	0,79	0,77	0,82	0,74
$\alpha_{B,pin1}$	1,39	1,00	0,81	1,11
$\alpha_{B,pin2}$	2,22	1,94	1,97	1,64
$\alpha_{V,pin1}$	5,54	2,93	1,06	0,56
$\alpha_{V,pin2}$	0,66	0,64	1,76	10,42

Taking into account Figure 3-14 and Figure 3-15, the flow rate of the carriers through those field lines towards the output depends on the on/off state of the channels. Under back irradiation the small absorption depth of the

violet photons across the back diode quenches the electric field there and consequently, the red collection (Red ON) almost disappears ($\alpha^{V}_{R,pin2} << 1$). Blue channel is absorbed across the front diode where the electric field was enhanced resulting in an increase collection of the blue channel ($\alpha^{V}_{B,pin2} > 1$). Since the green channel is absorbed across front and back diodes its collection is balanced by the increase collection in the front diode and its reduction at the back ($\alpha^{V}_{G,pin2} \sim 1$). The front violet background is absorbed at the surface of the front diode, increasing the electric field at the back diode, where the red and part of the green channels generate optical carriers. So, the collection is strongly enhanced ($\alpha^{V}_{R,pin1} >> 1$, $\alpha^{V}_{G,pin1} > 1$) while the blue collection stays near its dark value ($\alpha^{V}_{B,pin1} \sim 1$) [4, 7].

3.5.2 Violet optical bias control

Polychromatic combinations of the same red, green and blue input channels of Figure 3-22 but in different bit sequences was used to generate a multiplexed (MUX) signal.

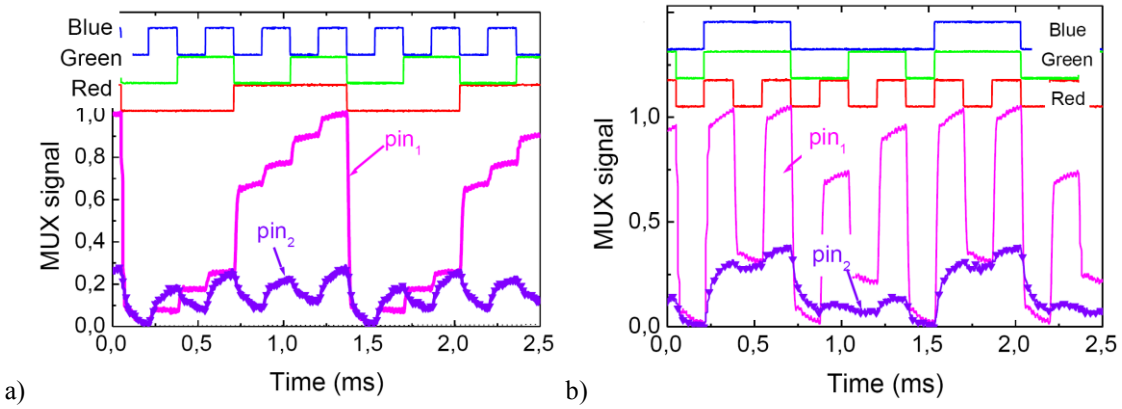

Figure 3-23 - Filtered output signals: a) front (pin1; lines) and back (pin2; symbols) violet irradiation. On the top, the optical signal used to transmit the information guide the eyes.

In Figure 3-23 the filtered signals under front (pin1) and back (pin2) violet light control are displayed. The signals were normalized to the maximum intensity under violet front irradiations to suppress the dependence on sensor and LEDs positioning. The bit sequences used to transmit the information are shown at the top of the figures.

Different gains for the RGB channels were obtained (Table 3-1). Due to this wavelength non-linearity under front violet background, the encoded

multiplexed signal presents as many levels as the possible RGB combinations, in a maximum of 2^3 (eight-level encode). Those levels can be grouped into two main classes due to the high amplification of the red channel ($\alpha^V_{R,pin1} >> 1$). The upper levels are ascribed to the presence of the red channel and the lower to its absence allowing the red channel decoder. Since under front irradiation the green channel is amplified ($\alpha^V_{G,pin1} > 1$), the highest levels, in both classes, are ascribed to the presence of the green channel and the lower ones to its lack (long-pass filter). Under back irradiation the red channel is suppressed ($\alpha^V_{R,pin2} << 1$), the blue enhanced ($\alpha^V_{B,pin2} > 1$) and the green reduced ($\alpha^V_{G,pin2} < 1$), so the encoded multiplexed signal presents a maximum of four separate levels (2^2). The highest levels correspond to the presence of the blue channel ON with or without the green ON respectively, and the other to its absence. The blue channel is then decoded using this simple algorithm (short-pass filter) [4].

3.6 Nonlinear Spectral gain

Several monochromatic pulsed lights separately (697 nm, 626 nm, 524 nm, 470 nm, 400 nm input channels; transmitted data) or combined (MUX signal) illuminated the device at 12000 bps. Steady state 390 nm bias at different intensities due to different LED input currents ($0 < I_{LED} < 30$ mA) were superimposed separately from both sides and the photocurrent was measured.

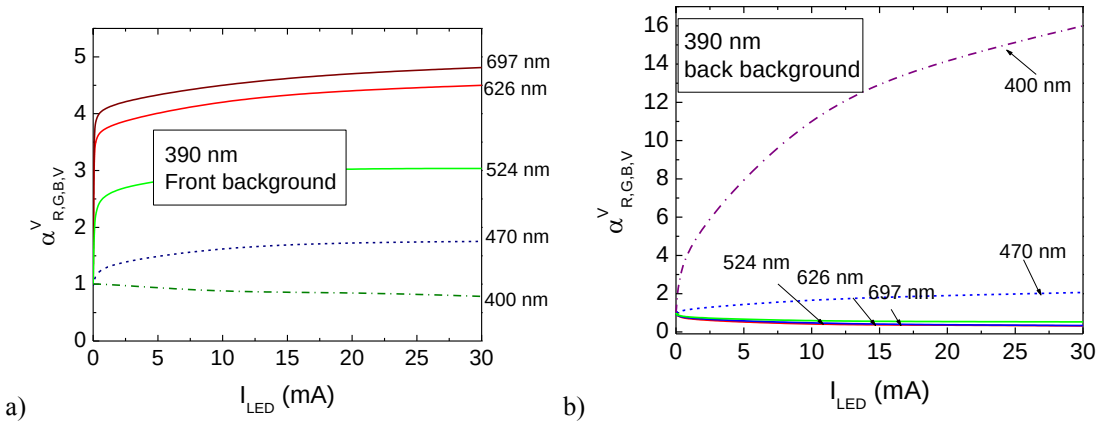

Figure 3-24 - a) Front and b) back optical gain at λ=390 nm irradiation and different input wavelengths.

For each individual channel the photocurrent was normalized to its value without irradiation (dark) and the photo-current gain ($\alpha_{VR,G,B,V}$)

determined. Figure 3-24 displays the different gain as a function of the drive currents of the lighting LED under front (a) and back (b) irradiation.

Results show that the gain depends mainly on the channel wavelength and slightly on the lighting intensity, for high fluxes. Even across narrow bandwidths, the gains are quite different. Under front irradiation (Figure 3-24a) the magnitude of the short wavelengths signals is quenched and enlarged in the long wavelengths range. The opposite happens when the background lighting is at the back side (Figure 3-24b). Here, the short wavelengths gain increases while the long wavelengths gain decreases. This behaviour can be used to build selective filters, where the gain of the short and long pass filters is controlled by optical bias either at the back or front sides. This nonlinearity allows identifying the different input channels in the visible range. Due to its low wavelength, the background light is absorbed at the top of the front diode and, due to the self-bias effect [13], increases the electric field at the back diode where the red incoming photons are absorbed according to their wavelengths (see Figure 3-1) resulting in an increased collection. Under back irradiation the electric field decreases mainly at the i-n back interface quenching the red/green input signals [14].

3.7 Optoelectronic Model

3.7.1 AC equivalent circuit

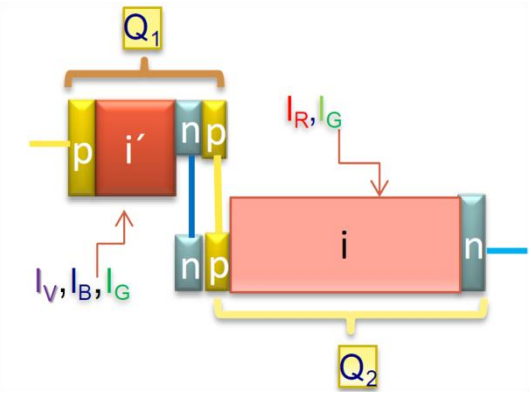

Figure 3-25 - Compound connected phototransistor equivalent model

The monolithic device (Figure 3-1) is modelled by the two-transistor model (Q_1-Q_2) shown in Figure 3-25. The two-phototransistor model is obtained by bisecting the two middle layers in two separate halves that can be considered to constitute pinp (Q_1) and npin (Q_2) phototransistors separately. In order to simulate the n-p internal junction, the collector and base of both transistors are shared [15].

The compound connected phototransistor model introduces a functional structure similar to the classic transistor. When the pi'npin device is reverse-biased, the base-emitter junction of both transistors are reverse biased and conceived as phototransistors, taking advantage of the amplifier action of adjacent collector junctions which are forward biased [15].

Based on the experimental results and device configuration an optoelectronic model, made out of a short- and a long-pass filter was developed [2], and is shown in Figure 3-26.

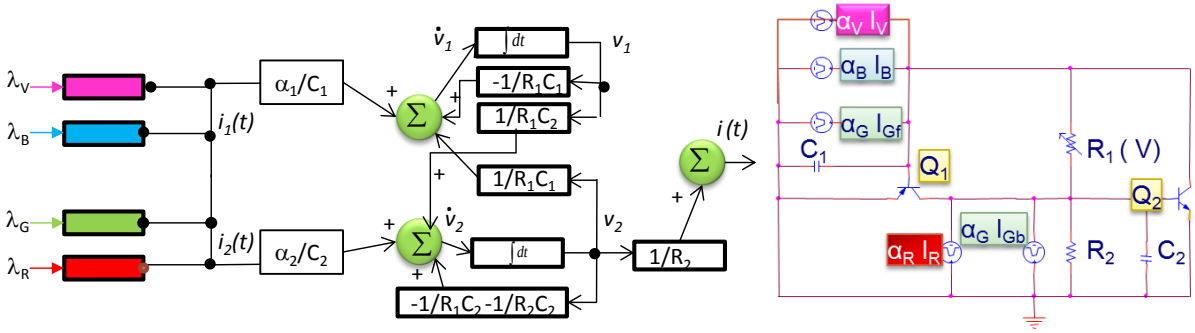

$$\frac{dv_{1,2}}{dt} = \begin{bmatrix} \frac{\alpha_1(\alpha_{V,B,G})}{C_1} \\ \frac{\alpha_2(\alpha_{R,G})}{C_2} \end{bmatrix} i_{1,2}(t) + \begin{bmatrix} -\frac{1}{R_1C_1} & \frac{1}{R_1C_1} \\ \frac{1}{R_1C_2} & -\frac{1}{R_1C_2} - \frac{1}{R_2C_2} \end{bmatrix} v_{1,2}(t) \quad ; \quad i(t) = \begin{bmatrix} 0 & \frac{1}{R_2} \end{bmatrix} v_{1,2}(t)$$

Figure 3-26 - a) Block diagram and *ac* equivalent circuit. b) Linear state equations.

In Figure 3-26a) the *ac* equivalent circuit and the block diagram of the optoelectronic state model are displayed. In Figure 3-26b) the linear state equations are shown. The use of amplifying elements (Q_1, Q_2), with resistors (R_1, R_2) and capacitors (C_1, C_2) in their feedback loops, synthesize the desired filter characteristics with $\alpha_{R,G,B,V}$ the optical gain. The input signals, $\lambda_{R,G,B,V}$ model the colour channels and *i(t)* the output signal. The amplifying elements, α_1 and α_2 are related with the optical gains and provide gain if needed or attenuate

unwanted wavelengths. The control matrix takes into account the enhancement or quenching of the channels (Figure 3-19) due to the steady state irradiation. Under front irradiation: $\alpha_2 >> \alpha_1$ and under back irradiation $\alpha_1 >> \alpha_2$. This affects the reverse photo capacitances, ($\alpha_{1,2}$ /$C_{1.2}$) that determine the influence of the system input on the state change (control matrix). The optoelectronic model with light biasing control has proven to be a good tool to design SiC multilayer add/drop filters. Furthermore, this model allows for extracting experimental parameters by fitting the model to the measured data.

3.7.2 Working principle

Under negative bias, the p-n internal junction is forward-biased and the external voltage drops mainly across both front and back reverse-biased junctions, mainly at the front one due to its higher resistivity. Under positive bias the internal junction becomes reverse biased.

The *ac* circuit representation displayed in Figure 3-26a) is supported by the complete dynamical large signal Ebers-Moll model with series resistances and capacities [4, 15].

The charge stored in the space-charge layers is modelled by the capacitor C_1 and C_2. R_1 and R_2 model the dynamical resistances of the internal and back junctions under different *dc* bias conditions. The operation is based upon the following strategic principle: the flow of current through the resistor connecting the two transistor bases is proportional to the difference in the voltages across both capacitors (charge storage buckets). The modified electrical model developed is the key of this strategic operation principle. The capacitors exhibit time-varying charge/voltage characteristics being the current across them the instantaneous rate of charge variation. If the device is biased negatively Q_1 and Q_2 are in their reverse active regions. Two optical gate connections ascribed to the different light penetration depths across the front (Q_1) and back (Q_2) phototransistors were considered to allow independent blue, red, green and violet channels transmission [15].

Five square-wave current sources with different intensities are used; three of them, with different frequencies to simulate the input violet (I_V), blue (I_B) and red (I_R) channels and the other two, with the same frequency but

different intensities, to simulate the green channel due to its asymmetrical absorption across both front (I_{Gf}) and back (I_{Gb}) phototransistors [15].

Once the *ac* sources are connected in the load loop an *ac* current flows through, establishing voltage modifications across the two capacitors. During the simultaneous transmission of the three independent bit sequences, the set-up in this capacitive circuit loop is constantly changing in magnitude and direction. This means that the voltage across one capacitor builds up until its maximum and the voltage across the other builds up to a minimum. The system collapses and builds up in the opposite direction. It tends to saturate and then leave the saturation state because of the cyclic operation. This results in changes on the reactance of both capacitors. The use of separate capacitances on a single resistance R_1 results in a charging current gain proportional to the ratio between collector currents. The *dc* voltage, according to its strength, aids or opposes the *ac* currents. So, when the pi'npin device is reverse-biased, the base-emitter junction of both transistors are inversely polarized and conceived as phototransistors, taking, so, advantage of the amplifier action of adjacent collector junctions which are polarized directly. This results in a current gain proportional to the ratio between both collector currents. Under positive bias the internal junction becomes reverse-biased [15].

The external current depends not only on the balance between violet, blue, green and red photocurrents (I_V I_B I_{Gf} I_{Gb} I_R) but also on the end of each half-cycle of each modulated current. Here, the movement of charge carriers with an increase/decrease in the irradiation, results in a charging or a displacement current similar to the current ($i=C\ dV/dt$) that charges the capacitors C_1 and C_2 in opposite ways [15].

Assuming that the frequency is low enough so that quasi-statics is maintained, the incremental capacitances are used to evaluate the total charge stored. So, the junction capacitance and diffusion capacitance would behave as if they have been kept in parallel. Because inherently they are leaky capacitors, C_1 and C_2, need to store higher charge that has also to be supplied. This charge will appear as a current component. The leaky capacitors can be represented as parallel combinations of ideal capacitors and resistances. The current would be the superposition of two components: one leakage current that is in-phase with

the voltage and one displacement-capacitive-current which is out of phase with the voltage [15].

3.7.3 Transfer Characteristics

To illustrate the transfer characteristics effects due to changes in steady state light, *dc* control voltage or applied light pulses the following steps in the operation and control of the optoelectronic circuit are considered:

Positive voltage bias control.

Only an *ac* current is flowing through the load capacitance C_2. The device has high ohmic resistance (high R_1) and remains in its non conducting state unless a light pulse (I_2 or I_2+I_4) is applied to the base of Q_2. This pulse causes Q_2 to conduct as the reversed biased n-p internal junction behaves like a capacitor inducing a charging current across R_2. No amplification effect was detected since Q_1 acts as a load and no charges are transferred between C_1 and C_2 (see Figure 3-27) [15].

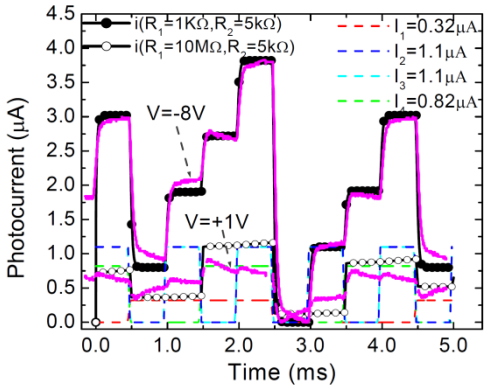

Figure 3-27 - Multiplexed simulated (symbols), current sources (dash lines) and experimental (solid lines) under negative (R1=1 kΩ; -8 V) and positive (R1=10 MΩ; +1 V) *dc* bias without any background.

Negative dc voltage bias control.

Under negative bias the device has low ohmic resistance (low R_1) the base emitter junction of both transistors are inversely polarized and conceived as phototransistors, thus taking advantage of the amplifier action of neighbouring collector junctions, which are polarized directly. This results in a charging current gain proportional to the ratio between both collector currents (C_1/C_2). The device behaves like an optoelectronic controlled transmission

system that stores, amplifies and transports the minority carriers generated by the current pulses, through the capacitors C_1 and C_2. Here, the *dc* voltage control creates a voltage across one or both capacitors which, when superimposed with an *ac* pulse, collectively saturates the circuit. No additional change in the voltage across the capacitors occurs. This results in maximum power transfer to the load. (see Figure 3-27 and Figure 3-28) [15].

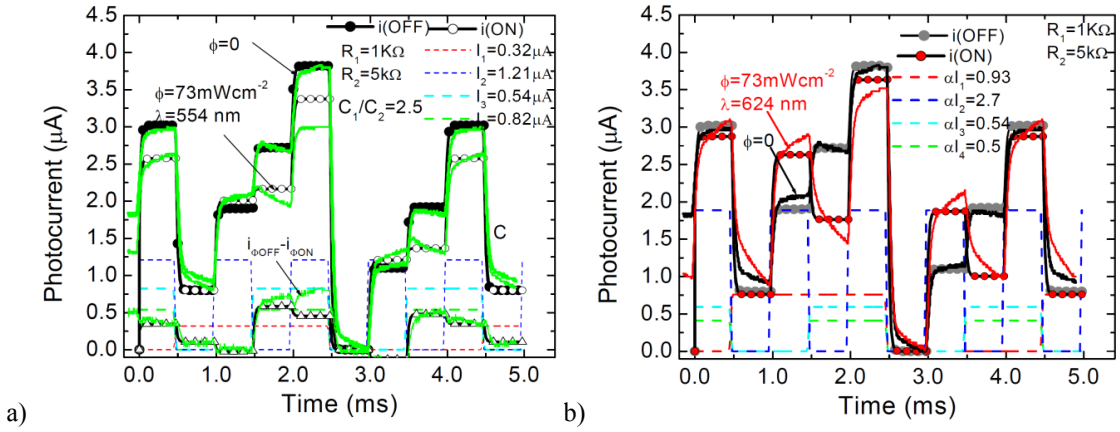

Figure 3-28 - Multiplexed simulated (symbols), current sources (dash lines) and experimental (solid lines): under negative (R1=1 kΩ; -8 V) *dc* bias and green (a) and red (b) backgrounds.

Optical bias control.

Depending on its wavelength the optical bias changes the amplitude of the *ac* current sources by an α factor, and so the voltages across one or both capacitors. Blue, red or green irradiations move asymmetrically the bases of Q_1, Q_2 or both toward (away) their emitter voltages, self-forward (reverse) effect, resulting, respectively in lower (higher) values of I_1, I_2, I_3 and I_4 when compared with no optical bias. The circuit can leave the saturation resulting in a wavelength controlled power transfer to the load that allows tuning an input channel from the stream (Figure 3-27) or to optically de-multiplex a polychromatic channel (Figure 3-28) [15].

3.8 Opto-Electronic Conversion

For an optoelectronic digital capture system, opto-electronic conversion is the relationship between the optical input levels and the corresponding digital output levels. We use an 8-bit priority encoder as an example to illustrate how a logic function is mapped onto the proposed directed-logic

circuit. An encoder has a number of inputs, only one of which is in the 1 state, and an N-bit code is generated, depending upon which of the inputs is excited.

To analyze the device under information-modulated wave and uniform irradiation, three monochromatic pulsed lights separately (red, green and blue input channels, Figure 3-29a) or combined (multiplexed signal, Figure 3-29b) illuminated the device at 6000 bps. Steady state violet optical bias was superimposed separately from the front (solid lines, pin1) and the back (dash lines, pin2) sides and the photocurrent generated measured at -8 V.

The transient signals were normalized to their values without background in Figure 3-29a. In Figure 3-29b) the normalized multiplexed signal under front (symbols) and back (lines) violet irradiation is displayed. On the top of the figure the signals used to drive the input channels are shown to guide the eyes into the ON/OFF channel states.

Even under transient conditions the front background presents a nonlinear dependence on the wavelength. It enhances mainly the light-to-dark sensitivity in the medium-long wavelength ranges. Violet radiation is absorbed at the top of the front diode, increasing the electric field at the least absorbing cell (see Figure 3-15a), the back diode. So the collection is strongly enhanced (α^{V}_{Gpin1}=2.2, α^{V}_{Rpin1}=3.1) while the blue collection stays near its dark value (α^{V}_{Bpin1}=1.1). Under back irradiation the small absorption depth of the violet photons across the back diode quenches the electric field and so, the red collection almost disappears (α^{V}_{Rpin2}=0.2). Blue channel is absorbed across the front diode where the electric field is enhanced resulting in an increase collection of the blue channel (α^{V}_{Bpin1}=1.6). Since the green channel is absorbed across front and back diodes its collection is balanced by the increased collection in the front diode and its reduction at the back one (α^{V}_{Gpin2}=0.7).

The truth tables of both encoders of Figure 3-29, that perform 8-to-1 MUX function, are also shown in Figure 3-30. In the inputs (x_0….x_7), the index of each bit is related to the first (highest) nonzero logic input. Here, the MUX device selects, through the violet background, one of the eight input logic signals and sends it to the output ($y=x_S$). The output is a three-bit [$S_2S_1S_0$] binary RGB number that may identify one of eight possible inputs.

To understand this mapping, in Figure 3-29, for the input x_7 and output S_2, the first nonzero logic input is 7 ($2^2+2^1+2^0$), which corresponds an output [111]. Those OR gates are expressed, respectively, as: $S_2=x_7+x_6+x_5+x_4$ under front irradiation (Figure 3-30a) and $S_2=x_7+x_3+x_5+x1$ under back light (Figure 3-30b).

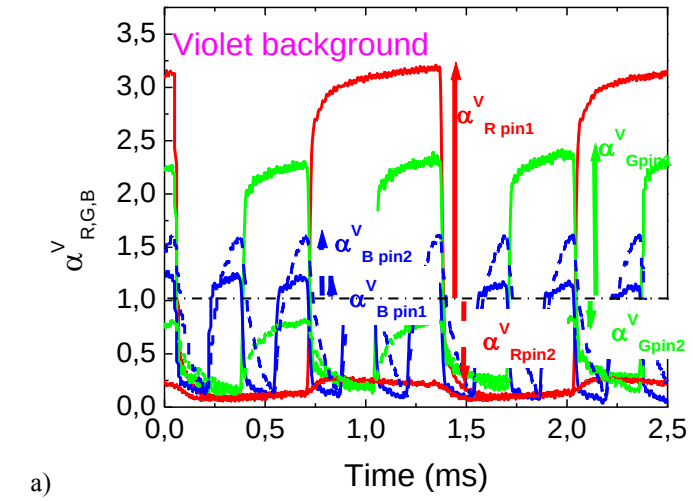

a)

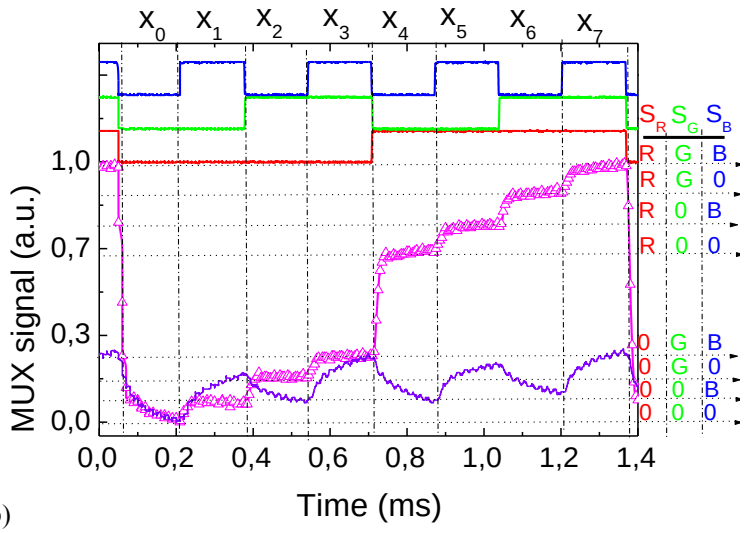

b)

Figure 3-29 - a) Normalized red, green and blue transient signals at -8V with violet (400 nm) steady state optical bias applied from the front side (α_{pin1}) and from the back side (α_{pin2}). b) Multiplexed output signal under front (symbols) and back (line) violet irradiation.

Violet irradiation is applied from the front (pin1; $\alpha^V_{Rpin1}>>1$, $\alpha^V_{Gpin1}>1$ and $\alpha^V_{Bpin}\sim1$) and back (pin2; $\alpha^V_{Rpin2}<<1$, $\alpha^V_{Gpin2}<1$ and $\alpha^V_{Bpin2}>1$) sides (see Figure 3-8d and Figure 3-29a). Under front irradiation (Figure 3-29b) the 2^3 levels can be grouped into two main classes due to the high amplification of the red channel. The upper four levels are ascribed to the presence of the red

channel ON, and the lower four to its absence, allowing the red channel decoder (4-to-1 multiplexer; long-pass filter function). Since under front irradiation the green channel is amplified the two highest levels, in both classes, are ascribed to the presence of the green channel and the two lower ones to its lack [9].

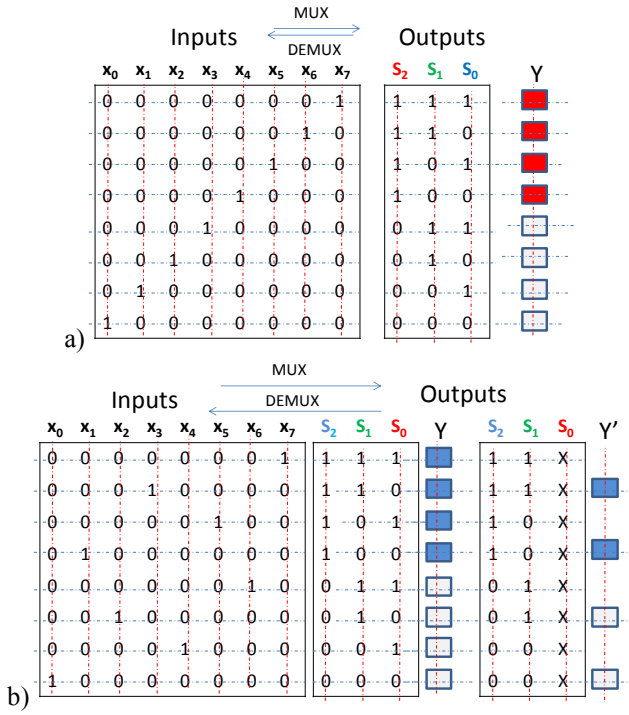

Figure 3-30 - Truth tables of the encoders that perform 8-to-1 multiplexer (MUX) function, under front (a) and back (b) violet irradiations (x means " not significant").

Under back irradiation, the blue channel is enhanced; the green reduced the red almost suppressed. The encoded multiplexed signal has the eight sublevels grouped also into two main levels, the higher where the blue channel is ON and the lower where it is OFF (4-to-1 multiplexer; short-pass filter function). In each main level the four existent sublevels are grouped in two classes, with and without the channel green ON. Each of those sublevels split into two near ones, attributed to the presence or absence of the red channel. If we consider this red output bit "not significant" only four separate levels (2^2) are considered and the logic MUX function is converted into a logic filter function. The blue channel is then decoded.

Like regular binary numbers, the binary RGB code is an arithmetic code and so, it is weighted, i.e. there is specific weights assigned to each bit position. Under front violet irradiation, the most significant digit, the left most bit, in the

RGB code is the red (α^{V}_{Rpin1}>>1). Going from the left to right, the next is the green (α^{V}_{Gpin1}>1) and the last is the blue (α^{V}_{Bpin1}~1). Under back violet irradiation, the left most bit is the blue. Going from the left to right, the next is the green and last the red. So, the correspondence between the outputs S_2, S_1, S_0, in Figure 3-30 and the on/off state of the input channels, S_R, S_G, S_B, in Figure 3-29 are obvious.

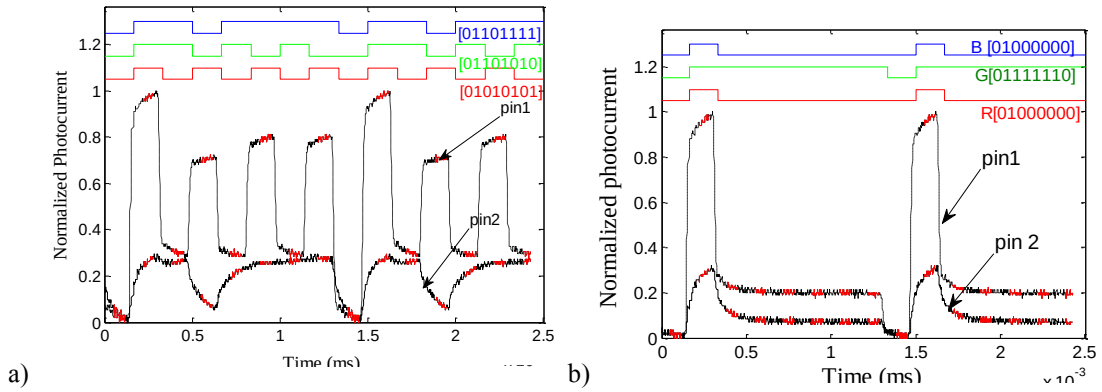

Figure 3-31 - MUX signal under front and back irradiation. On the top the DEMUX signals obtained using the decoder algorithm is displayed as well as the binary bit sequences.

We have used this simple algorithm to decode the multiplex signal. The results are displayed in Figure 3-31 for two different bit sequences. An excellent fit was obtained.

Results show that the pi'npin multilayered structure becomes reconfigurable under front and back irradiation. They perform WDM optoelectronic logic functions providing photonic functions such as signal amplification, filtering and switching. So, by means of optical control applied to the front or back diodes, the photonic function is modified from a long- to a short-pass filter, giving a step reconfiguration of the device [9].

3.9 Visible and Infrared Tuning

3.9.1 Visible and Near Infrared Tuning

Several monochromatic pulsed lights separately (850 nm, 697 nm, 626 nm, 524 nm, 470 nm, 400 nm; input channels) or combined (MUX signal) illuminated the device at 12000 bps. Steady state 390 nm bias at different

intensities due to different LED input currents (0< I_{LED} <30 mA) were superimposed separately from both sides and the photocurrent was measured.

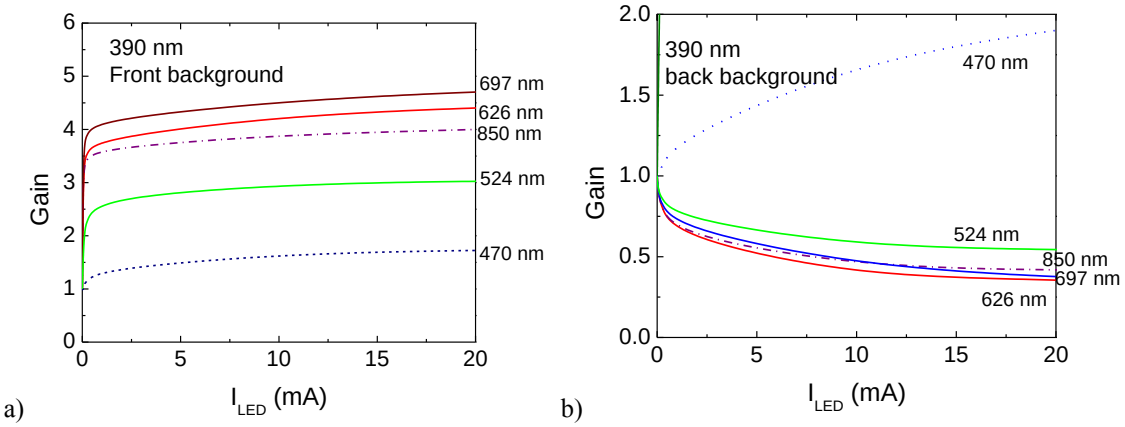

Figure 3-32 - a) Front and b) back optical gain at λ=390 nm irradiation and different input wavelengths.

For each individual channel the photocurrent was normalized to its value without irradiation (dark) and the photocurrent gain determined. Figure 3-32 displays the different gain as a function of the drive currents of the lighting LED under front and back irradiation. Results show that the gain depends mainly on the channel wavelength and slightly on the lighting intensity [1]. Even across narrow bandwidths, the photocurrent gains are quite different. This nonlinearity allows the identification of the different input channels in the visible/infrared ranges. To exemplify, in Figure 3-33a), the gain of the 850 nm input channel, under front irradiation and different intensities, is displayed. In Figure 3-33b) the MUX signals due to the combination of the 850 nm, 697 nm, 626 nm and 524 nm input channels are presented. At the top the signals used to drive the input channels are shown to guide the eyes into the on/off states.

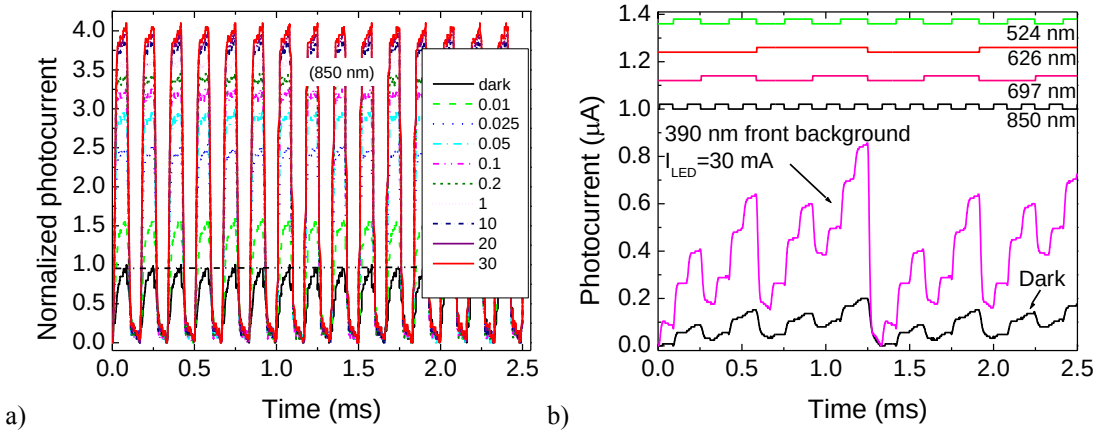

Figure 3-33 - a) Optical gain at 390 nm front irradiation and different intensities. b) Combined polychromatic signal with and without 390 nm front irradiation and different bit sequences.

Results confirm that, even under transient conditions, the input channels present different gains, depending on their wavelengths [5]. This nonlinearity, due to capacitive effect at the internal interface [1, 5] allows channel recognition and so, a multiplexed information, due to several visible/infrared signals encoded in the same optical transmission path, can be decoded through a simple algorithm [5] that takes into account the channel gains and the illumination side (see Figure 3-32). Under front irradiation the sensor sensitivity to long wavelengths is enhanced and presents different sensitivities in a narrow red/infrared bandwidth when compared without background. The combination of the four channels under irradiation points out to the presence of all the possible sixteen (2^4) on/off states, clearly observed in Figure 3-33b). Here, each level is ordered by the correspondent gains in a 4 bit binary code [X_{697}, X_{626}, X_{850}, X_{524}] with X=1 if the channel is on and X=0 if it is off. The functional principle is based on the adjustable penetration depths of the photons into the front and back diodes (Figure 3-1) which is linked to their absorption coefficient in the intrinsic front and back collection areas. Front irradiation is strongly absorbed at the beginning of the front diode and, due to the self-bias effect, increases the electric field at the back diode where the red/infrared incoming photons are absorbed accordingly their penetration depths, and so to their wavelengths, resulting in an increased collection. Under back irradiation the electric field decreases mainly at the i-n back interface quenching the red/infrared signals and enhancing the blue /violet ones. Depending on the illumination side and intensity, the device sensitivity is tailored and shifted toward the long or short wavelength ranges leading to linearly profiled collection areas. So, by switching between front and back irradiation the photonic function is modified from a long- to a short-pass wavelength filter, alternately selecting the red/infrared or the blue/violet channels, and making the bridge between the visible and the infrared regions. The green region is recognized through the use of both filters [17].

3.9.2 Red and Infrared Tuning

Three monochromatic pulsed lights separately (645 nm, 697 nm, 880 nm input channels,) or combined (MUX signal; Figure 3-34) illuminated the device at 12000 bps. Steady state 390 nm bias at different intensities (5 $\mu Wcm^{-2} < \varphi_{F,B} <$

3000 μWcm^{-2}) were superimposed separately from the front and the back device side and the photocurrent was measured. The intensity to drive the LEDs was adjusted to generate almost the same intensities without applied optical bias. In Figure 3-32a), the transient signals are presented under front irradiation and in Figure 3-32b) under back light. The current level was set to zero when all the input channels were off. On the top, the signals used to drive the input channels are shown to guide the eyes into the on/off channel states [3].

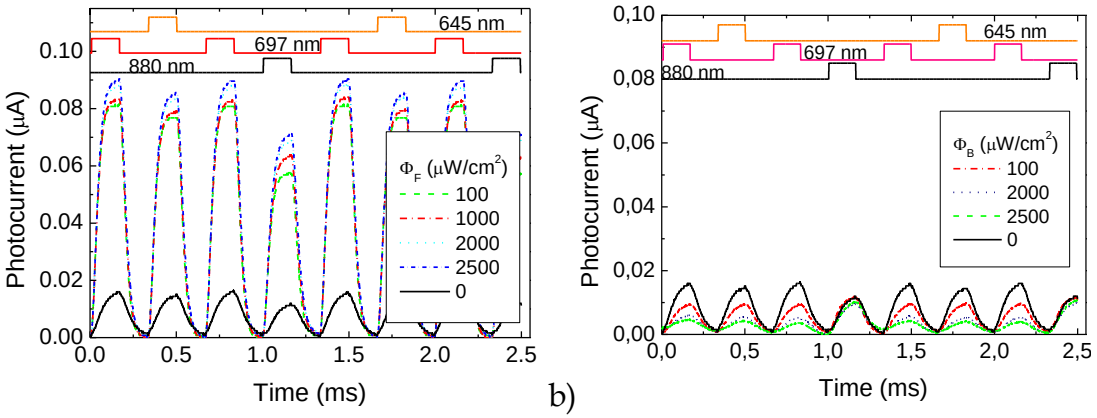

Figure 3-34 - Front (a) and back (b) spectral photocurrent signal using λ=390 nm irradiation at different intensities.

As expected from Figure 3-12, in the red/infrared spectral ranges, the optical gain depends on optical bias intensity and on the wavelength of the input channels. Results show that, even under transient conditions and using commercial visible and NIR LEDs, the background side and intensity alters the signal magnitude of the input channels. Under front irradiation, as the light flux increases, the magnitudes of all the input channels increases being higher at 697 nm then at 645 nm or 880 nm. Under back irradiation, as the flux intensity increases the magnitude of the channels decreases, quickly in the visible range and stays almost constant in the infrared range. This nonlinearity provides the possibility for selective tuning of the visible and IR wavelengths allowing their recognition. In Table 3-2 the optical gains for the individual input channels are displayed under front (α_F) and back (α_B) irradiation. In Figure 3-35, the MUX signals due to the combination of the same wavelength channels but under two different bit sequences are displayed, under front and back irradiation. The signals were normalized to their values without background. In Figure 3-35a)

none of the channels are simultaneously on while in Figure 3-35b) an overlap between the 880 nm and the 697 nm channels occurs [3].

Table 3-2 - Optical gains under front and back irradiation.

Input channel (nm)	645	697	880
α_F	4.0	5.0	3.7
α_B	0.3	0.3	0.8

Results show that by shining 390 nm light, separately, from both sides and using appropriate intensity, it is possible to tune different wavelengths in the VIS-NIR range.

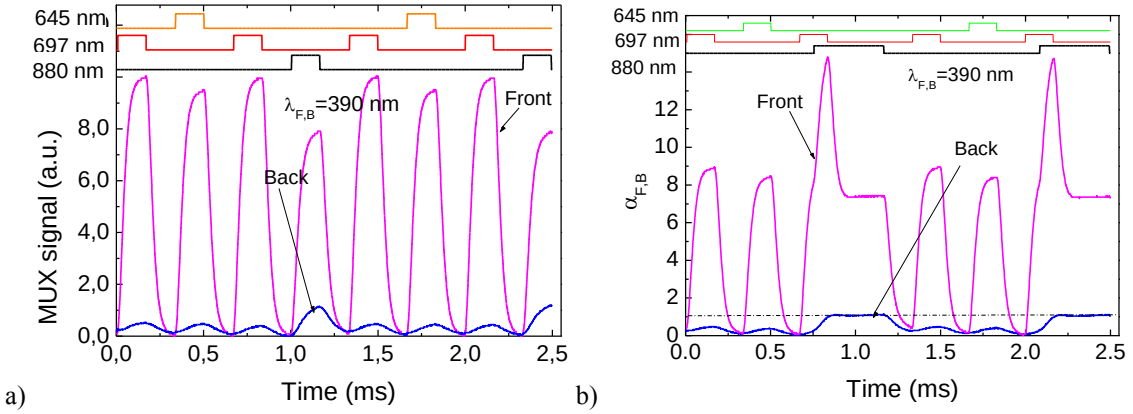

Figure 3-35 - Front and back MUX signals under front and back λ=390 nm irradiation and different bit sequences.

Under front and back irradiation the gain of the three input channels is different ($\alpha_{F,B}$, Table 3-2). This nonlinearity allows identifying the different input channels in a narrow red/infrared range. Near-UV radiation is absorbed at the beginning of the front diode and, due to the self-bias effect, increases the electric field at the back diode where the red/infrared incoming photons (see Figure 3-3) are absorbed accordingly to their wavelengths (see Figure 3-12) resulting in an increased collection. Under back irradiation the electric field decreases mainly at the i-n back interface quenching the red input signals. The infrared signal stays near its value without back bias. This effect may be due to the increased absorption under back irradiation (Figure 3-3) that increases the number of carriers generated by the infra-red photons. So, by switching between front to back irradiation the photonic function is modified from a long-

to a band-pass filter, alternately selecting the red or the infrared channels, making the bridge between the visible and the infrared regions [3].

3.9.3 Bridge between Red and Near Infrared WDM

The spectral sensitivity under different front and back backgrounds intensities was analysed [18] through spectral response measurements (see Section 3.1), and the optical gain (α), is displayed in Figure 3-3 and Figure 3-12, where the background intensity (φ) was changed between 5μWcm^{-2} and 3800 μWcm^{-2}.

Results show that the optical gains have opposite behaviour under front and back irradiations. Under front irradiation (Figure 3-12c) and low flux, the gain is high in the infrared region, presents a well-defined peak at 750 nm and strongly quenches in the visible range. As the power intensity increases the peak shifts to the visible range and the spectral sensitivity can be deconvoluted into two peaks, one in the red range that slightly increases with the back-ground intensity and another, in the green range, that strongly increases with it. In the blue range the gain is much lower. This shows the controlled long-pass filtering properties of the device. Under back bias (Figure 3-12d) the gain in the blue/violet range is high and has a maximum near 420 nm even at low intensities. It strongly lowers between 450 nm and 700 nm, acting as a short-pass filter in the visible range. Also, in the infrared the gain is higher than in the visible range. Thus, back irradiation, tunes the violet/blue region of the visible spectrum whatever the flux intensity, while front irradiation and depending on the back-ground intensity selects the infrared or the visible spectral ranges; low fluxes select the near infrared region and cuts the visible one, the reddish part of the spectrum is selected at medium fluxes, and high fluxes tune the red/green ranges.

Several monochromatic pulsed lights separately (880 nm, 697 nm, 626 nm, 524 nm, 470 nm, 400 nm; input channels) or combined (MUX signal) illuminated the device at 12000 bps. Steady state 390 nm optical bias with different intensities was superimposed separately from the back and front sides and the photocurrent measured. For each individual channel the photocurrent gain under irradiation was determined. In Figure 3-36 these gains are displayed

as a function of the background lighting under front (lines) and back (symbols) irradiation.

Three monochromatic pulsed lights separately (645 nm, 697 nm, and 880 nm input channels) or combined (MUX signal) illuminated the device at 12000 bps. Steady state 390 nm bias (5 $\mu Wcm^{-2} < \varphi_F, B < 3000\ \mu Wcm^{-2}$) were superimposed separately from both sides and the photocurrent was measured. The intensity driving the LEDs was adjusted to give the same intensities without applied optical bias.

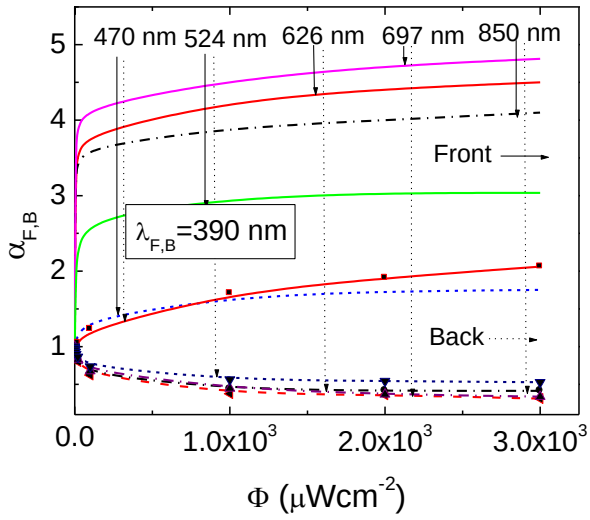

Figure 3-36 - Front and back optical gain at λ=390 nm irradiation and different input wavelengths.

Results show that the gain depends mainly on the channel wavelength and to some extent on the lighting intensity. Even across narrow bandwidths, the photocurrent gains are quite different. This nonlinearity allows identifying the different input channels in the visible/infrared ranges [19].

3.9.4 Visible and Infrared tuning

Three monochromatic pulsed lights separately (645 nm, 697 nm, and 880 nm input channels) or combined (MUX signal) illuminated the device at 12000 bps. Steady state 390 nm bias (5 $\mu Wcm^{-2} < \varphi_F, B < 3000\ \mu Wcm^{-2}$) were superimposed separately from both sides and the photocurrent was measured. The intensity driving the LEDs was adjusted to give the same intensities without applied optical bias.

In Figure 3-37 the multiplexed signals are presented under front and back irradiations. On top, the signals used to drive the input channels are shown to guide the eyes into the on/off channel states.

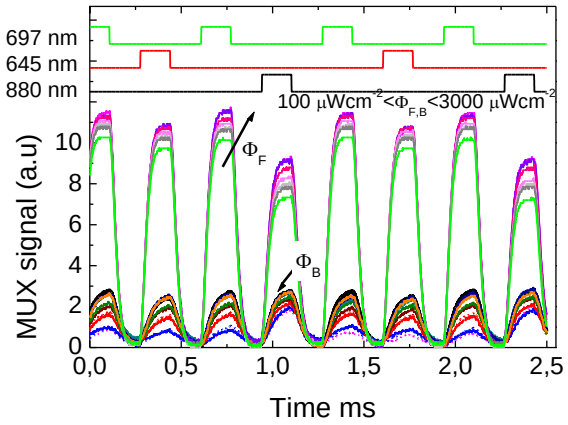

Figure 3-37 - Front and back spectral photocurrents at λ=390 nm irradiation and different intensities.

As expected from Figure 3-36, in the red/infrared spectral ranges, the optical gain depends mainly on the wavelength of the input channels and on the optical bias side. Using commercial visible and infrared LEDs, the background side and intensity alters the signal magnitude of the input channels [19].

Under front irradiation, as the light flux increases, the magnitude of all the input channels increase being higher at 697 nm than at 645 nm or 880 nm. Under back irradiation, as the flux intensity increases the magnitude of the channels decreases, in a fast way in the visible range and very slowly in the infrared range. This nonlinearity provides the possibility for selective tuning of the visible and infrared wavelengths allowing channel recognition. In Figure 3-38, the MUX signals due to two possible combinations of 697 nm, 645 nm and 880 nm input channels with different bit sequences are displayed, under front and back 3000 μWcm^{-2} irradiation. The driving signals are displayed on the top of the figures [19].

Under front and back irradiation the gains of the three input channels are different ($\alpha_{F,B}$, Figure 3-36 and Figure 3-37). This nonlinearity allows identifying the different input channels in a slight red/infrared range. The 390 nm background is absorbed at the top of the front diode and, due to the self-bias effect, increases the electric field at the back diode where the red/infrared

incoming photons are absorbed according to their wavelengths, resulting in an increased collection (α_{697}=4.1, α_{645}=3.7, α_{880}=3.2).

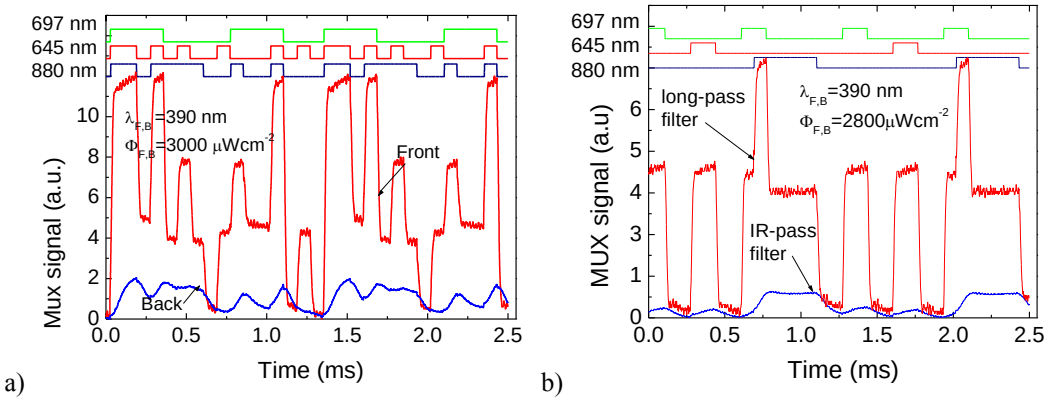

Figure 3-38 - Front and back MUX signals under front and back λ=390 nm irradiation and different bit sequences.

Under back irradiation the electric field decreases mainly at the back diode quenching the red input signals ($\alpha_{645,\ 697}$=0.27) The infrared signal is less reduced (α_{880}=0.65). This different behaviour in the infrared range may be due to the increased absorption under back irradiation (Figure 3-3b) that increases the number of carriers generated by the infra-red photons. So, by switching between front to back irradiation the photonic function is modified from a long- to an IR-pass filter, allowing alternately the selection of the red or the infrared channels and making the bridge between the visible and the infrared regions [19].

3.10 Summary

The pi'npin device is a sensor constituted by two stacked pin structures (p(a-SiC:H)-i'(a-SiC:H)-n(a-SiC:H)-p(a-SiC:H)-i(a-Si:H)-n(a-Si:H)) sandwiched between two transparent contacts one at each end of the tandem structure.

The device deposited over a glass substrate allows the structure to be illuminated on both sides; the front surface which is in direct contact with the glass and the back surface which is furthest away from the glass.

Built with different intrinsic layer thicknesses and each pin structure with different elements allows for the depth of absorption of the visible light to

be distinguished in two different ranges, the blue approximately from 400 to 500 nm and the red from 500 to 800 nm.

By setting different electrical polarizations the spectral gain of the mentioned ranges can be changed allowing the sensor to be used as a selective filter.

Fixing the electrical polarization, an equivalent selective filtering can be accomplished by setting an optical bias either at the front surface of the device or at the back surface. This optical bias is a ultra-violet wavelength.

The study of the pi'npin device was directed to the use of a fixed electrical operating point and then changing the bias by using the ultra-violet irradiation on either side of the sensor.

The operating point of the pi'npin device is set at -8 V; inversely polarized. The ultra-violet irradiation uses LED's with wavelengths around 390 nm. The optical bias is a steady state illumination flux.

The front surface is used as the signal input side and allows any number of different wavelengths to impinge upon it. The light sources are LEDs preferably where each LED has a single wavelength in the visible spectrum. Study with signal LEDs in the ultra-violet (390 and 400 nm) and near infra-red wavelengths (700, 850 and 875 nm) was also made.

The sensor presents different gains at each wavelength. The gain is defined as the ratio between the photocurrent with and without a specific background illumination.

The difference in gains helps the identification of a selected wavelength. The most used wavelengths in the study were the ultra-violet (390 and 400 nm), blue (470 nm), green (524 nm) and red (626 nm).

The background illumination at the front side enhances the gain of wavelengths in the 500 to 800 nm range and quenches those in the 400 to 500 nm. The opposite occurs when the background illumination of the device is at the back; the wavelengths 500 to 800 nm are quenched and those in the 400 to 500 nm range are enhanced.

The device also shows an enhanced gain in the near infra-red range (700 to 900 nm) for low flux illumination of the front background with ultra violet (390 nm) lighting.

The non linear spectral gain allows the combination of three different wavelengths (626, 524 and 470 nm) in a multiplexer configuration producing the dark signal. The combination can then be recovered using the back and front illumination of the backgrounds. The data rate shows better results at 4000 bps, and at other rates used in the experiments 6000 bps and 12000 bps it is still possible to recover the signals.

An optoelectronic model has been updated since it was generated by the different setups used, and the simulation results are coherent with the experimental results.

3.11 References

[1] M. Vieira, P. Louro, M. Fernandes, M. A. Vieira, Q. Torre, and M. Caparica, "Three Transducers Embedded into One Single SiC Photodetector : LSP Direct Image Sensor , Optical Amplifier and Demux Device," in *Advances in Photodiodes*, vol. March Ch19, G. F. D. Betta, Ed. Intech, 2011, pp. 403–426.

[2] G. De Cesare, F. Irrera, F. Lemmi, F. Palma, and M. Tucci, "a-Si:H/a-SiC:H Heterostructure for Bias-Controlled Photodetectors," *MRS Proc.*, vol. 336, p. 885, Feb. 2011.

[3] M. Vieira, M. A. Vieira, V. Silva, I. Rodrigues, and P. Louro, "Near-UV background as a bridge between visible and infrared communication," *MRS Proc.*, 2014.

[4] M. A. Vieira, M. Vieira, P. Louro, V. Silva, and A. Fantoni, "Integrated photonic filters based on SiC multilayer structures," *Appl. Surf. Sci.*, vol. 275, pp. 185–192, Jun. 2013.

[5] M. A. Vieira, M. Vieira, J. Costa, P. Louro, M. Fernandes, and A. Fantoni, "Double Pin Photodiodes with Two Optical Gate Connections for Light Triggering.," *Sensors & Transducers*, vol. 10, no. Special issue, pp. 96–120, 2011.

[6] M. A. Vieira, M. Vieira, P. Louro, V. Silva, and A. S. Garção, "Photodetector with integrated optical thin film filters," *J. Phys. Conf. Ser.*, vol. 421, p. 012011, Mar. 2013.

[7] A. Fantoni, M. Vieira, and R. Martins, "Simulation of hydrogenated amorphous and microcrystalline silicon optoelectronic devices," *Math. Comput. Simul.*, vol. 49, no. 4–5, pp. 381–401, Sep. 1999.

[8] A. S. Ferlauto, G. M. Ferreira, J. M. Pearce, C. R. Wronski, R. W. Collins, X. Deng, and G. Ganguly, "Analytical model for the optical functions of amorphous semiconductors and its applications for thin film solar cells," *Thin Solid Films*, vol. 455–456, pp. 388–392, May 2004.

[9] M. Vieira, M. A. Vieira, P. Louro, A. Fantoni, and V. Silva, "Reconfigurable SiC Embedded Photonic Structures with Self Optical Bias Control," *Plasmonics*, vol. 8, no. 1, pp. 45–51, Sep. 2012.

[10] M. Vieira, M. A. Vieira, P. Louro, V. Silva, and J. Costa, "SiC multilayer add/drop filter for optical interconnects," *MRS Proc.*, vol. 1559, pp. mrss13–1559–aa02–06, May 2013.

[11] M. A. Vieira, M. Vieira, P. Louro, V. Silva, J. Costa, and A. Fantoni, "SiC Multilayer Structures as Light Controlled Photonic Active Filters," *Plasmonics*, vol. 8, no. 1, pp. 63–70, Aug. 2012.

[12] V. Silva, M. A. Vieira, P. Louro, and M. Vieira, "Optoelectronic digital capture device based on Si/C multilayer heterostuctures," in *Technological Innovation for the Internet of Things*, Springer Berlin Heidelberg, 2013, pp. 555–562.

[13] V. Van, T. A. Ibrahim, K. Ritter, P. P. Absil, F. G. Johnson, R. Grover, J. Goldhar, and P.-T. Ho, "All-optical nonlinear switching in GaAs-AlGaAs microring resonators," *Photonics Technol. Lett. IEEE*, vol. 14, no. 1, pp. 74–76, 2002.

[14] M. A. Vieira, M. Vieira, V. Silva, P. Louro, and M. Barata, "Error control on spectral data of four-wave mixing based on a-SiC technology," *Phys. status solidi*, Jan. 2015.

[15] M. A. Vieira, "Three Transducers for One Photodetector: essays for optical communications," FCT-UNL Universidade Nova de Lisboa, 2012.

[16] M. A. Vieira, M. Vieira, P. Louro, M. Fernandes, A. Fantoni, and M. Barata, "Voltage Controlled Amorphous Si/SiC Phototransistors and Photodiodes as Wavelength Selective Devices: Theoretical and Electrical Approaches," *MRS Proc.*, vol. 1153, pp. 1153–A08–03, Jan. 2011.

[17] V. Silva, I. Rodrigues, M. A. Vieira, P. Louro, and M. Vieira, "Increased sensitivity in a-SiC pinpin multilayers in the VIS-NIR range under UV light," *MRS Proc.*, 2014.

[18] M. A. Vieira, P. Louro, M. Vieira, A. Fantoni, and A. Steiger-Garcao, "Light-Activated Amplification in Si-C Tandem Devices: A Capacitive Active Filter Model," *IEEE Sens. J.*, vol. 12, no. 6, pp. 1755–1762, Jun. 2012.

[19] M. Vieira, M. a. Vieira, I. Rodrigues, V. Silva, and P. Louro, "Tuning optical a-SiC/a-Si active filters by UV bias light in the visible and infrared spectral ranges," *Phys. Status Solidi Curr. Top. Solid State Phys.*, vol. 2, no. 11–12, pp. 1674–1677, Nov. 2014.

4

4 Multiplexer

Communication involves the transmission and reception of data that both receiver and transmitter understand. The communication channel between the receiver and transmitter may have characteristics that do not allow the data to be transmitted just as it is. The data may suffer a transformation prior to transmission (encoding) and then at the receiver an inverse transformation must be applied (decoding) to retrieve the original data. Several transformations may be applied, so the data may de encoded several times through different algorithms and at different stages of the transmission. The successful reception of the data obliges to equivalent decoding and in the reverse order of their application. There are many different encoding/decoding algorithms which have direct influence on the bandwidth of the signals and the total size of encoded data. Encoding may be made at the physical media, like modulation, or at the higher levels of communication as encryption [1].

Communication media have bandwidths that are much higher than the bandwidth of a single signal. To increase the communication efficiency several signals are sent through the same media. Multiplexing is a technique used to include two or more signals into the same media. Demultiplexing is the inverse technique that retrieves one or more channels from that media. Multiplexing

and demultiplexing can be made by dividing time into slots in which each channel is transmitted, TDM (Time Division Multiplexing), or by dividing the frequency spectrum, with each signal allocated into a different bandwidth, FDM (Frequency Division Multiplexing), or using different wavelengths for each signal, WDM (Wavelength Division Multiplexing) [2].

Light-emitting Diode (LED) is a very effective lighting technology due to its high brightness, long life, energy efficiency, durability, affordable cost, optical spectrum and its colour range for creative use. Their use as communication devices with a photo-diode as receptor has been used for many years in hand held devices to control televisions and other media equipment and with higher rates between computational devices [3]. This communication path has been used in the near infra-red (NIR) range but due to the increasing LED lighting in homes and offices the idea to use them for visible light communications (VLC) is present in many working groups. The IEEE (Institute of Electrical and Electronics Engineers) task group 7 has come up with the IEEE 802.15.7 VLC PHY/MAC standard proposal for the physical (PHY) and medium access control (MAC) for VLC communications [4]. The Internet use and its most popular protocols also have been studied for their performance over VLC [5]. Economic issues that will eventually guide the VLC outcome are also on the run [6].

This section uses LEDs modulated by digital data signals that are multiplexed and demultiplexed using the p'inpin sensor.

4.1 WDM working principle

4.2 The multiplexing and demultiplexing device

In Figure 4-1 the device configuration is depicted in both multiplexing (a) and demultiplexing (b) modes. Here, multiple monochromatic (Figure 4-1a) or a single polychromatic (Figure 4-1b) beams are directed to the device where they are absorbed, accordingly to each wavelength, giving rise to a time and wavelength dependent electrical field modulation across it [7].

In the multiplexing mode the device faces the modulated light incoming together from the fibres, each with a wavelength in a specific range (R, G, B channels). The combined effect of each input channel is then converted to an electrical signal via the WDM device Figure 4-1a) keeping the data of the input channels (wavelength and bite rate) [8], [9].

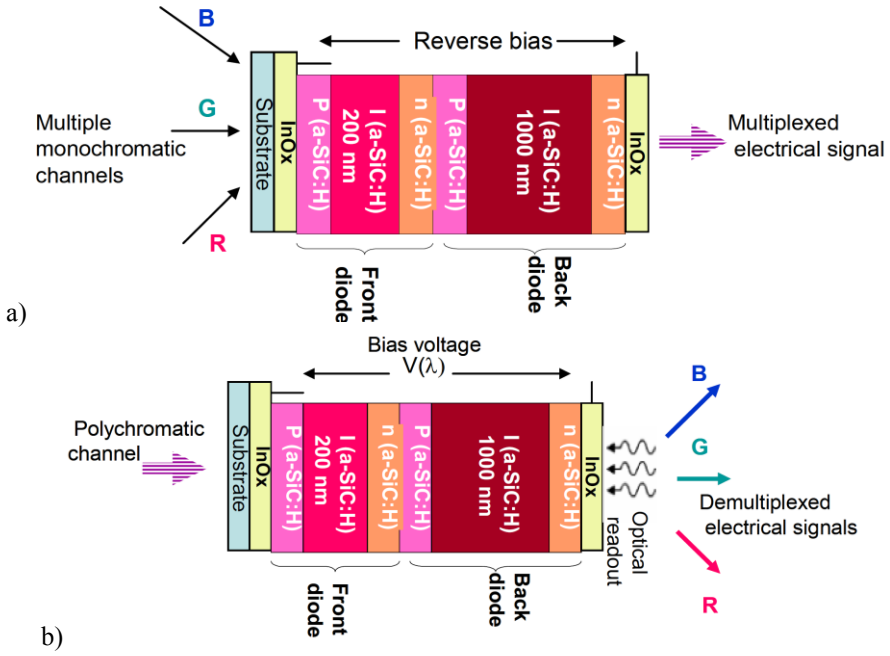

Figure 4-1 – WDM device configuration a) Multiplexing mode b) Demultiplexing mode.

In the demultiplexing mode a polychromatic light beam (mixture of different wavelength) is projected onto the device and the signal measured at appropriated applied voltages. Here, the spectral sensibility of the device is voltage controlled allowing the recognition of the RGB channels Figure 4-1b) [10].

4.3 WDM operation

Figure 4-2 displays the spectral photocurrent, measured along the visible spectrum, under reverse bias without and with optical light bias focusing the device from the front side.

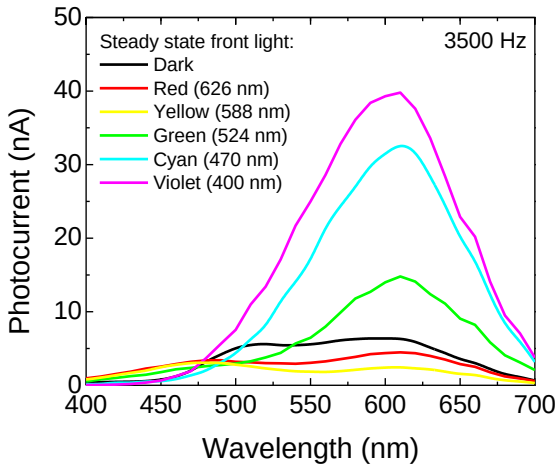

Figure 4-2 - Spectral photocurrent under dark conditions and using steady state light of different wavelengths by the device front side.

Results of Figure 4-2 show that the use of steady state light bias from the front side, i.e., from the a-SiC:H structure, enhances the photocurrent in the range of wavelengths longer than 500 nm when using background light of short wavelength (400 nm, 470 nm and 524 nm). For optical bias of longer wavelengths (588 nm and 624 nm) the photocurrent signal is decreased. On the remaining part of the spectrum an opposite behaviour is observed as the amplification effect occurs for longer light bias wavelengths and the reduction

of the signal for shorter wavelengths. Thus, the use of a short wavelength light source as optical bias amplifies both green and red optical channels.

The enhancement of the photocurrent signal using different optical bias for the background light result is an effective method for tuning the device sensitivity and detecting the input optical channels [11].

4.3.1 Back steady state optical bias

Figure 4-3 displays the spectral photocurrent using back steady state illumination of several wavelengths at different optical intensities. For comparison the spectral photocurrent (right axis) of the individual front and back, hererostructures (dash lines) are superimposed, in order to show their optical filter behaviour in the blue and red spectral regions. The front diode, based on a- SiC:H, cuts the red component of the spectrum while the back one, based on a-Si:H, cuts the blue component.

Under back steady state optical bias the observed photocurrent curves show for every wavelength a similar trend, which shows that the optical biasing from the back side (a-Si:H) is not so much dependent on the background light wavelength. Generally, in the range of wavelengths shorter than 480 nm it is observed an increase of the signal for every background, and a decrease in the complimentary range.

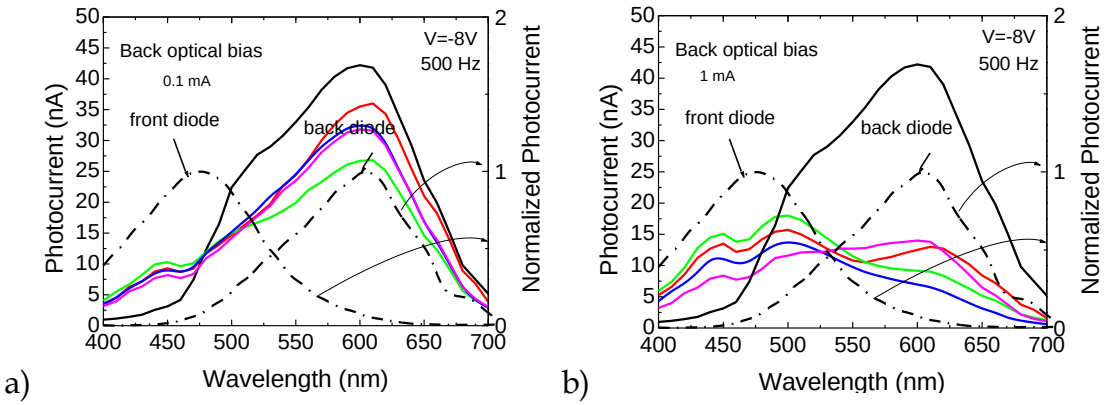

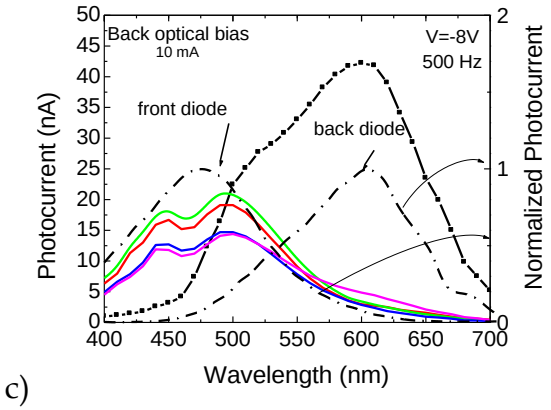

c)

Figure 4-3 - Spectral photocurrent using back steady state illumination of several wavelengths at different optical intensities.

The main difference occurs with the variation of the background light optical intensity. For low optical power (Figure 4-3a) the photocurrent is similar to the measured output signal measured without any background light, showing however an increased value in the short wavelength range (400-470 nm). When the optical power of the background light increases (Figure 4-3b) the photocurrent increases in the short wavelength range and decreases in the long wavelength region. For high optical power values of the background light (Figure 4-3c) this trend moves to the enhancement of the sensitivity in the short wavelength range and to the extinction of the signal in the long range. This trend suggests a change in the operating device heterostructure. The use of high intensity back steady state light actuates the front photodiode and the response is mainly confined to the short wavelength range. At the same time the back photodiode stops working and the signal in the long wavelength range is strongly decreased [11].

4.3.2 Transient input signals

The analysis of the transient device response used three monochromatic waveform optical signals (red, green and blue input channels) that illuminated the device from the front side (see Figure 3-1). Optical bias was also used to soak uniformly the device separately from the back and front sides of the device.

The device was reverse biased (-8 V). In Figure 4-4 the transient signals of each individual channel without and with front and back background illumination are plotted.

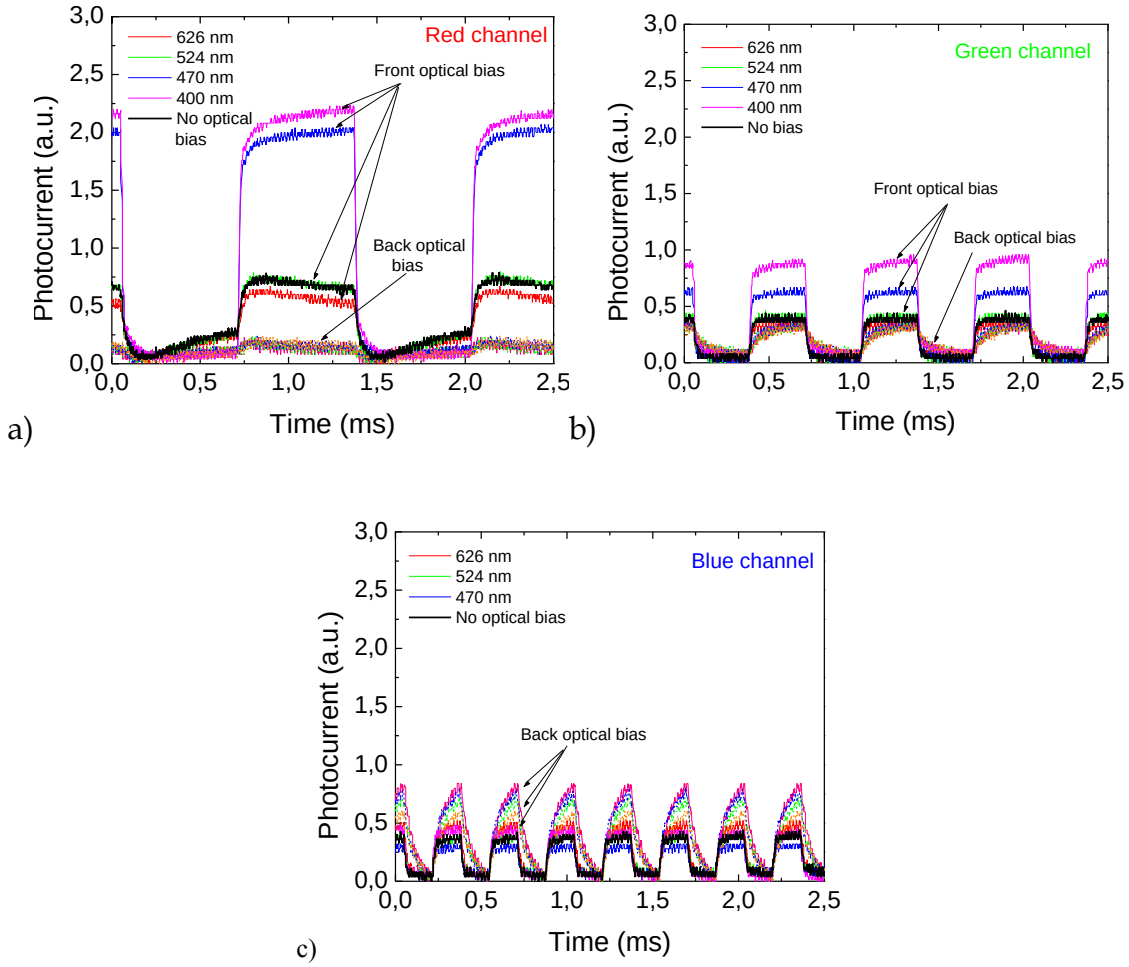

Figure 4-4 - Red, green and blue transient input signals under front and back optical bias of different wavelengths.

As predicted from spectral response data (Figure 4-2 and Figure 4-3) the red channel (Figure 4-4a) at 624 nm (long wavelength range) is strongly enhanced under front short wavelength optical bias (400 nm and 470 nm). Under back optical bias the red channel is strongly reduced for any wavelength of the impinging light. In the green channel (Figure 4-4b) a similar trend is observed although with a smaller amplification factor. In the blue channel (Figure 4-4c) a different trend is observed as the most important effect for the

amplification of the signal is the use of back optical bias instead of front illumination, as happened for the red and green channels.

This different transient response of the input channels under different optical bias conditions allows the decoding of the input signals. Thus the use of a short front wavelength for the optical bias (400 nm) will strongly amplify the red channel, produce an increase in the green channel and make no effect on the blue channel. On the other hand, if the same wavelength light is used from the back side this will result in amplification of the blue channel and attenuation of the red channel, while the green channel will not be modified [11].

4.3.3 Transient mux signal

In order to test the decoding performance of the device using violet (400 nm) front and back optical bias, different combined red, green and blue optical waveform signals were used.

Figure 4-5 displays the transient multiplexed signal under reverse bias using different optical bias conditions during the signal acquisition process: no optical bias (dark line), and front violet (violet line) and back violet light (cyan line) for the steady state light.

The output multiplexed signal, obtained with the combination of the three optical sources, depends on the side of the background illumination and on the ON-OFF state of each input optical channel. In order to decode the input channels both multiplexed signals measured with back and front steady state illumination were divided into several time slots, each corresponding to a different optical state.

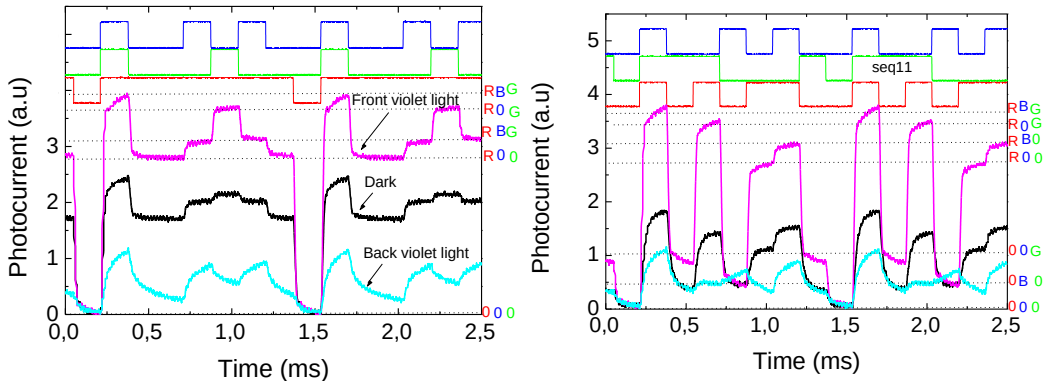

Figure 4-5 - MUX signals acquired without (dark line) and with front (violet lines) and back (cyan lines) violet optical bias using two different combinations of the red, green and blue optical signals.

In the signal measured by the device front side (violet lines in Figure 4-5) the highest levels correspond to the presence of the red input channel, while the lowest ones to its absence. This mechanism allows the immediate recognition of the ON-OFF states for the red channel. Attending to the signal measured with violet illumination from the back side the same logic can be used (cyan lines in Figure 4-5). Here the highest levels are assigned to the presence of the blue input signal and the lowest levels to its lack, which allows the immediate decoding of the blue channel. Thus, both red and blue channels can be immediately tuned by using adequate biasing light for the background. The green channel is ON in the two highest photocurrent thresholds of each measured signal. The integration of the recovery information of each channel allows then the decoding of the whole data transmitted in the multiplexed signal. Using this simple key algorithm the independent red, green and blue bit sequences can be decoded as shown in Figure 4-6, which are in agreement with the signals acquired for the independent channels (Figure 4-5) [11].

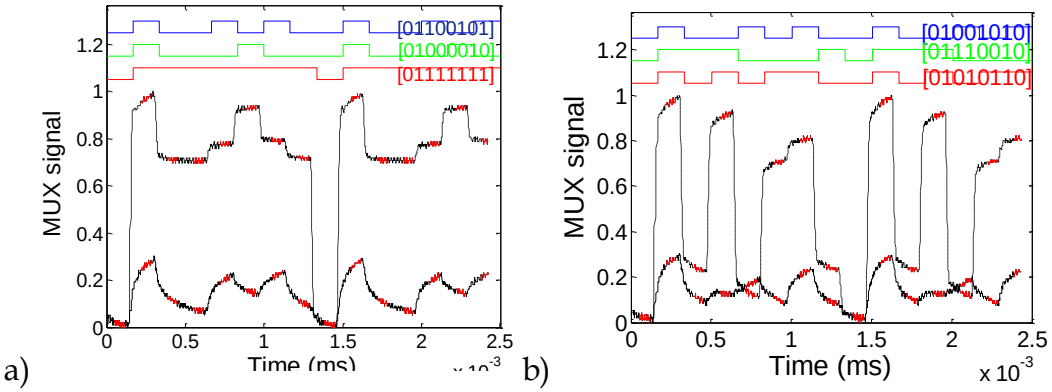

Figure 4-6 - MUX signals under front and back irradiation. On the top the DEMUX signals obtained using the decoder algorithm is displayed as well as the binary bit sequences.

4.4 Add / Drop filters

For an optoelectronic digital capture system, opto-electronic conversion is the relationship between the optical inputs and the corresponding digital output levels. The implementation of a wavelength division multiplexer requires that the channel wavelength may be tailored such that add/drop filters with different spectral locations, may be cascaded. Here, tailoring the filter wavelength is achieved by changing the violet background from the back to the front side.

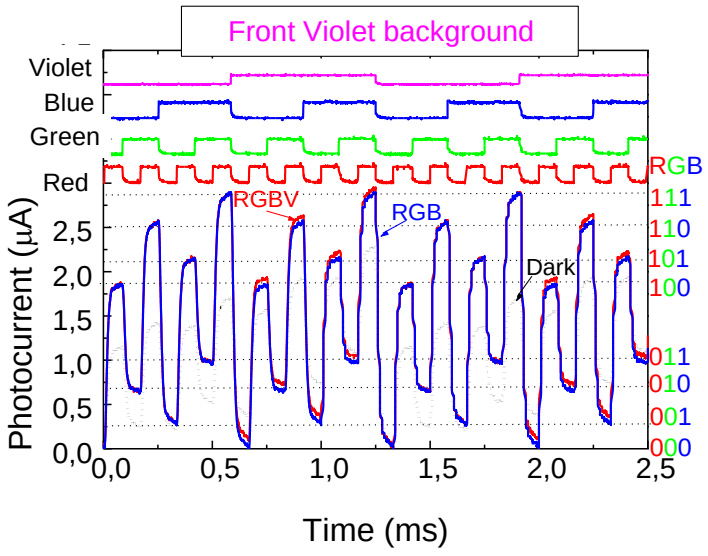

Figure 4-7 - Multiplexed signal under front violet irradiation and without it.

The MUX signals due to the combination of the input channels of Figure 3-21 (R, G, B, V) are displayed without and under front (Figure 4-7) and back (Figure 4-8) violet irradiations. On the top the signals used to drive the input channels are displayed showing the presence of all possible sixteen *on/off* states. To show the backgrounds add/drop filter effect, in Figure 4-7 the RGB and in Figure 4-8 the GBV combined multiplexed signals are shown. Results show that the device is a two tuneable background connected filter and acts as a wavelength selective switch.

Without applied background (dark) sixteen output levels are observed each one corresponding to one of the possible 4-channel *on/off* configurations (16-to-1 multiplexer).

Under applied optical bias, the side that has background illumination affects the form and the magnitude of the MUX signal in opposite ways. Under front irradiation (Figure 4-7) the violet channel quenches, and so, the difference between the multiplex signals with and without the violet channel *on* is irrelevant. This means that under front irradiation the transmission of the violet channel changes from high to low and so, the output signal has only eight separate levels (horizontal dot lines) that can be assigned to the 2^3 *on/off* possible states of an 8-to-1 RGB multiplexer. The levels are weighted by the optical gains of each channel, so, the selection index for this 8-element look-up table (in the right hand-side) is a 3-bit binary [RGB] code. The violet channel was switched to the drop port and the others continue in the transmission line. Under back irradiation the magnitude of the red channel is strongly reduced. The 8-to-1 look up table (dot lines) is clear and the 3-assigned bit binary [VBG] code displayed in the right side of Figure 4-8 [11]. So, the quenching of the red channel drops it to the drop port and the others continue in the transmission line. By using the add/drop SiC based filter a usable portion of the optical visible spectrum can be partitioned into wavelength bands to make signal

separation possible at the receivers. The advantage of optic background tuning lies in its structural simplicity. The front background selects the red channel and drops the violet while the back background adds the violet and drops the red. It provides a low-cost solution in optical and optoelectronic interconnection technologies according to their suitability of adoption in optical cross connections, switches and routers [12].

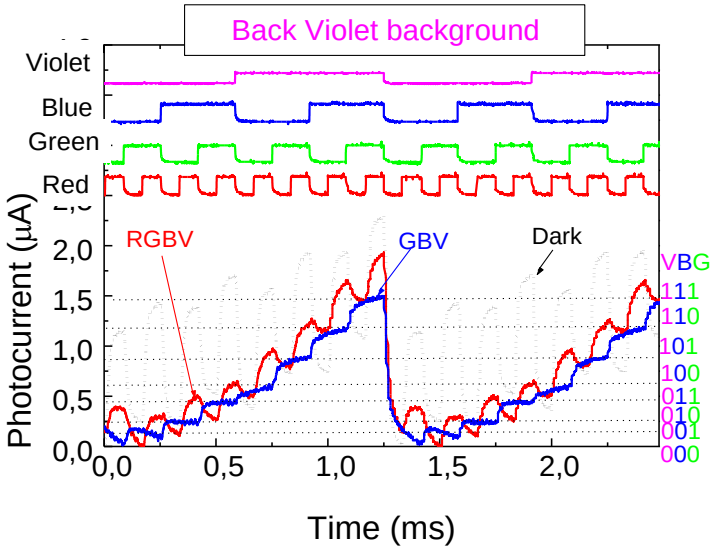

Figure 4-8 - Multiplexed signal under back violet irradiation and without it.

The add/drop filter concept is extended to implement a 1 by 4 WDM. Results have shown that under front or back irradiation, each of the four channels, in turn, is enhanced or quenched. The logic MUX function is converted into a logic filter function and each channel can be decoded as a data signal to be routed to a selected destination. Figure 4-9a) displays the normalized MUX signals due to the combination of the input channels of Figure 3-21. On the top, the signals used to drive the input channels are displayed. Under front irradiation, the 2^4 levels are detected (horizontal dot lines) and grouped into two main classes due to the high amplification of the red channel (Figure 4-9a). The upper eight (2^3) levels are ascribed to the presence of the red channel (R=1), and the lower eight to its absence (R=0), allowing the red channel decoder (8-to-1 multiplexer; long-pass filter function). Since under front

irradiation the green channel is also amplified, the four (2^2) highest levels, in both classes, are ascribed to the presence of the green channel (G=1) and the four lower ones to its lack (G=0). The blue channel is slightly amplified, so, in each group of 4 entries, two subclasses (2^1) can be found: the two higher levels correspond to the presence of the blue channel (B=1) and the two lowers to its absence (B=0). Finally, each group of 2 entries have two very near sublevels, the higher where the violet channels is ON (V=1) and the lower where it is missing (V=0). Under back irradiation, the violet channel is strongly enhanced, the blue channel slightly enhanced and the green and red reduced (Figure 3-21b). The encoded multiplexed signal also has sixteen sublevels but ordered in a different way. Two classes are observed, one composed by the eight higher levels, where the violet channel is ON (V=1) and the other including the eight lower levels where it is OFF (V=0) (8-to-1 multiplexer; short-pass filter function) allowing the violet channel decoder (see bottom of Figure 4-9a)). Each group of eight levels can still be grouped in two classes of four levels each, with and without the blue channel ON. Taking into account Figure 4-8, those four near sublevels are ordered. The higher has both red and green channels ON, the lower both OFF and in-between only one of them is missing, the red or the green [12].

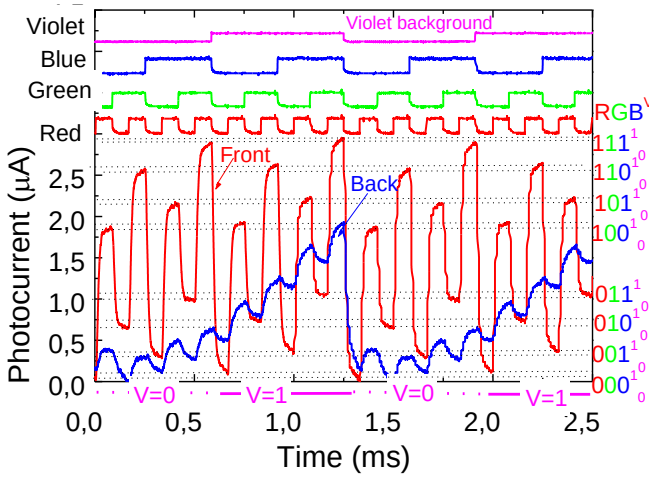

a)

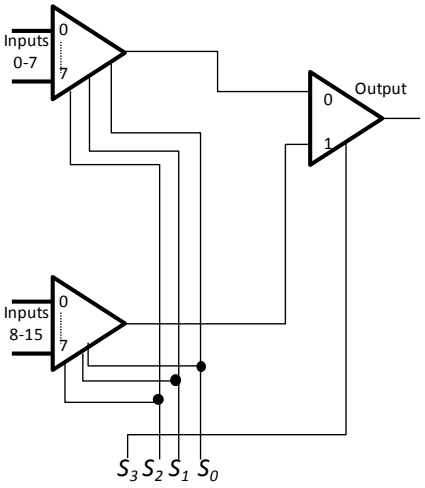

b)

Figure 4-9 - a) Normalized multiplexed signal under front and back violet irradiation. On the top the signals used to drive the input channels are shown. b) Schematic of a pi'npin 16-element table look-up.

The selection index for both 16-element look-up tables is a 4-bit binary code of the form S_3, S_2, S_1, S_0 where Sn means the colour channel and n weights, under front and back irradiations, the bit position though the different amplification factors (see Figure 3-19) . So, the multiplexer select code, under front irradiation, represents an address, *RGBV*, into the ordered inputs while under back irradiation it will be of the form *VBRG*. We may view those 16-element look-up tables, as consisting of two look-ups, one to select the proper group of 8, and pick the red under front irradiation or the violet under back background. Each group of 8 inputs requires 3 bits for picking the proper group of 8 and for specifying an input. In Figure 4-9b) the schematic of the pin/pin a-SiC:H 16-element table look-up is displayed. Here, if S_3=R then the S_2=G, S_1=B and S_0=V; if S_3=V the 4-bit binary code will be *VBGR*. By using both look-up tables any multiplex signal can be decoded [12].

4.5 Encoder / Decoder

Four monochromatic pulsed lights, separately (R, G, B and V input channels) illuminated the device at 12000 bps. Steady state violet optical bias was superimposed separately from the front (Figure 4-10a) and the back (Figure

4-10b) sides and without it and the photocurrent measured at -8 V. The signals were normalized to their values without applied background. The optical gain (amplification factor) for the four individual channels ($\alpha^{V}_{R,G,B,V}$) under front and back irradiation are also displayed [13].

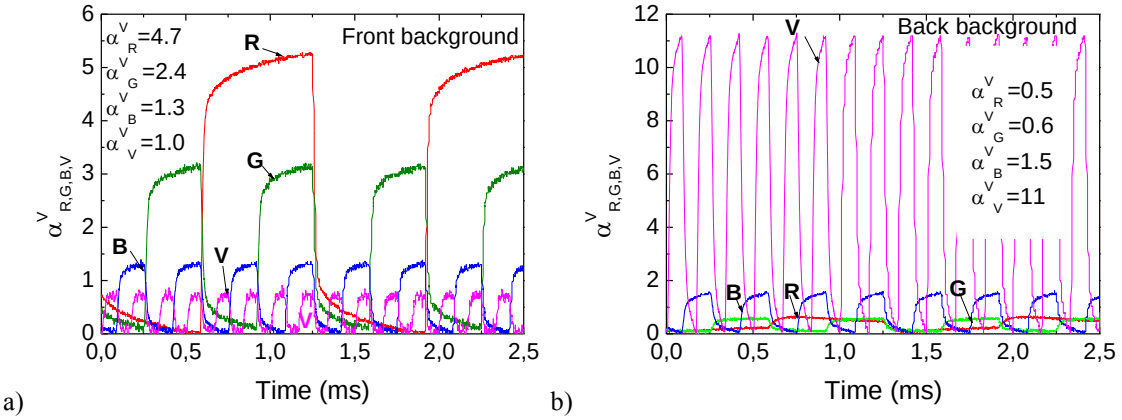

Figure 4-10 - Red (R), green (G), blue (B) and violet (V) input channels, under violet optical bias applied from the front (a) and from the back (b) sides and normalized to their values without background.

Results show that, even under transient conditions and using commercial LEDs as pulsed light sources, the background side affects the signal magnitude of the colour channels. As shown in Figure 3-16 and Figure 3-17, under front irradiation, it enhances mainly the spectral sensitivity in the medium-long wavelength ranges (α^{V}_{R}=4.7, α^{V}_{G}=2.4). Violet radiation is absorbed at the top of the front diode, increasing the electric field at the back diode [14] where the red and part of the green incoming photons are absorbed (see Figure 3-1). Under back irradiation the electric field increases mainly near the front p-i' interface where the violet and part of the blue incoming channels generate most of the photocarriers (α^{V}_{V}=11, α^{V}_{B}=1.5). So, by switching between front to back irradiation the photonic function is modified from a long- to a short-pass filter alternately selecting the red or the violet channels [13].

Four combined monochromatic pulsed lights (multiplexed signal, Figure 4-11) illuminated the device at 12000 bps. Steady state violet optical bias was superimposed separately from the back and the front sides and the photocurrent was measured [13].

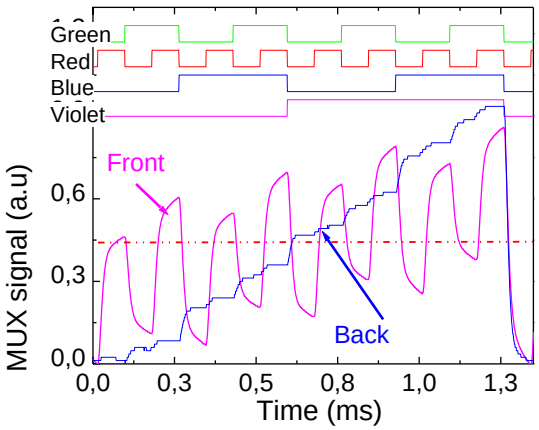

Figure 4-11 - Multiplexed signal under front and back violet irradiation. On the top the signals used to drive the input channels are shown to guide the eyes into the ON/OFF channel states.

Results show that, even under transient conditions and in the presence of several channels simultaneously, the side of the background affects the form and the magnitude of the MUX signal in opposite ways [15]. Under front and back irradiation, sixteen levels (2^4) are detected and grouped into different subgroups due to the different gains of the same colour channel under front and back irradiations (see arrows in Figure 4-11). The dash-dot line is the threshold for both. Under front irradiation the eight upper levels are ascribed to the presence of the red channel ON and the lowers to its absence, while under back irradiation the higher eight corresponds to the presence of the violet channel ON and the lower to its lack. This allows, respectively, the decoding of the red and violet channels (8-to-1 multiplexer; long- and short-pass filter functions). As under front irradiation the green channel is amplified ($\alpha^{V}_{G}>1$), the blue channel stays in its value, and the violet is almost suppressed. Under back illumination the blue channel is enhanced and the green and red are reduced ($\alpha^{V}_{B}>1$ and α^{V}_{R} and $\alpha^{V}_{G}<1$). It is then possible to ascribe a specific weight assigned to each bit position [16]. Due to the different optical gains (Figure 4-10), the selection index for those ordered 16-element is a 4-bit binary [RGBV] code under front irradiation or a 4-bit binary [VBGR] under violet illumination. The multiplexer select code represents an address or index, into the sixteen ordered inputs [13].

4.5.1 CODER/DECODER DEVICE

In Figure 4-12, the MUX signals due to the combination of the red, green, blue and violet visible input channels is displayed under front and back irradiations. On top the signals used to drive the input channels are also displayed. Figure 4-12a) shows the normalized MUX signals due to the combination of all the sixteen possible input channels.

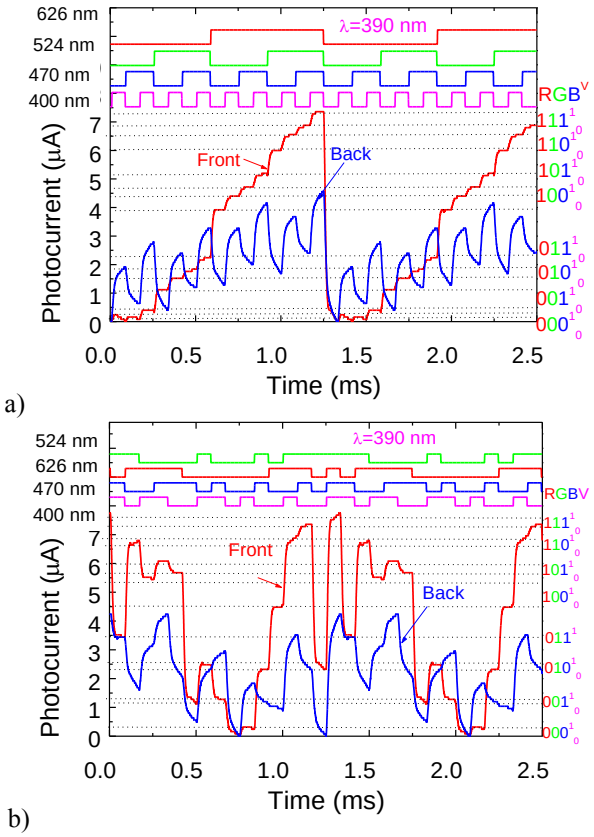

Figure 4-12 - MUX/DEMUX signals under 390 nm front and back UV irradiation and decoded RGBV binary bit sequences. On top the signals used to drive the input channels are shown.

In Figure 4-12b) a random combination is presented to test the decoding methodology. Under front or back irradiation, each of those four channels, by turn, is enhanced or quenched (see Figure 3-12). So, 2^4 ordered levels are detected (horizontal dotted lines) and grouped into two main classes due to the high amplification of the red channel (α_{626}=5.5). The upper eight (2^3) levels are ascribed to the presence of the red channel (R=1), and the lower eight to its absence (R=0), allowing to decode the red channel. Since under front irradiation

the green channel is also amplified (α_{524}=2.5) the four (2^2) highest levels, in both classes, are ascribed to the presence of the green channel (G=1) and the four lower ones to its lack (G=0). The blue channel is slightly amplified (α_{470}=1.1). So, in each group of 4 entries, two subclasses (2^1) can be found: the two set of higher levels correspond to the presence of the blue channel (B=1) and the two lowers to its absence (B=0). Finally, each group of 2 entries have two very near sublevels, the higher where the violet channels is ON (V=1) and the lower where it is missing (V=0). In the right side of the figure the sixteen RGBV sublevels are inserted. Under back irradiation, the violet channel is strongly enhanced, the blue channel slightly and the green and red reduced (Figure 3-12b). So, from the front and back information the different bit sequences were decoded and the signal demultiplexed [7].

4.5.2 MUX/DEMUX devices

Based on the above explained filtering properties of the device and the different gains for the RGB channels (Table 3-1), a decoding algorithm was implemented in Matlab and tested [17].

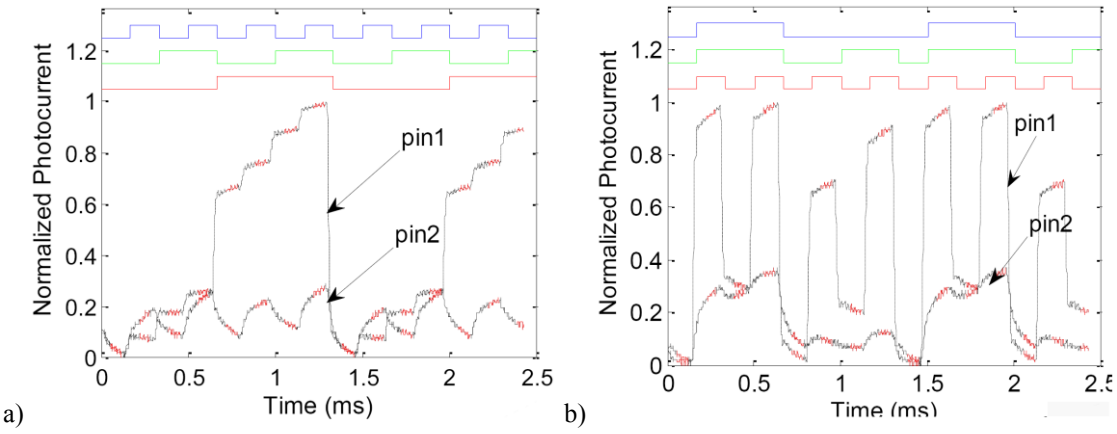

Figure 4-13 - MUX/DEMUX signals under front (pin1) and back (pin2) irradiation.

In all tested sequences the RGB signals were correctly decoded, as exemplified in Figure 4-13. Here, on the top the DEMUX signals obtained using the decoder algorithm are displayed. The correspondent binary bit sequences

are in agreement with the optical signal used to transmit the information (Figure 3-21).

Results show that by means of violet optical bias control, the MUX photonic function may be modified, giving reconfiguration. This new method, based on wavelength background processing techniques enables the optical routing [17].

4.6 Four channel WDM

To analyze the device under information-modulated wave and uniform irradiation, four monochromatic pulsed lights, separately (red, green, blue and violet input channels; R, G, B, V) illuminated the device at 6000 bps. Steady state violet optical bias was superimposed separately from the front (Figure 4-14a) and the back (Figure 4-14b) sides and the photocurrent generated measured at -8 V. In both figures the signals, without applied optical bias, are shown. The ratio between the photocurrents with and without background (amplification factor) for the four individual channels ($\alpha_{R\ front}$, $\alpha_{G\ front}$, $\alpha_{B\ front}$, $\alpha_{V\ front}$) are also displayed.

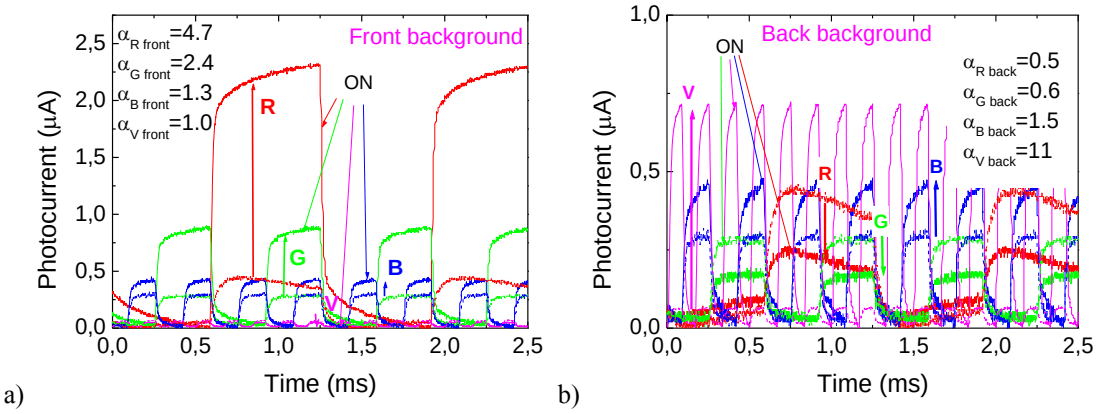

Figure 4-14 - Red (R), green (G) and blue (B) and violet (V) input channels, at -8V, without and under violet steady state optical bias (ON) applied from the front side (a) and from the back side (b).

Results show that when steady state irradiation is imposed the output photocurrent due to the input signals exhibits a nonlinear dependence on the wavelength. Under front irradiation, the light-to-dark sensitivity is enhanced mainly in the long- medium wavelength ranges. Violet radiation is absorbed at the top of the front diode, increasing the electric field at the least absorbing cell [14], the back diode, where the red and part of the green channels generate optical carriers. So, red and green collection are strongly enhanced (α_{Rfront}=4.7, α_{Gfront}=2.4), the blue lightly increases (α_{Bfront}=1.3) and the violet one stays near its dark value (α_{Bpin1}=1.0). Under back irradiation, the small absorption depth of the violet photons in the back diode enhances the electric field at the front diode and so, the red and green collections are reduced (α_{Rback}=0.5, α_{Gback}=0.6). The violet and the blue channels are absorbed across the front diode resulting in an increase collection for the blue (α_{Bback}=1.5) and enormous increase for the violet (α_{Vback}=11.0) since its absorption occurs near the front p-i´ interface where the electric field suffers the larger increase [18].

4.6.1 Input channels

Four monochromatic pulsed lights separately (red, green, blue and violet input channels) or combined (multiplexed signal) illuminated the device at 12000 bps. Steady state violet bias was superimposed separately from the front and the back sides and the photocurrent was measured and plotted in Figure 4-14. The transient signals were normalized to their values without background and, for each individual channel, the mean values of the optical gains added. Results show that the illuminations of the background sides alter the signal magnitude of the input channels. This nonlinearity provides the possibility for selective removal or addition of wavelengths. As expected from Figure 3-18, under front irradiation it enhances mainly the spectral sensitivity in the medium-long wavelength ranges (α^{V}_{R}=7.3, α^{V}_{G}=3.2). Violet radiation is

absorbed at the top of the front diode, increasing the electric field at the back diode [19] where the red and part of the green incoming photons are absorbed.

Under back irradiation the electric field increases mainly near the front p-n interface where the violet and part of the blue incoming channels generate most of the photocarriers (α^{V}_{V}=11, α^{V}_{B}=1.5). So, by switching between front to back irradiation the photonic function is modified from a long- to a short-pass filter allowing, alternately selecting the red or the violet channels [12].

4.6.2 Multiplexed output

For an optoelectronic digital capture system, opto-electronic conversion is the relationship between the optical inputs and the corresponding digital output levels. The implementation of a wavelength division multiplexer requires that the channel wavelength may be tailored such that add/drop filters with different spectral locations, may be cascaded. A set of four channels with random data illuminated the device at 12000 bps and is shown in Figure 4-15.

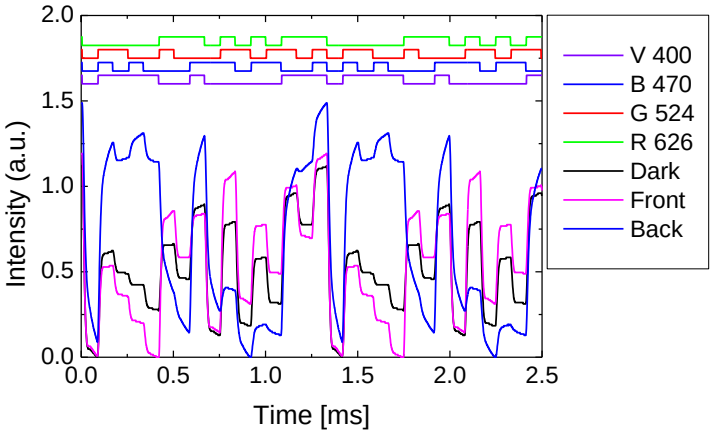

Figure 4-15 – Random 4 channel multiplexed signals

Here, tailoring the filter wavelength is achieved by changing the violet background from the front to the back side. The MUX signals (R, G, B, V) due to the combination of the input channels are displayed without and under front and back violet irradiations in a random sequence in Figure 4-15. On the top the

signals used to drive the input channels are displayed showing the presence of all possible sixteen on/off states. To show the backgrounds add/drop filter effect, the RGB and the GBV combined multiplexed signal are shown [11].

Results show that the device is a two tuneable background connected filter and acts as a wavelength selective switch. Without applied background (dark) sixteen output levels are observed each one correspondent to a one of the possible 4-channel on/off configurations (16-to-1 multiplexer) [12].

4.7 Five channel WDM

The multiplexing of four channels, each at 12000 bps allows for a raw transmission rate of 4*12000 = 48000 bps. Adding another channel, would allow for a raw transmission rate of 60000 bps. Two selectors, the front and back illumination of the background, are used to select the channels. As a summary the front illumination would sieve two channels and the back illumination would sieve the other two. When introducing another channel, the selection process may become more complex. To study the five channels multiplexer an experiment was made and the result is displayed in Figure 4-16.

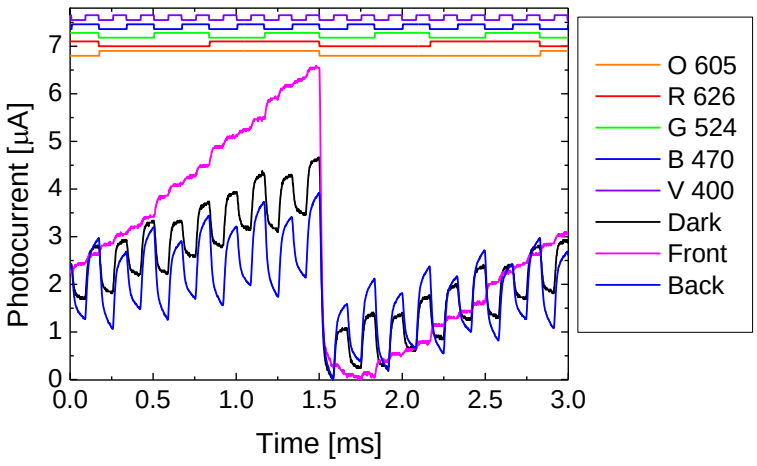

Figure 4-16 – A five channel multiplexer output.

Shown in Figure 4-16 is the output of the pi'npin when it is bathed by the signal wavelengths (dark) and simultaneously by the front illumination of the background (front) and the background at the back of the device (back). At the top of the figure there are the digital input signals that were applied to the LEDs, they contain the data of each channel. These digital signals help guiding the eyes to the front signal and showing that all 32 combinations are there. The back signal follows the violet input channel (400 nm) very strongly and distinguishes between dubious classifications of the front signal. The blue (470 nm) channel can also be recovered by the back signal. After the extraction of both violet and blue channels, the red (626 nm), orange (605 nm) and green (524 nm) can be easily identified.

The orange (605 nm) wavelength can be extracted because the gain of that wavelength (α_{Ofront}=4.53, α_{Oback}=0.54) is different from the other gains. Using the clustering explained further in Section 7, applied to the front and back signals of Figure 4-16 results in what is shown in Figure 4-17.

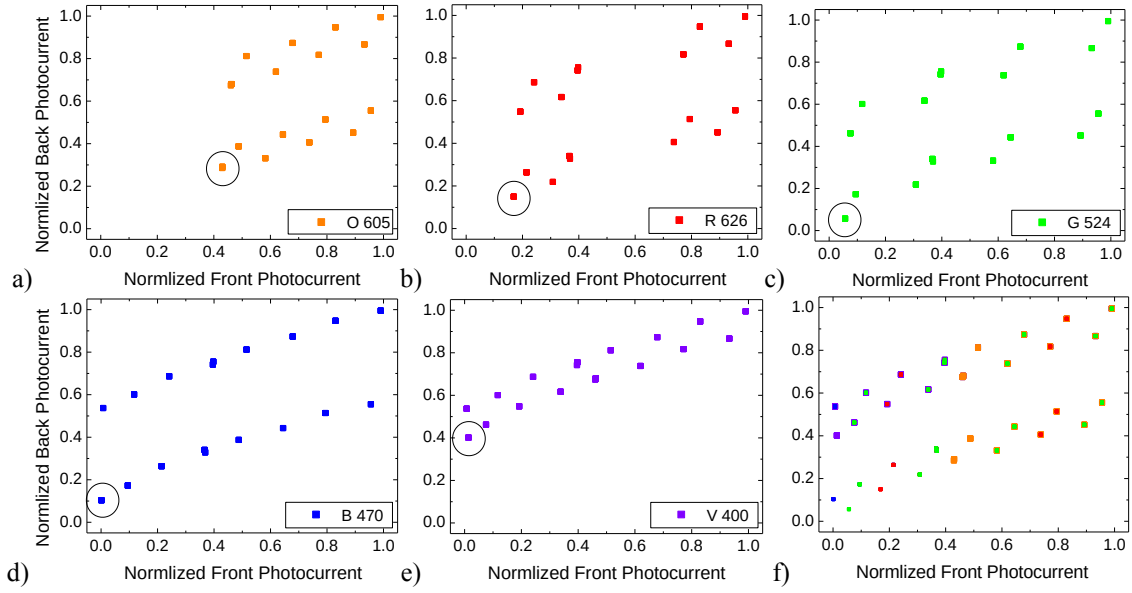

Figure 4-17 – Clusters of a) O 605 b) R 626 c) G 524 d) B 470 e) V 400 and f) all ORGBV.

The pi'npin sensor responds to the orange O 605 nm signal depending on the other signals that are also shining at the sensor. With four different

wavelengths, 2^4 possible combinations lead to the 16 areas in Figure 4-17a). The area marked with a circle belongs to the influence of O 605 when no other signal wavelength is active. The clusters for the other wavelengths are also shown in Figure 4-17b) to e). The graph of Figure 4-17f) is the over position of all individual wavelengths. There are only 31 areas on this graph because de 00000 bit is not plotted, as each individual graph only indicates where the wavelength is active.

4.8 n-channel WDM

To construct the above multiplexers some settings were commonly used and these should be followed for the use of an n-channel multiplexer. The n-channels should be equally balanced around the 500 nm point, this is so due to the different behaviour that the wavelength gain has when front or back illumination is used. The further away from the 500 nm, the higher the distance from the unit gain, to a certain extent until it decreases.

The starting point is to know the gain that the pi'npin has for each wavelength when it is subject to the front or back illuminations of its surfaces'; the front gain and the back gain respectively. Then the wavelengths are ordered by descending front gains. For an n-channel multiplexer, n different wavelengths are necessary. To adjust the flux intensity of each led by setting its' current, an input data pattern must be used, easy to be identified by the researcher. A simple pattern that holds all possible 2^n binary combinations is the sequential counting from 0 up to 2^n-1. The n bits used for that sequence from the highest order digit to the lowest order bit are distributed by the above ordered wavelengths; the wavelength with the highest front gain holds the highest order bit.

The ultra violet illumination of the front surface is switched on and maintained in its steady state during the configuration of the flux of all channels. The currents are then set incrementally, by switching on the LEDs starting from the high order bits. One by one the LEDs are switched on, and the current is adjusted to make sure that all 2^k levels are visible when there is k LEDs on out of all n LEDs. If needed, slight adjustments must be made to the already k set currents due to the entry of the next k+1 LED. This setting ensures that 2^n levels are visible for an n-channel multiplexer, like the one shown in Figure 4-16. The flux intensity should also be the lowest possible so that there is no saturation of the electrical equipment, and that all signals are within an appropriate range for the amplification and conversion. To ensure the optimal flux, it may be necessary to swap the LEDs between levels (see Figure 4-18). If this is done, then the process of setting each LED current must be repeated.

After setting the currents, the front ultra violet illumination is switched off and the back ultra violet illumination is set alight. The output signal should be observed to ensure that the wavelengths shorter than 500 nm are visible. For s <= n wavelengths shorter than 500 nm there should be 2^s different output levels. If this is not the case, then slight adjustments of the current of those s LEDs must be made followed by the process of the current setting explained above. This all process should be repeated from this new setting point till all levels are distinctly visible.

This setting process ensures that the classification process will have a reduced number of errors, and that all multiplexers have the same calibration method. This is important when different wavelength combinations are used for the same number of channels.

The choice of the wavelengths to use is also important. The 500nm turning point is used to balance the wavelengths used so that for n channels

n/2 wavelengths should be found on each side of the 500 nm wavelength. For odd number of channels either side can have the odd number. This balancing is due to the fact that there are only two selectors.

An example of a 7 bit multiplexer is shown in Figure 4-18.

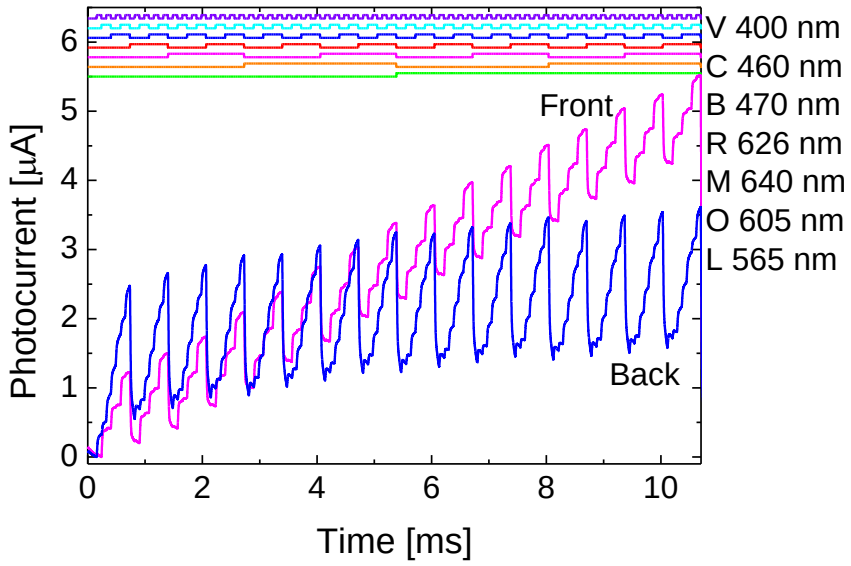

Figure 4-18 – Multiplexed signal with seven input channels.

Seven different wavelengths L 565 nm, O 605 nm, M 640 nm, R 626 nm, B 470 nm, C 460 nm, V 400 nm illuminated the p'inpin sensor as shown by the top signals in Figure 4-18 that are there to guide the eyes into the figure. The front and back signals were obtained by the front and back ultra-violet illumination of the backgrounds, respectively. In this example, the illumination of each led was tuned to minimize the overall illumination, that is why instead of the ladder like response of the front signal in Figure 4-16, the front signal in Figure 4-18, goes up and down although still presenting the full 2^7 (128) combinations.

4.9 Conclusion

The pi'npin device works as a selective filter controlled by the optical bias. The optical bias is a steady state ultra-violet wavelength. The optical bias can be set either at the front or at the back surface of the device. When the optical bias is set at the front surface of the device the gain of the visible spectrum from 500 to 800 nm is enhanced and in the 400 to 500 nm range it is quenched. The opposite occurs when the bias is set at the back surface; wavelengths in the 400 to 500 nm wavelength range are enhanced and quenching occurs in the 500 to 800 nm wavelengths. This selective filter characteristic of the pi'npin device enables it to discriminate wavelengths from each side of the 500 nm wavelength turning point.

A simple and consequent application of the selective filter characteristic of the pi'npin is a 2 channel demultiplexer. Complementary to a demultiplexer is the multiplexer. An n-channel multiplexer is a device that has n input signals and $\log_2 n$ selecting inputs that are used to choose the input that is reproduced on the single output of the multiplexer. The n-channel demultiplexer is similar but has one input and n outputs.

Constructing a n-channel demultiplexer would necessitate the complete combinations of $\log_2 n$ selecting inputs. Using only the bias either at the front or at the back surfaces of the p'inpin device as a selector would only count as 2 possible combinations which could only enable a 2-channel demultiplexer. It is the non linear spectral gain of the pi'npin device in the 400 to 500 nm and 500 to 800 nm ranges that enables a more than 2-channel demultiplexer to be built.

Distributing the n-channels wavelengths equally in number by the two ranges 400 to 500 nm and 500 to 800 nm is the best way to implement the n-channel demultiplexer.

Experimentally a three, four, five and seven channel demultiplexers were built.

The configuration of the input channels was presented for the construction of any n-channel demultiplexer. The maximum number of channels that can be used with the pi'npin device was not defined in this chapter, but will be determined in a proceeding one.

The pi'npin device is also capable of multiplexing signals. To work in this mode it produces at its output an electrical signal that is the resultant of all n-channels that are applied to its front surface. A channel is a digital signal that modulates 100% by amplitude a single wavelength in the visible range, from 400 to 800 nm. An n-channel multiplexer is quite straight forward; n digital signals modulating 100% the amplitude of n different single wavelengths shinning upon the front surface of the pi'npin device.

The demultiplexing technique uses the pi'npin device as an n-channel multiplexer and then uses the optical bias to obtain the original n-channels.

In telecommunications it is common to retrieve one channel from the multiplexed transmission and to introduce a channel to the current transmission. This add-drop technique was also explored.

An almost straight forward application of the multiplexer and demultiplexer digital components is their use as a decoder and encoder device respectively; these two possibilities were also presented.

4.10References

[1] A. Tanenbaum and D. Wetherall, *Computer Networks*, 5th ed. Pearson Education International, 2011.

[2] G. A. Mahdiraji and A. F. Abas, "Advanced Modulation Formats and Multiplexing Techniques for Optical Telecommunication Systems," in *Trends in Telecommunications Technologies*, Intech, Ed. 2010, pp. 1–27.

[3] T. Komiyama, K. Kobayashi, K. Watanabe, T. Ohkubo, and Y. Kurihara, "Study of visible light communication system using RGB LED lights," in *Proceedings of SICE Annual Conference*, IEEE, 2011, pp. 1926–1928.

[4] S. Rajagopal, S. Lim, T. Bae, D. H. Kim, J. Son, I. S. Jang, D. Kim, D. W. Han, Y. Li, A. Yokoi, D. K. Jung, H. S. Shin, S. B. Park, K. W. Lee, S. A. Surra, F. Khan, T. G. Kang, and E. T. Won, "IEEE 802.15 Wireless Personal Area Networks," pp. 1–121, 2009.

[5] V. V Mai, N. Tran, T. C. Thang, and A. T. Pham, "Performance analysis of TCP over visible light communication networks with ARQ-SR protocol," pp. 1–9, 2014.

[6] H. Chowdhury, H. Bagheri, I. Ashraf, S. Tamoor-ul-hassan, and M. Katz, "Techno-Economic analysis of Visible Light Communications," *Proc. Tenth Int. Symp. Wirel. Commun. Syst. (ISWCS 2013)*, vol. 9, pp. 96–100, 2013.

[7] M. Vieira, M. Fernandes, J. Martins, P. Louro, A. Macarico, R. Schwarz, and M. B. Schubert, "Laser-scanned p-i-n photodiode (LSP) for image detection," *IEEE Sens. J.*, vol. 1, no. 2, p. 158, 2001.

[8] M. Vieira, P. Louro, M. A. Vieira, J. Costa, and M. Fernandes, "Direct color sensor, optical amplifier and demux device integrated on a single monolithic SiC photodetector," *Procedia Eng.*, vol. 5, pp. 232–235, Jan. 2010.

[9] P. Louro, M. Vieira, M. Fernandes, J. Costa, M. A. Vieira, J. Caeiro, N. Neves, and M. Barata, "Optical demultiplexer based on an a-SiC:H voltage controlled device," *Phys. status solidi*, p. NA–NA, Jan. 2010.

[10] M. A. Vieira, "Three Transducers for One Photodetector: essays for optical communications," FCT-UNL Universidade Nova de Lisboa, 2012.

[11] P. Louro, M. Vieira, M. A. Vieira, V. Silva, and A. Fantoni, "Novel device for implementation of WDM in the visible spectrum," *MRS Proc.*, vol. 1438, pp. mrss12–1438–m06–02, Sep. 2012.

[12] M. Vieira, M. A. Vieira, P. Louro, and V. Silva, "Reconfigurable active filters for optical communications," *(In Publ.*, pp. 1–5, 2013.

[13] V. Silva, M. A. Vieira, M. Vieira, P. Louro, A. Fantoni, and M. Barata, "Logic functions based on optical bias controlled SiC tandem devices," *Phys. Status Solidi*, vol. 11, no. 2, pp. 211–216, Feb. 2014.

[14] M. Vieira, A. Fantoni, P. Louro, M. Fernandes, R. Schwarz, G. Lavareda, and C. N. Carvalho, "Self-biasing effect in colour sensitive photodiodes based on double p-i-n a-SiC:H heterojunctions," *Vacuum*, vol. 82, no. 12, pp. 1512–1516, Aug. 2008.

[15] M. A. Vieira, M. Vieira, V. Silva, P. Louro, and M. Barata, "Optoelectronic logic functions using optical bias controlled SiC multilayer devices," *MRS Proc.*, vol. 1536, pp. 91–96, Jun. 2013.

[16] V. Silva, M. A. Vieira, P. Louro, and M. Vieira, "Optoelectronic digital capture device based on Si/C multilayer heterostuctures," in *Technological Innovation for the Internet of Things*, Springer Berlin Heidelberg, 2013, pp. 555–562.

[17] M. A. Vieira, M. Vieira, P. Louro, V. Silva, and A. Fantoni, "Integrated photonic filters based on SiC multilayer structures," *Appl. Surf. Sci.*, vol. 275, pp. 185–192, Jun. 2013.

[18] M. Vieira, M. A. Vieira, V. Silva, P. Louro, and J. Costa, "SiC monolithically integrated wavelength selector with 4 channels," *MRS Proc.*, vol. 1536, pp. 79–84, Jun. 2013.

[19] M. A. Vieira, M. Vieira, J. Costa, P. Louro, M. Fernandes, and A. Fantoni, "Double Pin Photodiodes with Two Optical Gate Connections for Light Triggering.," *Sensors & Transducers*, vol. 10, no. Special issue, pp. 96–120, 2011.

5

5 Logic Functions

The logic functions that are the basic of present digital technologies are mathematic operators of Boolean Algebra. The theoretical work done by George Boole in 1847 is presented in *"The mathematical analysis of Logic"* [1]. Using the Boolean logical functions with mathematical state theory more complex structures were built creating the reliable computers that are available at this date [2].

The Boolean logic functions, based in mathematical set theory, needed to construct any other complex logic functions, are the NOT (negation), and both or either an AND (conjunction) or an OR (disjunction) [3]. The implementation of these mathematical constructs in hardware has been done with several techniques, namely in the electronic domain, by RTL (resistor transistor logic), DTL (diode transistor logic), TTL (transistor transistor logic) among other families. The use of CMOS (complementary metal-oxide-semiconductor) logic improved the performance in several variables like, power consumption, speed, miniaturization and power supply [4].

In this chapter there is an approach to implement the basic logical functions on a pi'npin device [5].

Another logical function, the Majority function [6], which is also known as the voting function will also be implemented in this section.

5.1 Digital Light Signals

Logical functions are commonly used as logic gates [7] and by combining them, other logical functions are created, and some, due to their special function, are named. One of them is the multiplexer which is a combinational function. Due to its behaviour the multiplexer can also be used as a basic circuit which in turn can produce results as simple as the basic logic gates. There are three basic logical functions or operations: AND (conjunction), OR (disjunction) and NOT (inverse). The NOT function built with a multiplexer is presented in two different configurations in Figure 5-1. [8]

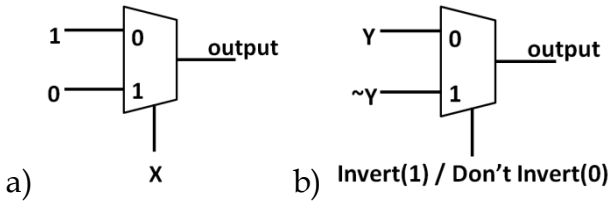

Figure 5-1 - A multiplexer used as an invert function.

The 2x1 multiplexer shown in Figure 5-1a) is composed by a selector input, X, which chooses one of the input signals to be set as the output. When X holds the 0 value, the 0 input is set at the output, in this case the output presents the value 1. Accordingly, when X is 1 the output is 0. This means that the output is the inverse of X.

In Figure 5-1b) the Invert signal is the selector that chooses between inputs Y and ~Y (NOT Y). The output follows the Y signal when the Invert selector is 0 and follows the ~Y signal when Invert is 1. By this setup, the Invert selector can choose between: a Y signal, or its inverse ~Y. This is the basis of the following work using the sensor's capability of being a multiplexer [9] to act as an inverter.

It is known that any logical function has only one of two possible values, either a True (T) or a False (F) [10]. The NOT is the inverse function which converts a T into a F and vice-versa. Using visible light to mimic the logic values that input the operations and their result, implies that the value T is the presence of light and the value F its absence. The inverse function must block the presence of light (T -> F) and when there is no light it has to emit it (F -> T) [10]. To do this with the pi'npin device implies another approach. The sensor

works as tuneable background filter (see Fig 3-19 and Fig 4-12). By defining the presence of a signal in one bandwidth as the T value and as F on the other, it is possible to define the inverse function of an input signal if that signal is composed by those two wavelengths. Here, the presence of a signal in the long-pass bandwidth was considered as a T logical value [10].

A digital light signal is defined, as a signal pair with two components, one from the long and another from the short filter ranges. One component's value is the inverse of the other [11].

Any long, short combination can be used, in the following examples the (Red, Blue) and the (Green, Violet) pair is used, chosen to have similar short-long distances. These pairs are presented in Figure 5-2, and were chosen because the distance in wavelength within each pair is similar.

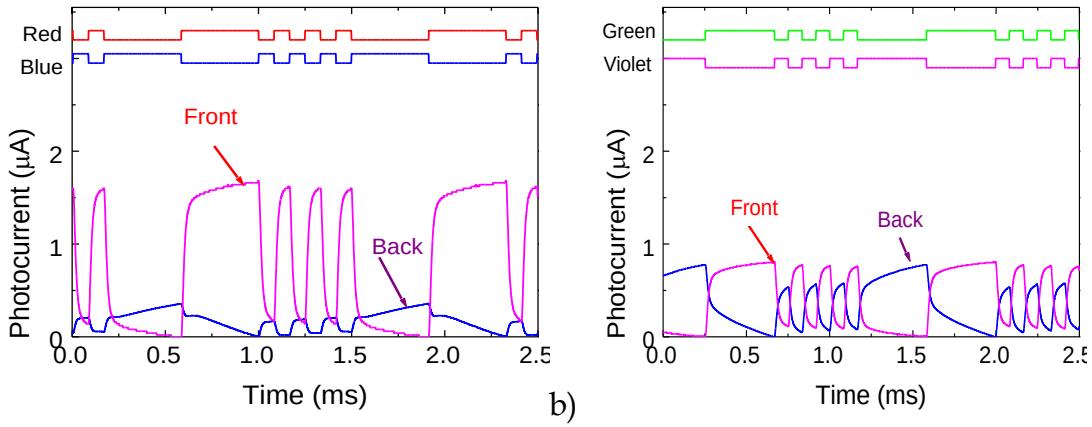

Figure 5-2 - Two examples of digital light signals: a) Red-Blue pair and b) Green-Violet pair.

Two different digital light signal pairs with the same data content are presented in Figure 5-2. By subjecting both digital light signal pairs to the Front and Back lighting of the background it is clear that the Front signal follows the Red and Green input signals and that the Back signal follows the Blue and Violet signals.

So, a visible digital light signal, D, is then the multiplex signal of two different wavelength channels, in the long and in the short wavelength ranges, under front and back violet irradiation, henceforth represented as D[L, S] where L and S represent the channel colour [10].

Transmitting a False or a True value for a long period of time would degrade the recovery of the output signals, as only the *ac* component is used. To improve the photocurrent output it is necessary that a True or False bit value changes in time during its bit length. This can be solved by using the Manchester coding which guarantees that there is a polarity change in the middle of each True or False bit time length. The photocurrent to be useful must be time dependent, so the logic signal, even if does not have its state changed, must vary in time. This obliges the digital signals to be synchronized and differential, thus a digital light signal must be Manchester coded [10], [11].

The Manchester code is one of the most common data coding methods. It provides a means of adding the data rate clock to the message to be used on the receiving end. Manchester coding also adds the benefit of always yielding an average DC level of 50%. In modulation types where the power output is a function of the message such as AM (Amplitude Modulation), the average power is constant and independent of the data stream being encoded. Manchester coding states that there will always be a transition of the message signal at the mid-point of the data bit frame. What occurs at the bit edges depends on the state of the previous bit frame and does not always produce a transition. A logical "1" is defined as a mid-point transition from low to high and a "0" is a mid-point transition from high to low [12].

A simple block diagram in Figure 5-3 shows how to produce a digital light signal from a plain digital signal.

The clock generator produces a digital square wave with a 50% duty-cycle (ratio between high-level signal and the wave length period). The clock and the digital signal input are exclusively-ored (XOR), which results in a signal that is identical to the clock signal whenever the digital signal holds a value of 0, and is equal to the inverse of the clock when the input digital signal has a high value; 1.

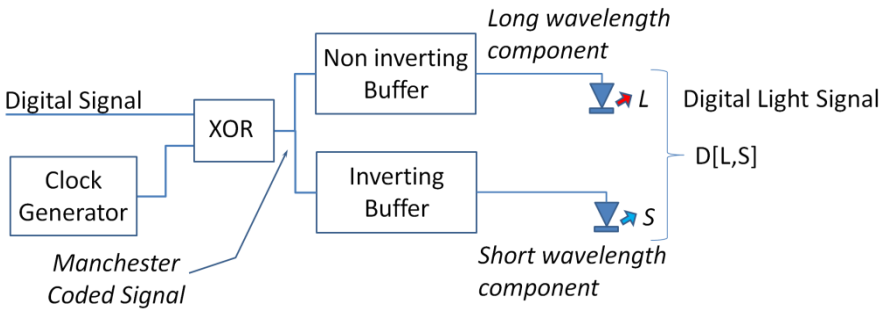

Figure 5-3 – Block diagram representing the generation of a Digital Light signal from a plain Digital Signal.

The output of the XOR between the clock and the digital signal is a Manchester coded signal, as shown in Figure 5-3. To obtain the digital light signal, two components must be generated from the Manchester coded signal. One which is identical to the Manchester coded signal, the Long wavelength component, and the other which is the inverse of the Manchester coded signal, the Short component. The inverse signal is obtained by an Inverting Buffer. The Long wavelength component is not directly connected to the Manchester coded signal as shown in the figure because a time delay equal to the one that the Inverting Buffer introduces is necessary so that both components of the digital light signal are synchronous and in phase.

Two examples of digital light signals with Manchester coding are shown in Figure 5-4

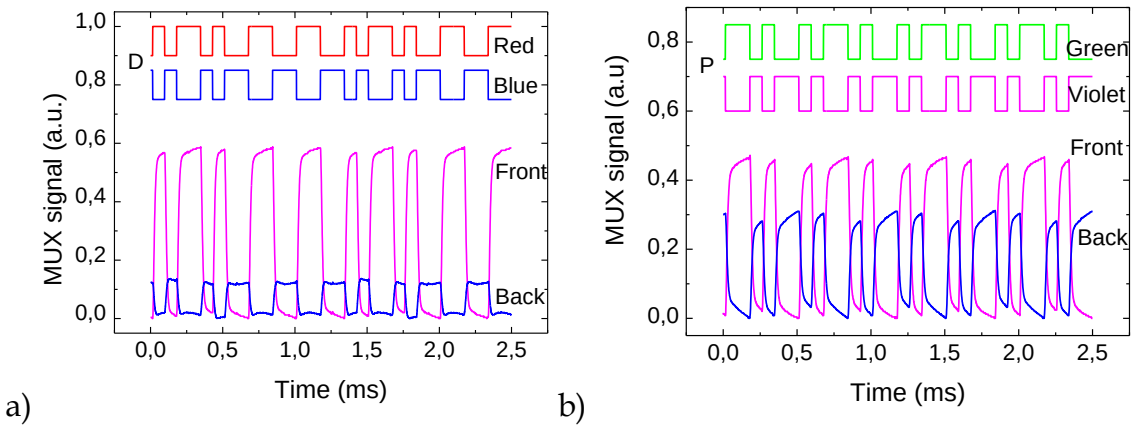

Figure 5-4 - Two examples of digital light signals and its MUX signals under front and back irradiation. At the top of both figures there are the signals used to drive the input channels and shown to guide the eyes into the ON/OFF channel states.

Figure 5-4 shows examples of two possible digital light signals: D[R, B] (a) and P[G, V] (b). Results show that by changing the background side at an appropriate intensity and wavelengths the digital light signal can be obtained describing, in the visible range, the basic logic functions [10].

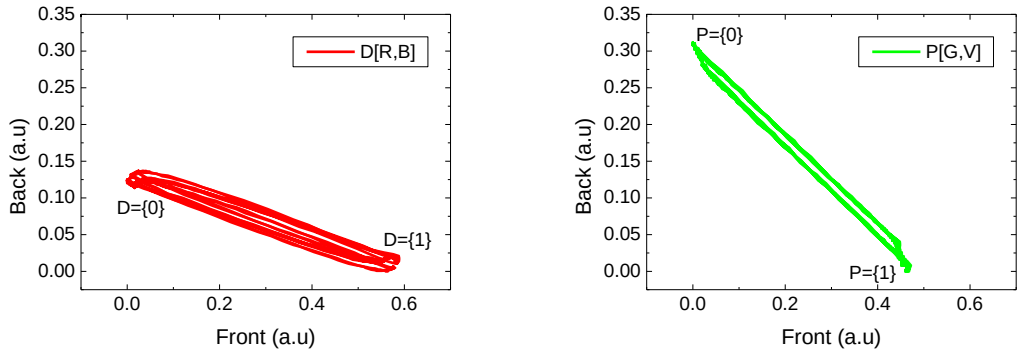

a) b)

Figure 5-5 – Scatter graphs of signals presented in Figure 5-4 a) D[R, B] b) P[G,V]

Figure 5-5 shows the scatter graphs of the signals presented in Figure 5-4. It is clear that only two values exist in each digital light signal D[R, B] = { {0}, {1} }, and P[G, V] = { {0}, {1} }. The scatter graph also shows that the front and back signal are inversely correlated, due to the negative slope of the graphs [13] as expected due to each digital light signal being a composition of a short and long wavelength [14].

A digital light signal can be written as Equation 5.1.

$$D[R,B] = [R(t)\cdot i_R \quad B(t)\cdot i_B] \times \begin{bmatrix} \alpha^{V}_{R,Front} & \alpha^{V}_{R,Back} \\ \alpha^{V}_{B,Front} & \alpha^{V}_{B,Back} \end{bmatrix} = [L_R(t) \quad S_B(t)] \quad (5.1)$$

R(t) is the digital sequence for example = {0,1,1,0,0,1,0,1} and B(t) the inverse of that sequence e.g. = {1,0,0,1,1,0,1,0}. The dark photocurrent for each wavelength is i_R for the Red and i_B for the Blue.

The L and S represent the signals in the long and short-wavelength range, respectively.

Under front and back irradiation, the D digital signal composed by the red and blue channels obeys to Equation 5.1 where $\alpha^{V}_{R;B,\ Front}$ and $\alpha^{V}_{R;B,\ Back}$ are respectively the optical gains under front and back violet background.

For the digital signal P with green and violet combination P[G, V] a similar equation results [$L_G(t)$ $S_V(t)$].

Some examples of different logic gates will be present in the following text as one of the device's possible applications [10].

5.2 NOT Gate

It is clear from Figure 5-4 that by using only two long and short wavelengths channels (the red and blue or the green and violet) an inverter can be built and controlled by the violet irradiation either at the back or front side of the device. Here, the true or false outcome is correlated to the relationship between the difference of both red and blue or green and violet components of the input signals [10].

Figure 5-1 showed a NOT function built with the use of a multiplexer, in a) the output signal is the inverse of A and in b) invert selects either Y or ~Y as the output, where ~Y is the inverse of Y. In the following examples 1 is the value True and 0 the value False [10].

Equations 5.2 and 5.3 show, respectively, for the circuit in Figure 5-1a) and Figure 5-1b) the corresponding transformations:

$$output = 1 \cdot {\sim}A + 0 \cdot A = {\sim}A \tag{5.2}$$

$$output = Y \cdot {\sim}Invert + {\sim}Y \cdot Invert = Y \oplus Invert \tag{5.3}$$

Equation 5.2 can be simplified as the XOR (exclusive OR) relation between Y and invert. If Invert is 0 then the output is Y otherwise the output is ~Y [10].

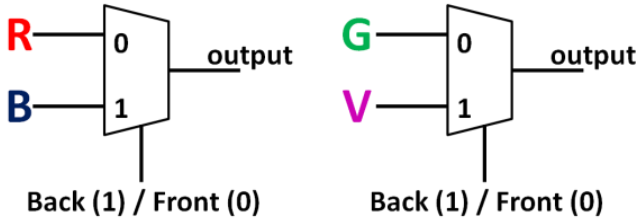

Figure 5-6 - NOT function using a digital light signal

Here, the digital light signal components are synchronized and differential; when one is *on* the other is *off* and vice-versa. This can be visualized in Figure 5-6a). Taking into account the Figure 5-1b) and signal D (Figure 5-4a) as an example, the Y input is the *red* (R) channel and the ~Y input is the *blue* (Y) one. The Invert input value 0 is the multiplexed signal under front illumination and the Invert value 1 is MUX signal under back illumination. The Invert selected as 0 results in the output of the sensor under front background, which is identical in a logic (on / off) point of view with the red signal in Figure 5-4a) and with the Green signal in Figure 5-4b). The *back* line, which is the output when Invert is 1, is identical to the *blue* signal in Figure 5-4a) and the *violet* signal in Figure 5-4b). This is the NOT function [10].

5.3 Combinations and Conditionals

A logical system block in which, for the same input combination presents the same output value, regardless of the sequence through which the input combinations are set in time, is considered stateless; it does not have memory. It also means that there is a logical function that defines the output.

Presented in Figure 5-7a) is a single input and single output system block and all their possible input and output combinations are represented in the table of Figure 5-7b).

a)

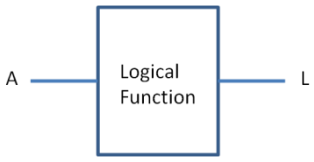

b)

input	possible L outputs			
A	0	A	~A	1
0	0	0	1	1
1	0	1	0	1

Figure 5-7 – a) Single input single output logical system and b) all possible input and output combinations.

Represented in Figure 5-7b) are all possible outputs for the input combinations. A stateless logical system with one logical input has two possible values (2^1). These two values can have four (2^2) different outcomes. The result L is always 0, which defines the absorption function. The result L is always equal to input A, then it defines the identity function. The result L is always equal to the inverse of input A (~A), then it defines the inverse function. The result L is always equal to 1, which defines the absorption function. Of the four possible combinations, only the inverse function produces a useful logical function. That function is the NOT.

Using the same approach with a logical function with two inputs and a single output the result is shown in Figure 5-8.

a)

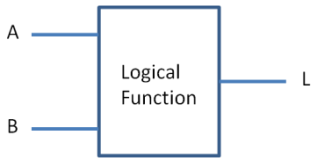

b)

Inputs		Possible L outputs															
A	B	0	~|	<	~A	>	~B	!=	~&	&	=	B	<=	A	>=	|	1
0	0	0	1	0	1	0	1	0	1	0	1	0	1	0	1	0	1
0	1	0	0	1	1	0	0	1	1	0	0	1	1	0	0	1	1
1	0	0	0	0	0	1	1	1	1	0	0	0	0	1	1	1	1
1	1	0	0	0	0	0	0	0	0	1	1	1	1	1	1	1	1

Figure 5-8 – a) Two input single output logical system and b) all possible input and output combinations.

A stateless logical system with two inputs has four (2^2) possible input combinations. These four combinations can produce sixteen (2^4) possible results, which are presented as a table in Figure 5-8b). From left to right the sixteen results are always 0, the inverse of (A or B) (~|), A less than B (<), not A (~A), A greater than B (>), not B (~B), A not equal to B (!=), the inverse of (A and B) (~&), A and B (&), A equal to B (=), B (B), A less than or equal to B (<=), A (A), A greater than or equal to B (>=), A or B (|), always 1. Observing all operations it is clear that half of them are the inverse of the other half.

Excluding the outputs 0, 1, A, B because they have not very useful logical operators, the most simple, non inverting operations are: <, >, &, =, |. From these operations the most widely used are the AND (&) the OR (|) and the XOR (!=) which is the *different* operator and used more frequently than the XAND (=) *equal* operator.

It is thus important to search for these widely used operators in any new technology that aims to implement logical functions. The use of the pi'npin structure as a possible technology to be used for logical operations leads to the study of the AND, OR and XOR logical functions in the following sections.

5.4 Interaction of two digital light signals

Logic operators besides the NOT have expressions with two variables. Boolean logic has the associative and commutative properties of algebra that are applied when more than two variables are involved. The number of input variables and the operation that produces a single logical output is called a gate. In this section two light variables are studied as the basic building block of a logical gate. In order to effectively classify the output of the logical gate the sampling of the signal will also be addressed.

Two different digital light signals D[R, B] (Figure 5-4a) and P[G, V] (Figure 5-4b) illuminated the device and their combination is presented in Figure 5-9 [10].

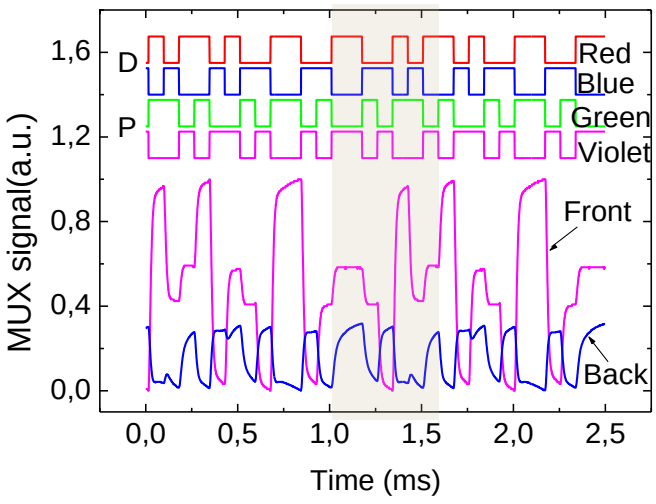

Figure 5-9 - Multiplexed signal due to the combination of P and D digital signals.

The interaction of two digital light signal pairs red-blue and green-violet is shown in Figure 5-9, where the top the input signals guide the eyes into the ON/OFF states. This signal is shown in Figure 5-10 as a scatter graph where the Front signal is set as the horizontal axis and the Back signal is set as the vertical axis.

The pattern selected in Figure 5-9 which holds all possible combinations of the D and P signal will be analysed in detail further in the text for sampling purposes.

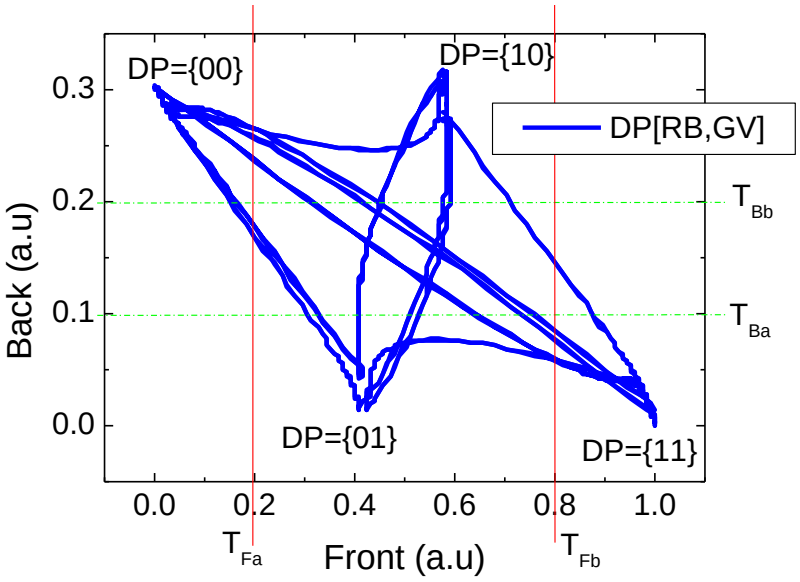

Figure 5-10 - Scatter graph of the Front and Back signals of Figure 5-9

Figure 5-10 shows both Front and Back signals in a scatter graph, where the line shows the sequence path where at each point, the front and back value are at the same time instant i.e. *functionOf(Front(t), Back(t))*. On the same figure the vertexes indicate the four possible combinations of the D and P digital light signals {00}, {01}, {10} and {11}. A simple classification grid can be used with threshold values which are drawn in solid and dashed lines on Figure 5-10, to classify the logical output.

The "eye/constellation" diagram shown in Figure 5-10 is wide enough indicating a good signal to noise ratio and that the classification of the sampled signal will be accurate. The eye diagram is a useful tool for the qualitative analysis of a signal used in digital transmission. It provides at-a-glance evaluation of system performance and can offer insight into the nature of

channel imperfections. Careful analysis of this visual display can give the user a first-order approximation of signal-to-noise, clock timing jitter and skew [15]. The constellation diagram, among many other attributes, provides a graphical insight into signal structure and the relationship among various modulation states. Given a digitally modulated signal, its constellation can be obtained by projecting individual modulation states onto a set of orthogonal basis functions the number of which is determined by the dimensionality of the signal. The most common constellations in use are two dimensional which map the signal onto a pattern of amplitude/phase states scattered on the 2D plane [16].

In this study the term eye or constellation diagram will be used interchangeably representing the scatter diagram of back vs front which provides a qualitative description of the distribution of the sampled points.

The sampling points grouped by clusters, constellation, can be visualized in Figure 5-11. The clustering will be discussed further into the text.

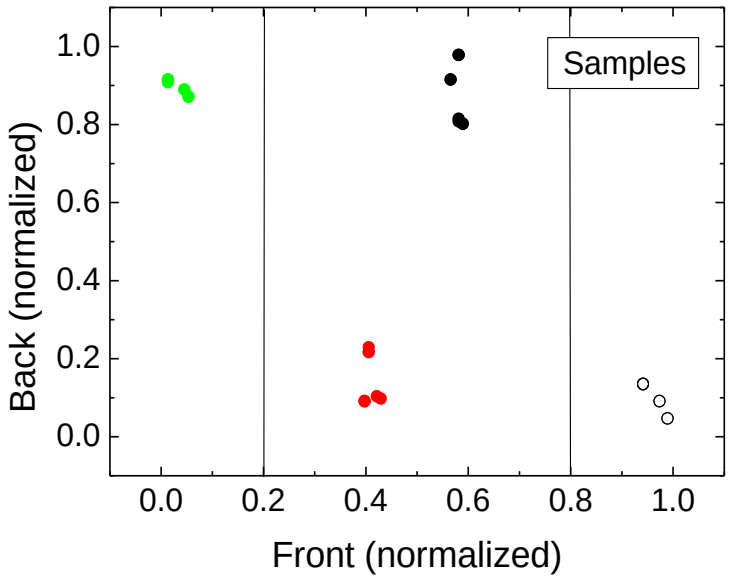

Figure 5-11 – Normalized data of Figure 5-10 showing sampling points.

Figure 5-11 displays the samples acquired from Figure 5-10 after normalization (signal within [0.0, 1.0]), and the clustering is clearly viewed which allows the classification of the data into four different values. The sampling was made at the end point of each bit (the reason for this position instead of the most common used at the middle of each bit is explained bellow). Adding the threshold lines to Figure 5-9 yields Figure 5-12.

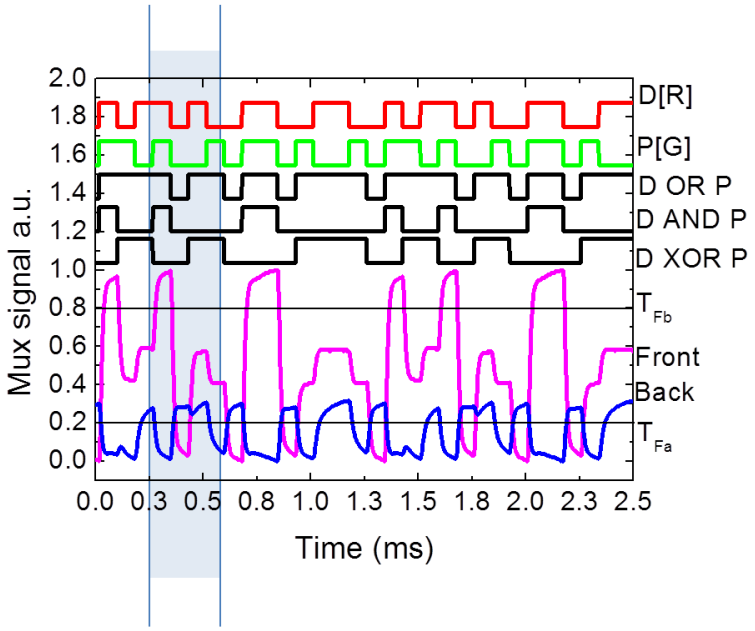

Figure 5-12 - Interaction of two digital light signals D and P. Threshold lines shown and expected result of the indicated logical operations.

Figure 5-12 is the same as the one shown in Figure 5-9 but the short-wavelength components (blue and violet) of the input signals are not shown to simplify the visualization. The black solid signal lines represent the expected result of the logical operations between both digital light signals D and P. Also shown are the two solid threshold lines (T_{Fa} and T_{Fb}) of Figure 5-10. The explanation of those logical operations follows in the next sections.

Table 5-1 – Digital logical operations of two input variables D and P

D	P	D AND P	D OR P	D XOR P
0	0	0	0	0
0	1	0	1	1
1	0	0	1	1
1	1	1	1	0

Table 5-1 represents all possible combinations of the digital light signals {DP} and the result according to the operations that can involve those two signals: D (AND, OR, XOR) P. These operations can be identified in the shadowed detail of Figure 5-12 and shown in Figure 5-13.

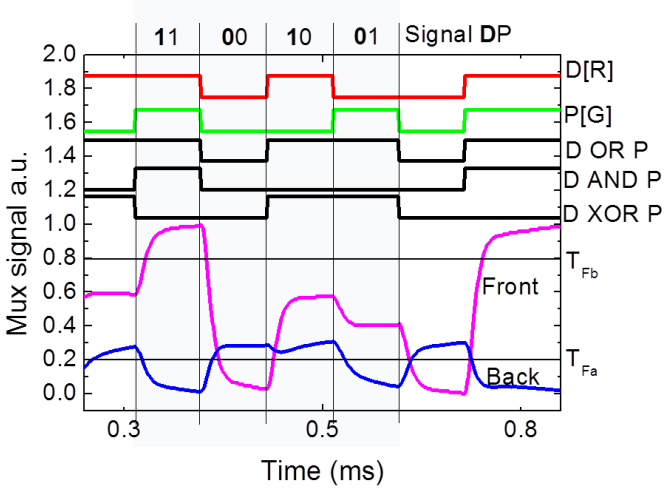

Figure 5-13 - Detail of the shadowed area of Figure 5-12

Figure 5-13 has all four possible combinations of the digital light signals {DP} represented by the D[R] and P[G] lines, and the solid thick black lines show the outcome of the operations indicated. The figure also displays the Front and Back output signals according to their respective illumination side. Two threshold lines that were chosen by observing Figure 5-10, aid the classification of the output signal.

5.5 AND Gate

The AND logical function (D AND P) is defined as having True as output if and only if both inputs {DP} have value True (Table 5-1) i.e. {11}. In Figure 5-13) under front irradiation it corresponds to both Red and Green channels on their ON state (the higher level under front illumination). Observing Figure 5-13 and the scatter function of Figure 5-10, it is possible to define a threshold line (T_{Fb}) above which any result represents the D AND P output function, isolating the {11} result. In our experimental conditions (Figure 5-13 and Figure 5-10) this threshold (T_{Fb}) cuts the multiplexed signal under front irradiation and yielding the "*D and P*" line which represents the AND output function to guide the eyes [5, 11, 13]. Figure 5-14 shows the AND classification on the scatter graph of Figure 5-11.

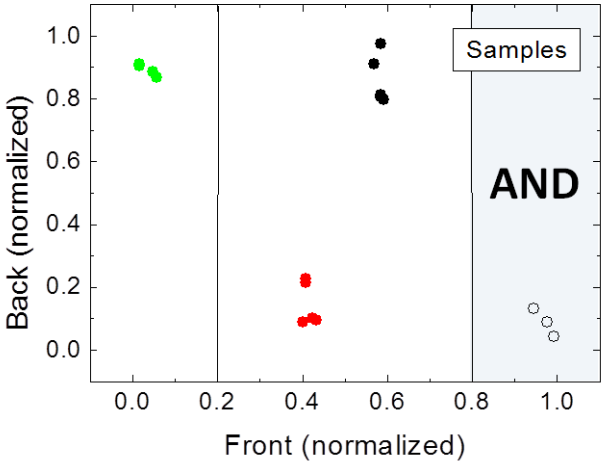

Figure 5-14 – AND output classification by threshold lines.

Figure 5-14 shows the cluster of the AND function. The correct digital output signal can be easily recovered with a single threshold line around 80% of the normalized [0.0, 1.0] front signal. The output must be above that line.

5.6 OR Gate

Another basic logic function is the OR. The OR logical function is defined as (D OR P) with output True if either or both {DP} are True or equivalently the output is False if and only if both {DP} are False, i.e. {00}. Taking into account Figure 5-13 and Figure 5-10 it corresponds to the presence under front irradiation of the red, green or both channels in its ON state. Observing both Figure 5-10 and Figure 5-13 it is possible to define a threshold line (T_{Fa}) above which any result is the D OR P function i.e. {{01}, {10}, {11}}. In Figure 5-13 this threshold line (T_{Fa}) cuts the multiplexed signal and yields the *"D OR P"* line which represents the OR output function to guide the eyes [5, 11, 13]. Figure 5-15 shows the OR classification on the scatter graph of Figure 5-11.

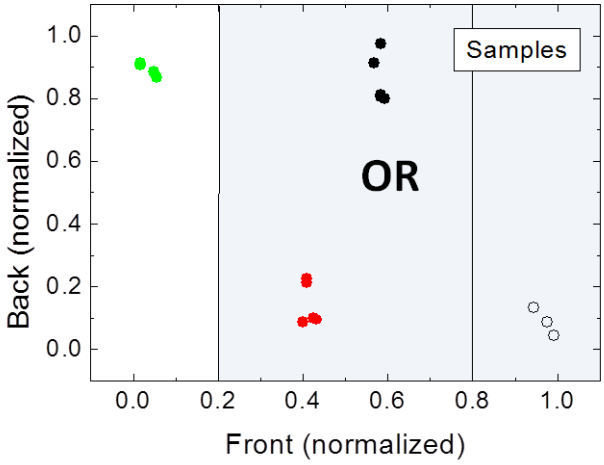

Figure 5-15 – OR output classification by threshold lines.

Figure 5-15 shows the clusters of the OR function. The correct digital output signal can be easily recovered with a single threshold line around 20% of the normalized [0.0, 1.0] front signal. The output must be above that line.

5.7 XOR gate

The Exclusive OR function, known as XOR, between two variables {DP} is True when only one of them holds the True value, i.e. {{01}, {10}}. It excludes the {11} from the OR. It can also be defined as the difference operation, which is True when the variables hold a value which is different from the other. Observing the scatter graph of Figure 5-10 it is possible to confine the {{01}, {10}} values between the two threshold lines T_{Fa} and T_{Fb}. In Figure 5-13 these two threshold lines (T_{Fa} and T_{Fb}) selects from the multiplexed Front signal the *"D XOR P"* line which represents the XOR output function to guide the eyes [5, 11, 13]. Figure 5-16 shows the OR classification on the scatter graph of Figure 5-11.

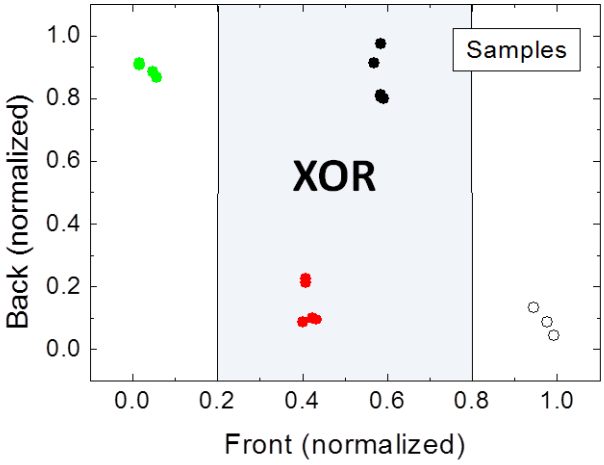

Figure 5-16 – XOR output classification by threshold lines.

Figure 5-16 shows the clusters of the XOR function. The correct digital output signal can be easily recovered with a two threshold lines around 20% and 80% of the normalized [0.0, 1.0] front signal. The output must be between both lines.

5.8 Sampling of the digital light signal

To determine the code produced by the sensor it is necessary to sample the output, classify it according to the clustering in which it fits best and present the code of that cluster.

The sampling algorithm is as follows: each bit time is oversampled such that its length is an odd number of samples (seven samples). The sampled bit value is then stored for further processing. The sampling point is chosen either from the beginning (sample 2), middle (sample 4) or end (sample 6) part of the bit. The oddS={2,4,6} value determines how close the sampling is to the edge (samples 1 and 7) of each bit.

The shaded portion of Figure 5-9 contains all possible values of the input digital light signals D and P, and is used as the same sampling pattern in the figures that follow. The input signal sequence {DP} is {10, 10, 01, 00, 11, 01, 10}, and this pattern is used to identify the best sampling point.

To choose the best sampling point of the output signals (Front and Back), experiments are shown with the same pattern sampled at the beginning (Figure 5-17 and Figure 5-18), middle (Figure 5-19 and Figure 5-20), and end part of the bit (Figure 5-21 and Figure 5-22).

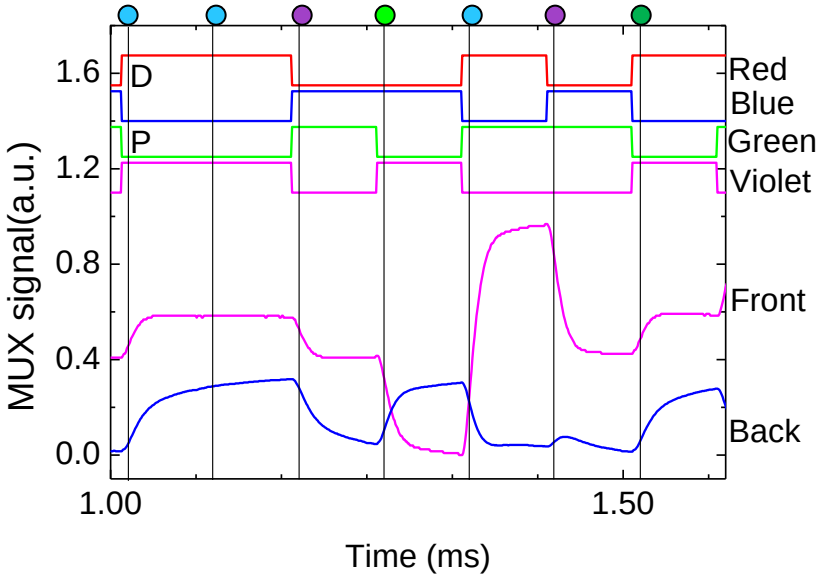

Figure 5-17 – Selected part of Figure 5-9 with the grid showing the sampling of the Front and Back signal at the beginning of each bit.

Figure 5-17 shows a grid which is set at the beginning part of each bit. At the top of the figure there are coloured circles that indicate the value of the {DP} signal sequence. These colours are the same on Figure 5-18 indicating the value of the sample at that selected point on the beginning of each bit. Represented in the same figure is the scatter graph of Figure 5-10 normalized to the unit, to guide the eyes.

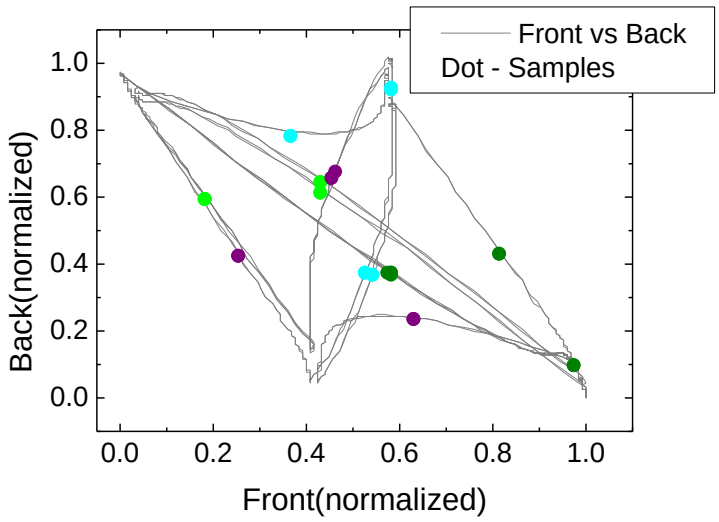

Figure 5-18 – Normalized data of Figure 5-10 showing sampling points at the beginning of each data bit.

The sampling spots in Figure 5-18 indicates the position of the sampling at the beginning of each bit and the value according to the digital input of signals D and P of Figure 5-9 are represented as four different colours. Results show that the signals are intertwined in a way that cannot be easily classified into the four different groups which are the only four different codes in the D and P signal.

Other possible sampling position is at the middle of each bit. This type of sampling is shown in Figure 5-19 and Figure 5-20.

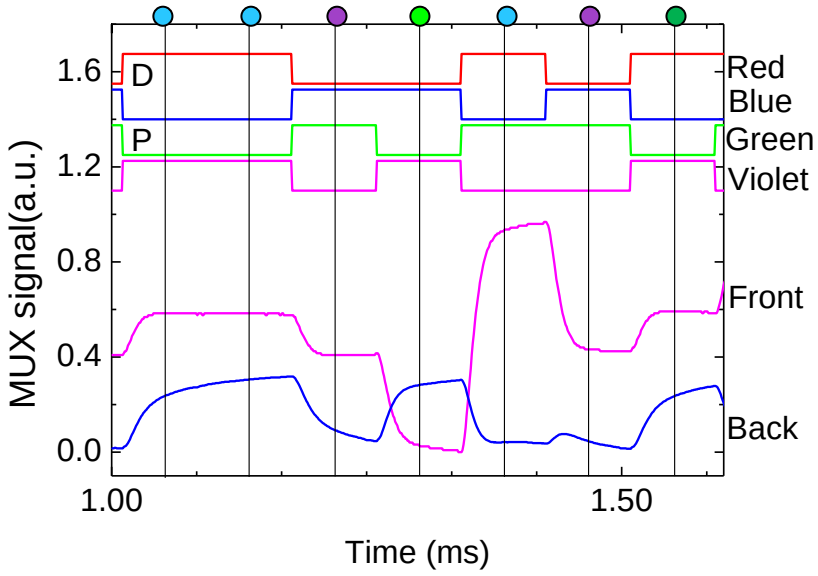

Figure 5-19 - Selected part of Figure 5-9 with the grid showing the sampling of the Front and Back signal at the middle of each bit.

Figure 5-19 shows the grid positioned at the sampling points of each bit. Observing the difference between the first two sampled bits on the left of Figure 5-19 and the same samples in Figure 5-17, it is clear that sampling the bit in the middle is preferable than at the beginning. This middle position is the one that is usually chosen for sampling purposes [17].

The representation of the Front and Back signals as a scatter graph with the sampling point positions is shown in Figure 5-20.

The sampled points are clearly found in four different groups, which imply that they can be easily classified and their code determined.

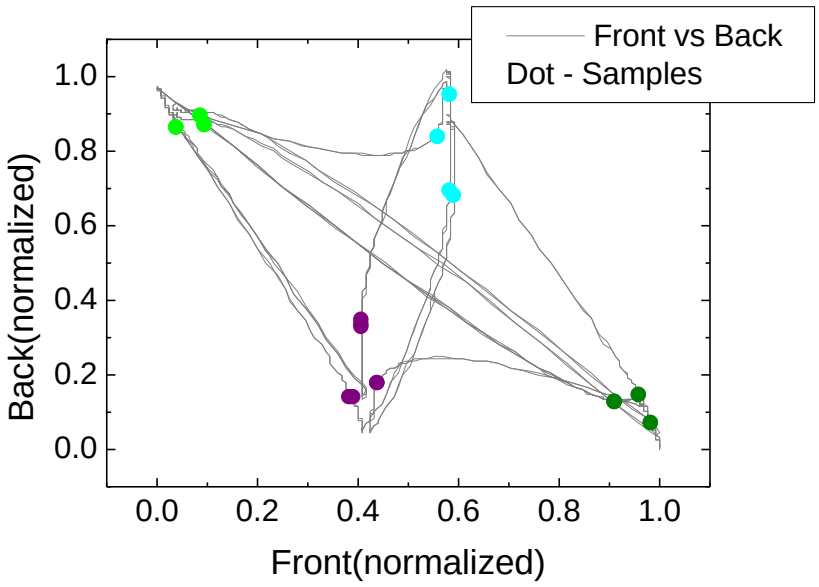

Figure 5-20 – Normalized data of Figure 5-10 showing sampling points at the middle of each data bit.

Figure 5-19 shows the scatter graph of the Front and Back signals of Figure 5-9 with the sampled points at the middle of each bit. Comparing with Figure 5-18 it is evident that the sampling points are a better choice as they group themselves into four distinct groups.

Another type of sampling, at the end of each bit, is shown in Figure 5-21.

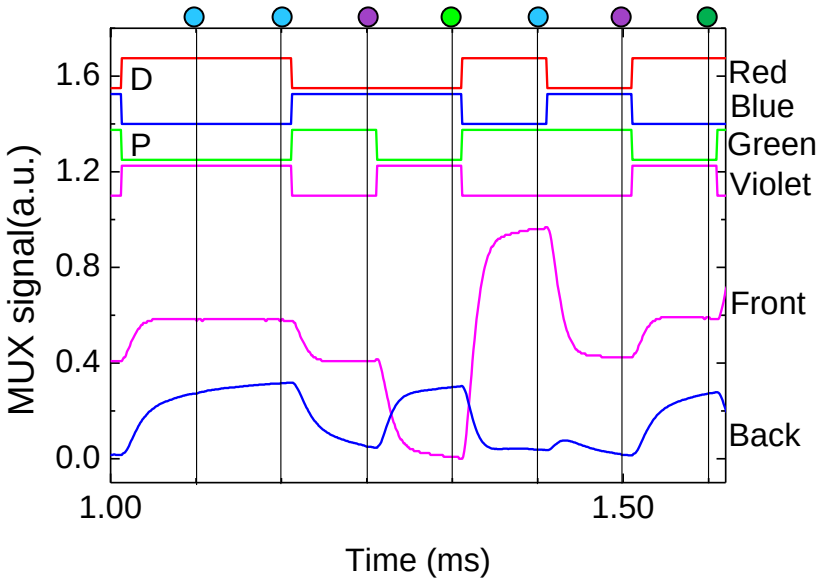

Figure 5-21 - Selected part of Figure 5-9 with the grid showing the sampling of the Front and Back signal at the end of each bit.

Figure 5-21 shows the same pattern of Figure 5-17 with the grid set at the sampling points at the end of each bit.

Comparing these sampling points with those of Figure 5-17 and Figure 5-19, they are set where the signal has less variation. The same signal is represented as a scatter graph in Figure 5-22.

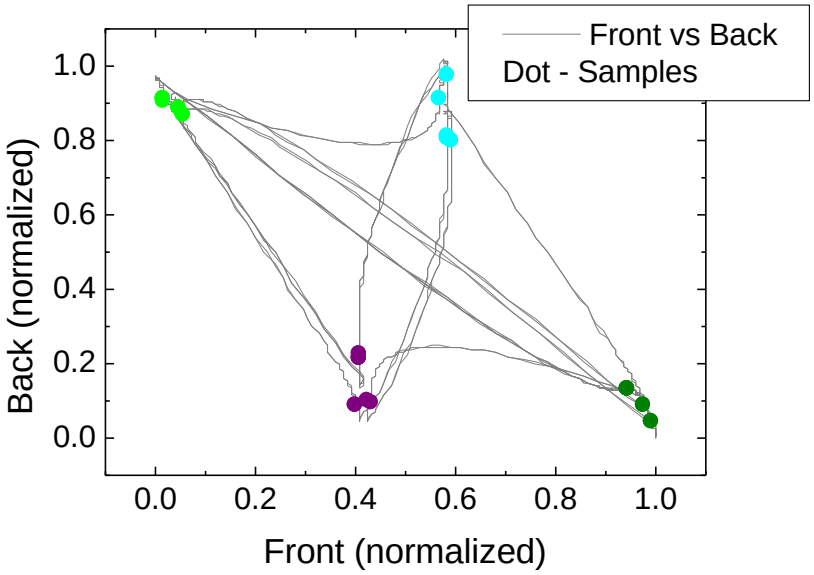

Figure 5-22 – Normalized data of Figure 5-10 showing sampling points at the end of each data bit.

Figure 5-22 shows the scatter graph of the Front and Back signals of Figure 5-17 with the sampling position at the end of each bit. The samples are grouped into four different clusters with allow for clear code identification of each sample. Comparing this figure with Figure 5-20, which also allows perfect sample identification, the samples are in this case more close to each other in the same cluster. Reducing the cluster area allows for more clusters to be included into the same graph if needed were it the case of three or more input digital light signals.

5.9 Interaction of three digital light signals

Logical gates can have more than one or two inputs, and with a well defined input to output function. A stateless logical system with three inputs has eight (2^3) possible input combinations. These eight combinations can

produce 256 (2^8) possible results, some of which are presented as a table in Figure 5-23.

a)

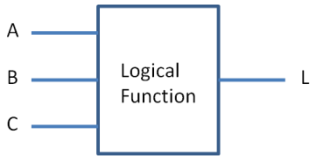

b)

Inputs			Some L outputs from the 256 possible ones													
A	B	C	0		&	|	~&	~|		even	odd		maj	min		1
0	0	0	0		0	0	1	1		1	0		0	1		1
0	0	1	0		0	1	1	0		0	1		0	1		1
0	1	0	0		0	1	1	0		0	1		0	1		1
0	1	1	0		0	1	1	0		1	0		1	0		1
1	0	0	0		0	1	1	0		0	1		0	1		1
1	0	1	0		0	1	1	0		1	0		1	0		1
1	1	0	0		0	1	1	0		1	0		1	0		1
1	1	1	0		1	1	0	0		0	1		1	0		1

Figure 5-23 – a) Three input single output logical system and b) a few input and output combinations from the 256 possible ones.

Figure 5-23 b) shows some logical operations that can be made with three Boolean inputs. Boolean Algebra theory provides properties that can be applied to these functions [1]. The commutative and associative properties hold for the functions shown in Figure 5-23 b). The AND (&), NOT AND (~&), OR (|), NOT OR (~|), have been shown before with two inputs. The EVEN and ODD functions have a Boolean value as output indicating if the number of inputs with value 1 is even or odd respectively. The ODD function is equivalent to the XOR function with two inputs, as shown before. The EVEN function is the NOT ODD. The functions MAJ and MIN have not been presented before.

The majority function (MAJ) indicates that the number of input bits set to 1 is equal or greater than half the number of inputs. It is also called the voting function; its output reflects the majority of 0 or 1 in the inputs. The minority function (MIN) is the inverse of MAJ (for an odd number of inputs) [18].

Using the pi'npin device with three digital input functions results in the signals presented in Figure 5-24.

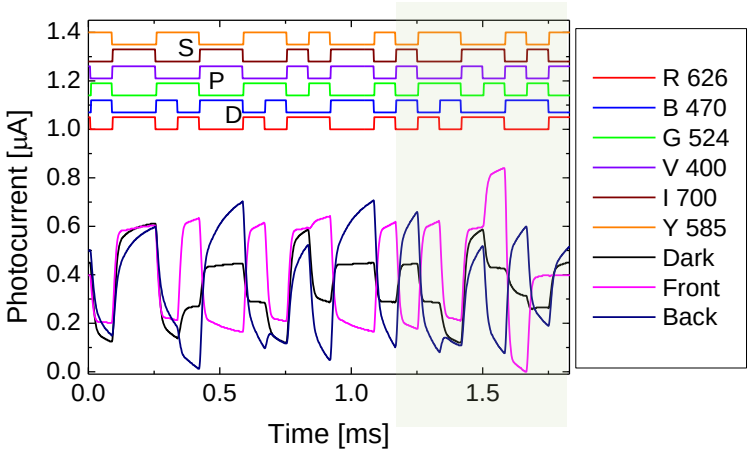

Figure 5-24 – Interaction of three digital light signals, D, P and S.

The interaction of three digital light signals, D, P and S is shown in Figure 5-24. The digital light signal, as stated above, is composed by two different wavelengths carrying differential data and Manchester coded. The three digital light signals are D={Red 625, Blue 470}, P={Green 524, Violet 400} and S={Infra 700, Yellow 585}. The Infa 700 deep red wavelength is close to the boundary of the visible and near infra-red. The shadowed area in the figure holds all possible combinations between the three signals. They can be seen in detail and explained further down in Figure 5-31.

The random sequence SEQ 00 shown is {DPS} = {010, 101, 101, 010, 110, 001, 001, 110, 010, 101, 110, 001, 001, 110, 001, 110, 010, 101, 111, 000, 011, 100}.

The highest output of the front signal in Figure 5-24 is coincident with the highest value of the {D, P, S}, 111, indicating that the Red 625, Green 524 and Infra 700, all wavelengths belonging to the red component of the digital light signal are on. Also the lowest value, 000 coincide with the blue part of the {D, P, S} combination being active.

The presence of the 000 and 111 must be ensured in all experiments to allow the outputs to be compared. To ease the comparison task all outputs must be normalized between 0 and 1. This normalization is reflected in the graph labels.

The normalization is made before the sampling occurs, which is observable as the position of the 000 and 111 values are near and not exactly on top of the maximum and minimum value of the coordinate, which is evident in Figure 5-25.

Sampling the Front and Back signals of Figure 5-24 and coding each sample as a binary value {D, P, S} according to the digital light signals results in Figure 5-25.

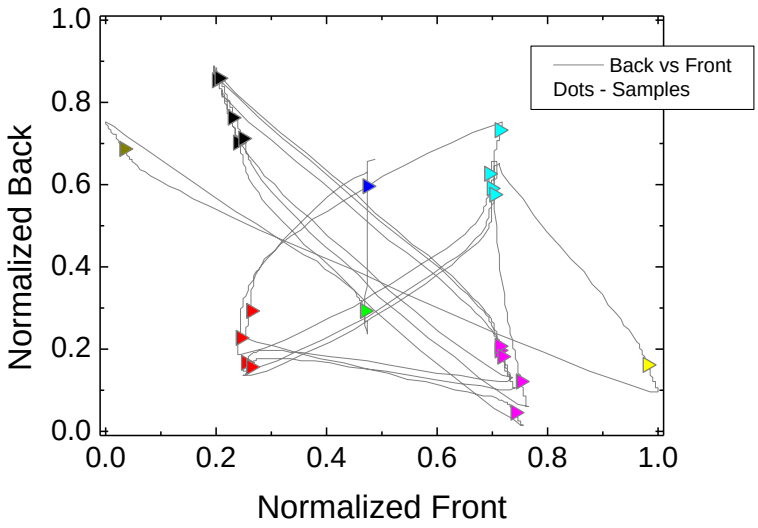

Figure 5-25 – Sample position and values of Front and Back signals of Figure 5-24.

Figure 5-25 shows the position where the Front and Back signals of Figure 5-24 were sampled. The same information is presented in Figure 5-26 with the inclusion of the binary code {D, P, S} held by the input digital light signals at those positions.

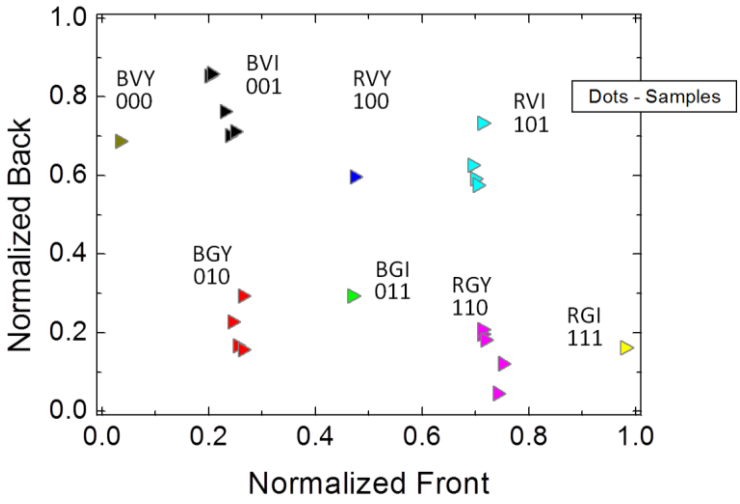

Figure 5-26 – Sampled Front and Back signals of Figure 5-24 and input {D, S, P} codes.

Figure 5-26 displays the codes of the samples of Figure 5-25 and coloured symbols indicating the same codification. The front and back signals were sampled at the end of each bit. Results show that the samples tend to group in clusters and there is a clear separation among the clusters. To verify the clustering a simple verification can be made with several random generated input sequences, and overlapping their sampled output signals in the same graph. The random sequences have all possible combinations of three digital light signals. Random sequence SEQ 01 is presented in Figure 5-27.

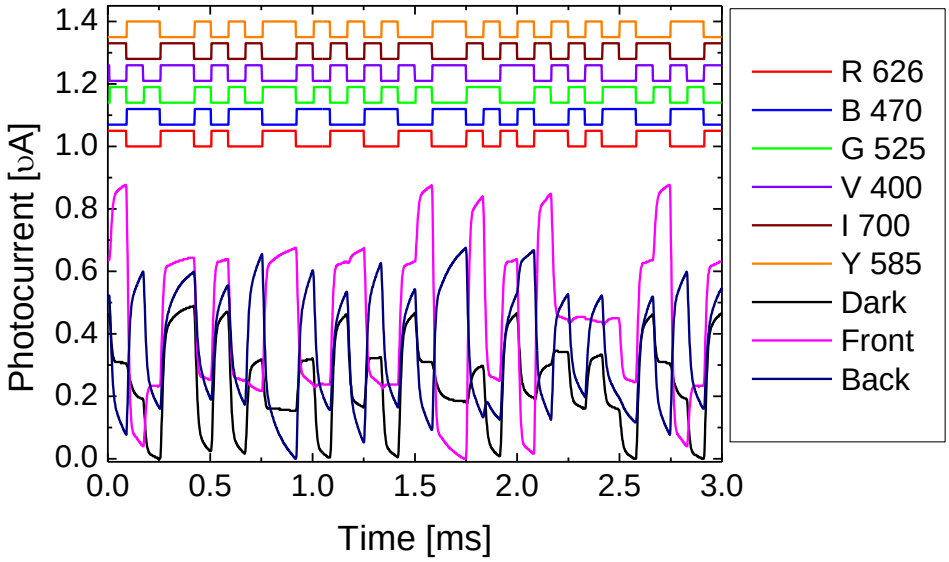

a)

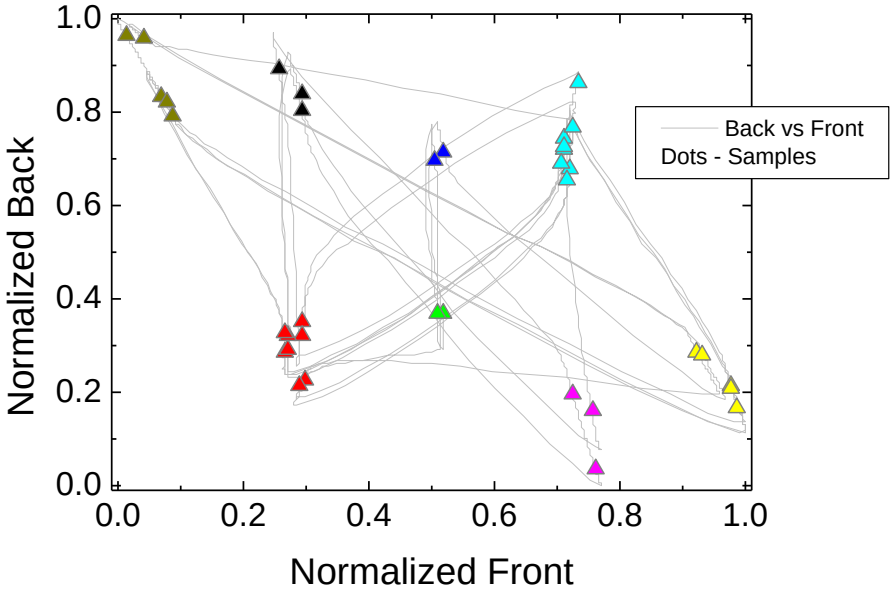

b)

Figure 5-27 – Random sequence (SEQ 01) of three digital light sequences

Figure 5-27 has a random sequence of 32 bits with three digital light signals D, P and S. The random sequence of SEQ 01 is {DPS} = {111, 000, 010, 101, 101, 010, 101, 010, 001, 110, 110, 001, 010, 101, 110, 001, 010, 101, 111, 000, 000, 111, 010, 101, 000, 111, 100, 011, 100, 011, 010, 101}. In this sequence there are only two repetitions of the values {100} and {011} which can be clearly seen in the middle of Figure 5-27b); {100} as two dark blue triangles and {011} as two green triangles within the sequence {…, 111, 100, 011, 100, 011, 010, …}

Another random sequence is presented in Figure 5-28

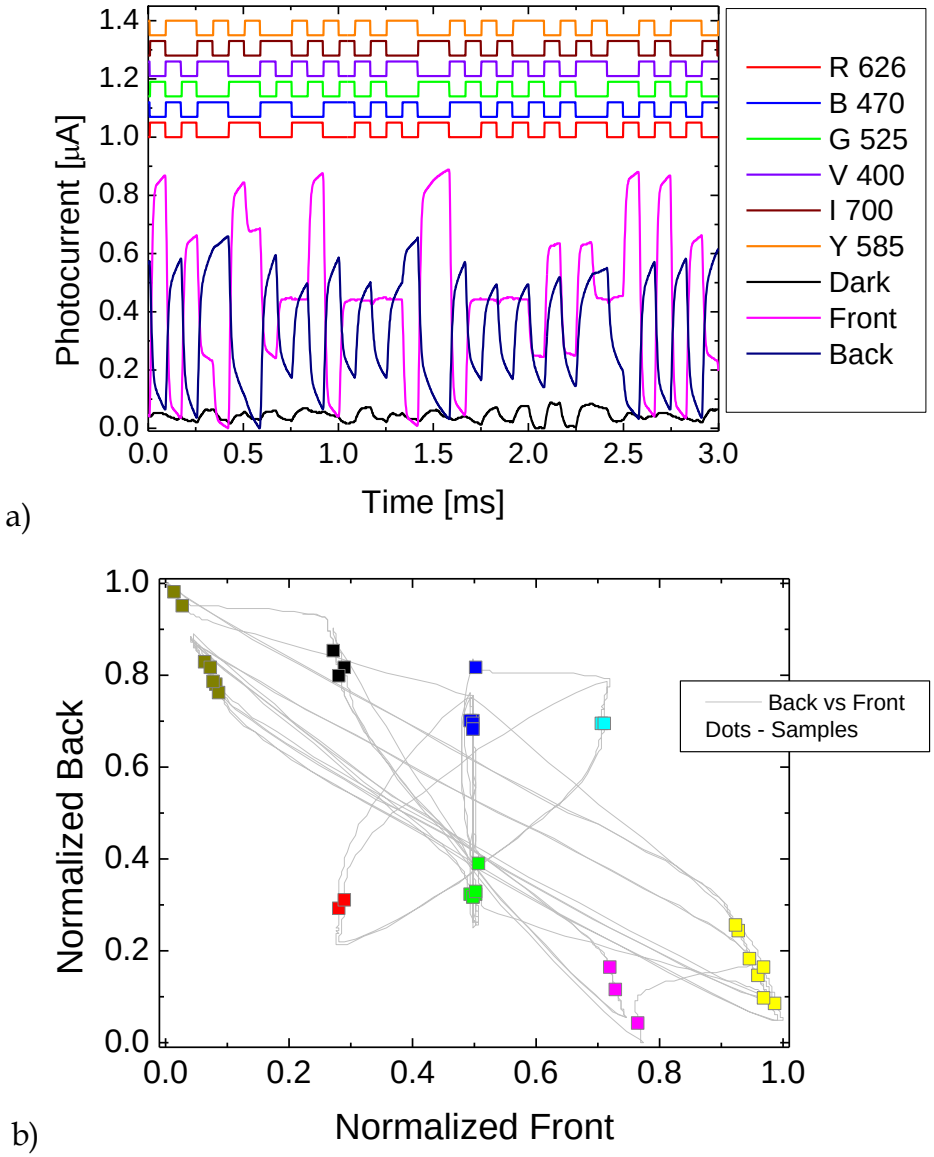

Figure 5-28 – Random sequence (SEQ 02) of three digital light sequences

Figure 5-28 presents the random sequence SEQ 02 of three digital light signals {DPS} = {111, 000, 110, 001, 000, 111, 110, 001, 011, 100, 011, 000, 011, 100, 011, 100, 000, 111, 111, 000, 011, 100, 011, 100, 010, 101, 010, 101, 100, 011, 111, 000}. All possible combinations are present as can be noted by the eight different sampling colours in Figure 5-28b).

Another random sequence is presented in Figure 5-29.

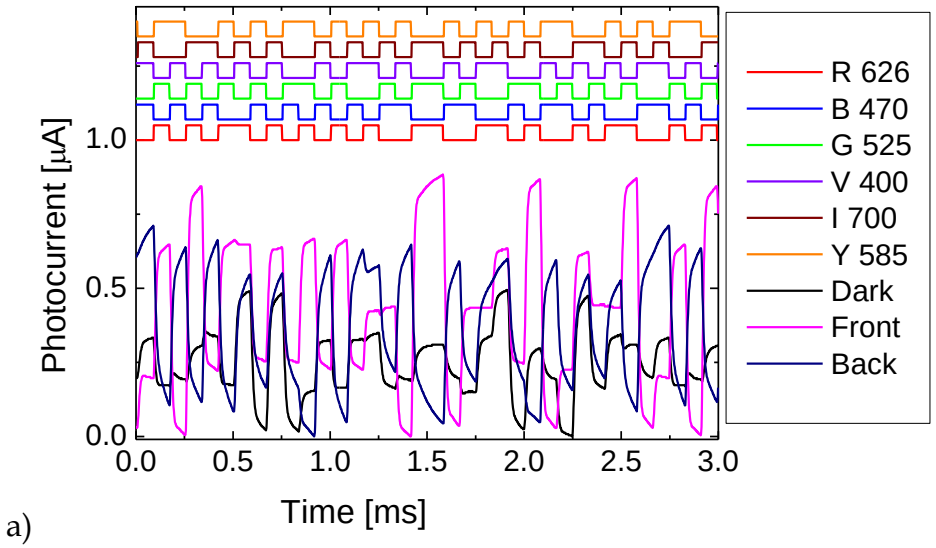

a)

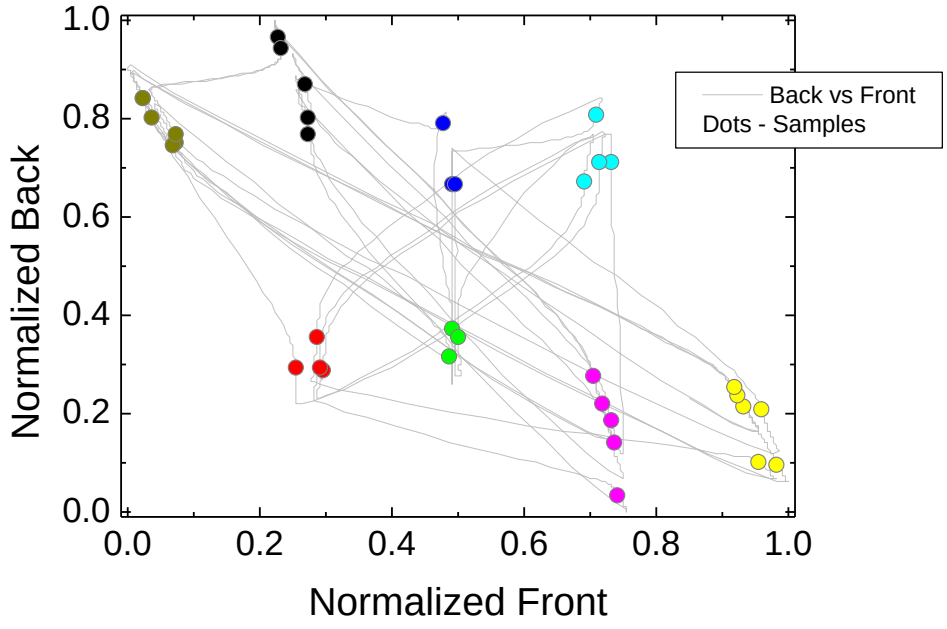

b)

Figure 5-29 – Random sequence (SEQ 03) of three digital light sequences

Figure 5-29 is the result of a random input sequence SEQ03 of three digital light signals defined by {DPS}={001, 110, 000, 111, 001, 110, 101, 010, 101, 010, 110, 001, 110, 001, 100, 011, 000, 111, 111, 000, 011, 100, 101, 010, 111, 000, 010, 101, 011, 100, 111, 000}.

Gathering all random sequences in the same graph yields the Figure 5-30.

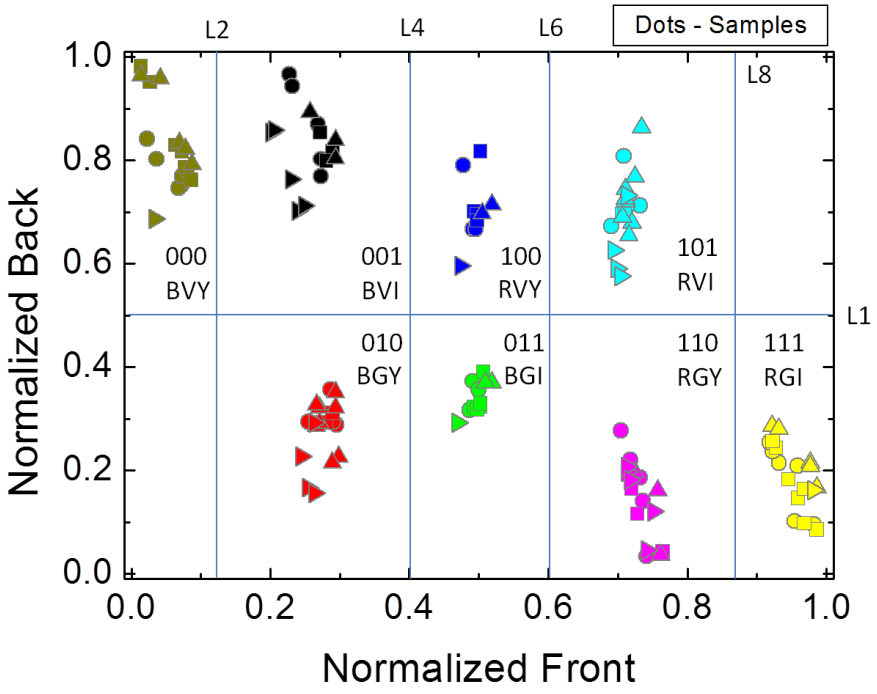

Figure 5-30 – Sampling points of Figure 5-25 and random sequences SEQ 01, SEQ 02, SEQ 03

Figure 5-30 shows all sequences with three digital light signals, the first sequence presented in Figure 5-24 with its scatter graph in Figure 5-25, and the random sequences SEQ 01, SEQ02 and SEQ 03 presented in Figure 5-27, Figure 5-28 and Figure 5-29. It is clear that the samples group as distinct clusters. The code of each input ant the LEDs that are alight are written in Figure 5-30. In the same figure, as a quick classification exercise, several lines were drawn in to divide the Front (L2, L4, L6, L8) and Back (L1) domain into distinguishable areas that hold the eight (2^3) possible outcomes in order to aid the recovery of the signal.

The shaded area of Figure 5-24 holds all possible combinations and it is shown in Figure 5-31 in another time scale for observation purposes. At the top of the figure there are the codes of the {DPS} sequence {001, 110, 010, 101, 111, 000, 011, 100} or in decimal, {1, 6, 2, 5, 7, 0, 3, 4}. The least significant bit is the S signal which accounts for the S[I, Y] digital signal pair. Manchester coding is used which ensures that a code is followed by its inverse, and if they are both summed the result, in this case with three bits (2^3-1), is 7.

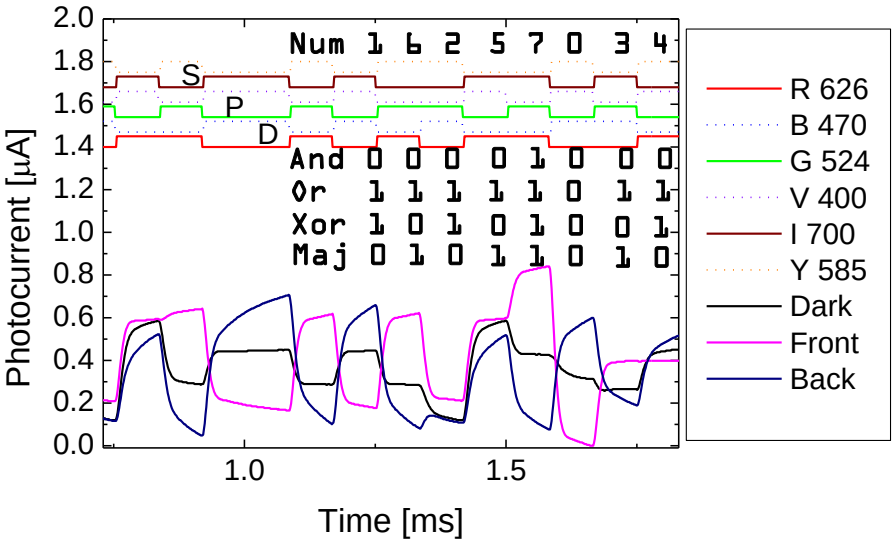

Figure 5-31 – Detail of marked range of Figure 5-24, with logical functions according to table of Figure 5-23b).

Figure 5-31 displays the three digital light signals {DPS} with one component, the reddish, in solid line and the bluish component as a dotted line for visualization purposes. In the same figure there are the logical operations that are being searched, the AND, OR, XOR and MAJ with the expected values for each bit. To determine the logical results the outcomes of the logical operations AND and OR are shaded in Figure 5-32.

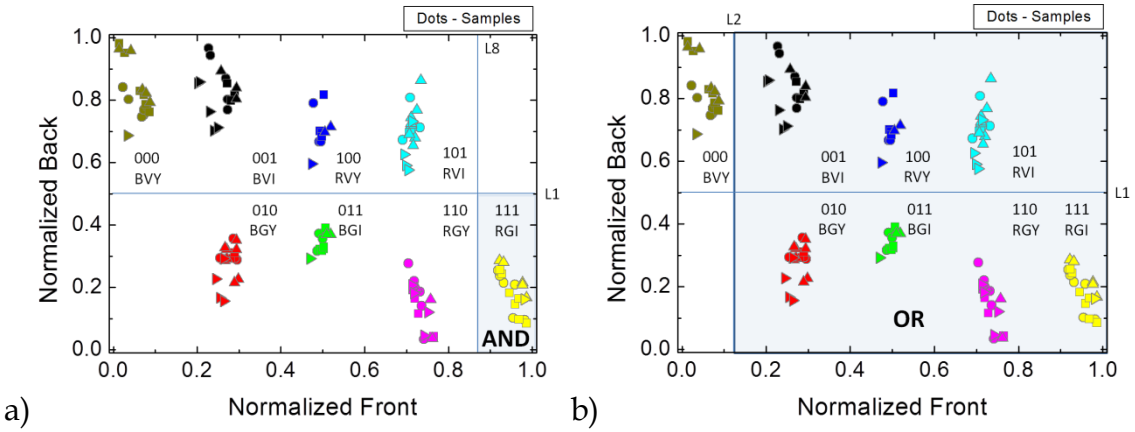

Figure 5-32 – Logical operations a) And, b) Or, with three bits

Figure 5-32a) represents clusters with all possible combinations of three digital light signals and in the shaded portion, delimited by the lines L8 and L1, is the AND logical operation, where all bits are set to 1. The AND is identified by the normalized Front signal above L8 and the normalized Back signal below L1. The OR logical function is shown in Figure 5-32b), identified by any

combination with a bit set to 1, which is the output whenever the normalized Front signal is above L2. Two other logical operations are presented in Figure 5-33.

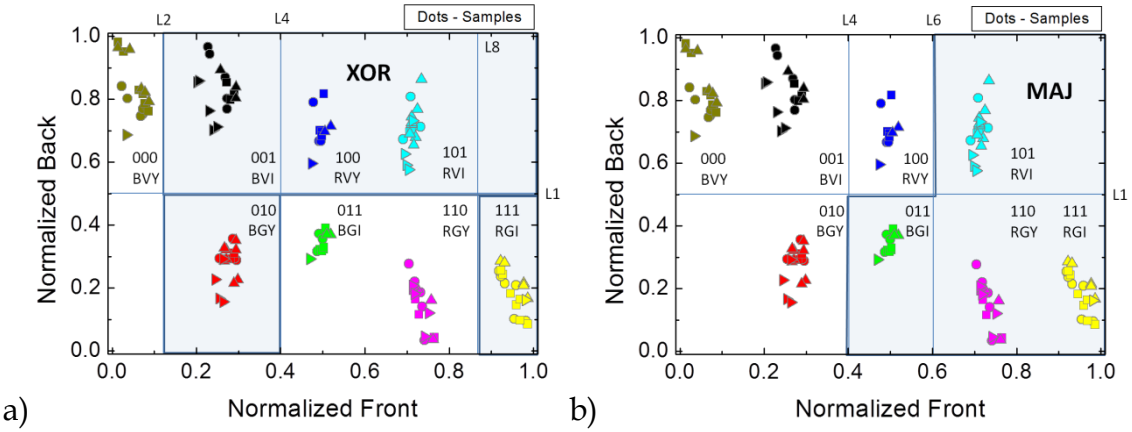

Figure 5-33 – The Logical operations a) XOR, b) MAJ, with three bits

The XOR operation, in which there are an odd number of bits set to 1, is identified in Figure 5-33a) by the shaded are confined by any Front signal normalized value above L2 excluding the values where the normalized Back signal is below L1 and the normalized Front signal is within the L4 to L8 range. The MAJ operation which is identified by two or more bits set to one is shown in Figure 5-33b) in which the result is the shaded area confined by the normalized Front signal values above L6 and also the output in which the normalized Back signal is below L1 and the normalized Front signal is above L4.

The results show that it is possible to build the AND, OR, XOR and MAJ functions with three digital light signals.

5.10Interaction of four and five digital light signals

To see if it is still possible to increase the number of digital channels and maintain the logical functions AND, OR, XOR and MAJ, experiments were made with four and five digital channels. The digital light signal definition implies that the addition of another channel is composed by two components. The Orange 605 nm and Lemon 565 nm wavelengths were chosen among the

available ones. A combination with four digital light signals is presented in Figure 5-34.

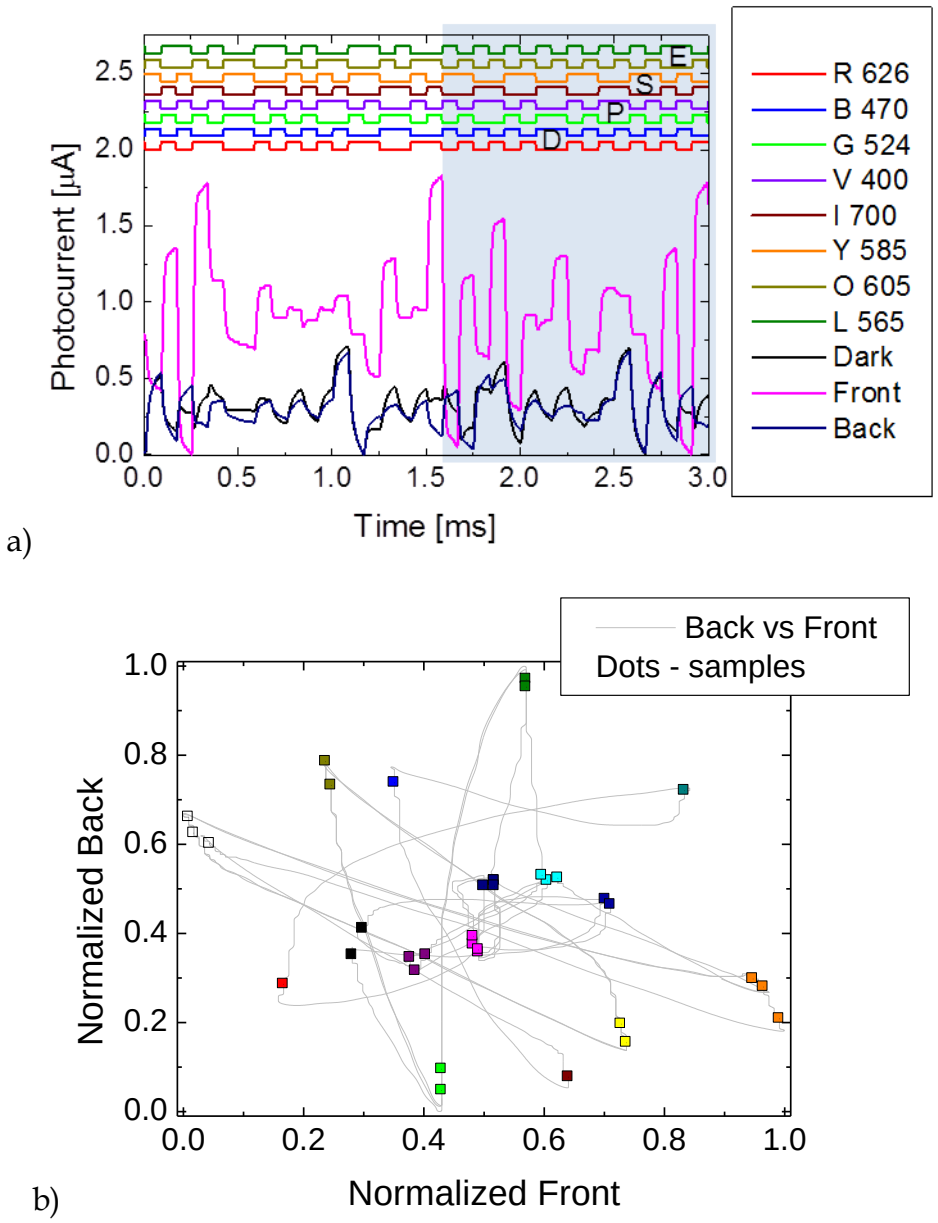

Figure 5-34 – Interaction of four digital light signals, D, P, S and E, a) time graph and b) scatter graph of normalized front and back output signals.

The interaction of four digital light signals, D, P, S and E is shown in Figure 5-34a). The digital light signals D, P and S are composed as before, and another digital light signal E[O, L]={Orange 605, Lemon 565} was added. All four channels are composed by two different wavelengths carrying differential data and Manchester coded. In Figure 5-34b) are the sampling points marked along the Back vs Front path shown in grey. As can be noted in this and the

following scatter figures, the eye diagram tends to close in the centre of the graph reducing the distance among different clusters. This may represent a difficulty in determining the correct coding of those samples. The shadowed area in Figure 5-34a) holds all possible combinations between the four signals. They can be seen in detail and explained further down along with Figure 5-35.

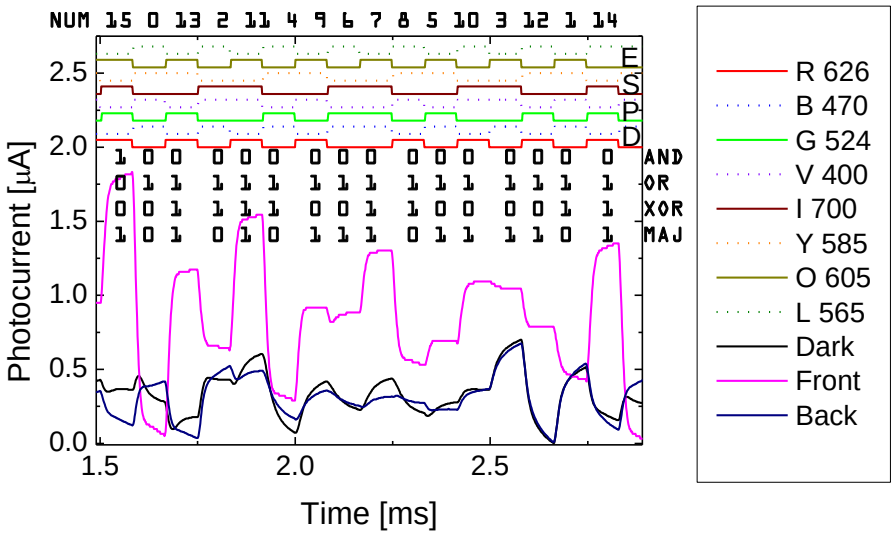

Figure 5-35 – Detail of marked range of Figure 5-34a), with expected values of the AND, OR, XOR and MAJ logical functions.

The highest output of the front signal in Figure 5-35 is coincident with the highest value of the {D, P, S, E}, 1111, indicating that the Red 625, Green 524, Infra 700 and Orange 605, are all wavelengths belonging to the red component of all digital light signals. Also the lowest value, 0000 coincides with the blue part of the {D, P, S, E} combination being active. It should be noticed that the "blue" components of digital light signals S (Y 585nm) and E (L 565nm) do not actually belong to the blue part of the spectrum. This is due to the fact that on the experimental setup, at this time, there were no other LEDs available. Although these signals can still be used for the logical functions AND, OR, XOR and MAJ, they cannot be used for the NOT function because it is not possible to enhance wavelengths above 500 nm with the ultra violet illumination at the back of the sensor, as shown in Figure 5-2.

At the top of Figure 5-35 there is the decimal representation of the binary sequence {D, P, S, E} where E[O, L] is the least significant bit. The sum of two consecutive numbers adding up to 15, (2^4-1), is an indication that the sequence is Manchester coded.

Follows three random sequences of four digital light signals shown in Figure 5-36 to Figure 5-38.

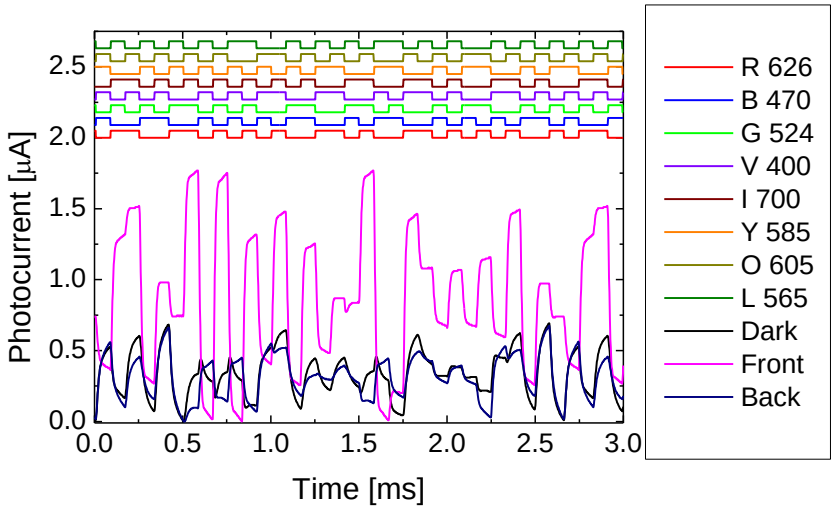

a)

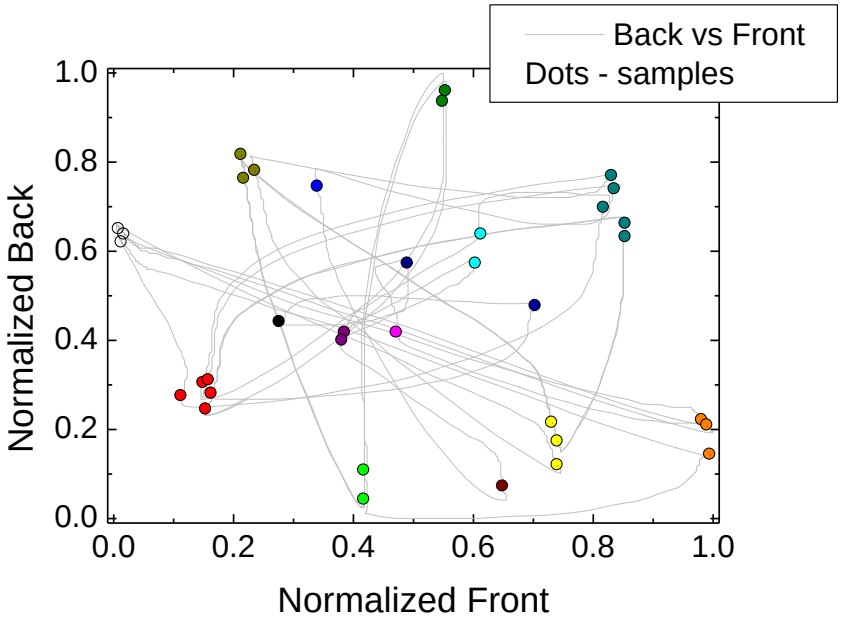

b)

Figure 5-36 – Random sequence (SEQ 41) of four digital light sequences

Figure 5-36 shows the random sequence SEQ41 with four digital light signals. The 32 bit random sequence is repeated in time to be seen and acquired by an oscilloscope, and the time frame presented has 36 bits. All experiments ensure the presence of the 0000 and 1111 to allow the outputs to be compared, and ease the normalization between 0 and 1, which occurs before the sampling.

All 16 possible combinations are present in the 32 bit sequence as can be seen by the 16 different clusters of Figure 5-36b). Another random sequence is shown in Figure 5-37.

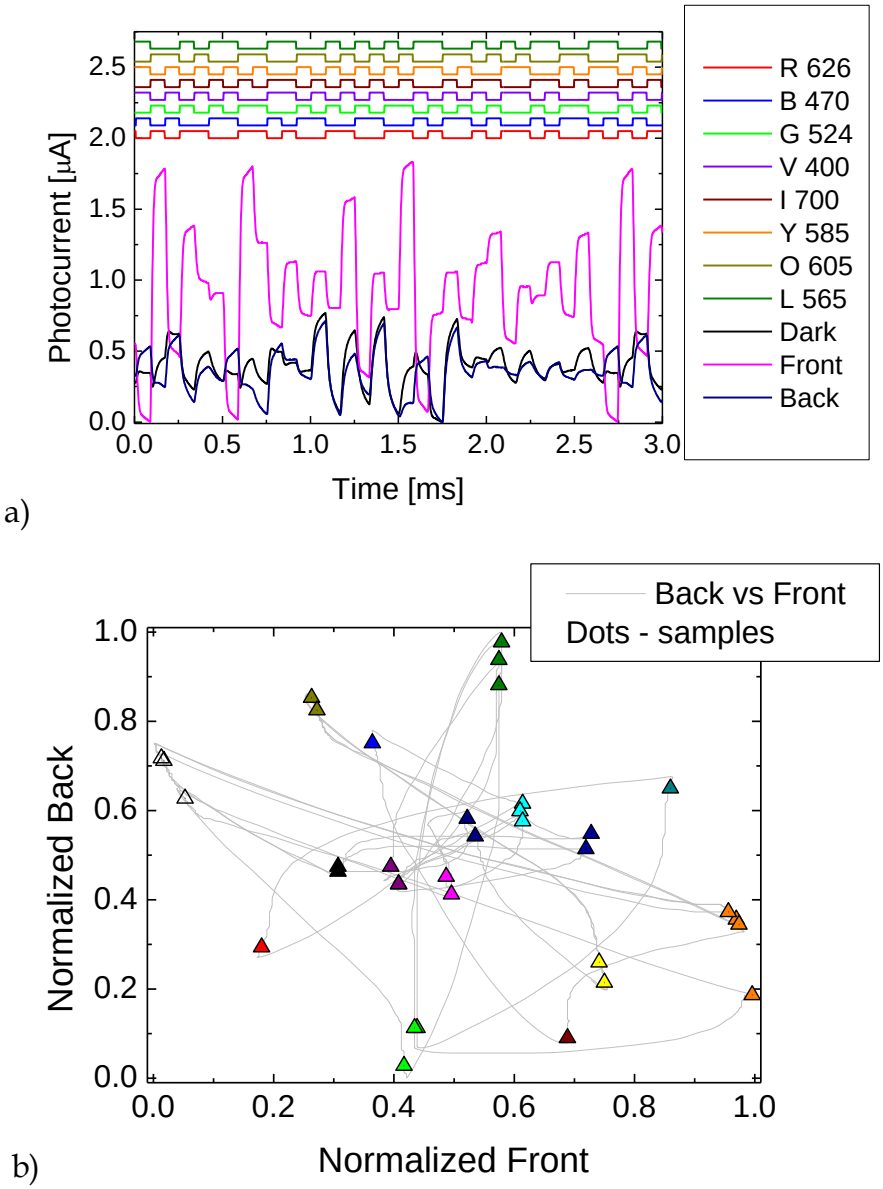

Figure 5-37 – Random sequence (SEQ 42) of four digital light sequences

Figure 5-37a) shows the time sequence of four digital light signals. The highest photocurrent output of the front signal is related to the maximum 1111 digital input sequence, and the lowest photocurrent value corresponds to the 0000 digital inputs. All samples were made at the end of each bit time, which

can be seen by the position of those samples in the scatter graph of Figure 5-37b) over the back vs front output signal line which represents a path in the scatter graph. The end of the bit position coincides with the vertexes of the path line in grey. Another random sequence is presented in Figure 5-38.

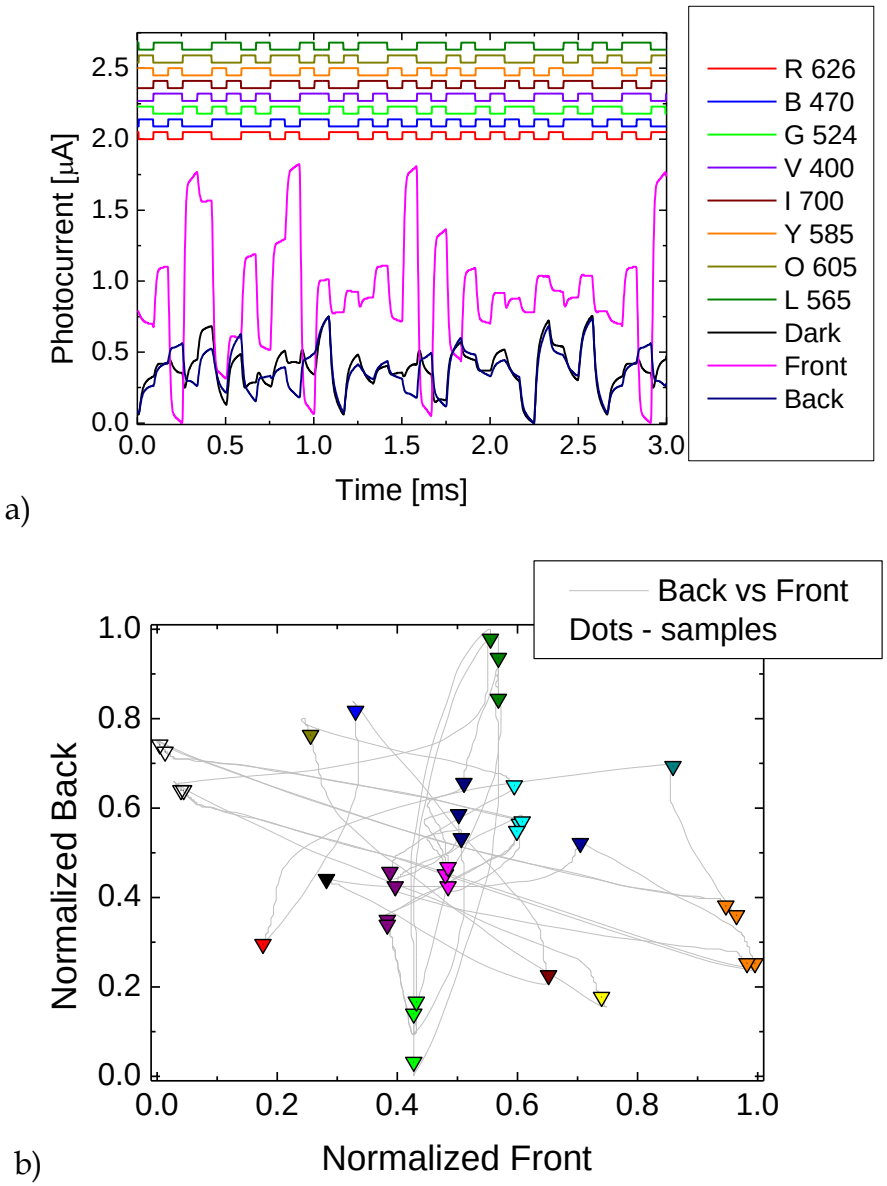

Figure 5-38 – Random sequence (SEQ 43) of four digital light sequences

Presented in Figure 5-38a) are 36 bits of a repeated 32 bit random sequence. Comparing the scatter distribution of the samples in Figure 5-38b) with their similar in Figure 5-36b) and Figure 5-37b), it can be observed that the repeated sequences in each graph tend to distribute themselves vertically, which is equivalent to say that for the same input values the front output signal

is more stable than the back output signal, i.e. the front is less dependent of the path than the back signal. Putting together all samples in the same figure this distribution is more evident as can be seen in Figure 5-39.

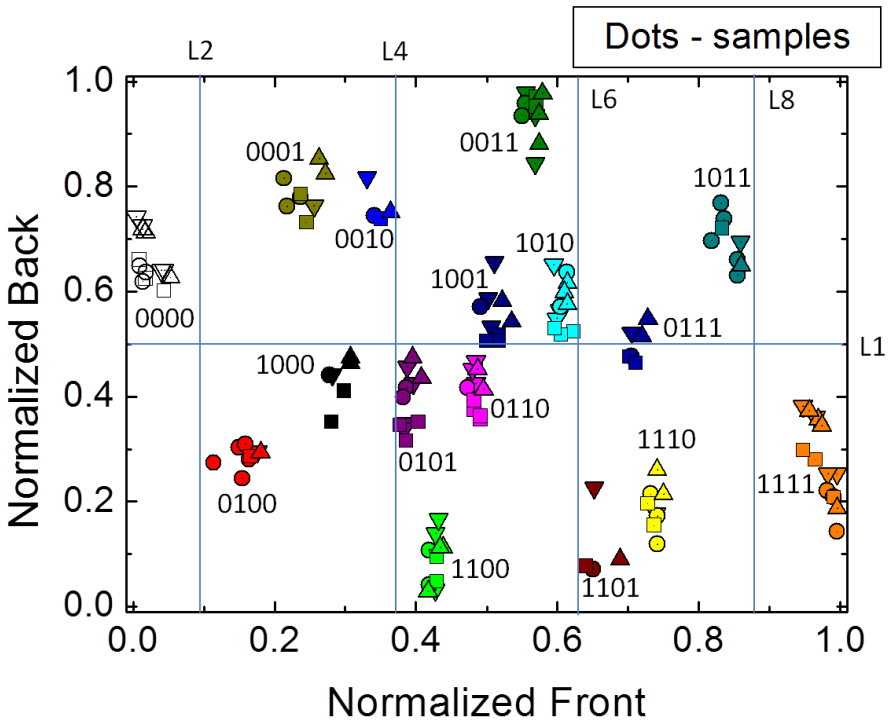

Figure 5-39 – Sampling points of Figure 5-34 and random sequences SEQ 41, SEQ 42, SEQ 43, all with four digital light signals.

Shown in Figure 5-39 there are all normalized samples of four digital light signals presented in Figure 5-35 to Figure 5-38. Also shown are the same level lines L1, L2, L4, L6 and L8 used for three digital light signal code recovery in Figure 5-30. At this stage, the interest in code recovery is for the identification of the logical output and not the exact code of the input bits. These five level lines are at this point sufficient enough to identify the output of the AND, OR, XOR and MAJ logical functions, as can be seen in the following Figure 5-40 and Figure 5-41. The level lines should in fact be subject to slight modifications for the efficient identification of the logical outputs for any four digital signal random sequences.

As noted before, the different clusters in the centre of Figure 5-39 are very close to each other which makes it difficult to identify unique codes, and an error of 4 bits can be easily made, for example between 1001 and 0110. The codes in which the digital light signals S and E change state in the {D, P, S, E}

tuple are the ones in which the "blue" component belongs to the red part of the spectrum. With the appropriate wavelengths the cluster distance should increase. Besides this aspect, the AND and OR logical functions are well defined as shown in Figure 5-40.

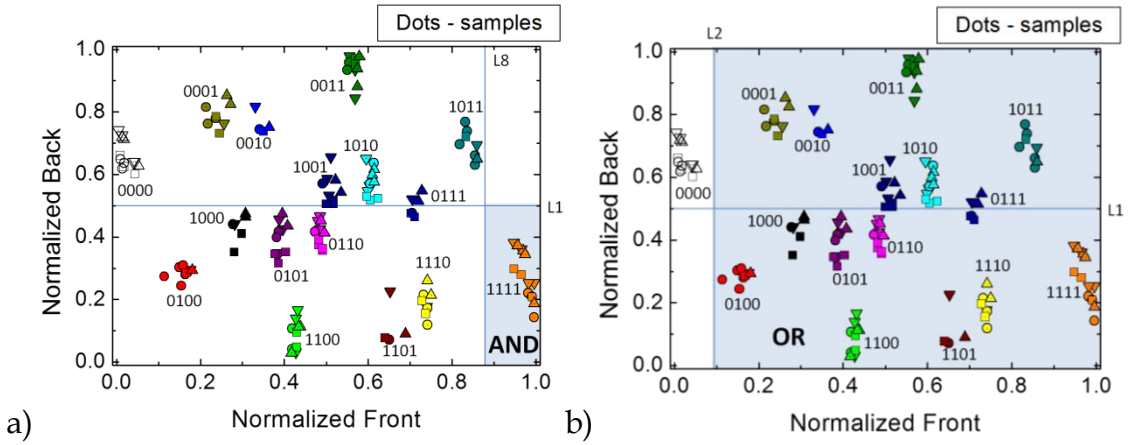

Figure 5-40 – Logical operations a) And, b) Or, with four bits

Figure 5-40a) shows how to identify the AND logical function, which is a single cluster in the shadowed area. Likewise is the OR logical function in Figure 5-40b), where the expected output is the whole domain except for a single cluster. These two output clusters are easily found as they represent the highest (AND, above L8) and the lowest (OR, above L2) values of the front signal, which can also be delimited by the back signal in which the AND is below the threshold line L1 and the OR above it.

Using the threshold lines other logical functions are identified in Figure 5-41

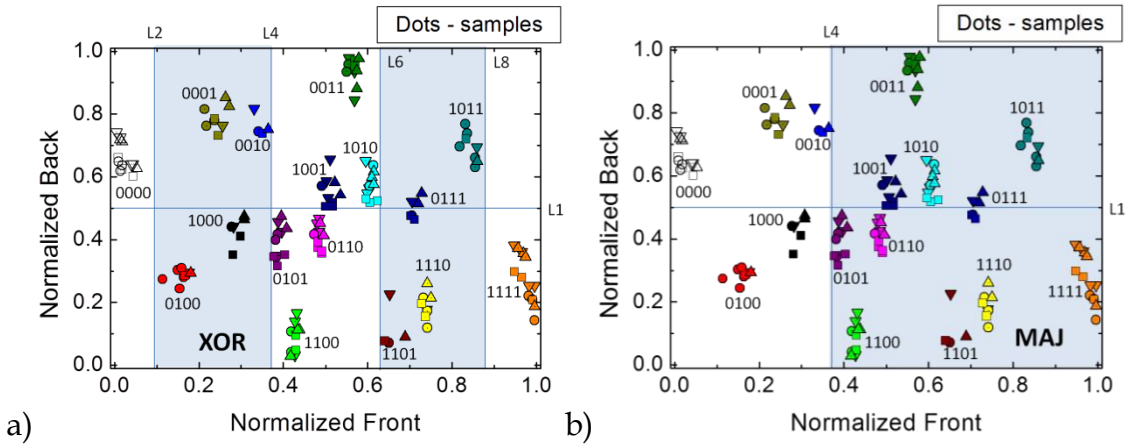

Figure 5-41 – Logical operations a) Xor, b) Maj, with four bits

The XOR logical function can be identified by the values of the front signal that lie between threshold lines L2-L4 and L6-L8, as can be seen in Figure 5-41a), where the result is all clusters with an odd number of 1 in its code. The logical function of Figure 5-41b) is the MAJ function. The majority function, as a voting function, has more meaning when there are an odd number of inputs, which is not the case of this four input function. Nevertheless it is defined as the output in which the number of 1 is at least half of the number of inputs. To exclude the half condition, the threshold line L6 can be used instead of the L4 delimiting the shadowed area of the figure.

By comparing the clustering of the shadowed areas of Figure 5-40 and Figure 5-41 it can be noted that on this particular case of four inputs the front output signal is enough to distinguish between all functions with the aid of the threshold lines.

5.11 The Adder

To build any complex digital function there is only a need for the NOT and either the AND or the OR gates. With only those two types of gates and the Boolean theory, different circuits can be made from a simple switch to a computer.

One useful circuit is the adder, which is used to sum two bits. The adder is built to work under the binary numeric base. A bit logical value True is a bit set to one and the value False is the bit set to 0. Summing bits is then a task of counting the number of bits that are set to 1 and produce an output in the binary base that represents that value.

To add more than two bits, a module called the full-adder is used because it can easily be concatenated with equal modules to produce an adder with any number of bits.

Using the pi'npin behaviour to use it as an adder can be twofold. Either as a simple two bit adder (also called a half adder) and use several pi'npin devices for more than two bits, or by adding as much bits as possible with a single p'inpin. The latter approach will be used in this work, and determining how

many bits can be summed at the same time minimizing the effort, whether hardware or software.

Presented in Figure 5-42 is the sum of two bits.

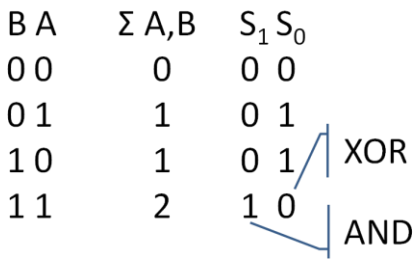

Figure 5-42 – Binary sum of two bits.

The sum of two bits is the smallest addition that can be made in binary. In Figure 5-42 there is the sum of two bits B and A. The sum in decimal base is {0 1, 2}, and the binary result {00, 01, 10}. The binary number S_1S_0 is composed by two digits with the following values $S_1=2^1=2$ and $S_0=2^0=1$.Observing the result of the binary sum with Table 5-1 it can be possible to determine that the lowest bit, S_0, has the same output of the XOR function with two variables and the high order bit, S_1, is the same as the AND function, with two variables. Both the sum and the logical operations AND, XOR, are commutative.

Examining the sum operation with three bits it is possible to present Figure 5-43.

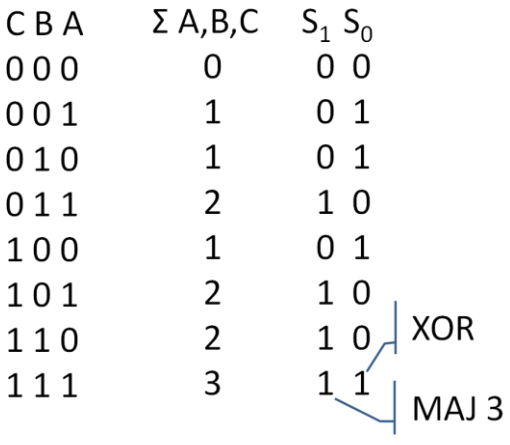

Figure 5-43 – Binary sum of three bits

The sum of three bits has a result between 0 and 3 in decimal base. Observing the binary output of each bit S_1 and S_0 individually and comparing

to the table of Figure 5-23b) the S_0 output is coincident with the odd column which is the XOR, and the S_1 output is coincident with the maj column which is the majoring of three, represented by MAJ3.

The sum of three binary bits is the basic building block of a binary adder, the full-adder. This is such because it can be considered as the sum of two binary digits being added to the carry-on of the previous digit. The result is always a two digit number, the low order S_0 is the digit with the same order of the sum and the high order bit S_1 is the carry-on of the next sum. A full-adder is schematically represented in Figure 5-44a).

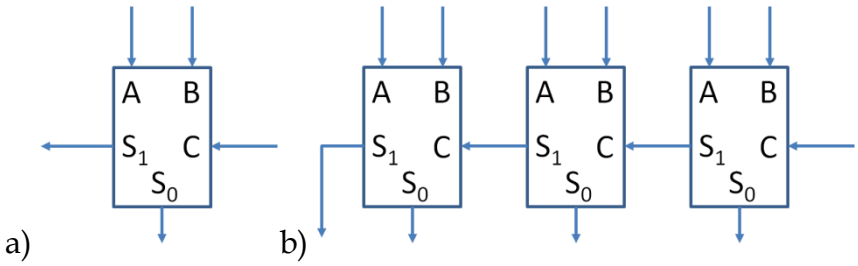

Figure 5-44 a) A three bit adder (full-adder), and a three binary digit adder.

By combining several full-adders it is possible to construct an adder with as many bits as needed, connecting them like Figure 5-44b). The figure shows a three digit sum with an entry for a Carry-in (C) and the four digit output in which the highest order bit is the Carry-out (S_1). The sum of two values with n digits produces a result with a maximum number of n+1 digits, despite the base in which the number is written in.

The sum of four bits is shown in Figure 5-45.

D C B A	Σ A,B,C,D	S_2 S_1 S_0	D C B A	Σ A,B,C,D	S_2 S_1 S_0
0 0 0 0	0	0 0 0	1 0 0 0	1	0 0 1
0 0 0 1	1	0 0 1	1 0 0 1	2	0 1 0
0 0 1 0	1	0 0 0	1 0 1 0	2	0 1 0
0 0 1 1	2	0 1 0	1 0 1 1	3	0 1 1
0 1 0 0	1	0 0 1	1 1 0 0	2	0 1 0
0 1 0 1	2	0 1 0	1 1 0 1	3	0 1 1
0 1 1 0	2	0 1 0	1 1 1 0	3	0 1 1
0 1 1 1	3	0 1 1	1 1 1 1	4	1 0 0

XOR

AND

Unkown

Figure 5-45 – Binary sum of four bits

The sum of four bits is presented in Figure 5-45. The highest order bit S_2 is easy to identify with the AND function of all inputs, and the lowest order bit S_0 is also identifiable with the XOR function of all bits. The result of the sum of four bits is an integer value between 0 and 4. The bit order S_1 is almost equal to the MAJ4. The MAJ4 function has a true output value whenever the number of bits is 2, 3 or 4. Observing Figure 5-45, the S_1 bit is active whenever the sum is 2 or 3. This is no known function, but it can still be built as the AND, XOR and MAJ functions are built. This unknown function which we can name QMAJ4 is the MAJ4 set except the AND set. This can easily be built observing Figure 5-40a) and Figure 5-41b), and delimiting the MAJ4 function with the level line L8 it is possible to build the QMAJ4 shown in Figure 5-46.

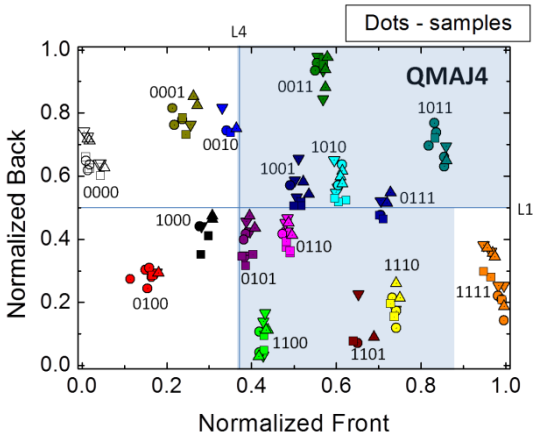

Figure 5-46 – Function for bit S_1

Shown in Figure 5-46 is the function for the S_1 bit of the result of the binary sum of four bits, called in this thesis QMAJ4 because it is almost like the MAJ4 function of Figure 5-41b).

With five or more bits the distribution of the number of bits is shown in Figure 5-47.

Number of bits	S_3	S_2	S_1	S_0
5	0	4,5	2,3	odd
6	0	4,5	2,3,6	odd
7	0	4,5,7	2,3,6	odd
8	8	4,5,7	2,3,6	odd

Figure 5-47 – Active output bits {S_3, S_2, S_1, S_0} for the summing of 5 to 8 number of bits.

With more bits involved in the sum the difficulty increases. In Figure 5-47 the sum of all bits is written in binary as {S_3, S_2, S_1, S_0}. The value of each bit depends on the count, and the numbers indicate when they are active. With 5 bits, the output S_2 must be active when all bits are 1 (AND) and also when there are 4 bits. But for 6 bits, when all bits are 1 (AND) the S_1 must be active and also when there are 2 or 3 bits set to 1. Different functions must be built for each number of bits that are being counted. Only the S_0 bit is common and does not change with the numbers of bits; it is always the odd number of bits, the XOR.

5.12Conclusion

The SiC:H sensor has the characteristic of a tuneable filter in two distinct bandwidths, the long and short wavelengths. By defining a digital light signal as the combination of two wavelengths, one from the long and other from the short bandwidth it is possible to identify the inverse function using the tuneable filter characteristic. The digital inverse function, known as the NOT, is a sine qua non expression in the digital domain.

The interaction of two digital light signals allow for the identification of other basic logical functions: AND, OR. The more complex digital function, the XOR is also a possible outcome of the sensor [8].

Results show that it is possible to use a single sensor to construct a NOT, AND, OR and XOR function with two digital light signals as input. The digital light signal is a composition of two wavelengths, one belonging to the short pass filter and the other to the long pass filter. One component has a data contents and the other has the inverse of that contents, both synchronous. This allowed the NOT function to be implemented by choosing the data contents with either a front or a back illumination of the background with violet light. Two digital light signals were presented simultaneously on the front surface of the sensor interact and their output, under front or back illumination is used as the result of a logical function [11]. To extract the logical functions only the multiplexed signal under front irradiation was used because it is not necessary to distinguish between the {01} and {10} input configuration [14, 19].

The sampling position within each bit has better results when it is set at the end of each received bit. This is due to the signal being more stable in its value, allowing a reduced cluster area for each code and thus increasing the distance between clusters.

The majority function, MAJ, is also possible to be implemented.

The interaction of two, three, four and five digital light signals have been shown. The use of other number of digital light signals can be used. The threshold lines number and values may need to change in that situation.

The easiest way to identify and define the logical output is by using threshold lines.

The threshold lines can also be used to build different functions. This is the case of the adder function.

The adder function can be as simple as summing 2 bits, the half-adder, 3 bits the full-adder and any other number of bits.

With two bits, nothing needs to be change, the output is of two functions, the AND and the XOR.

With three bits, nothing needs to change, the outputs is of two functions, the MAJ3 and the XOR.

With four or more bits, other functions using one or more threshold lines must be built, and the complexity increases with the increase of the number of bits.

As a suggestion, the pi'npin device should be used as a half or full-adder and exceptionally as a 4 bit adder function.

5.13 References

[1] G. Boole, "The mathematical analysis of Logic," 1847.

[2] H. Nishimura, "Boolean valued decomposition theory of states," *Publ. Res. Inst. Math. Sci.*, vol. 21, no. 5, pp. 1051–1058, 1985.

[3] A. Tanenbaum and T. Austin, *Structured computer organization*, 6th ed. Pearson Education International, 2013.

[4] Millman, *Microelctronics*. Mcgraw Hill.

[5] V. Silva, M. A. Vieira, P. Louro, and M. Vieira, "Optoelectronic digital capture device based on Si/C multilayer heterostuctures," in *Technological Innovation for the Internet of Things*, Springer Berlin Heidelberg, 2013, pp. 555–562.

[6] J. B. Moore and K. T. Tan, "Majority Logic Coding and its Multinomial Representation," no. 2, 1975.

[7] W. Stallings, *Computer Organization And Architecture Designing For Performance.*, 8th ed. Prentice Hall.

[8] V. Silva, M. A. Vieira, P. Louro, M. Barata, and M. Vieira, "Simple and complex logical functions in a SiC tandem device," in *Technological Innovation for Collective Awareness Systems*, 2014, pp. 592–601.

[9] M. Vieira, M. A. Vieira, V. Silva, P. Louro, and J. Costa, "SiC monolithically integrated wavelength selector with 4 channels," *MRS Proc.*, vol. 1536, pp. 79–84, Jun. 2013.

[10] V. Silva, M. A. Vieira, M. Vieira, P. Louro, A. Fantoni, and M. Barata, "Logic functions based on optical bias controlled SiC tandem devices," *Phys. Status Solidi*, vol. 11, no. 2, pp. 211–216, Feb. 2014.

[11] V. Silva, M. Vieira, P. Louro, and M. Barata, "Logical functions in a tandem SiC device," *Microelectron. Eng.*, vol. 126, pp. 79–83, Jun. 2014.

[12] ATMEL, "Manchester Coding Basics: Application Note," 2009.

[13] W. Navidi, *Statistics - for Engineers and Scientists*, 3rd ed. McGraw-Hill Professional, 2010.

[14] V. Silva, M. A. Vieira, P. Louro, M. Barata, and M. Vieira, "AND, OR, NOT Logical Functions in a SiC Tandem Device," *Procedia Technol.*, vol. 17, pp. 557–565, 2014.

[15] G. Breed, "Analyzing Signals Using the Eye Diagram," *High Freq. Electron.*, pp. 50–54, 2005.

[16] B. G. Mobasseri, "Digital modulation classification using constellation shape," *Signal Processing*, vol. 80, no. 2, pp. 251–277, 2000.

[17] G. C. Valley, "Photonic analog-to-digital converters.," *Opt. Express*, vol. 15, no. 5, pp. 1955–1982, 2007.

[18] E. Pacuit and S. Salame, “Majority Logic,” in *Principles of Knowledge Representation and Reasoning*, KR 04., C. W. and M.-A. W. D. Dubois, Ed. 2004, pp. 598–605.

[19] M. A. Vieira, M. Vieira, V. Silva, P. Louro, and M. Barata, “Optoelectronic logic functions using optical bias controlled SiC multilayer devices,” *MRS Proc.*, vol. 1536, pp. 91–96, Jun. 2013.

6

6 Memory Function

The p'inpin device has been used throughout this work as a stateless component which means that its output is only dependent of its inputs regardless of the outcome history of past inputs or outputs. This however does not hold when the outputs are observed as a sequence of inputs. The identification of the input sequence, using a classification function with the output of the pi'npin, shows that past sequences do influence the output of the device which does in fact hold a memory of the illumination beforehand. Although this is a difficult task for signal identification it is necessary to understand this phenomenon to ease the identification task and also to use it as an advantage by constructing a volatile memory with the pi'npin device.

6.1 Paradigm change

The observations made to indicate that there is a memory function that characterizes the pi'npin device started when the readings of the dark signal did not remain constant between experiments. Initially it was assumed that there was an influence of noise from the surrounding equipment and other devices. Several modifications were gradually made to the experimental setup to reduce the influence of the noise sources. Presently the device is inside a Faraday cage with coaxial cables connecting the device to the equipment, but the cables that connect the LEDs to the drivers are not yet coaxial which would further reduce the electromagnetic noise.

To understand the start condition of the pi'npin device and its influence over the output, changes were made to the software of the user interface and that of the microcontroller that drives the LEDs. These changes allow static readings to be made. The selection of a start condition, programmable delays and the possibility of short sequences, all time controlled and with adequate triggering for the oscilloscope, allowed the study that is presented in this section.

The optical bias as a steady lighting has been used in all experiments till this point, for example, as different applications namely the WDM communication element and digital light logical functions [1]–[3]. To use the device as a volatile memory the optical bias paradigm is changed and looked upon as two light Control signals; the Front Control and the Back Control signal [4]. On this section they are no longer steady state, but impulses.

6.2 Conceptual approach

The experimental setup with the relative positioning of the LEDs and the pi'npin device can be visualized in Figure 6-1 along with the measuring and control equipment. The PiscaLed system [5, 6] controls the LED currents and their on/off timing patterns.

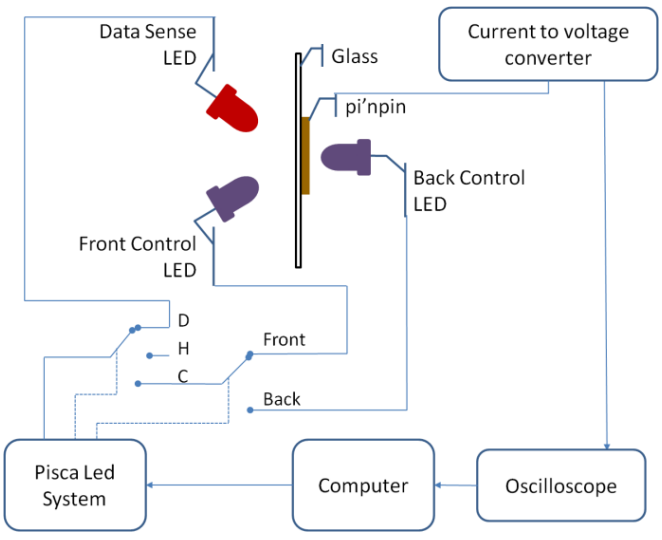

Figure 6-1 - Experimental Setup showing LEDs and their relative position with the p'inpin device and the D (Data), H (Hibernation) and C (Control) phases as switches.

To use the device as a volatile memory there are is a sequential operation with three phases, the Control, the Hibernation and the Data phase. During the Control phase only the Front Control and the Back Control signals may be presented to the sensor. The Hibernation phase has no illumination signals; the sensor is in complete darkness. During the Data phase the sensor is subjected to the Data Sense signal. These phases can be represented by switches, shown in Figure 6-1.

The Front and Back Control signals use a 390 nm LED, set with a current intensity of 5 mA and 20 mA respectively. These values differ, so that the output of the pi'npin may be similar. The Data Sense signal is a single 626 nm LED channel pulsed at 6000 Hz, set with a current intensity of 5 mA. These current intensity values were chosen so as to allow a clear visualization of the memory effect in the oscilloscope and consequentially in the graphical figures of this section, while avoiding saturation of the current to voltage converter equipment.

A signal labeled as Dark is the photocurrent output when there are no Control signals and only the Data Sense signal is applied. It is used here as a reference.

To introduce the memory theme a simple experiment is shown in Figure 6-2a). On the top of the figure, there are the signals to guide the eyes.

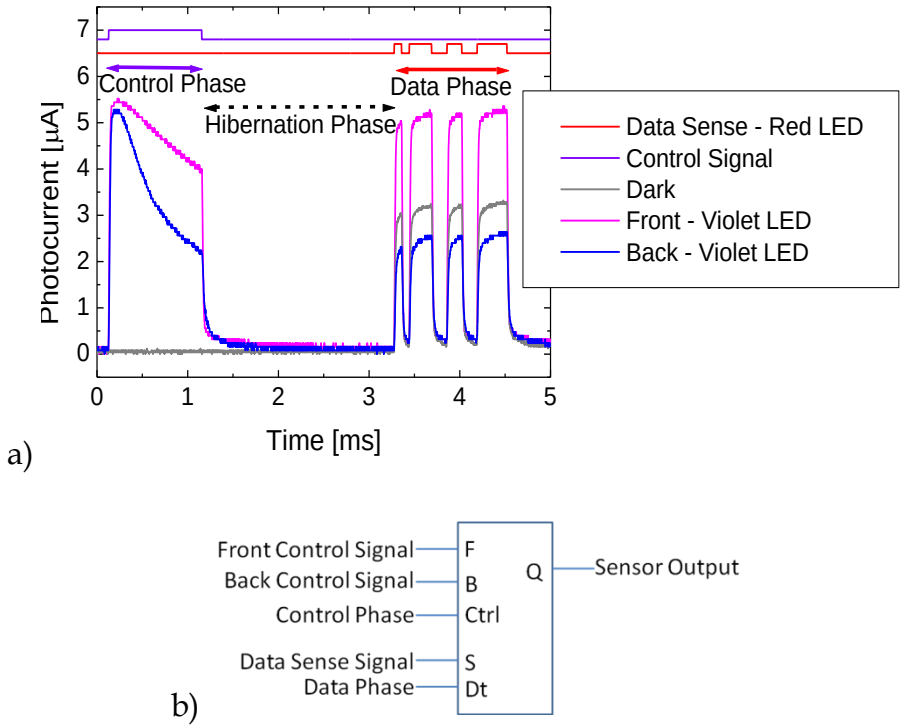

Figure 6-2 – a) Three outputs represented by the different conditions: Dark, Front Control and Back Control, on the same plot. b) Digital component of the equivalent pi'npin setup.

The experiment shown in Figure 6-2a) is the result of the following sequential actions:

i.) The Data Sense signal is applied and the pi'npin sensor's output is plotted and named Dark in Figure 6-2a).

ii.) The Back Control signal is applied during 1 ms, followed by complete darkness during 2 ms, and then the Data Sense signal is applied. The output is plotted and named Back in Figure 6-2a).

iii.) The Front Control signal is applied during 1 ms, followed by complete darkness during 2 ms, and then the Data Sense signal is applied. The output is plotted and named Front in Figure 6-2a).

These sequential actions were spaced in time between them by more than 2 minutes. This to ensure that one action does not have a big influence on the next one.

Observing Figure 6-2a) between 3 and 5 ms it is notable the reduced output of the Back in relation to the Dark, and the enhanced output of the Front in relation to the Dark. There is an influence of the Control signal over the Data

Sense signal, even though they are not both on simultaneously. Let the output be represented by the function *f(control, sense)*.

To model this effect a digital component is presented in Figure 6-2b). The digital component has all the input signals on the left hand side and the output signal on the right hand side.

The Control Phase input enables the Front Control and the Back Control signal, and the Data Phase input enables the Data Sense signal.

The operation of the digital component is better described with the aid of Table 6-1.

Table 6-1 – Automata state variable table

Row	Inputs					Internal State		Output
	F	B	Ctrl	S	Dt	$Store_{act}$	$Store_{nxt}$	Q
1	F	0	1	-	0	-	F	-
2	0	B	1	-	0	-	B	-
3	-	-	0	-	0	$Store_{act}$	$Store_{act}$	0
4	-	-	0	S	1	$Store_{act}$	$Store_{act}$	$f(Store_{act},S)$
5	-	-	1	-	1	-	-	-

Presented in Table 6-1 are the automata transition states of the digital component. In this table the (-) symbol represents a *don't care* value, which means that whatever the value that the variable has on that state, it does not interfere on the subsequent action. When the (-) is used as an output it means that the output in that case should not be considered. The (1) symbol means that the signal is active, and the (0) symbol that the signal is not active.

When a letter is used (F, B or S) means that it is a variable that can have either 0 or 1, and the row where they occur is valid for whatever value those variables hold.

The internal state is defined by variable Store, which is represented as $Store_{act}$ indicating the value that it holds in the present state. $Store_{nxt}$ represents the value that Store will hold due to the input values; the next state.

Row 1 indicates that when the Control phase is active and the input Front Control as a value F the next state will be set with that value. Row 2 indicates

that when the Control phase is active and the input Back Control as a value B the next state will be set with that value.

Row 1 and 2 also imply that the Front and Back Control are not set simultaneously.

Row 3 shows that when there is neither a Control phase nor a Data phase the internal state variable will hold the same value; i.e. during the Hibernation phase the Store value does not change, and that the output is inactive while the internal state is maintained: $Store_{nxt} = Store_{act}$.

Row 4 indicates that when the Data phase is active the sensor output is a function of the present value of the internal state variable Store and of the Data Sense signal S; output = *f(control, sense)*.

Row 5 indicates that if the Control phase and Data phase are set simultaneously the component will have unpredictable results.

The three phases, Control, Hibernation and Data have to be studied for the understanding of the memory effect. The approach used in the next section will focus on the current intensity and duration in time of the Control phase. Some time setting will be fixed and others vary to better observe and understand the results.

6.3 Memory effect

The study of the memory effect is presented by changing several parameters. Here the Control Signal intensity (Front and Back) is changed between 1.5 mA and 30 mA. After defining the best intensity, the length of the Control signal is changed between 1ms and 3000 ms. These values were chosen because the memory effect is observable above 1 ms, and the 3000 ms value because after that the outputs slightly change. As there is always an influence due to past signals, the Dark condition is considered as such when there is no illumination of the pi'npin device for more than 20000 ms. This value was found as appropriate during the experiments. All experiments start from an initial Dark condition.

Control signal intensity: the Front Control signal is active during the control phase for 1 ms, then follows an hibernation phase of 0.25 ms after which a Data signal is presented to the sensor. This sequence is repeated with different currents of the Front Control LED. The output is pictured in Figure 6-3.

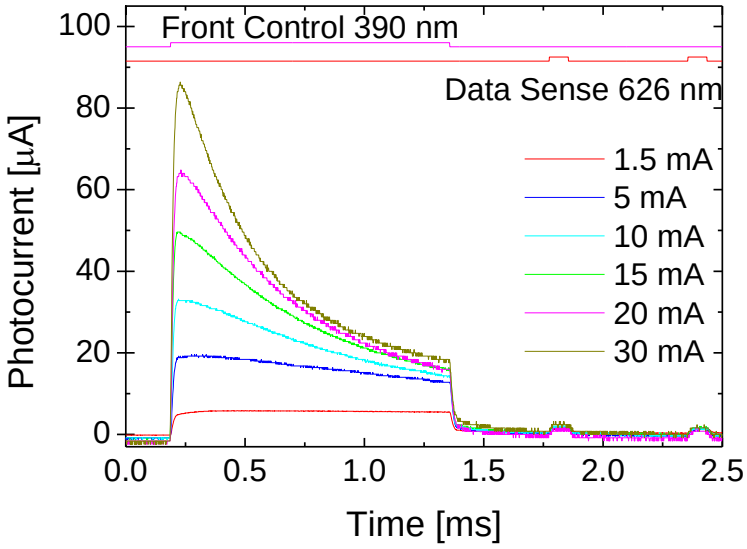

Figure 6-3 – Time response of the Front Control and Data channel 626 nm with different control LED currents. Control (C), Hibernation (H) and Data (D) phases marked to guide the eyes.

Results show that the output during the control is uniform for low intensity light fluxes and presents saturation effects for high intensity light flux. There is also an influence of the control phase over the output Data Sense signal which is not visible on Figure 6-3 and Figure 6-4, although this occurs in both figures, the values are too small to be seen.

The Dark signal is not shown in Figure 6-3 or Figure 6-4.

The same method of Figure 6-3 is applied to the Back Control signal and presented in Figure 6-4; it shows the influence of the Back Control signal over the Data Sense signal after an Hibernation Phase duration of 0.25 ms. The Back Control signal is active during the control phase for 1 ms, then follows an Hibernation Phase of 0.25 ms after which a Data Sense signal is presented to the pi'npin device.

The Back Control signal intensity is chosen within the same range, from 1.5 mA to 30 mA.

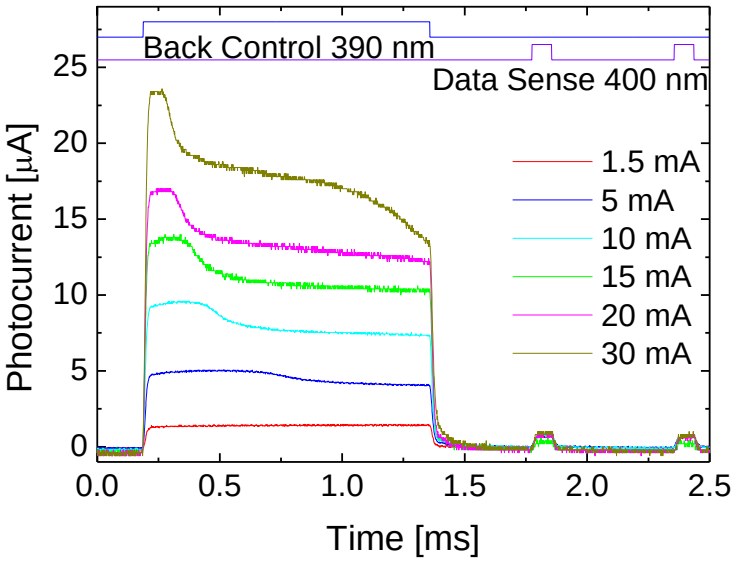

Figure 6-4 – Time response of the Back Control and Data channel 400 nm, with different control LED currents. Control (C), Hibernation (H) and Data (D) phases marked to guide the eyes.

Results show that the Data Sense output has negligible changes with variations of either the Front Control signal or the Back Control signal in the 1.5 mA to 30 mA range.

The 1.5 mA Front Control signal and the 1.5 mA Back Control signal, due to their uniform amplitude during the Control phase will be used as a setting for the next experiments. This 1.5 mA is chosen so far as the best Control Signal intensity.

Control signal duration: the Front Control signal is active during the control phase with a LED current of 1.5 mA, after that follows the hibernation phase of 0.25 ms after which a Data Sense signal is presented to the sensor. This sequence is repeated with different durations of the control phase. The output is pictured in Figure 6-5.

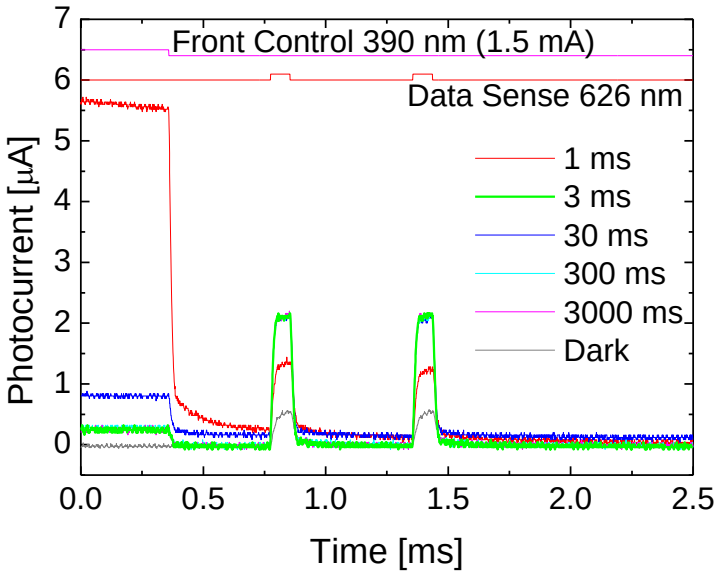

Figure 6-5 – Time response of the Front Control and Data channel 626 nm with different control duration time. Control (C), Hibernation (H) and Data (D) phases marked to guide the eyes.

Figure 6-5 shows the p'inpin response to the Front Control signal followed by a Data signal. All Front Control experiments have the same 1.5 mA current impulse which is maintained during different lengths in time. This results in a smaller value response of the pi'npin device at the end of the Front Control impulse. The response of the pi'npin to the same Data Sense signal is enhanced when a previous Front Control signal has a length wider than 3 ms. In all Front Control lengths, the output response is always higher than the Dark condition, in which there is no Front Control Signal, and only the Data Sense Signal is applied. This Data Sense gain is due to the previous Front Control signal, which implies a delayed influence; a memory effect.

The same Control Signal length in time method is applied to the Back Control signal and presented in Figure 6-6.

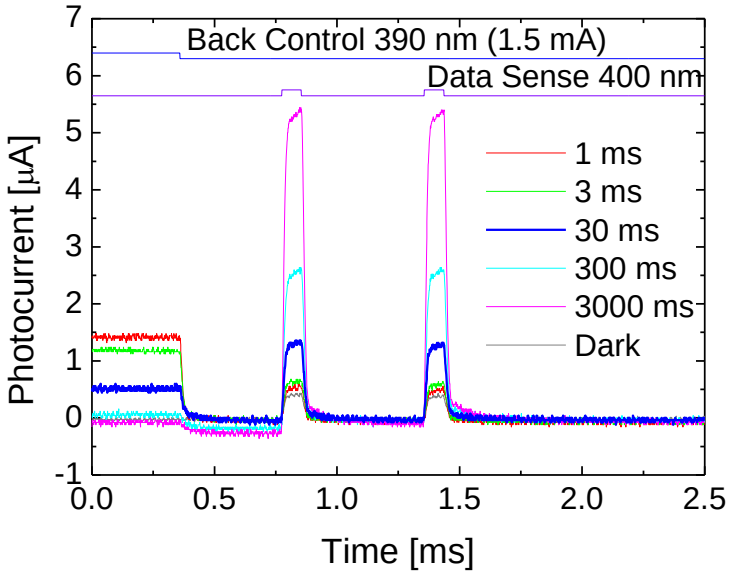

Figure 6-6 – Time response of the Back Control and Data channel 400 nm, with different control duration time. Control (C), Hibernation (H) and Data (D) phases marked to guide the eyes.

Results show that the control phase has a strong influence on the signal of the Data phase. The gain, defined as the ratio between the output signal with a Control phase and the Dark signal, increases with the Control phase time. The output is enhanced for Control phase duration bigger than 30 ms.

The Control Signal used in the next set of experiments, except where stated otherwise, is chosen according to the following criteria: the intensity is the 30 mA used to drive the pi'npin background lighting in other research papers [5], and the impulse duration should be as small as possible to increase repeated operations ratio. From both Figure 6-3 and Figure 6-6 the control signal impulse duration of 3 ms is chosen due to its relatively high value after the control phase.

Control Signal Phase duration: this study uses Control signals with different time duration, from 1 to 5 ms. After each Control signal, follows a fixed Hibernation phase that lasts 3 ms after which a Data Sense signal is applied.

The results of the applied Front Control signals, is presented in Figure 6-7.

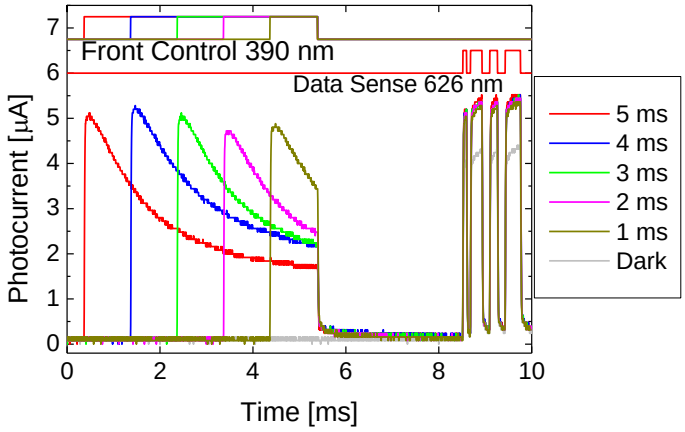

Figure 6-7 – Front Control signals with different lengths in time followed by a fixed Hibernation time and the same Data Sense signal.

At the top of Figure 6-7, there are the signals to guide the eyes. Results show that there is almost no difference to the output produced by the applied Data Sense signal despite differences in the length of the applied Front Control signal. The Data Sense signal output is enhanced in relation to the Dark reference which is in conformance with the spectral gain presented in Section 3.3.5.

Figure 6-8 shows the results for the applied Back Control signals.

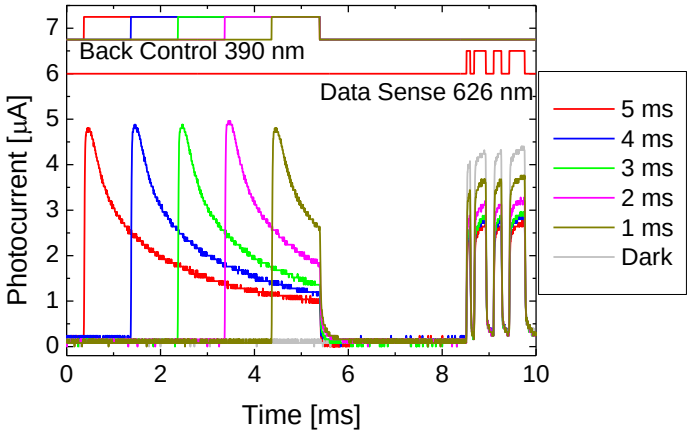

Figure 6-8 – Back Control signals with different lengths in time followed by a fixed Hibernation time and the same Data Sense signal.

Presented in Figure 6-8 at the top, there are the signals to guide the eyes. The results show that higher duration of the Back Control signals reduces more the output of the applied signal when comparing it to the Dark reference. Comparing Figure 6-7 and Figure 6-8 on the Data Sense signal output, it is possible to infer the side on which a Control signal was set.

Constant Control plus Hibernation time: for visualization purposes the sum of the Control phase time plus the Hibernation phase time remains constant with a value of 3.1 ms. On successive experiments the focus will be on the Control signal duration, from 0.1 ms to 3 ms. The aim is to have the highest difference in photocurrent of the Data Sense signal output comparing the results of the applied Front Control or Back Control signal. The Data Sense signal is the same on all experiments, and is a random digital sequence.

Presented in Figure 6-9 is the experimental result of different Front Control signals followed by a short sequence of a Data Sense signal.

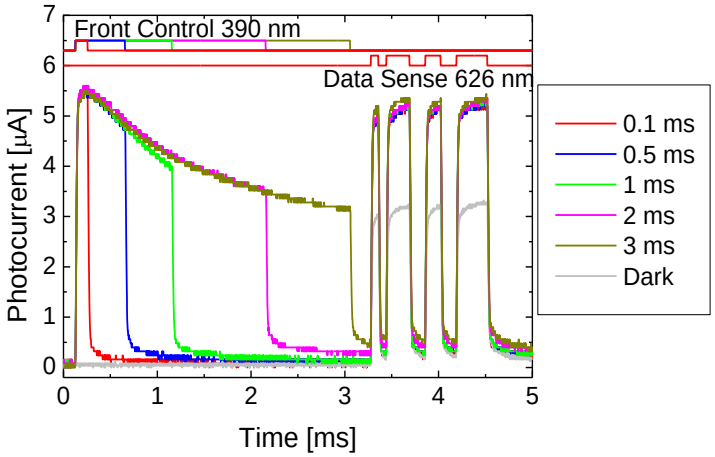

Figure 6-9 – Front Control signals with different lengths in time followed by the same Data Sense signal.

At the top of Figure 6-9, there are the signals to guide the eyes. Results show that there is almost no difference to the output produced by the applied Data Sense signal despite differences in the length of the applied Front Control signal. The Data Sense signal output is enhanced relatively to the Dark reference which is in conformance with the spectral gain presented in Section 3.3.5.

Figure 6-10 is the result of different Back Control signals followed by a short sequence of a Data Sense signal.

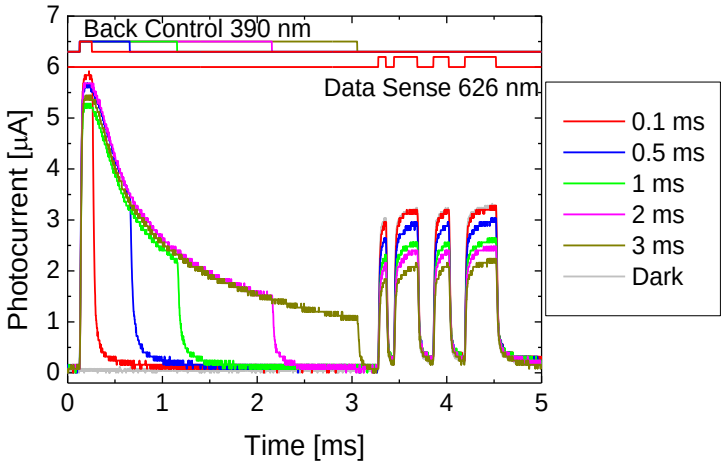

Figure 6-10 – Back Control signals with different lengths in time followed by the same Data Sense signal.

At the top of Figure 6-10, there are the signals to guide the eyes. Results show that the output produced by the applied Data Sense signal reduces with the increase of the duration in time of the Back Control signal. The Data Sense signal output is quenched related to the Dark reference which is in conformance with the spectral gain presented in Section 3.3.5.

Observing both figures Figure 6-9 and Figure 6-10 it is clear that, the longer in time the Front and Back Control signals are the higher the photocurrent output difference between the Data Sense signals is.

Data Sense signal Phase duration: in order to study the decay of the stored value through time an experiment was set in which the Data Sense signal used in the previous experiments is repeated cyclically with a 0.5 ms interval. This is shown in Figure 6-11, where the signals at the top guide the eyes. Presented in Figure 6-11, there are the results of the applied Front and Back Control signals each with duration of 3ms followed by a Hibernation phase of 3ms. The Data Sense signal sequence is equivalent to 16 cycles at a frequency of 6000Hz. These 16 cycles are then repeated.

Results show that there is amplitude decay in time of the output Data Sense signal despite the Control signal is either Front or Back. The decay rate, were it linear, is roughly twice higher in the Front Control signal (-83 µA/s) than in the Back Control signal (-46 µA/s) which means that they instead of crossing will maintain an amplitude equivalent to the Dark reference signal.

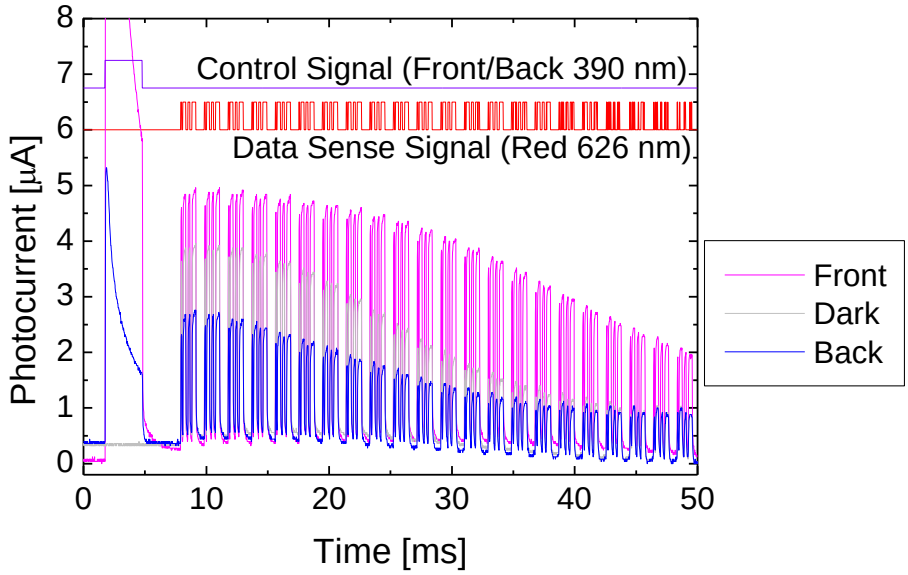

Figure 6-11 – Front and Back Control signals followed by the a Data Sense signal with a pattern in a repeated cycle.

Furthermore, the decayed amplitude of the Data Sense signal due to the Front Control signal will eventually be less than the highest amplitude of the Data Sense signal due to the Back Control signal. Observing Figure 6-11 that would occur around 25 ms; this determines the volatile memory hold time.

6.4 Memory Application

This memory effect can have several applications. Here there are two possible uses: one as the identification of the last of two consecutive events, and the other involving a digital light signal.

6.4.1 Two consecutive events

An application of the memory effect would result in the use of successive Front Control or Back Control signals followed by several Data Sense signals. The possible Front Control followed by a Back Control or vice-versa before a Data Sense signal must also be considered. These situations are presented next [7].

The sensor is initially not illuminated with a Control signal and is subjected to a Data signal with a wavelength of 626 nm with an intensity of 5

mA and with duration of a bit transmitted at 12000 bps (83 μs). This bit is repeated 8 times every 10 ms. The total sequence lasts 80 ms. This is shown in Figure 6-12. The output photocurrent response value is 4.8 μA (below 5 μA). This value is roughly the same during the 8 impulses. This is the Dark readings reference because there is no Control signal, this 5 μA line is drawn in further figures for comparison with other output responses.

Control signal at the back or front side: the same sequence is used throughout the next experiments but with previous different Control signals. The Control signals illuminate the back or front side of the pi'npin device. These are shown in Figure 6-13 through Figure 6-16.

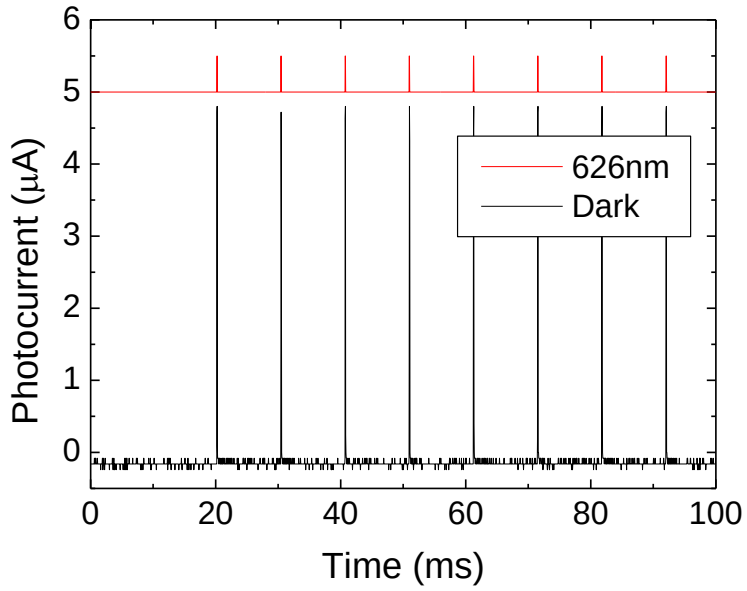

Figure 6-12 – Time response of the Data channel 626 nm without control signals (Dark readings). On top the 626 nm signal marked to guide the eyes.

The sensor was illuminated with a Control signal of 390 nm wavelength 3 ms wide and with a current intensity of 30 mA. After 10 ms the sequence shown in Figure 6-12 illuminated the device. The result is shown in Figure 6-13.

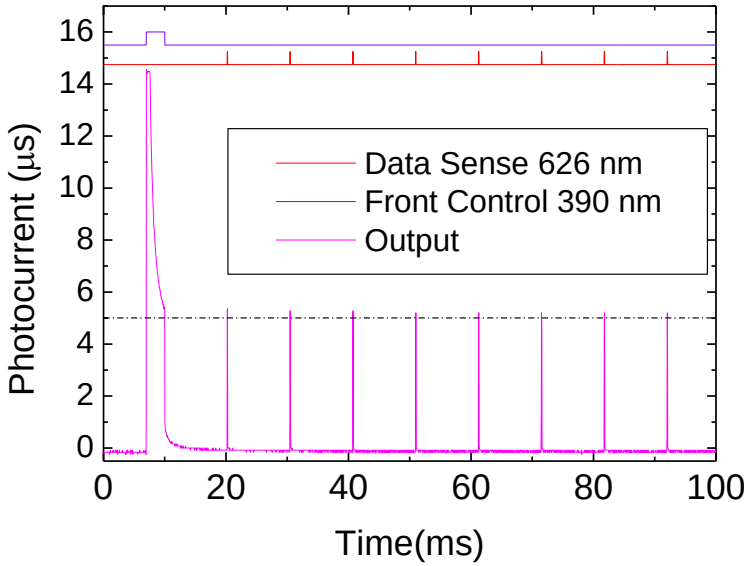

Figure 6-13 – Time response of the Front Control signal followed by a Data Sense channel 626 nm sequences. On top there are the 626 nm Data Sense and Control signal to guide the eyes.

A threshold line of 5 µA is shown in Figure 6-13 indicating that the output signal is above the Dark output reference of Figure 6-12. This shows there is an influence of the Front signal throughout the 80 ms that span the Data signal input. The Front control event was memorized.

Note that the peaks of the Control signals in Figure 6-13 and Figure 6-14 are much higher than the 14 µA value shown; this is so because of the saturation of the current to voltage converter equipment used to measure the photocurrent output. The saturation does not affect the rest of the output which is of concern to this paper. The same artefact can also be seen on the following Figure 6-15 and Figure 6-16.

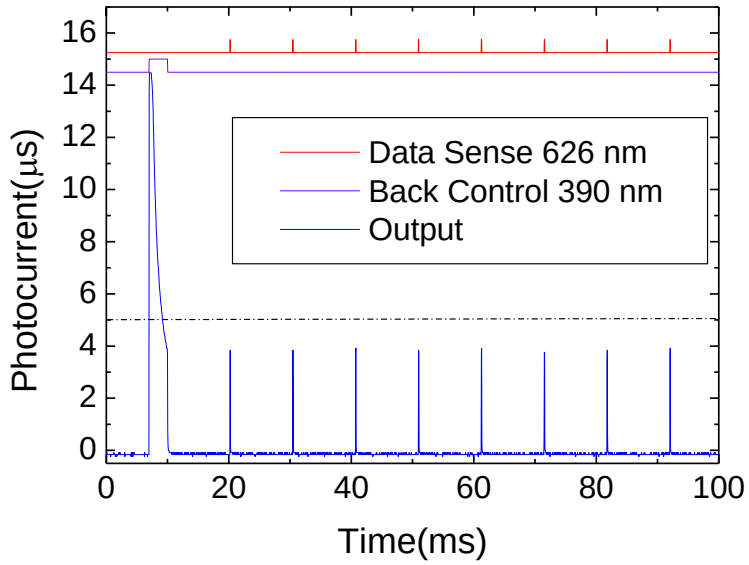

Figure 6-14 – Time response of the Back Control signal followed by a Data Sense channel 626 nm sequences. At the top there are the Data Sense and Control signals to guide the eyes into the figure.

Figure 6-14 shows the output of the pi'npin sensor when the sequence of Figure 6-12 illuminates the sensor after the Control signal has illuminated the back of the pi'npin sensor. A threshold line of 5 µA is shown indicating that the output is well below the Dark reference of Figure 6-12. This indicates that the Back Control signal event was memorized.

Two Control signals at the back and front side: the same sequence of Figure 6-12 is used. The Control signals illuminate both the back and front side, one before the other with two possibilities: Back before Front, and Front before Back combinations.

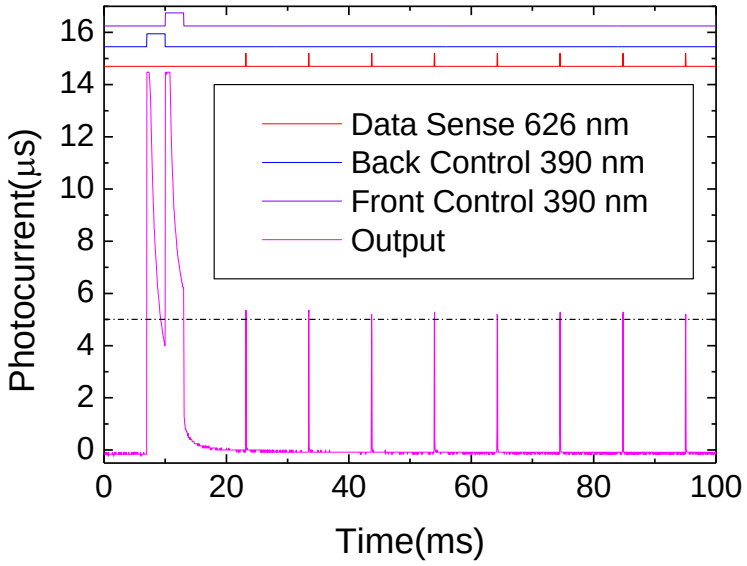

Figure 6-15 – Time response of the Back before Front Control signal followed by a Data Sense channel 626 nm sequences. At the top there are the Data Sense and Control signals to guide the eyes.

Figure 6-15 shows the output of the pi'npin sensor when an initial Back Control signal illuminates the device immediately followed by a Front control signal with the same 3 ms duration and 30 mA current intensity. Afterwards, 10 ms later, the Data signal sequence of Figure 6-12 illuminates the pi'npin sensor. The output is above the 5 μA threshold which identifies the Front signal condition shown in Figure 6-13. This means that the Front control event was memorized.

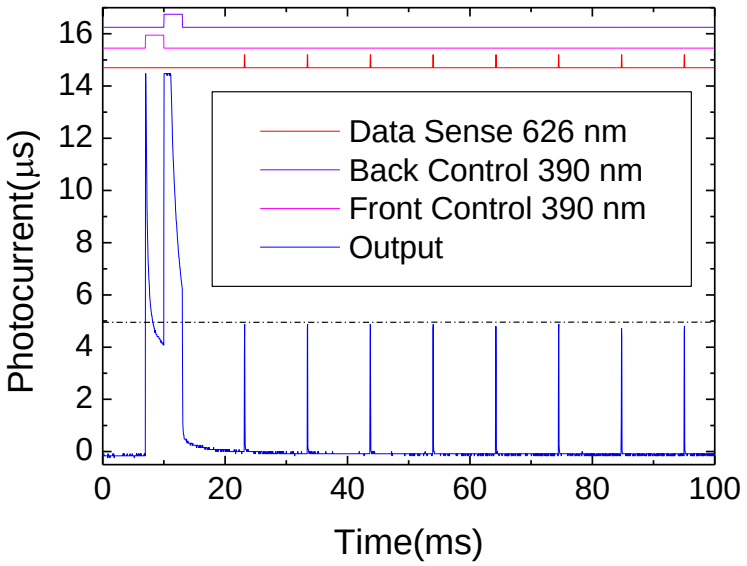

Figure 6-16 – Time response of the Front before Back Control signal followed by a Data Sense channel 626 nm sequences. At the top the Data Sense and Control signals to guide the eyes.

Figure 6-16 shows the output of the pi'npin sensor when subjected to the Front before Back combination. The Front Control signal illuminated the device immediately followed by the Back Control signal. The sequence of Figure 6-12 followed 10 ms later. The threshold line (5 μA) is shown indicating that the pi'npin photocurrent output is below that value. This opposes the Back before Front condition shown in Figure 6-15. This means that the Back control event can be identified. The expected result would be that of Figure 6-14 which is much lower than the threshold line. This difference is due to the strong influence of the Front Control signal.

6.4.2 Digital light signal application

The digital light signal D[L, S] that was introduced on the previous chapter is now used here as the Data Sense signal.

An experiment that applies the findings of this chapter and that of the digital light signal is shown in Figure 6-17.

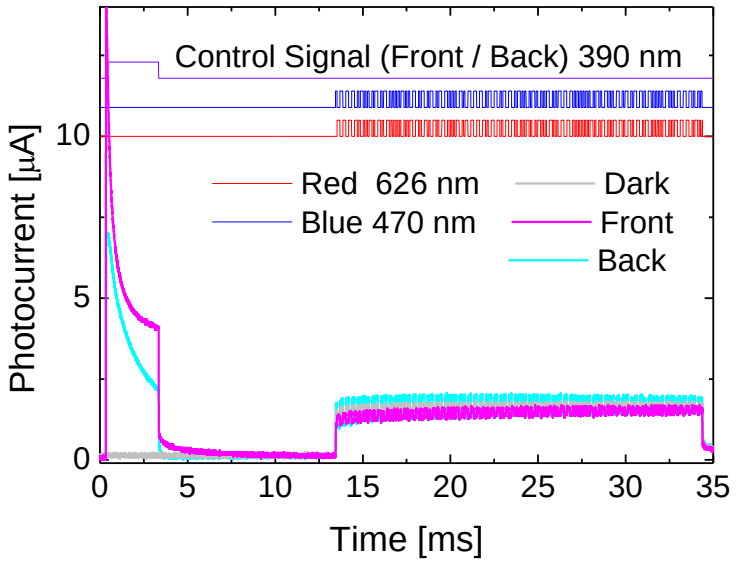

Figure 6-17 – A digital light signal D[R, B]={Red, Blue} used as a Data Sense signal.

The experiment shown in Figure 6-17 was done in three steps. First the Dark signal was acquired with the digital light signal D[R, B]={Red, Blue}. As defined, the digital light signal has two components one on each side of the 500 nm wavelength, and both signals are Manchester coded with one being the inverse of the other. Next the Front Control signal, an ultra violet light of 390

nm bathed the front surface of the pi'npin device for 3 ms, followed by 10 ms of darkness, with no lighting whatsoever upon either surface of the device. Then the same digital light signal was applied as the Data Sense signal. The output is called the Front signal.

The same procedure was made to acquire the Dark signal, by using the Back Control signal of 3 ms, followed by 10 ms of darkness and the same digital light signal as before.

The Digital Sense signal output of Figure 6-17 is shown in Figure 6-18 with another time scale.

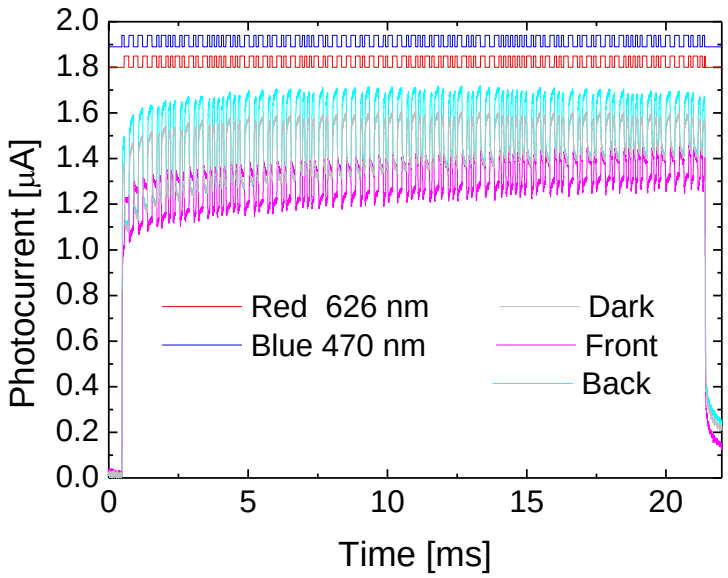

Figure 6-18 – Detail of the digital light signal D[R, B] of Figure 6-17 with 128 data bits.

Presented in Figure 6-18 is a sequence of 256 bits with a bit rate of 12000 bps that represent the Manchester coding of 128 bits of data at a data rate of 6000 Baud.

A detail of Figure 6-18 is shown in Figure 6-19.

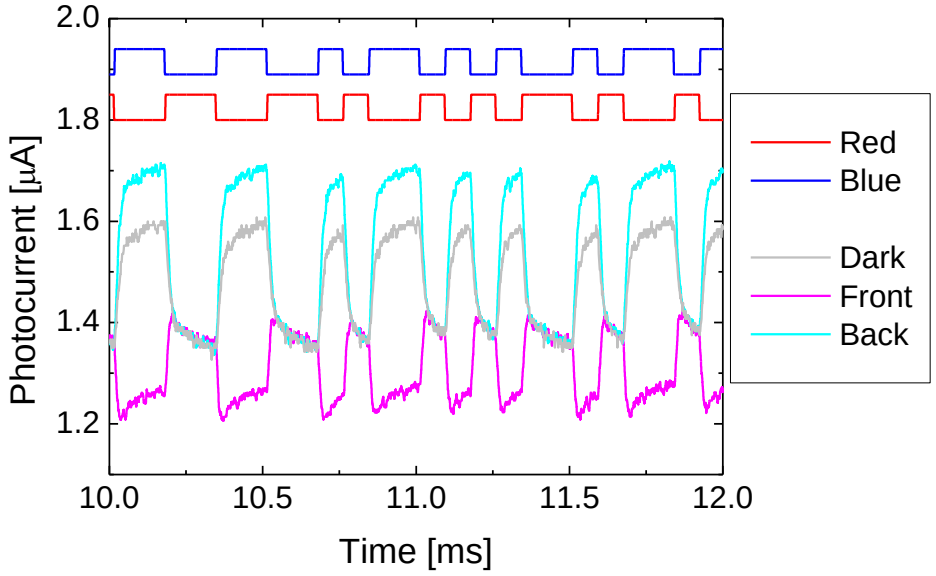

Figure 6-19 – Detail of Figure 6-18

The pi'npin output signal shown in Figure 6-19 is the result of the Data Sense signal input without any Control signal (dark) and with a Front Control signal (front) and Back Control signal (back). Observing the dark signal it resembles the blue component of the digital light signal {Red, Blue} that was used as a Data Sense signal. When a Back Control signal is used, the output enhances the blue component and that is why the back signal in the figure has bigger amplitude than the dark one. Consequently the Front Control signal results in the front signal that follows the red component of the digital light signal. As expected the front and back signals are inverted in relation to one another. The behaviour of this experiment is shown as a digital circuit in Figure 6-20.

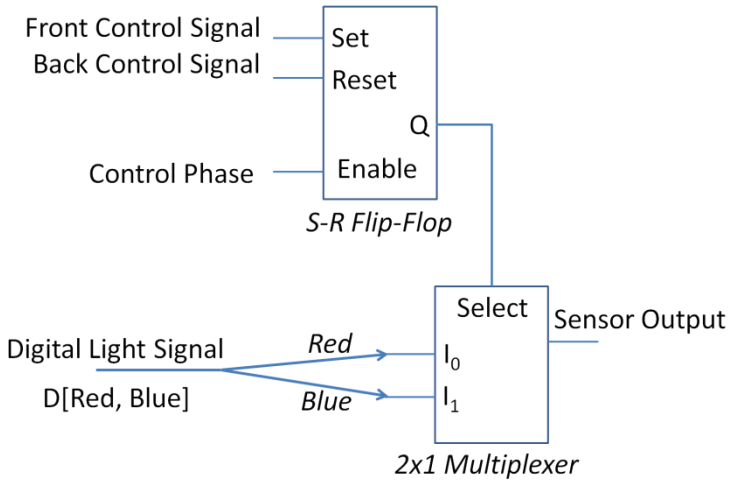

Figure 6-20 – Equivalent digital circuit of the behaviour of Figure 6-17.

The behaviour of the experiment shown in Figure 6-17 can be modelled by the digital circuit shown in Figure 6-20. The *S-R Flip-Flop* is a memory component that stores a digital value 1 when the Set is active and a digital value of 0 when the Reset is active; by definition the output is unpredictable when both Set and Reset are active. The Enable input has to be active for the Set and Reset to work accordingly, otherwise the output Q holds its value. The *2x1 Multiplexer* component reproduces at its output the input signal connected to I_0 or I_1 that is chosen by the Select input. The digital light signal D[Red, Blue] has two components; the red is connected to input I_0 and the blue is connected to input I_1. Summing up, the Sensor output is equal to the red or blue component of the input digital light signal depending on the stored value given by a previous Front or Back Control signal respectively.

As a side effect, for only using one Data Sense signal and being Manchester coded, the output signal can be improved if the Back and Front are subtracted from each other due to the complementary content of those signals. The result is presented in Figure 6-21.

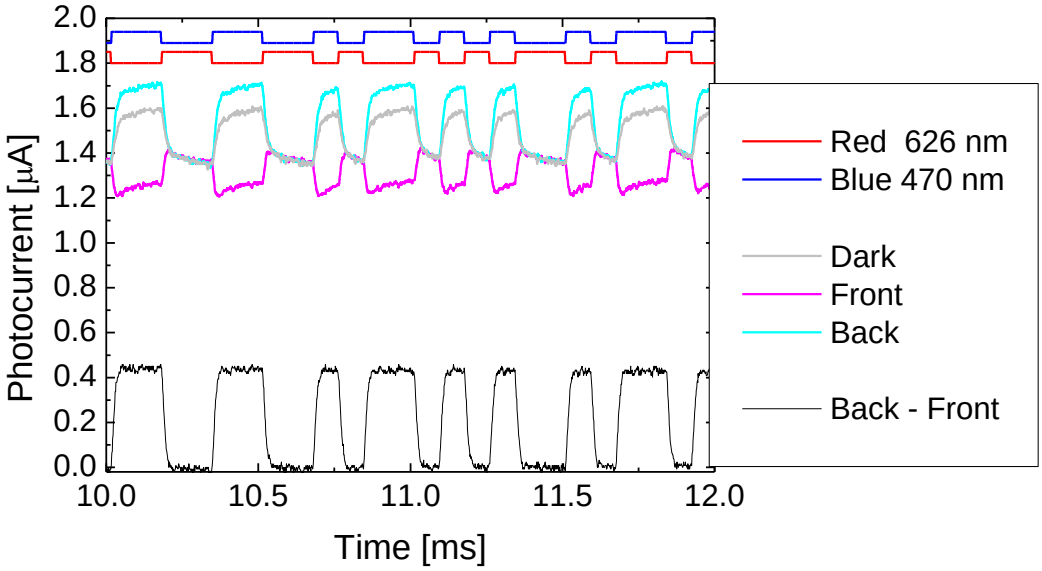

Figure 6-21 – Difference between the Back and Front output signals.

Due to the complementary nature of the Back and Front signals following the short and long components of the digital light signal (Blue and Red respectively) that are Manchester coded, the result of their difference is an improved square wave, shown in Figure 6-21.

6.5 Conclusion

Short term memory is achieved by the capacitive junctions of an amorphous SiC pi'npin device that can be illuminated on both front and back surfaces by an impulse.

The Control phase's duration and intensity directly influences the Data phase output.

The approach of using Control signals as a selector has successful results as long as the Data Sense signal time duration is less than 25ms. It is possible to know by comparing the amplitudes of the Dark signal output to Data Sense signal output to know if the Control signal beforehand was a Control Front or a Control Back signal.

The Control signal event is recognized 10 ms afterwards by the Data Sense signal which is used as a reading probe. When the Control signal is applied to the front of the sensor the output is higher that a selected threshold (5 μA) and

when the Control signal is applied to the back of the sensor the output is below that same threshold. This recognizes the side in which the Control signal was applied.

When two Control signals are applied one after the other, on different sides, the results show that the output still recognizes the last Control signal applied. Thus the Back before Front signal is recognized as the Front Control signal being selected, and the Front before Back is recognized as the Back Control signal being selected.

The device can work as a memory, in which the Front Control signal is the Set and the Back Control signal the Reset. The Data signal is the reading probe and the pi'npin sensor output indicates with each reading, if there was previously a Front Control or a Back Control signal.

Two possible applications were shown, one in which a sequence of two different Control signals result on selecting as output the equivalent of the lastly applied Control Signal. The other is the result of a digital light signal used as a Data Sense signal and the pi'npin device reproduces either the red or the blue component, of the digital light signal, depending on which Control signal was used. A Front Control signal leads the pi'npin to consequently reproduce the red component of the digital light signal, and the Back Control results in the reproduction of the blue component. Using this application with a digital light signal frame of 128 data Manchester coded bits, shows another way to use the pi'npin device as a two channel multiplexer.

As a final conclusion it is important to refer that a volatile memory can indeed be built using a single pi'npin device.

6.6 References

[1] V. Silva, M. A. Vieira, M. Vieira, P. Louro, A. Fantoni, and M. Barata, "Logic functions based on optical bias controlled SiC tandem devices," *Phys. Status Solidi*, vol. 11, no. 2, pp. 211–216, Feb. 2014.

[2] P. Louro, M. Vieira, J. Costa, M. A. Vieira, M. Fernandes, A. Fantoni, and M. Barata, "a-SiC:H Based Devices as Optical Demultiplexers," *MRS Proc.*, vol. 1246, pp. 1246–B07–07, Feb. 2011.

[3] V. Silva, M. A. Vieira, P. Louro, M. Barata, and M. Vieira, “Simple and complex logical functions in a SiC tandem device,” in *Technological Innovation for Collective Awareness Systems*, 2014, pp. 592–601.

[4] V. Silva, M. Barata, M. A. Vieira, P. Louro, and M. Vieira, “Light Memory Operation Based on a Double Pin SiC Device,” in *Technological Innovation for Cloud-Based Engineering Systems*, T. A. B. Luis M. Camarinha-Matos and F. M. Giovanni Di Orio, Eds. Springer International Publishing, 2015, pp. 265–272.

[5] V. Silva, “PiscaLed - User’s Manual,” *GIAMOS - ISEL - Inst. Super. Eng. Lisboa*, p. 34, 2013.

[6] V. Silva, “PiscaLed - Technical Manual,” *GIAMOS - ISEL - Inst. Super. Eng. Lisboa*, p. 46, 2013.

[7] V. Silva, M. Vieira, M. A. Vieira, P. Louro, and M. Barata, “Light memory function in a double pin SiC device,” *Microelectron. Eng.*, 2015.

7

7 Validation

A very important step in research is to validate the findings. This can be made by other researchers that dwell with the same topic, or by providing results that can be thoroughly analysed, or by resources that can be easily used like programs, or any other way that is efficient to confirm the research made. In this section, the *IndicaLed* program is presented that analyses the results obtained through the experimentation process [1]. This is a milestone on the work group as it provides an instrument to spread the research domain of the a-SiC:H device. The program must be sufficiently flexible to allow the researcher to change all variables, allow different approaches, include new ones, and still maintain a solid core that is not altered so that a common methodology can be used as reference. There are several topics that are necessary to understand the working principle of the validation process.

When digital data is converted to a photon emission, such that a value of 0 is no photonic emission and a value of 1 is a continuous photonic emission, then this kind of modulation is 100% amplitude modulation, and the coding is NRZ (Non Return to Zero), which means that during the data bit time (whether 0 or 1), the photonic emission does not change. Represented in Figure 7-1 is a data bit sequence of a 0 followed by a 1, and they are both coded using NRZ and Manchester. The NRZ representation is the direct translation of the 0 bit into a 0 amplitude signal and the 1 bit value is translated into the maximum amplitude value. The result is a square wave identical to the data bit values.

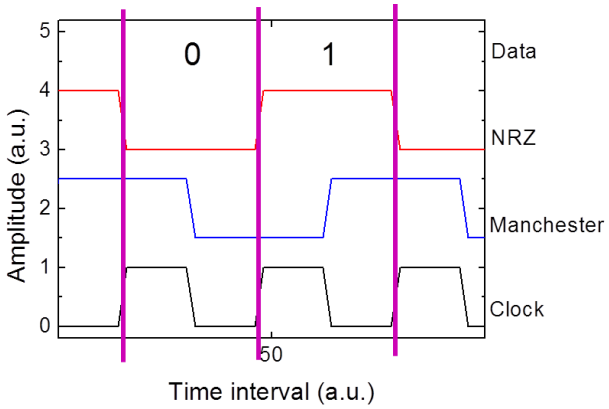

Figure 7-1 – A data bit of 0 and 1 coded with NRZ and Manchester.

The Manchester signal however changes during each data bit time. In Figure 7-1 a clock signal is represented to help visualizing the generation of the Manchester signal. The 0 value data bit translated to Manchester coding follows the clock signal during the bit time, and the 1 value bit translated to Manchester is identical to the inverse of the clock signal. A more complete graph is shown in Figure 7-2.

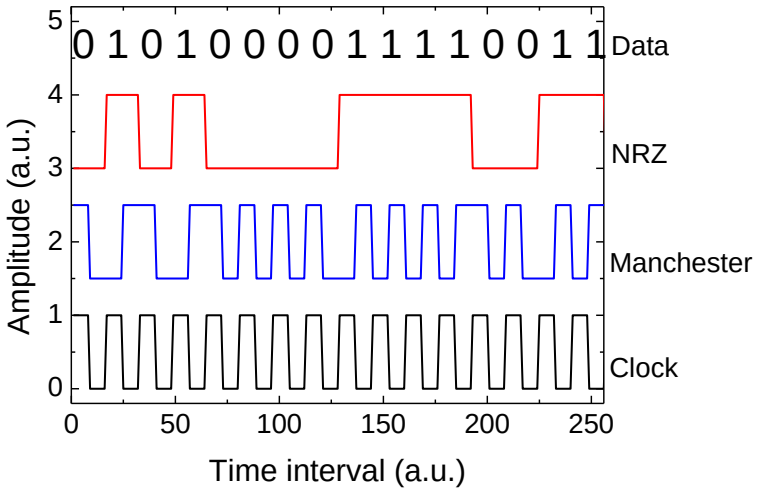

Figure 7-2 – A random sequence of data bits coded in NRZ and Manchester.

Observing Figure 7-2, the NRZ signal follows the direct translation of the data bit values, written as numbers at the top of the figure. Long periods of 0 or 1 still have the same length in NRZ. The Manchester coded signal only has two different frequencies; it is either equal to the clock frequency or half of that frequency. A phase change occurs at a 0 to 1 and 1 to 0 boundary.

The data of each channel produces a photocurrent that must change in time or otherwise it will act as an optical bias. This means that the channel has

to be encoded in a way, that a continuous sequence of 0 or 1 or random values as input, yields an output that changes in time. The Manchester coding is a simple and effective option to use [1, 2]. The receiver system must decode the Manchester coding and deliver the input data [4]. This process involves the sampling of the received signal and determining where each bit starts. The bits received are then classified, by clustering, so that the original data is correctly understood[5].

7.1 Validation Methodology

To ensure that all logical functions work it is necessary to show results that are independent of any specific input configuration. The experimental method is presented in Figure 7-3. A random code generator will drive the signal LEDs (A). They will shine over the sensor. The sensor biased at -8 V will be subjected to front and back illumination of the pi'npin surfaces (C). The output, filtered and amplified (B) will then have a result code (D). The code (D) is then compared to the original input (A) and statistical methods will be used to determine the feasibility of the whole system.

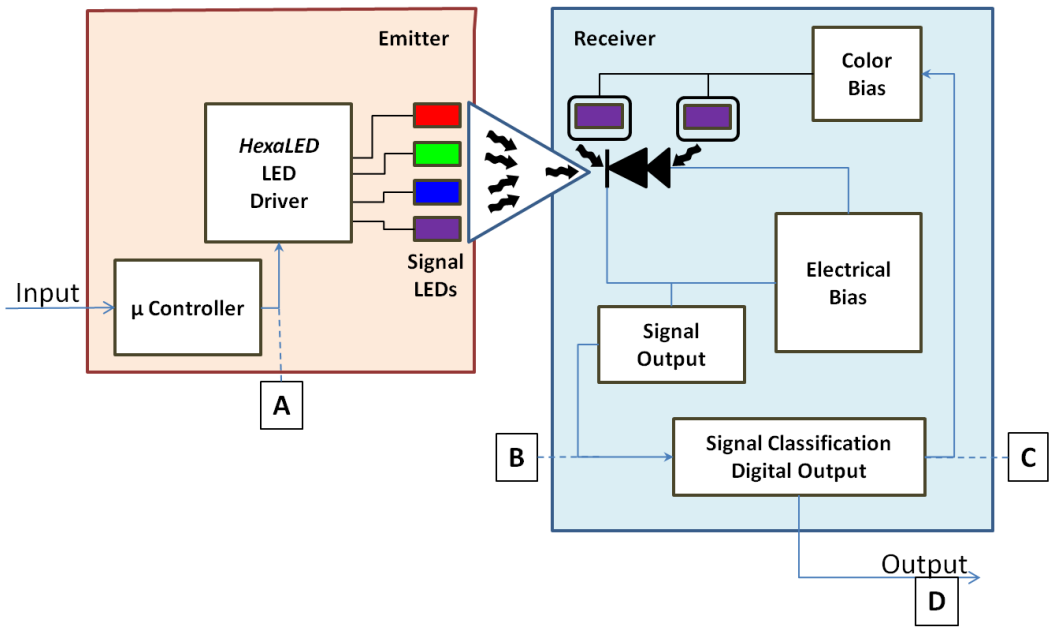

Figure 7-3 – Emitter and Receiver block diagram.

The input signals must be applied to the red, green, blue and violet LEDs as shown in Figure 7-3. These LEDs must be carefully aligned to ensure that

they shine over the whole sensor surface. The LEDs are 5 cm away from the sensor, and the sensor is 1 cm x 1 cm. This means that the LED must have a viewing angle bigger than arctan 0.5/5 ≈ 5.7 degrees if positioned in the centre of the sensor. The LEDs are common commercially available and have viewing angles of 15, 60 and 120 degrees. The signal LEDs are positioned as close to the perpendicular of the sensor as possible.

The same type of LEDs is used for the background illumination. The background LEDS are positioned in the centre perpendicular to the sensor. The back LED has the closest distance from the sensor, < 1 cm. The front LED is 5 cm from the sensor.

Each LED is positioned to ensure full sensor coverage and does not shadow the other LEDS.

The signal LEDs have a very low current applied, usually bellow 3 mA, and the background illumination LEDs have a high current over 20 mA.

Presented in Figure 7-4 is the block diagram of the validation process.

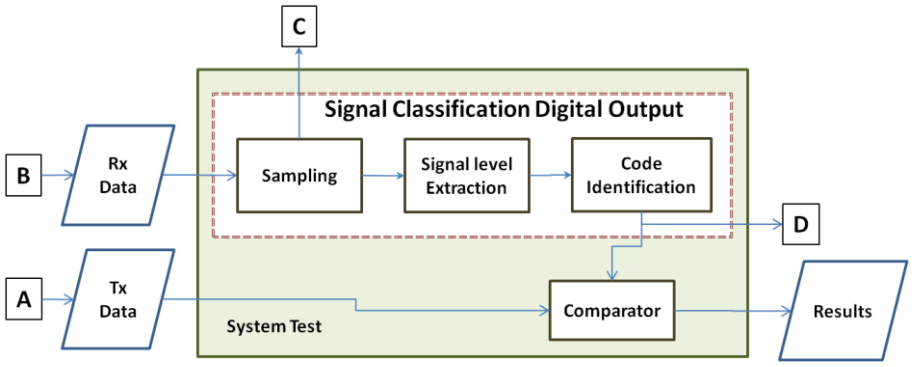

Figure 7-4 – Block diagram of the Validation process.

The block diagram of the validation process is shown in Figure 7-4. The input (Tx data) and output (Rx data) of the device can be recorded in a file for post analysis. Data logging over time is also a possible construction option if necessary; especially for time dependent experiments as in the case of a sample which varies over time and is positioned between the signal inputs and the sensor.

The Received data (B) is processed so that a digital code is obtained (D), also called the estimated code further into the text. This estimated code is then

compared to the transmitted data (A) which is also named the original code further into the text. Comparing both the estimated and original code, (Results), will account for the overhaul validation of the communication system.

7.2 The Samples

The oscilloscope used is a 4 channel digital oscilloscope with 8 bits vertical resolution (recently replaced by an 8 and 12 bits one). By selecting the visualization of the input signals applied to the LEDs that shine over the pi'npin device, the digital signals are then stored in the computer by a program that communicates with the oscilloscope. The same procedure is made with the output of the pi'npin device. As a working example three input channels shine upon the pi'npin device at 12000 bps. The collected data is composed by those three channels and the dark, front and back output of the pi'npin device. The horizontal resolution selected on the oscilloscope provides, 5000 readings over 6000 μs. This means that the oscilloscope displays $12000 * 6000x10^{-6} = 72$ bits of the input data sequence. Each bit has a length of 5000 / 72 = 69.4 samples. All 5000 values of a sequence is written into a table in the Origin file, and each 5000 rows is composed by the following column order: time, all digital input channels, dark, front and back output signal, shown in Figure 7-5b). A small range of the table data converted into a graph is shown in Figure 7-5a).

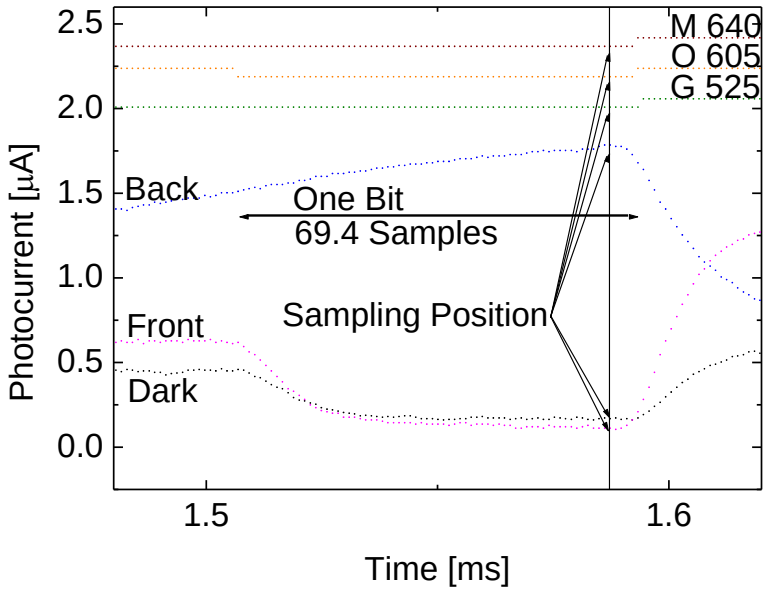

a)

b)

Data6 - Alea 54

	A[X]	B[Y]	C[Y]	D[Y]	E[Y]	F[Y]	G[Y]	H[Y]	I[Y]	J[Y]	K[Y]	L[Y]	M[Y]	N[Y]
	Time	G524	C460	O605	N430	M640	B470	R626	V400	L565	U390	Dark	Front	Back
215	2.568E-4	2.05	2.09	2.18	2.32	2.41	2.45	2.59	2.63	2.72	2.86	0.28945	0.75578	0.60301
216	2.58E-4	2.05	2.09	2.18	2.32	2.41	2.45	2.59	2.63	2.72	2.86	0.28543	0.74774	0.60301
217	2.592E-4	2.05	2.09	2.18	2.32	2.41	2.45	2.59	2.63	2.72	2.86	0.28141	0.7397	0.58693
218	2.604E-4	2.05	2.09	2.18	2.32	2.41	2.45	2.59	2.63	2.72	2.86	0.28141	0.74774	0.59497
219	2.616E-4	2	2.09	2.18	2.32	2.41	2.45	2.59	2.63	2.72	2.86	0.27739	0.7397	0.59497
220	2.628E-4	2	2.09	2.18	2.27	2.36	2.45	2.54	2.63	2.72	2.81	0.27337	0.72362	0.58693
221	2.64E-4	2	2.09	2.18	2.27	2.36	2.45	2.54	2.63	2.72	2.81	0.26533	0.69146	0.57889
222	2.652E-4	2	2.14	2.18	2.27	2.36	2.45	2.54	2.63	2.72	2.81	0.25729	0.67538	0.60301
223	2.664E-4	2	2.14	2.23	2.27	2.36	2.45	2.54	2.63	2.72	2.81	0.25327	0.66734	0.62714
224	2.676E-4	2	2.14	2.23	2.27	2.36	2.45	2.54	2.68	2.77	2.81	0.24925	0.63518	0.65126
225	2.688E-4	2	2.14	2.23	2.27	2.36	2.5	2.54	2.68	2.77	2.81	0.25729	0.62714	0.68342
226	2.7E-4	2	2.14	2.23	2.27	2.36	2.5	2.54	2.68	2.77	2.81	0.26935	0.6191	0.72362
227	2.712E-4	2	2.14	2.23	2.27	2.36	2.5	2.54	2.68	2.77	2.81	0.27739	0.61106	0.76382

Figure 7-5 – a) One data bit sample, and b) part of the sampled data in a table.

Figure 7-5a) shows the sample of a bit with the conditions addressed before. A bit has an integer number of samples, which means that some bits will be 69 samples in length and others 70 samples. The sampling point should be as close to the end of the bit as possible because the signals have a very slow setup time. Another aspect that must be considered is the fact that the LED driver used with the PiscaLed controller has 16 outputs, and the last four outputs are used as the digital signals to be displayed on the oscilloscope [6]. The driver has a graduated delay circuit between outputs, with a fixed delay of 20 ns when changing the state of each output, this to minimize a large inrush current [7]. Due to the delay, there can be a difference of up to 15 * 20 ns = 300 ns in each digital channel. According to the example described above, 300 ns is the time of $(5000 / 6000 \times 10^{-6}) \times 300\ 10^{-9} = 0.25$ samples. This delay is insignificant for this example, and for the majority of the experiments, but it can influence a difference of one bit. The digital channel values are also the result of an

analogue to digital conversion in which a hysteresis of 1/3 is used (explained further into the section, see Figure 7-10), which may introduce an offset of more than one sample.

Another delay is between the oscilloscope channels, when there are more than one of the 4 channels selected, the sampling time is divided by the active channels, which means that there is a delay of one sample between consecutive channels. Summing up all influences the number of different bits among the samples of digital channels can be of 1 + 4 + 1 = 6 bits. Observing the cells marked in table of Figure 7-5b) it can be noted the difference in samples when all 10 digital channels change state synchronously and simultaneously according to the instructions sent to the hardware. The sampling of the 10 digital signals was made in groups of three which can also account for a difference in one bit to the cycling of the sequence triggered by a bit from the hardware. On the table displayed, the changing of the digital state is spread over 7 samples. This lap difference is important because a sample can be digitally coded with error if the sampling position is too close to the transition, which might mislead the classification process when comparing this original coding with the estimated code. Allowing a misalignment error of 7 samples in 72 gives a maximum sampling position of (72 - 7) / 72 = 90.3%

7.3 The frame

Data is produced by the PiscaLed which illuminates the LEDs that impinge upon the pi'npin device. The PiscaLed has two fixed modes, one in which it repeats a sequence of 16 bits (2^4), and another with 32 bits (2^5). The content of each bit is configurable. These 16 or 32 bit sequences have been used in almost all sequences presented in this work. Another mode is much more flexible and made for the validation process; in this mode a data frame with a maximum length of 1024 bits can be defined. It may include some of the 16 or 32 bit sequences used previously and or include random bits. It is also possible to define a Start of Header (SOH) and End of Text (EOT) patterns. The SOH is sent before the data and the EOT after the data. The available 1024 bits include both SOH and EOT headers [8].

The SOH and EOT are used to help delimit the data. The SOH can also be used to send a preamble by setting adequate values. A preamble is a sequence of bits that when transmitted sends a wave that can be used to synchronize the clock at the receiver. The validation process needs to synchronize the clock, as it will be discussed in the next section, and the normalization of the input values between 0.0 and 1.0 need the maximum and minimum values to be known. These values can be supplied by the preamble pattern. To minimize the DC component of the signal, a Manchester coding can be used; otherwise the normalization process will err. To compensate the DC component, if there is no Manchester coding, the normalization process must be changed to remove the mean value of the signal, or, as it is done in previous experiments, by setting the oscilloscope readings to AC mode. An example of a data frame is shown in Figure 7-6.

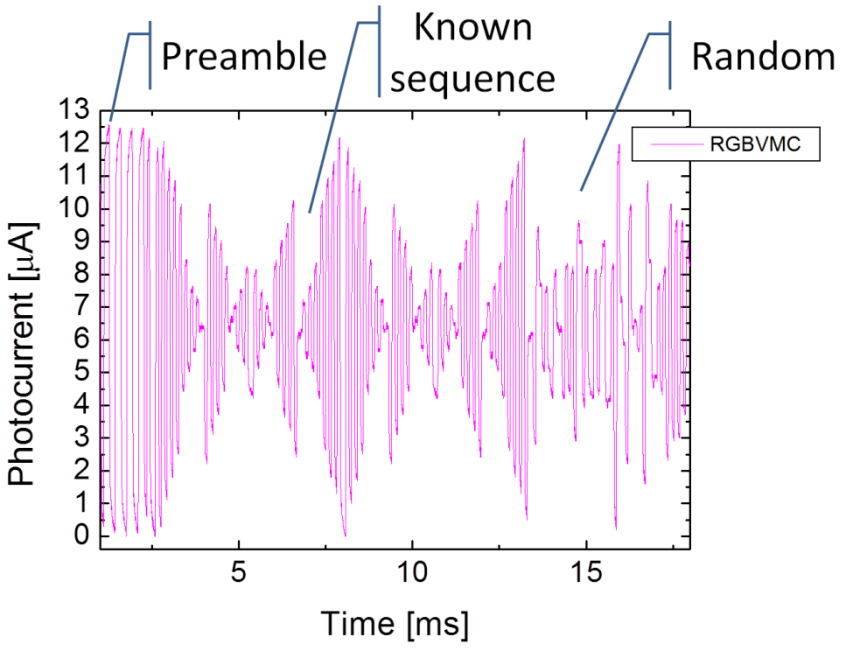

Figure 7-6 – Part of a 24 ms data frame with 256 bits.

A data frame of three digital light signals (Red-Blue, Green-Violet and Magenta-Cyan) impinged upon the pi'npin sensor while the front violet illumination is on. The 256 data bits were recorded in 24 ms and part of that frame can be seen in Figure 7-6. On the same figure the preamble can be seen with a sequence in which all three digital light signals are on the 1 state followed by a 0 state. There are only four preamble bits because they are

Manchester coded and the count is eight in all. Following the preamble is a known sequence of 32 bits repeated twice and then random values to fill in the 256 bits. The lowest photocurrent is 0 μA by definition; when the input values are read the minimum is set to 0 μA; that is why there is an apparent DC component in the figure.

7.4 The process

The output of the pi'npin device is a set of three values registered at three different moments in time. First the pi'npin device is impinged with the light signal inputs without any background lighting, and the output is registered and named the Dark signal. Next, while the same input sequence flood the p'inpin device it is also subjected to a constant background lighting on the front surface; the output is registered and named the Front signal. Last, the same input sequence floods the pi'npin device while it is subjected to background lighting at the back surface, the output signal is registered and named the Back signal. The three different readings are made through the oscilloscope with the external trigger connected to the input signal driving equipment, so that the whole sequence is stable in all readings. Enough time is given between the three readings so that there is no influence among each other.

All output samples are stored in an Origin project file, which also includes the original input sequence that is also sampled through the oscilloscope to ensure the correct attribution of the timing event (through the external trigger).

Classification can be made through the Origin program by observation, but it is preferable to have an automatic classification procedure to eventually use the same process for on-the-fly readings. With this in mind and to implement the proposed validation methodology of Figure 7-3 a program in Java was built to accomplish the System Test block of the validation process (Figure 7-4).

The program is built by several independent blocks which run concurrently (i.e. simultaneously) on the same computer. Each of these blocks has the structure of Figure 7-7.

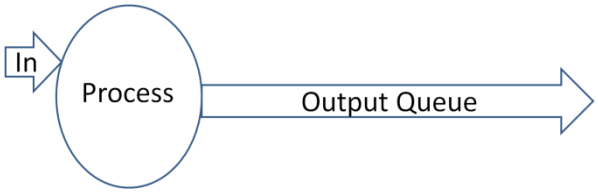

Figure 7-7 – Basic building block

Shown in Figure 7-7 is the graphical representation of the class *Systema* that handles all or part of the samples acquired from the pi'npin device's output. Each object of type *Systema,* to run concurrently, needs a thread which is labelled *Process* in Figure 7-7. Each process waits for an input (In), processes it and stores the result in a queue (Output Queue). The Output Queue of a *Systema* is connected to the input (In) of another *Systema* object. The queues can hold any number of results. Their use is to account for differences of the duration in time of each *Process* and also the random execution of all *Process* threads that although running concurrently, still have to be distributed one by one to the available processing cores of the computer.

The *Systema* class also allows for several inputs and output queues to be held by a specific object. The whole automatic classification method is shown in Figure 7-8.

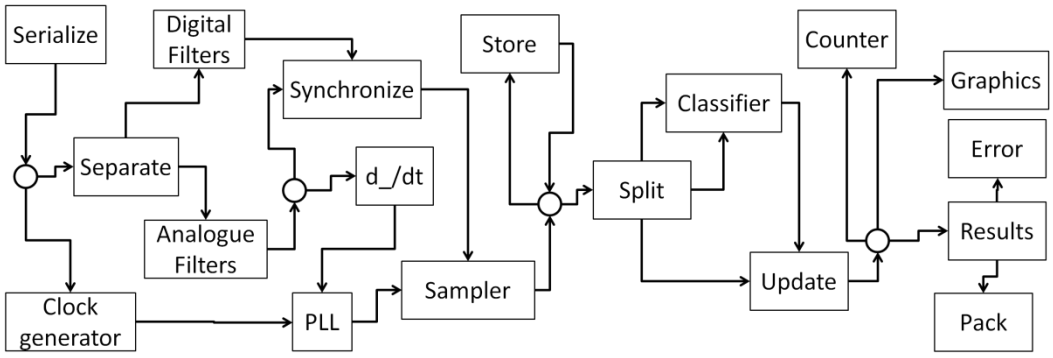

Figure 7-8 – Block diagram of the pi'npin validation process.

Figure 7-8 shows all objects that build up the validation process. Each block shown is a *Systema* object.

The entry point of the samples is through the *Serialize* process. Here the samples can have at least three possible sources: a file, the clipboard or directly from the sampling equipment. Despite of the selected source all samples are treated independently from them. In this work only the clipboard entry was

implemented because of the simple interface that the clipboard allows to input the data directly from the Origin program. This also allows a visual perception of the chosen data. Samples are stored by input order on the Output Queue of the *Serialize* block. Each sample is an object of type *Sample*. Each *Sample* holds the dark, front and back sampled values, the original code, and the estimated code. The original code is the digital input channels sampled with the same timing as the pi'npin output signals. The estimated code is set at the end of the validation process by the classification method chosen. With this data, it is possible to analyse each *Sample* object and produce statistical results.

The *Serialize* is also responsible for the normalization of the sample values. The normalization clamps the values within the [0.0, +1.0] range. Several configuration options explained below allow for the previous definition of the maximum and minimum value of each dark, front and back sample sequence to effectively produce the clamping function.

Several *Connection* blocks, that also belong to the *Systema* class, shown as circles in the figure, are only used to duplicate the input into all output queues; no transformation is made to the data.

The *Separate* separates the *Sample* object into the analogue component, composed by the dark, front and back values, on a single queue, and separates the *Sample* object into the digital component splitting all digital channels individually into different queues. This separation is made because of the different operations that have to be done to all those signals in the explanation that follows, and is shown as a diagram in Figure 7-9.

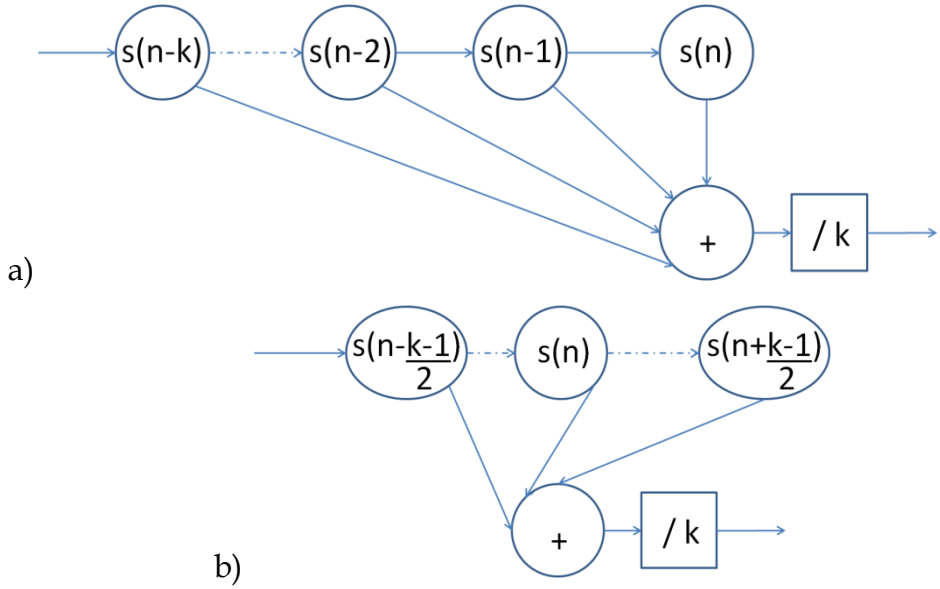

Figure 7-9 – Schematics of the *AnalogueFilter*

The *AnalogueFilter* shown in Figure 7-9 is the implementation of a moving average filter; the moving average filter is optimal for a common task: reducing random noise while retaining a sharp step response. This makes it the premier filter for time domain encoded signals [9]. The value of k is configurable and is set to 3 by default; it indicates the number of points in the average. As Figure 7-9a) indicates, the average is over the last k samples, which will produce a relative shift between the output and input of the filter. This shift can be reduced by weighting (k-1)/2 samples from each side, with k being an odd number. In the *AnalogueFilter* implementation, Figure 7-9a), there is a relative shift which is welcomed because it compensates by (k-1)/2 with k odd, the misalignment discussed in previous section 7.2.

While the *AnalogueFilter* object produces real numbers as output, the *DigitalFilter* shown in Figure 7-10 produces logical values.

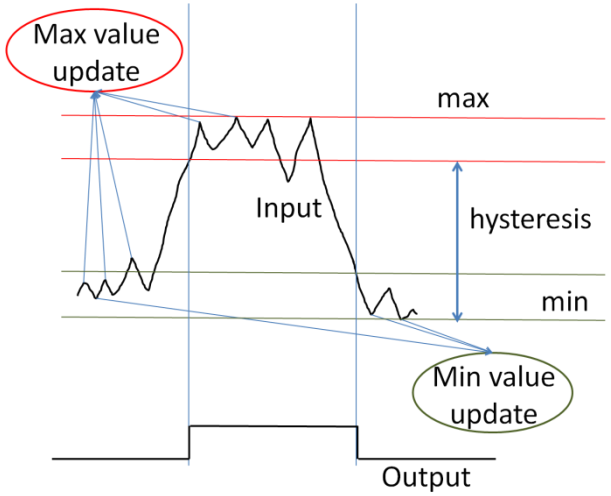

Figure 7-10 – *DigitalFilter* basic function.

The *DigitalFilter* object is for a single input channel, and its working principle is shown in Figure 7-10. Initially the max and min variable are set with the first input value. Then for several input samples the min and max values will eventually hold the highest and lowest values of the input square wave. After that, a value to change state must overflow the hysteresis gap. If the digital signal is considered at a low logical level, it will only change state to the high level if the input signal is above the min value plus the hysteresis value. The same occurs when stepping downwards; the value must be less than the max minus the hysteresis value to be considered a low level output signal. Both input and output signal forms can be seen in Figure 7-10. The number of samples needed to define the max and min values depends on the input pattern. The pattern can be forced, like a preamble which will be explained further down, in which a 0 to 1 or a 1 to 0 transition is known to be found, or waiting till the pattern appears and then fill in the max and min values. While the min and max values are not stable, all input samples are stored in a temporary queue. When the min and max values are set, the temporary queue is emptied and the calculations made into the output queue of the *DigitalFilter*. All subsequent input samples are immediately calculated and added to the output queue. As said, there are several *DigitalFilter* objects, each with its own max and min value to be determined, and to make sure that there is synchronization in the whole process, a *Synchronize* object gathers all output queues as shown in Figure 7-8 and explained next.

The *Synchronize* block has as many digital inputs as the number of channels, and has one analogue input. Here the original *Sample* object that was split by the *Separate* object is reunited with the normalized [0.0, +1.0] dark, front and back signals and the corresponding digital input code. The sample order is maintained.

At this stage a sample is well determined in its digital and analogue components. Now it is necessary to identify each data bit which is composed according to the example by 69.4 samples. It is necessary to find out when to start the counting. This is done by several objects that are marked in Figure 7-11.

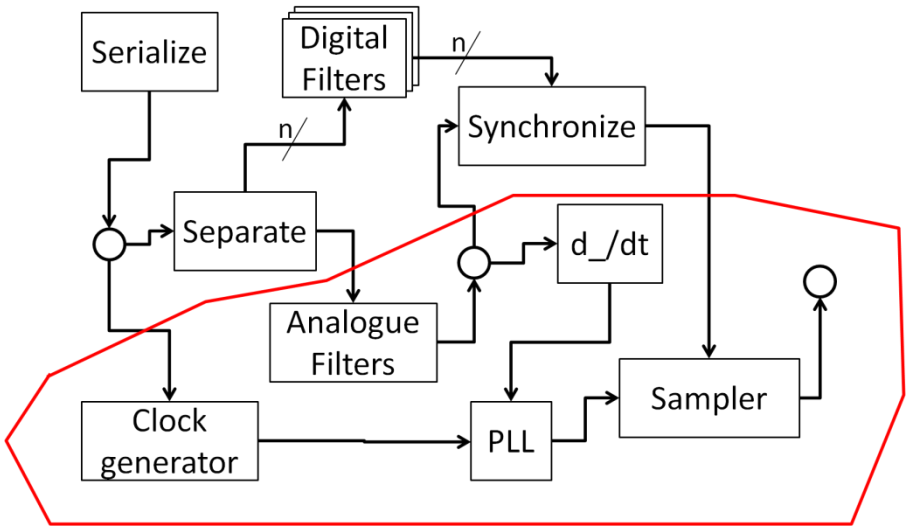

Figure 7-11 – Part of the validation schema with highlighted blocks that deal with the data bit.

A detail of Figure 7-8 is shown in Figure 7-11 highlighted with the objects that are necessary to aid in the determination of a data bit.

To better understand the flow of the events please keep in mind that there is no time involved in the validation schema, but samples that are fed into the system and follow paths asynchronously. Where there is need to synchronize the sample, specific synchronization blocks are available like the *Synchronize*.

The Clock object generates an impulse for each sample that is available in the *Serialize* output queue. It is equivalent to the clock with the highest frequency in the system, were it made in hardware.

The *Differentiate* object receives all analogue data and differentiates it. When any of the dark, front or back signals have a difference between samples

above a programmable threshold, a high level value is added to its output queue and a low value otherwise. The reason for this object is to identify transitions in the samples that may be related to data bit transitions.

The *PLL* object is a reflection of a Phase Locked Loop system. Its' main purpose is to find the transition of a data bit in a sequence of samples. The expected bit size is known and configurable, in this example the value of 69.4 would be set as 70 samples per data bit. A counter associated to the clock sets a value in the output queue indicating the start of a bit transition whenever it reaches the configured sample length. The counter is advanced or retarded depending on the input value from the differential *Differentiate* object. This is the attempt to adapt the output as close to the bit transitions as possible. This process occurs throughout the whole sample sequence, which will expectedly produce bits with lengths of 69 or 70 bits in length according to the example that is being used throughout this section. The result of the PLL object is a sequence of spaces indicating the samples and a mark that indicates a transition of a data bit.

The *Sampler* object receives from its input queues the samples and the marking indicating the sample that is associated with the beginning of a new data bit. This object has several configuration options which can be seen in Figure 7-12.

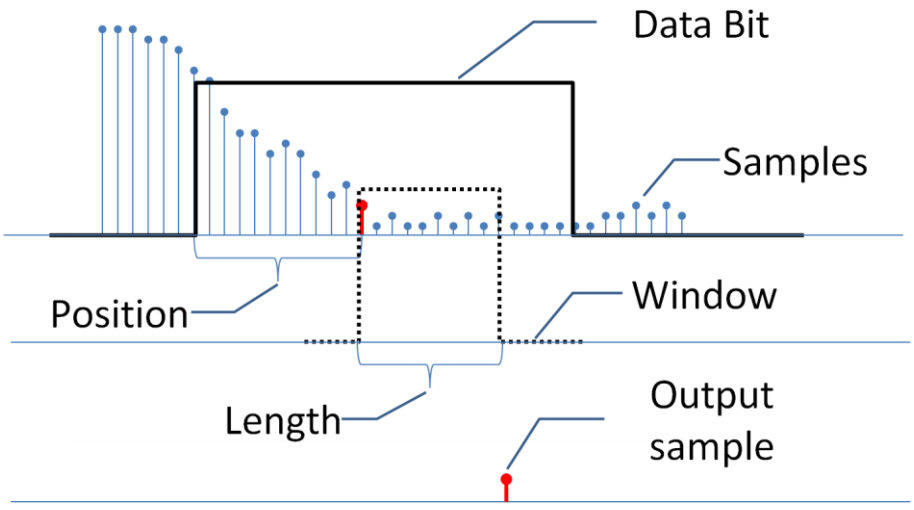

Figure 7-12 – The sampling of a data bit

A data bit is composed by several samples, 69 or 70 according to the example that is being followed in this section. These samples are represented in Figure 7-12 inside the *Data Bit* delimitation line. A window positioned at a percentage of the data bit's length marks the sample, coloured red in the figure, that will be added to the output queue. That sample value depends on the configuration, and it can have the mean value of all samples inside the window; i.e. dark, front and back have their corresponding mean value. The sample chosen is a *Sample* object, thus it holds the input digital code, which means that according to the explanation above the position must be less than 90.3 %. The default values are: position = 90 %, window = 10 % and sample value = mean of all samples inside the window. The output queue of the *Sampler* object has, according to the default setup, one sample for each data bit. From this point onwards only data bits are present on the output queues, which means, with the example that is being followed, there are 72 *Sample* objects on the output queue of the *Sampler* object which is connected to a Connection object. The new starting point, from the *Sampler* object, with the rest of the validation process is shown as a detail in Figure 7-13

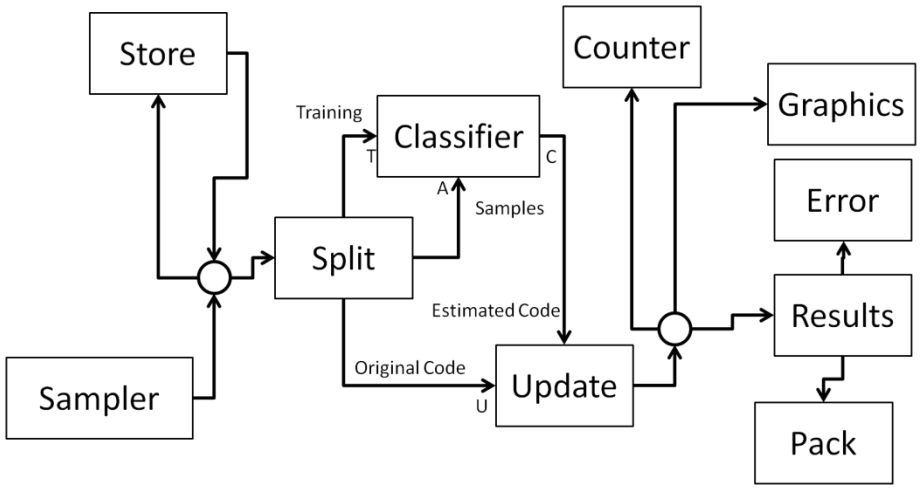

Figure 7-13 – Detail of Figure 7-8 showing the Classifier input and output

The *Store* keeps all data bit samples to be used repeatedly; for example in the case of training sequences for specific classifiers. The interaction with the *Store* object allows the training sequence to be stored or not and cleared for another sequence. It is only limited by the computer memory. A careful observation of Figure 7-13 reveals that the output of the *Store* object is connected to the *Connection* which connects to the entry of *Split*. This path

allows data bits that enter the *Connection* to be stored in the *Store* object while being fed into the *Split* object as well. Then, in turn, if needed, the *Store* object can feed the *Split* object with all data bits in the same order in which they were stored. This process does not empty the *Store* object which can repeat the feeding process under program control.

The classification core of the validation process is represented in Figure 7-14.

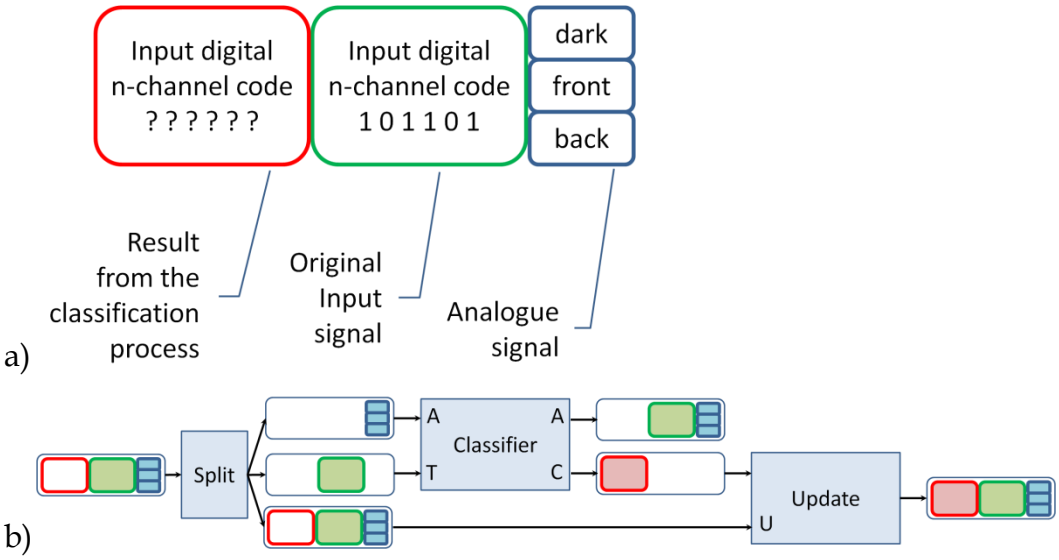

Figure 7-14 – Representation of the *Sample* object and b) the *Split*, *Classifier* and *Update* objects with input / output objects

The *Sample* object is partially represented in Figure 7-14a). It has the analogue part that is the pi'npin output (dark, front and back) when the n-channel input sequence (ex: 101101 in the figure) shinned upon the pi'npin. The classifier has to determine the input code (ex: 101101) only from the analogue part (A input). Classifiers are of several types, some of them needing the original code (T input) to train the classification process beforehand. Figure 7-14b) shows the general data flow for all classifiers. The *Split* object separates the *Sample* object into three parts. Two of them, the analogue part (A) and original digital code (T) are fed into the classifier. The classifier is program controlled and can be set into the training mode, which uses the original digital part of the sample (T). Nevertheless, a classification code is produced and added to the output queue (C). The third part (U) which is a copy of the data bit *Sample* object is sent to the *Update* object which awaits the result from the classification process. The *Update* object completes the *Sample* object by inserting

the estimated code (C) into the data bit sample. It is then ready for statistical analysis.

The *Classifier* has two outputs; the unused one (A) is for debugging purposes and is connected to a graphic object for display.

The complete *Sample* object is copied from the Classifier (one of the possible classifiers chosen) into several *Systema* objects: the *Counter*, *Graphics*, *Results*, (with *Error* and *Pack)*, as can be seen on the right part of Figure 7-13 with all objects connected to the *Connection* represented by a circle.

The *Counter* object is used to count all data bits and ensure that the classification process has been complete before allowing another attempt either by the *Serialize* object or by the *Store* object. The *Counter* object is used as a validation synchronization point.

The *Graphics* object displays all *Sample* objects. It is only used as a debugging tool.

The *Pack* object keeps all *Sample* objects. By program control it stores into the computer's clipboard all *Pack*'s contents so that the result can be used for another program, for example the Origin chart program.

The *Results* object does the statistical analysis of each *Sample* object and of the whole set. Total number of completely correct codes, and errors by counting the number of bit errors in each channel, and whether they are false positives (a 1 which is supposed to be a 0) or false negatives (a 0 which is supposed to be a 1). It also displays the total error in percentage.

By program control the statistics can be cleared, several block configurations altered, training sequences stored and deleted, configurations downloaded or uploaded from files, and new data sequences entered into the whole system. It is also possible to define the number of channels and to choose one classifier from a set of classifiers. It is easy to add a new classifier by programming and adding it to the ones that are already programmed.

7.5 The classifiers

The whole validation schematics presented in Figure 7-8 is the structural support for the classification process which is done by the *Classifier* in that figure. There are presently three programmed classifiers: NeuronalNetwork, Levels, and Clusters.

Each classifier has two inputs A and T and two outputs A and C, shown in Figure 7-14. The A input has the *Sample* object and contains the dark, front and back values. The same object is written to output A for debugging purposes. The T input holds the original digital data code and is used to train the classifier if it uses a supervised strategy for classification. By program control, the classifier can be set to supervised training or classification mode. Whatever mode the classifier is in, it always writes a value that is understood as the classification code associated to the A sample into output C.

7.5.1 Neural Network classifier

The classifier *NeuronalNetwork* object is a back propagation implementation of a supervised multi-layered perceptron neural network [10]. An example with four channels is shown in Figure 7-15.

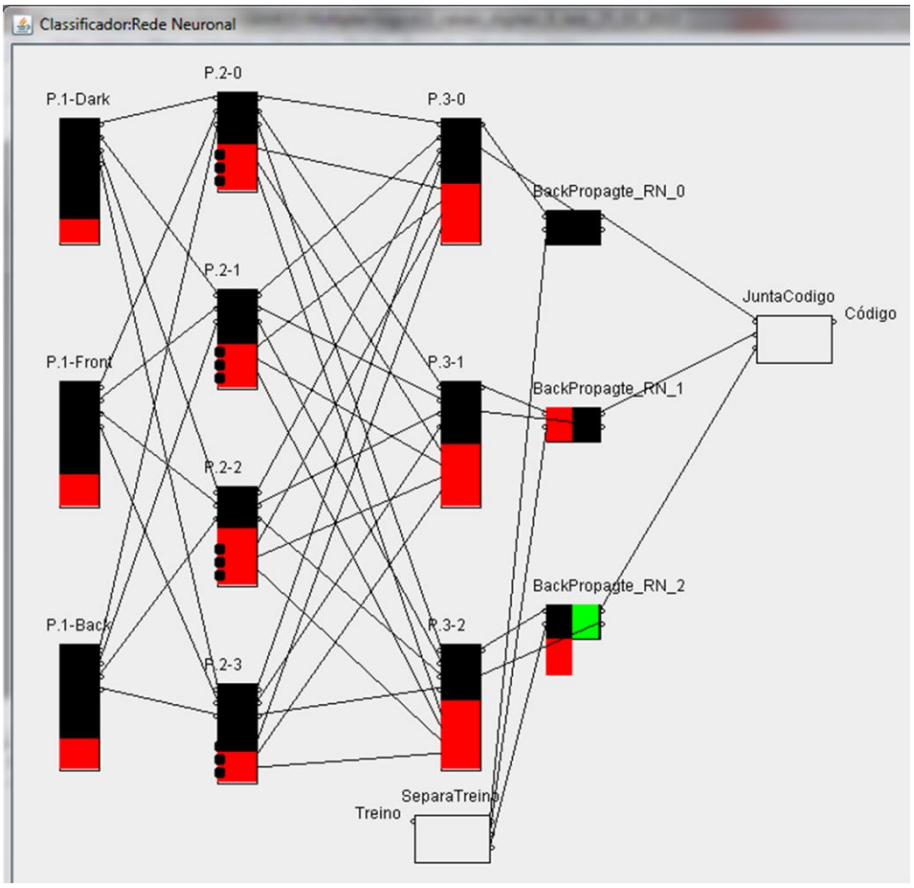

Figure 7-15 – Neural network classifier *NeuronalNetwork*.

Figure 7-15 is a view of all the objects that compose the *NeuronalNetwork* object classifier that implements a neural network. In the figure, the *Training* input is connected to input terminal T, and output *Code* to the output terminal C, both terminals shown in Figure 7-14. The red colours in the three layers of perceptron on the left of Figure 7-15 are a level indication [0.0, +1.0] of the value of the perceptron after the threshold function (explained below). The red and green colours on the column of object at the right signify the following: The green colour indicates a logic level of 1, and the black part the logic level of 0. The value present in the figure is from top to bottom {001}. This is the value that the neural network produced. The red part indicates the error that the output has. If it is black means no error, if the red part is instead of the black means a error of 1 (false negative), and if it beneath the black it is a error of -1 (false positive). This means that the network has the output {001} but it should have the output {010}. This type of visualization is for debugging purposes and used when cycling over the data bits, step by step, under program control.

All outputs marked with a dark spot in Figure 7-15 are unused terminations.

A multi-layer neural network has an input layer, which is composed by the three perceptron objects on the left side of Figure 7-15: P.1-Dark, P.1-Front and P.1-Back. These input perceptrons receive the sample *Sample* object that enters the classifier block through input A, shown in Figure 7-14. All input perceptrons are directly connected to the four hidden-layer perceptrons: P.2-0 to P.2-3. These four hidden-layer perceptrons are connected to the output perceptrons P3-0 to P3-3. The number of perceptrons is defined by the following: there are three different input values dark, front and back, which define the number of input perceptrons, and in the case of Figure 7-15 it is the four digital channels which define the number of output perceptrons on the output layer. The hidden-layer can be composed by more than one layer, and the recommended number of perceptrons is the sum of the input plus the output and should be less than twice the number of inputs [11]. This sets a hidden-layer with four to six perceptrons. The number four is chosen by default. Each perceptron has a structure shown in Figure 7-16.

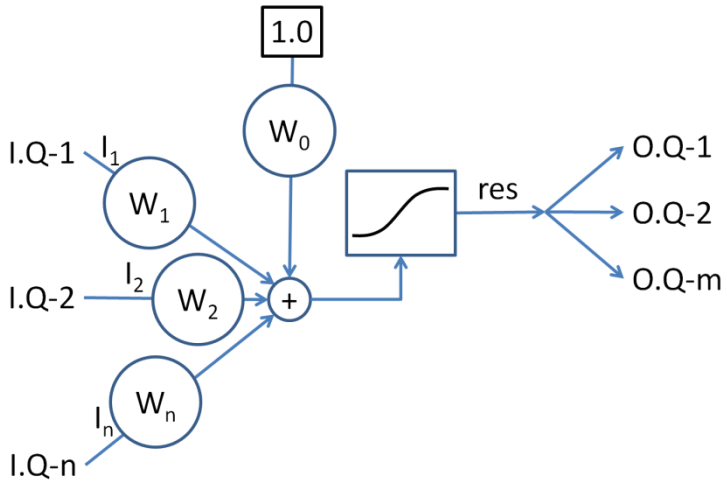

Figure 7-16 – The perceptron in feed-forward mode

The basic function of the perceptron represented in Figure 7-16 is as follows: input values are removed from the input queues I.Q-i and multiplied by their corresponding weight W_i and all summed up. The summed value is then used as a parameter in a threshold function which guarantees an output value between 0.0 and 1.0. The output of the threshold function is then copied

to all output queues O.Q-i. A bias can be set by weight W_0 that is always multiplied by 1.0. The threshold function is a sigmoid $sigmoid(x)=1/(1+e^{-x})$ [9].

The input perceptrons are hollow; they only copy the value from their, only one, input queue to all output queues. The hidden-layer and output layer perceptrons are active and work according to Figure 7-16 [12].

The setting of the weights is made by training. The training mode of the perceptron is made by inserting the expected code in the output and propagating the error (difference between the result and the expected code) through all perceptrons and slightly changing the weights [12]. The back-propagation mode of each perceptron is shown in Figure 7-17

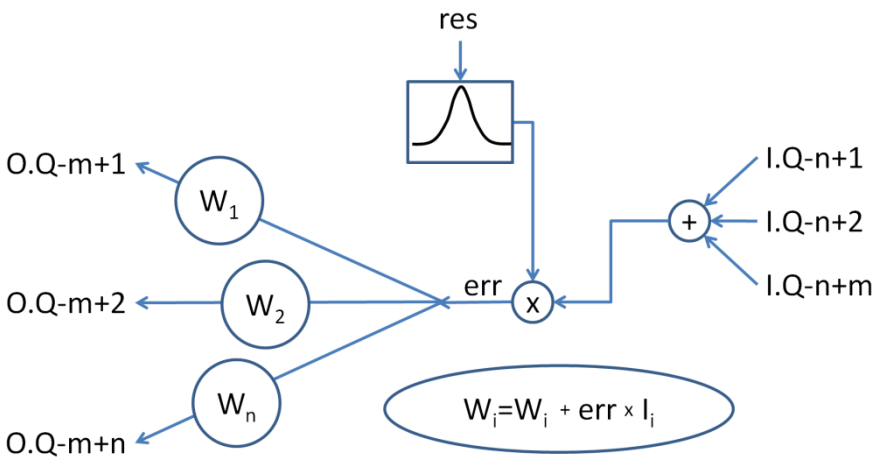

Figure 7-17 – Perceptron in back-propagation mode

All perceptrons except for the input perceptrons that are passive have the back-propagation mode shown in Figure 7-17. The input queues bring results from the end chain and the output queues propagate the error through the weights in the direction of the source chain. The threshold function used is the first derivate of the sigmoid *derivSigmoid(x) = sigmoid(x) (1-sigmoid(x))*. The res value is the output value for that perceptron and is the same res indicated in Figure 7-16.

The error propagation shown in Figure 7-17 is the process by which the error err of a perceptron is sent back to the input perceptrons multiplied by their weight W_i. The weights W_i inside each perceptron are updated after propagating the errors. The update is such that $W_i=W_i+err * I_i$, in which I_i is the value of each input shown in Figure 7-16.

The back-propagation starts in the BackPropagate object, one for each channel, shown in Figure 7-15. The internal function of this object is shown in Figure 7-18.

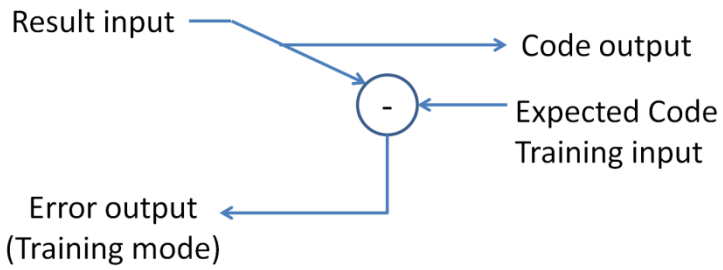

Figure 7-18 – *NeuronalNetwork* object function

At the end of the neural network, a *NeuronalNetwork* object is found for each output node. The operation made at this point is shown in Figure 7-18. The result is always written to the output queue. For debugging purposes the error is always calculated. The error is the difference between the result and the expected code. The expected code is available from the training queue (input T in Figure 7-14). In case of supervised training, the error is fed back into the output nodes of the neural network as shown in Figure 7-18.

This type of classifier based on the neural network theory can be improved. That improvement however would be a task too heavy to accomplish during this work. The neural implementation herein is very simple and has some positive results which will be discussed in section 7.7.

7.5.2 *Level Classifier*

Another classifier, *Levels*, uses level lines to distinguish between different samples. This classifier is an implementation of a tree classifier [13]. The output signal domain of the front and back signals is divided by several level lines. These lines eventually create several rectangles. Each rectangle is attributed with a classification code. The number of channels, n, indicates that there must be at least 2^n different rectangles. The same code can be attributed to more than one rectangle. An example is shown in Figure 7-19.

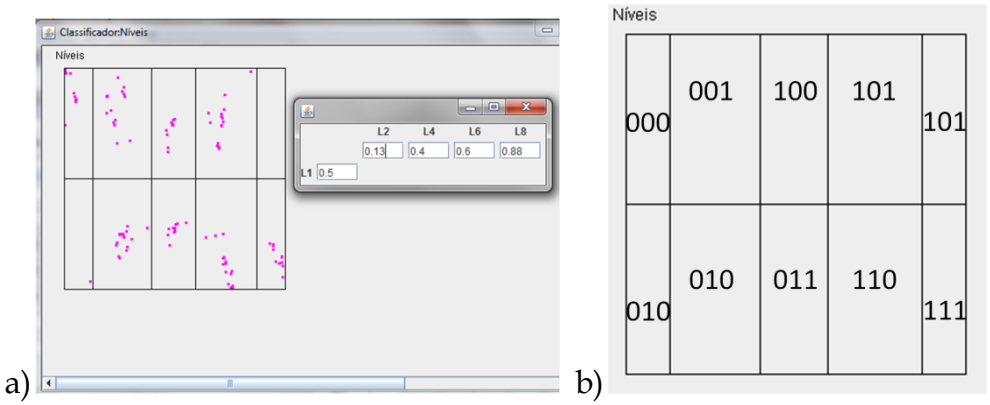

Figure 7-19 – Classifier *Levels* with three channels.

The *Levels* classifier is parameterized by the number of channels, and value of the level lines. The level line values used in Figure 7-19a) and the code distribution in Figure 7-19b) come from results of a previous chapter. An example with a different number of channels is presented in Figure 7-20.

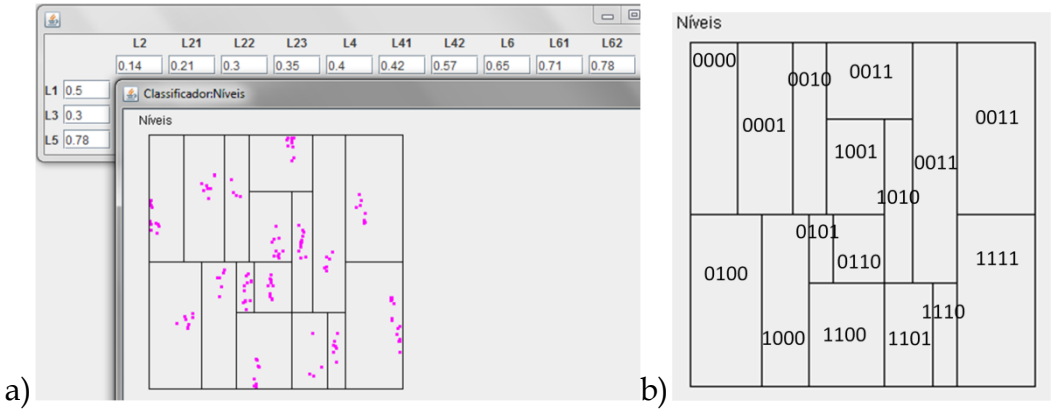

Figure 7-20 – Four channel *Levels* classifier

A rather more complex distribution is necessary when the number of channels increase like the one shown in Figure 7-20, where four data channels are distributed into 2^4 rectangles. The number of levels chosen was minimized and their values are from results of a previous chapter.

The *Levels* object does not need training. Though a *Levels* classifier can be built in which the levels are searched for after a clustering process delimits the codes into small areas.

This classification has excellent results and their discussion will be provided in section 7.7.

7.5.3 *Cluster Classifier*

The cluster classifier does not have any initial barrier, thresholds or marked areas, it is implemented by the *Cluster* object and a three channel classifier is shown in Figure 7-21.

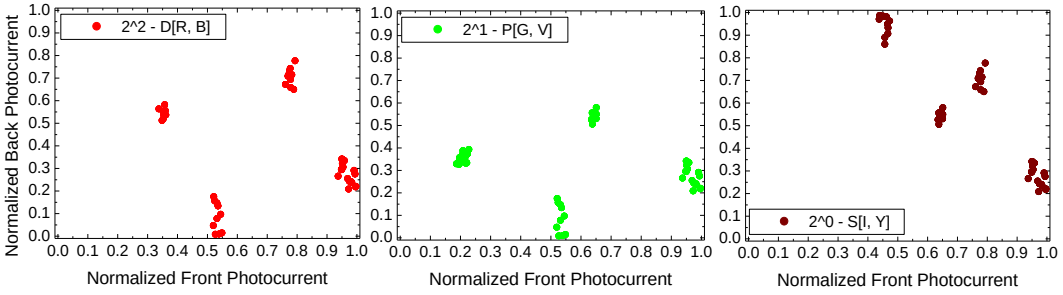

Figure 7-21 – Result of the training / classification of the *Cluster* classifier.

The *Cluster* classifier uses clustering that is spread into as many maps as the number of channels. An example for three channels can be seen in Figure 7-21. The figure represents the result of the training with a few sequences. Each point is then inflated by one point in all directions spanning nine values altogether like the detail shown in Figure 7-22.

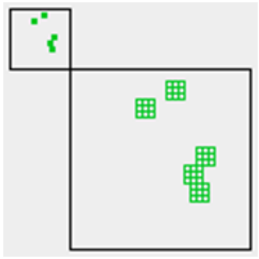

Figure 7-22 – Detail of 5 samples after inflation

Five samples were stored by training and inflated afterwards and then shown in Figure 7-22, inside the little square. A magnification tool included in the program allows an insight to that cluster showing in the big square the result of the inflation process. Further processing can be made to the clusters at the end of the training process so that inflation of the whole cluster will eventually join areas in which the probability of belonging to the same cluster is high. This joining process is not yet made at the time of this writing.

The input channels used in Figure 7-21 are three digital light signals D[R, B], P[G, V] and S[I, Y]. The wavelengths are as follows: R(626 nm), B(470 nm), G(524 nm), V(400 nm), I(700nm) and Y(585 nm). The binary weight was chosen

to be D=2^2, P=2^1 and S=2^0. Each cluster shows where the digital light signal has the value of True (1). The result of the classification process was copied to the Origin and shown as a graph.

To build Figure 7-21 three frames with 36 random data bits in each one of the three channels that make up the frame were used.

As a viewing exercise the three maps of Figure 7-21 were put one in top of the other with different sizes for each map and shown in Figure 7-23. Each cluster is represented by the wavelength colour of the long range component of the digital light signal, and next to each cluster there is the binary code and its decimal base correspondent value in brackets. If the binary weight were different than the above chosen one, the clusters would not change from their position, only the binary value, and decimal, would change.

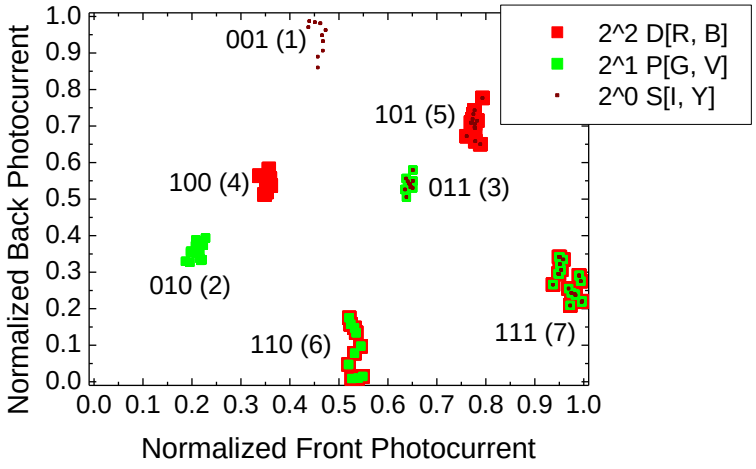

Figure 7-23 – All clusters of Figure 7-21 joined in the same map with different sizes for visualization purposes.

There are seven visible clusters in Figure 7-23, from top to bottom and from left to right, using only the long range component of the digital signal: {G, R, I, RG, GI, RI, RGI}. The missing code is invisible; it is the one where there is no R, or G or I. This means that this type of clustering produces a high number of false negative errors, indicating a 0 where there should be a 1 in the code.

As with the above classifiers, results with the *Cluster* object will be discussed in Section 7.7.

7.6 The program

The validation program has an initial user interface which is shown in Figure 7-24.

The user must choose the configuration to use for the validation process. This is done by selecting the attributes in the opening user interface shown in Figure 7-24. The number of channels must be chosen and cannot be changed after selecting the Classifier. The Bit rate is that of the data bit in the sample sequence. The initial position of the sample within a bit time is set to 90% and its length to 10%. These are the best values and can be changed whenever the user wants to. The *AnalogueFilter* object, described in section 7.4, uses the mean value of a defined number of bits which is set to 3 by default. This value can be changed if the user wants to.

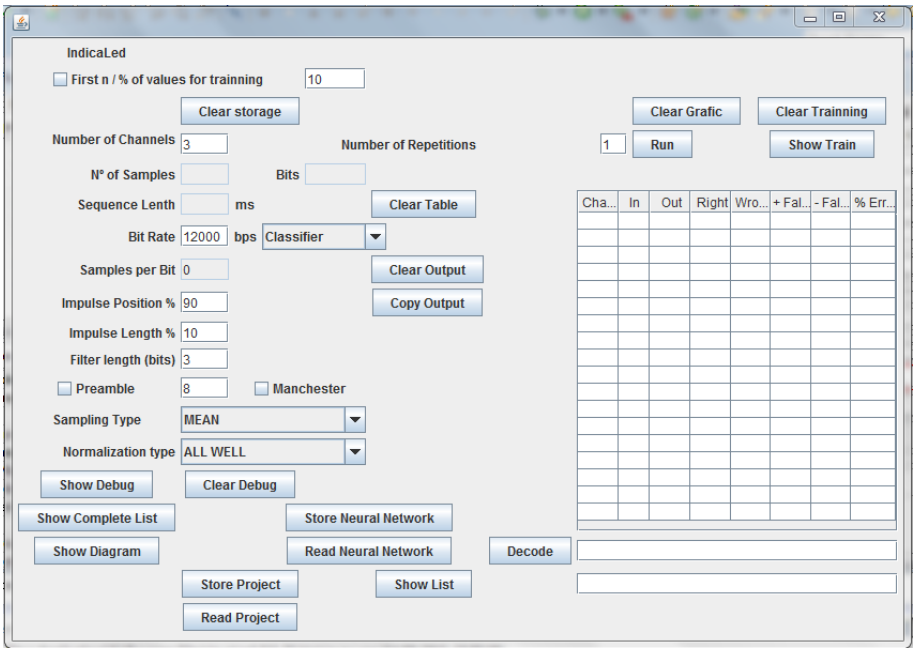

Figure 7-24 – The *IndicaLed* validation program's user interface.

In case of the validation of frames, it is possible to set the use of the preamble with a default of 8 bits. These bits are used only for synchronization and determination of the maximum and minimum values (of the dark, front and back signals), and are removed from the classification process. This removal is necessary because the several blocks like the *AnalogueFilter* and *PLL* objects that are on the sample path are not ready yet to process the samples

because the maximum and minimum values must be known. The default number of 8 is considered enough for the correct classification to take part.

The setting of different data bit sampling can be set by *Sampling type* and the normalization algorithms can also be chosen from *Normalization type*.

After choosing the Classifier, some other option can be chosen. Figure 7-25 displays the *Cluster* classifier after some training.

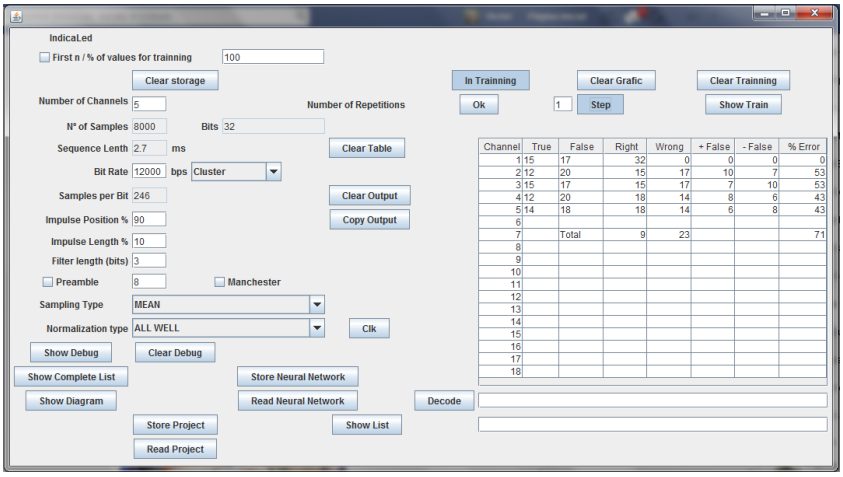

Figure 7-25 – The user interface when using a classifier, ex: *Cluster*.

After choosing a classifier, like *Cluster* in Figure 7-25, and some samples have been inserted, the missing values in Figure 7-24, *Nº of Samples*, *Sequence Length*, *Samples per Bit*, *Bits*, are filled in, as seen in Figure 7-25. To train the classifier it is necessary to store the training patterns. This is done by clicking in *Store*. The top part of the interface is shown in Figure 7-26.

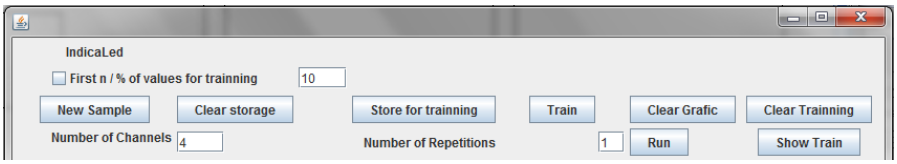

Figure 7-26 – Keep samples for training

When the top part of the interface is as shown in Figure 7-26, all input samples are stored, by clicking in *Store*, depending on the percentage chosen, or by option, the selected number of data bits. Then the training proceeds by clicking in *Train* and the interface presents itself as Figure 7-27.

Figure 7-27 – User interface in Train mode

When in training the top of the user interface has the appearance of Figure 7-27. The same stored samples are used every time the Ok button is clicked. As of this writing there is no random option for the order of the training sequence. The result of the training can be visualized in an appropriate window or the training can be reset. There is also an option, using the toggle button *Run*, to feed the samples either automatically or manually. In manual mode a *Clk* button appears and when clicked does a step by step sequence of training. This manual option can also be used when not in the training mode. The *Clk* button can be seen in Figure 7-25. The training or classification results can be visualized in Figure 7-28.

Channel	True	False	Right	Wrong	+ False	- False	% Error
1	15	17	32	0	0	0	0
2	12	20	15	17	10	7	53
3	15	17	15	17	7	10	53
4	12	20	18	14	8	6	43
5	14	18	18	14	6	8	43
6							
7		Total	9	23			71

Figure 7-28 – Results of a sampling sequence.

Displayed in Figure 7-28 is the result of a sampling sequence after classification (errors were deliberately produced by swapping input channel data from channel 2 with 3 and 4 with 5). The number of channels is five. There were 9+23 = 32 samples classified. Only 9 of those samples were correctly classified against 23 with at least one error which leads to an error of 71%. Each channel can be analysed independently. Channel 1 also had 32 samples, 32 of which were correctly classified. Channel 2 only had 15 correct samples from a total of 32, and 17 with error which gives a channel error of 53%. The errors are of two types: either a 1 was expected and turned out to be a 0, which is a false negative, or the opposite, where an expected 0 turned out to be a 1 which is a false positive.

It is important to note that even with errors in each channel below 60% the resulting error rate is above 70%. This indicates that the error as a whole, lowest possible, is what is expected of a good classifier. The difference between false positives and false negatives can be due to the classifier used, for example the cluster classifier, *Cluster*, has a higher probability to produce false negatives.

The *IndicaLed* has other functionalities like the writing to the clipboard of the classification results to be used in the Origin program. These other functionalities are not written here because they are not strictly necessary for the classification and analysis of the results. Decoding of the received message sent by the PiscaLed frame is also possible, with result in ASCII and hexadecimal.

7.7 Discussion

The classifiers neural, levels and cluster were used with 3, 4, 5 and 7 digital channels (3, 4, 5 and 7 wavelengths respectively). Experiments were also made with 3, 4 and 5 digital light signals (6, 8 and 10 wavelengths respectively).

The neural classifier does not provide adequate results. The percentage of correctly classified codes is around 50%, but since there are only two possible outcomes for each channel, 0 or 1, the 50% indicates that the output is as good as a random guess. The neural classifier, to be used as a solution, must be improved by the most recent research of that particular area. Another aspect that may improve this kind of classifier is the inclusion of a few of memory states. Observing the scatter graphs, for example SEQ 43 in Figure 5-38, the blue samples near the front, back coordinates (0.6, 0.6), they are in three groups, and these groups depend on the previous value before that sample; the two samples that are almost overlapping came from the previous value, coordinates (0.0, 0.7). This memory state converts samples into vectors, and this vectoring can also be applied in future trends to the cluster classifier to improve it, as it is generally, the best of all the solutions presented in this thesis.

The threshold lines are effective for three channels, but still they must move according to the illumination of the digital channels. When correctly set,

almost 100% of success is achieved. With four channels it is possible to identify but the success is around 65%.

The cluster classifier has results above 70% up to 100% in any number of channels. With three channels the success is almost 100%.

Follows an example of a five channel classifier, with four different types of data sets: NRZ, Manchester, NRZ paired channels and Manchester paired channels (digital light signals). Each data set is composed by five different frames each with five channels and each channel with 1031 random bits each were used to construct the graphs that follow.

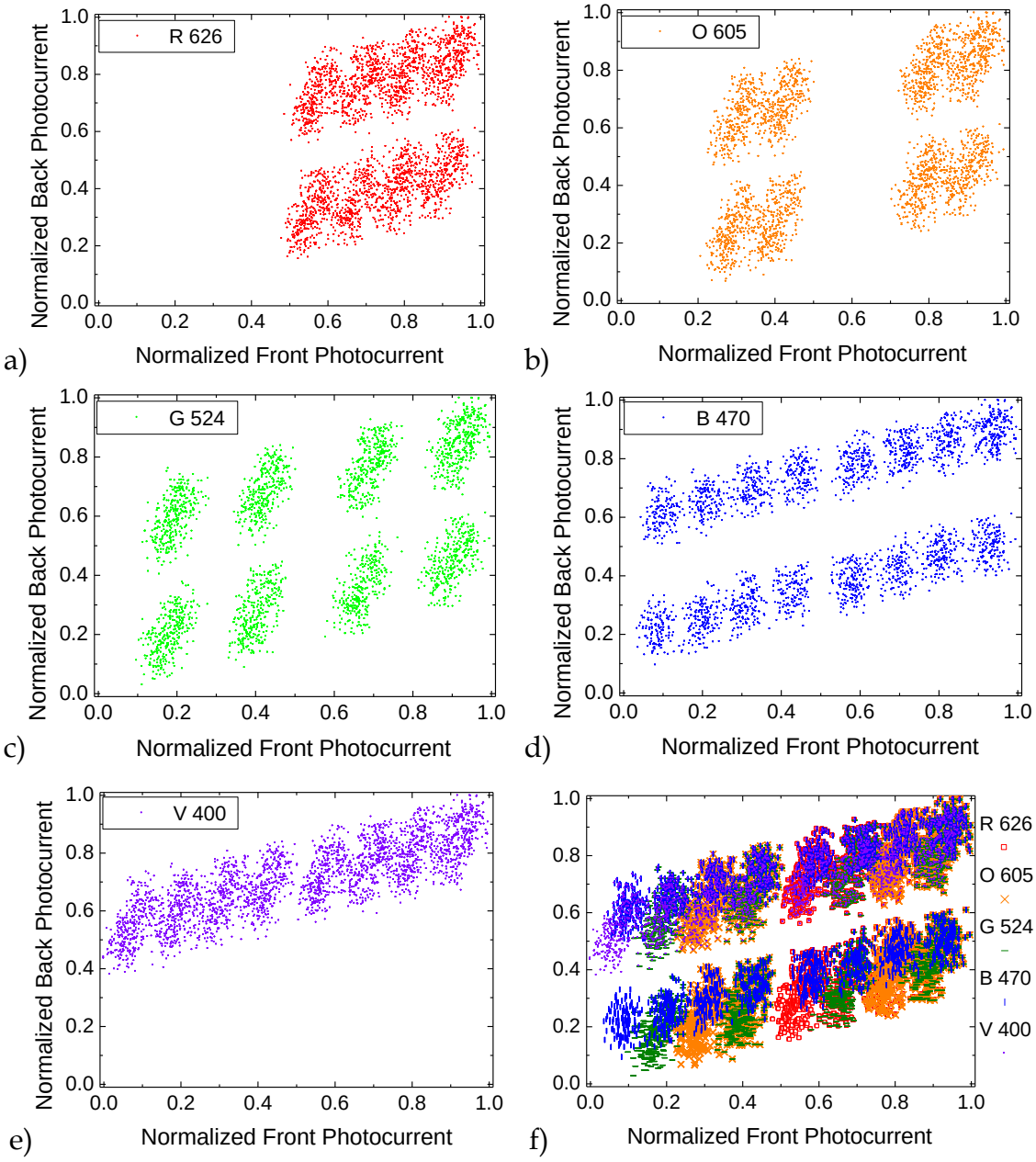

Figure 7-29 – Five channel received data NRZ coded a) Red 640 nm, b) Orange 605 nm, c) Green 524 nm, d) Blue 470 nm, e) Violet 400 nm, and f) all together.

Figure 7-29 shows the five channel data recovered by the cluster classifier. The result of 5*1031 random bits should be distributed by 2^5=32 different clusters; 16 of which a channel has its bit as 1 and the other 16 with the bit as 0. Observing the Figure 7-29a) through e), only 8 different clusters seem to be identified in each. The overlapping of all clusters yields Figure 7-29f) in which symbols and the same colours are used to distinguish the five channels.

Using the same setup but instead of NRZ, Manchester coding is used in Figure 7-30.

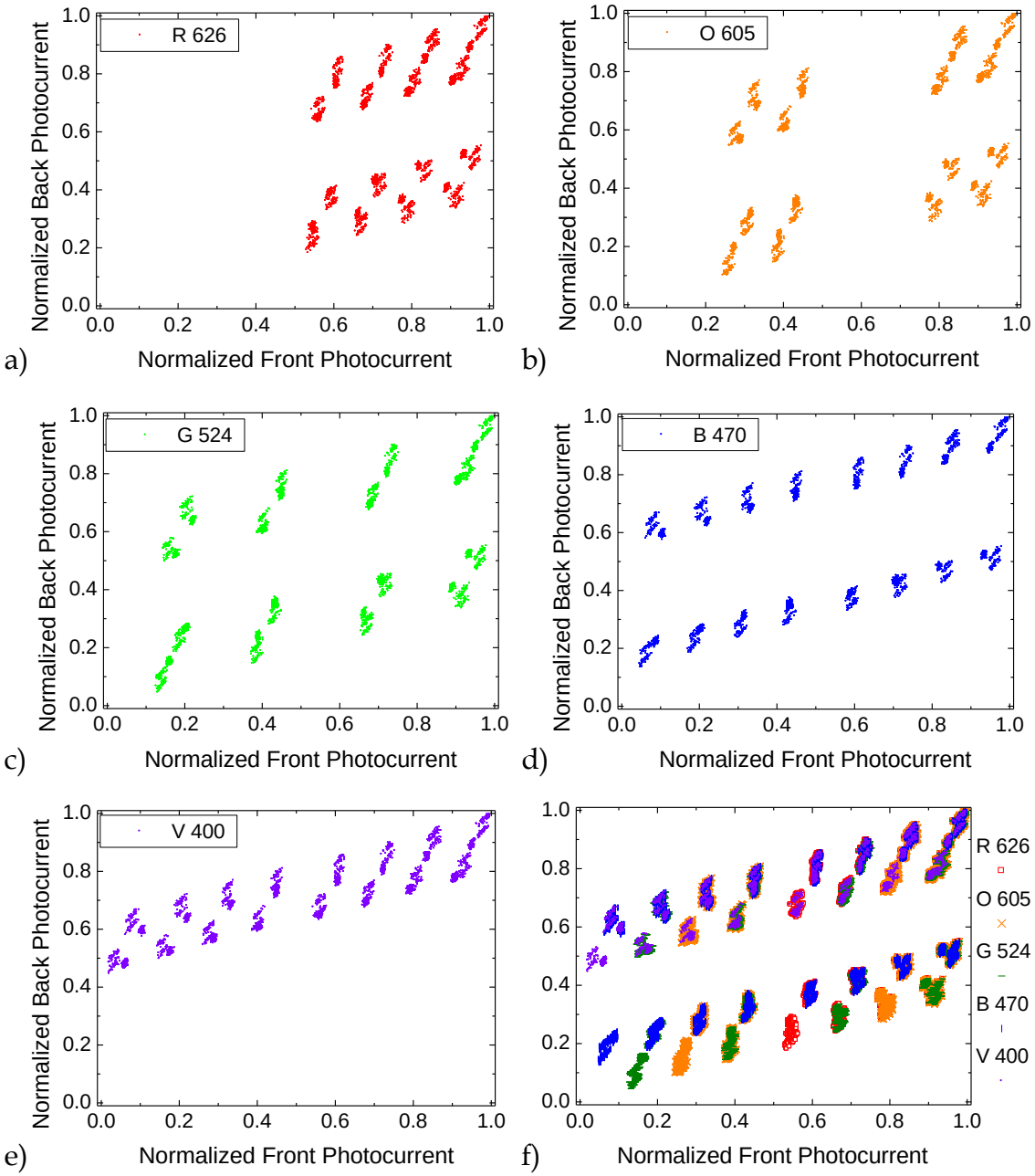

Figure 7-30 - Five channel received data Manchester coded a) Red 640 nm, b) Orange 605 nm, c) Green 524 nm, d) Blue 470 nm, e) Violet 400 nm, and f) all together.

Figure 7-30 shows the clustering of Manchester coded signals. Comparing them to their equivalent in Figure 7-29 the cluster are much sharper and denser. There are 31 different clusters seen in Figure 7-30f), ranging the codes 1 to 31, and the 0 code (00000) is not visible because it is the cluster in which there is no bit set to 1. The 31 clusters are not distinguishable in Figure 7-29f). Manchester

coding has clear advantages and should be used in the digital channels that input the p'inpin device.

A strategy used in chapter 5 was the use of two wavelengths for each channel. This paired set is shown in Figure 7-31.

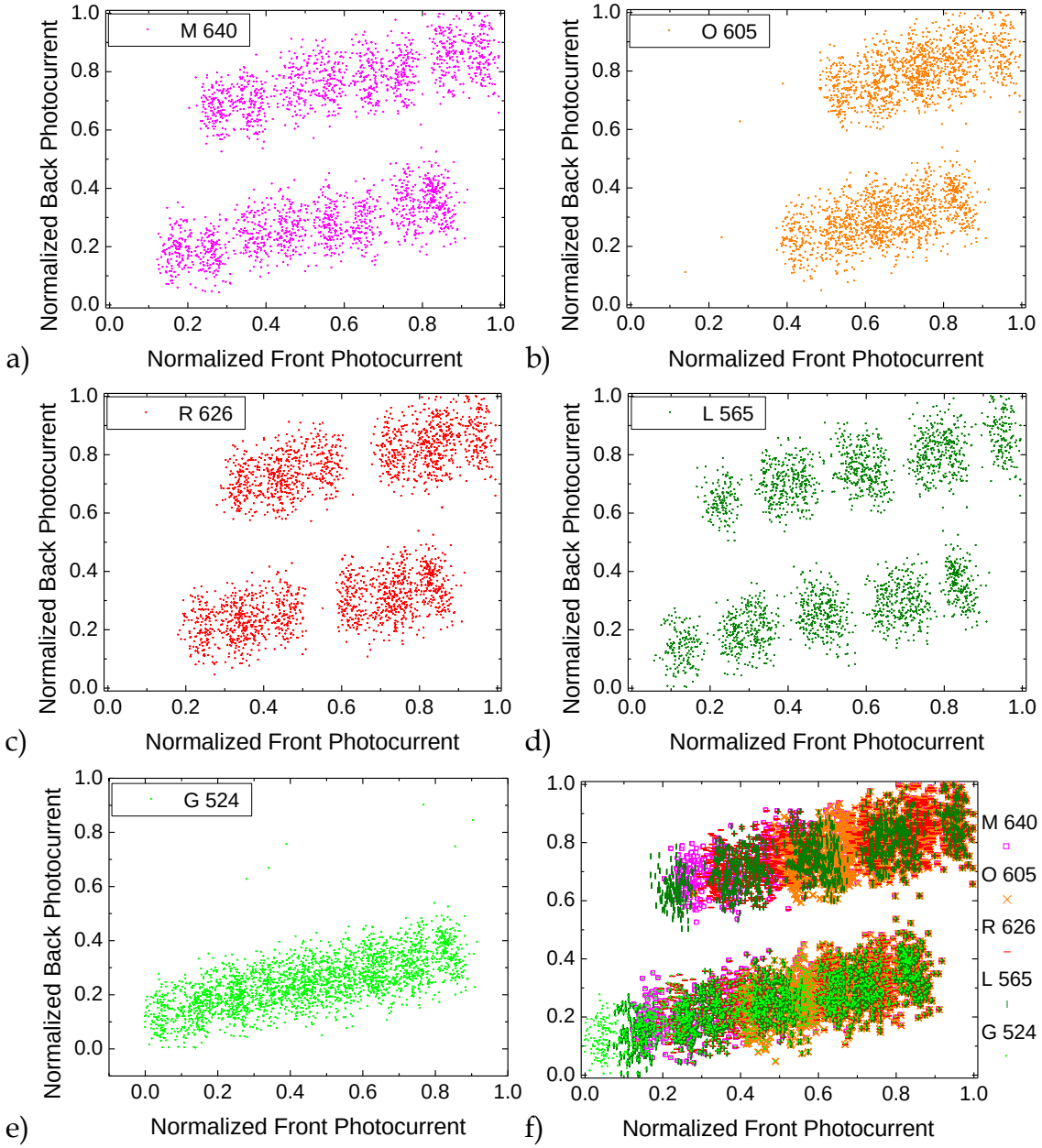

Figure 7-31 - Five channel received data paired NRZ coded a) Magenta 640 nm, b) Orange 605 nm, c) Red 626 nm, d) Lime 565 nm, e) Green 524 nm, and f) all together.

The graphs shown in Figure 7-31 are the result of five paired channels, which means that each channel is composed by a pair of wavelengths, one

above 500nm and the other below 500 nm: M [640, 470], O [605, 430], R [626, 400], L [565, 390], G [524, 460]; the values are wavelengths in nm.

The total number of wavelengths is ten (5*2) that result in Figure 7-31, and comparing with the five wavelengths that result in Figure 7-29 it is difficult to choose which approach is best. Observing in both figures the one that has all channels overlapped, Figure 7-29f) and Figure 7-31f), the Figure 7-31f) seems sharper and with denser clusters. The comparison with Figure 7-31 must be made with Figure 7-32 where the same paired channels are Manchester coded.

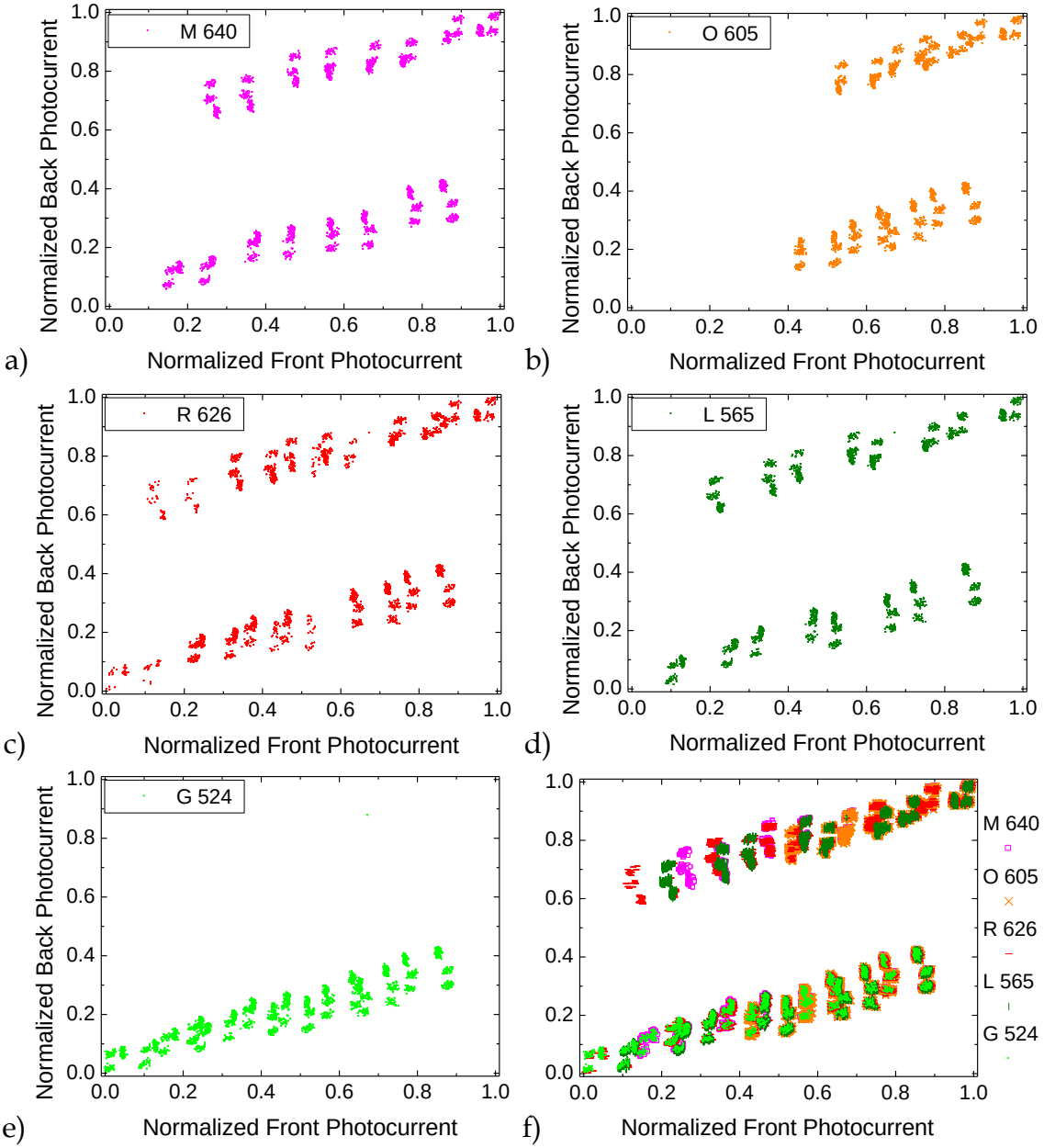

Figure 7-32 - Five channel received data paired Manchester coded a) Magenta 640 nm, b) Orange 605 nm, c) Red 626 nm, d) Lime 565 nm, e) Green 524 nm, and f) all together.

The paired signals Manchester coded in Figure 7-32 are by definition digital light signals, as stated in Chapter 5. The clusters are of all four sets the most sharper and dense, and it is even possible to visualize sub clusters (apparently three) that compose the cluster with the same code. This sub clustering is related to the previous value that was subjected to the sensor; this clustering classifier can be improved with the inclusion of vectors.

There are other variables that can be changed, for example the luminous intensity of the front and back lighting. Several examples with the same data of Figure 7-32 but with different front and back lighting is shown in Figure 7-33.

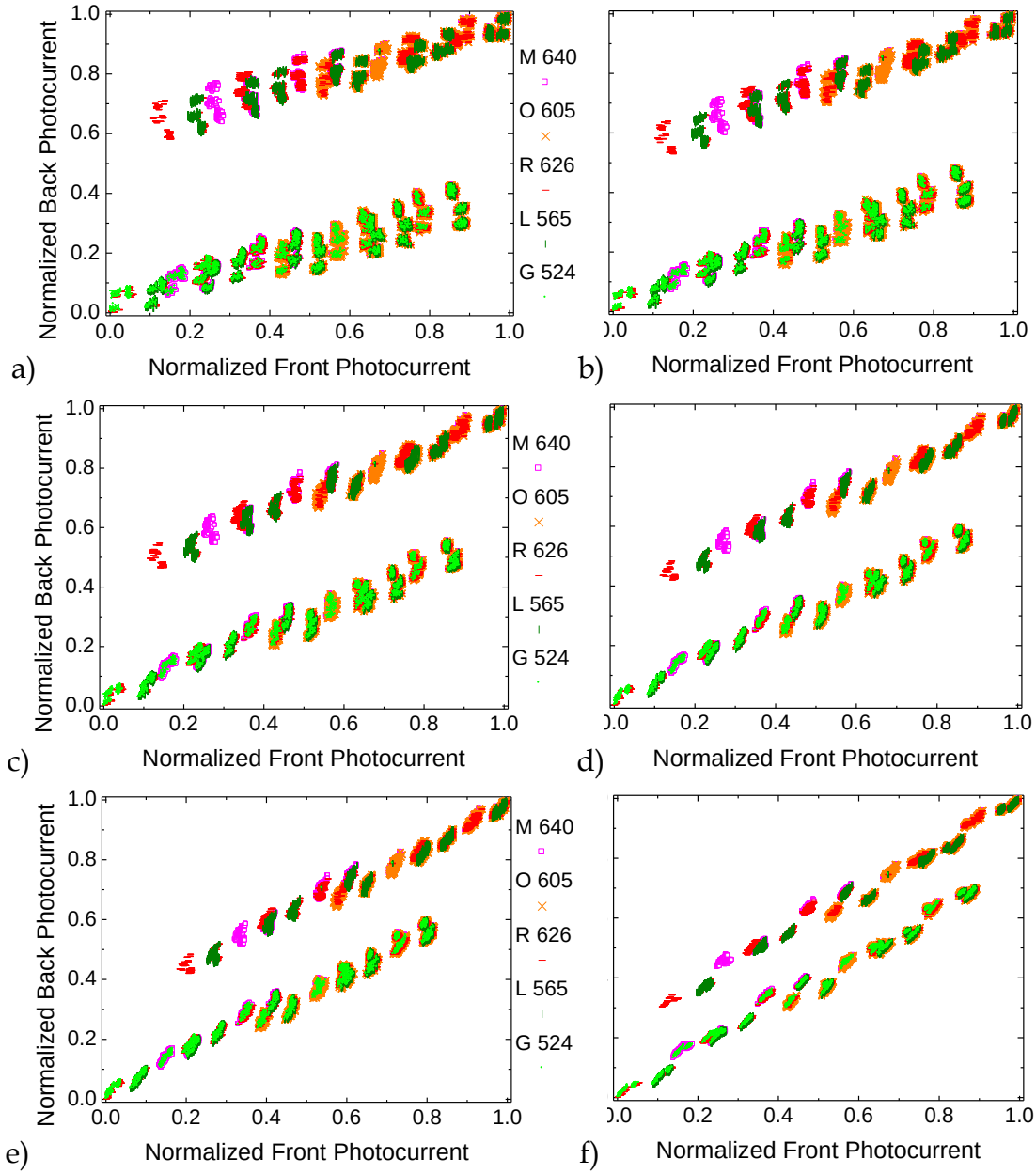

Figure 7-33 – Front Back illumination a) 30, 30 b) 20, 20, c) 10, 10 d) 5, 5 e) 0.5, 5 f) 20, 0.5 in mA

Different illumination combinations are presented in Figure 7-33. The selection of the paired wavelengths for each channel and their individual current setting also play an important part in the clustering of the received signals. Almost all experiments in this thesis were made with the front and back illumination set to 30 mA. From Figure 7-33 there seems to be little difference between Figure 7-33a) and Figure 7-33b) if the current is set to 20 mA. Future research is needed to choose the optimal illumination for the front and back bias.

7.8 Conclusion

The validation process is very important in the determination of the success of the classification of the electrical output of the pi'npin sensor when a known light input is present on its surfaces'. An accurate and effective classification with a very low Bit Error Rate (BER) will allow the pi'npin sensor and its classification procedure to be used in communication links, logical applications or equivalent. The validation is a difficult task because the sensor has a non linear response. There is also a slight influence of past bit sequences on the present bit that is being classified.

To aid the classification there are many known techniques with a solid theoretic background. Of these a few were selected to study the behaviour of the pi'npin device. These are the neural network, the clustering and the tree classifiers.

The study of the classifiers is out of the scope of this work. They are though used in their simple versions, and can be enhanced within the working group that supports this work in future trends.

The *IndicaLed* program is written in Java and has an object oriented concurrent approach. Different circuits from the one used, see Figure 7-8, can be easily implemented, saved and restored. Other classifiers can be built and can be compared on-the-fly with others, by designing a circuit in which both classifiers are simultaneously fed with the same samples, and then changing the results table to fit in the other classifiers.

The validation process has several indicators, the errors and their type, that help choosing the most adequate classifier for a type of application used by the pi'npin device.

The ultimate result of the pi'npin device in this work are logical outputs, thus the analysis table only reflects logical errors and success. If the analogue output of the pi'npin has to be studied the analysis table can easily be changed.

Although the *IndicaLed* is being used exclusively by the pi'npin experiments it is flexible enough for an equivalent use with any kind of sensor.

The pi'npin device has only one electrical output that is read in three different modes, the dark, the front and the back, regarding the background illumination is either off, on the front or at the back of the device. For the *IndicaLed* program these are three different signals and are treated as such. The *IndicaLed* is thus a program that allows the classification and analysis of results for a device with multiple inputs (the channels) and multiple outputs.

All three dark, front and back signals are available for any classifier, but the classifier may not use them all. The important issue for a classifier is that it must produce one output pattern for each input pattern. If this is not the case, then the objects to which the classifier connects must change to engage that behaviour.

The *IndicaLed* is very flexible and adapts itself for different input data. The same configuration can be used with input samples of different lengths and sampling frequencies. The only parameter that must not change after it is defined is the number of channels and bit rate. In case of error in the input of the samples, for example missing rows or missing columns, only the input process is terminated and reseted so that it is ready for the next set of input samples.

The classification output can be stored into the clipboard and then used as input for any other program, like the Origin to represent data in graphical form.

The *IndicaLed* is a valuable asset in conjunction with the *PiscaLed* that provides the illumination pattern of the LEDs that shine upon the pi'npin device.

Classification can be improved by choosing adequate front and back illumination that produces dense clusters and increase the distance between clusters. When using digital light signals, with two wavelengths for each channel, the careful selection of those pairs also improves the cluster density.

The best classifier used in this thesis is the one that uses clustering. The output signals due to the different rise and fall times, and cross gains (the gain is dependent on the wavelengths that shine over the front or back surfaces), are not transitive: If input code A is followed by input code C, the output when C is present is different if the input code A is followed by B and then by C. This effect is the vectoring term used in the last section, and if it is added to a cluster type classifier the classification will improve. Another strategy is to identify the codes that can follow a particular code and by that careful selection reduce the vectoring thus making quasi transitive paths. A communication protocol with data coding would easily ensure the coding scheme that would follow those paths.

7.9 References

[1] V. Silva, "IndicaLed," *GIAMOS - ISEL - Inst. Super. Eng. Lisboa*, p. 29, 2015.

[2] A. Tanenbaum and D. Wetherall, *Computer Networks*, 5th ed. Pearson Education International, 2011.

[3] R. Blahut, *Algebraic Codes for Data Transmission*, Electrical. University of Illinois at Urbana – Champaign.

[4] B. Streetman and S. K. Banerjee, *Solid State Electronic Devices*, 6th ed. Prentice Hall, 2006.

[5] A. K. Jain, N. Murty, and P. Flynn, "Data Clustering: A Review," *ACM Comput. Surv.*, vol. 31, no. 3, pp. 264–323, 1999.

[6] V. Silva, "PiscaLed - Technical Manual," *GIAMOS - ISEL - Inst. Super. Eng. Lisboa*, p. 46, 2013.

[7] Texas Instruments, "TLC5922 - Led Driver."

[8] V. Silva, "PiscaLed - User's Manual," *GIAMOS - ISEL - Inst. Super. Eng. Lisboa*, p. 34, 2013.

[9] S. W. S. Smith, *The scientist and engineer's guide to digital signal processing*, vol. 3, no. 3. California Technical Publishing, 1997.

[10] S. B. Kotsiantis, "Supervised Machine Learning : A Review of Classification Techniques," *Informatica*, vol. 31, pp. 249–268, 2007.

[11] S. Karsoliya, "Approximating Number of Hidden layer neurons in Multiple Hidden Layer BPNN Architecture," *Int. J. Eng. Trends Technol.*, vol. 3, no. 6, pp. 714–717, 2012.

[12] P. J. Braspenning, F. Thuijsman, and A. Weijters, *Artificial neural networks: an introduction to ANN theory and practice*, vol. 931. 1995.

[13] P. J. Flynn, "Data Clustering : A Review," vol. 31, no. 3, 2000.

8

8 Conclusion

The double pin structure which has been the fundamental issue of this work (p(a-SiC:H)-i'(a-SiC:H)-n(a-SiC:H) -p(a-SiC:H)-i(a-Si:H)-n(a-Si:H)) is a photosensitive device.

A earlier stage of this continued research using similar structures by the GIAMOS working group has provided several topics like the multiplexer/demultiplexer which motivated this thesis bringing up some questions. In this chapter, the discussion of results will lead to their response. The questions are grouped in three sets.

The first set involves the multiplexer and demultiplexer capabilities of the pi'npin sensor:

- How many channels in the visible light range can be transmitted by WDM with a a-SiC:H/a-Si:H sensor selecting the desired channel with visible light?
- What wavelengths ranges are best suited for the de-multiplexing function?
- How to de-multiplex light channels using light selectors with one sensor.

The second set dwells with the research of logical functions that can be built by using one pi'npin sensor as a logical component:

- Which are the logical functions that can be translated by this sensor?
- How to build complex logical functions with the device.

The last set was a result of the observation of the behaviour of the pi'npin device and the difficulties that arose due to the recovery of the signals of the other set of questions:

- How to build a memory due to charges stored by light.

In all experiments that use the pi'npin device as a multiplexer, demultiplexer, logical function or volatile memory, it is inverse biased electrically (-8 V). The input signals are all within the visible spectrum 400-800 nm. The optical bias is used by ultra-violet irradiation (390, 400 nm). The difference between a signal and optical bias is that a signal is a pulsed sequence of light while the bias is a fixed, steady state, continuous flux of light.

8.1 Multiplexer / Demultiplexer

The multiplexer is the simplest application of the pi'npin sensor. Any wavelength that shines upon any of the surfaces of the device produces a photocurrent. The multiplexing capability must use different wavelengths because each wavelength produces a different output. This is so due to the non linear characteristics of the pi'npin structure.

The light sources are from common, single wavelength, LEDs. The wavelength width of each LED is measured at the spectral distribution of half the power of the peak wavelength. This value depends on the specific LED used and values from 17 to 47 nm are common. For calculations, a value of 20 nm will be used as the wavelength width, which will set each LED wavelength λ_L as being in the range [λ_L -10, λ_L +10] nm. Two wavelengths are considered different if their peak values are at least 10 nm apart. This 10 nm separation was experimentally tested with LEDs; 390 and 400, 460 and 470 nm.

In the 400-800 nm range, it is possible to fit (800-400)/10 + 1 = 41 different wavelengths. The multiplexer, with the LED technology used, is capable of handling 41 different channels.

The experiments made showed that LEDs above 700 nm must have a very high light flux compared to the 400-700 nm range so that their signal can be used in the full 400-800 nm range. This difference in lighting poses a great difficulty in the gain and saturation of the equipment. This drops the maximum multiplexer channel number to (700-400)/10 +1 = 31 light channels.

Another limitation comes from the suggested distribution of the channels around the 500 nm wavelength. The suggestion is that the number of wavelengths should be balanced by a difference of one, on each side of the 500 nm value. This means that (500-400)/10 +1 = 11 wavelengths are in the 400 to 500 nm range and 12 wavelengths in the 500 to 700 range. The multiplexer with this 11+12 = 23 channel distribution results in an output electrical signal that can be recovered by the method exploited in this work. This does not invalidate, of course, a 31 channel multiplexer.

The methodology used for signal recovery is based on the optical bias of the pi'npin device at the front surface, which results in an electrical signal called front, and on the bias of the back surface of the device resulting on a back signal. Both surfaces are not illuminated simultaneously. The front and back signals are acquired after the transition from front to back illumination of the surfaces is made and the output has settled and considered as a steady state illumination of the surface.

These transitions are shown in Figure 8-1.

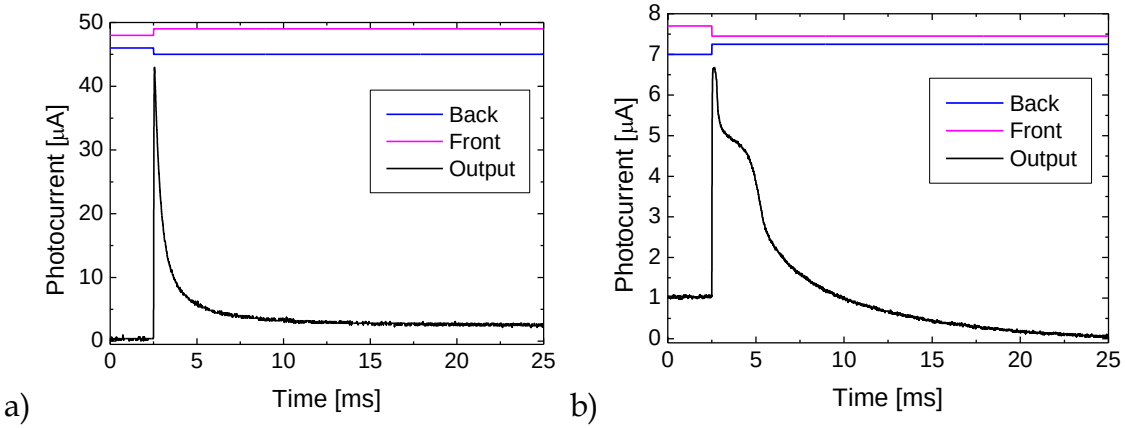

Figure 8-1 – Background transition a) Back to Front and b) Front to Back

The transition of background lighting from the back surface to the front one is shown in Figure 8-1a). The spike in the output signal is due to the fact that the memory effect due to the previous illumination on the back surface enhanced the gain on the blue part of the visible spectrum and thus the switching *on* of the front bias is a change in flux which is considered as a signal. When the front illumination maintains its state the photocurrent maintains its value. Note that the zero photocurrent value in the figure represents the lowest value of photocurrent and not a DC value.

In Figure 8-1b) is shown the front to back transition of the illumination of the pi'npin surfaces. The sevenfold difference to the previous spike shows that the front illumination decreases a change in the back surface in the ultra-violet. This kind of signal has not been studied yet. The back illumination takes more time to reach a stable operation point. Observing both figures roughly the back to front transition takes 5 ms and the front to back transition 15 ms.

The data signals used by each channel is set in this work as 12000 bps, which means that for signal recovery a minimum sampling frequency of 24000Hz is necessary. The period is 1/24000 = 0.04167 ms. These timings (0.04 ms << 15 ms) invalidate the front and back optical bias to be used as selectors during the demultiplexation process.

To build an effective demultiplexer that is used in run time, two pi'npin devices have to be used; one with optical bias in the front surface and the other

with optical bias at the back surface, and in both the same multiplexed signal input impinges on both front sides.

By using two pi'npin devices, and the 23 channel limit discussed above, one pi'npin would only need to distinguish 12 channels and the other 11. This means that 2^{12} different levels have to be identified. The analogue to digital converter must at least have 13 bits or more to account for at least a one bit of quantization error.

Summing up, using the p'inpin device as the photosensitive device for the demultiplexing of a previous multiplexed n-channel system, the research study shows that there can be at the most 23 channels with different wavelength sources divided in two groups, 400-500 nm and 500-700 nm, each having n/2 wavelengths, where n is the number of channels used, and the odd one out belonging to the 500-700 nm range group, because being wider it can hold more channels. Two pi'npin devices must be used for an effective real time acquisition system, where one of the devices has front background illumination and the other with the illumination on its back surface.

One pi'npin device can be used in a system that repeats twice the same multiplexed frame allowing for a 5ms / 15 ms repetition so that the background lighting can cicely be switched from back to front to back, thus maintaining a steady state optical bias. Although this is a possible solution it is a far less efficient than the two pi'npin solution.

The multiplexer/demultiplexer working with channels with a data rate of 12000 bps is capable of a total transmission of n x 12000 bps, which defines a total of 23x12000 = 276000 bps. This data rate however can cause classification difficulties due to the fact that continuous sequences of 0 or of 1 would influence the classification process due to the memory effect. A scrambler can reduce these 0 and 1 sequences but possible classification errors can jeopardize several bits. By using Manchester coded signals in all channels, the classification is improved and voiding the scrambler. In this situation the data rate falls to 6000 Baud in each channel and a total of 6000*23 = 138000 Baud.

8.2 Logic functions

Another topic that was researched is related to the use of the pi'npin device as a logic component. The logic functions are based on set theory and in particular Boolean Algebra. Operators, properties and rules of the Boolean algebra allow transformation of some functions into others. The only operation that cannot be transformed by any other is the NOT, the inverter function.

For the pi'npin to be used as a generic logic component it must perform the NOT operation. This inverter function indicates that there must be a logical low output when there is a high input value, and a low input value must result in a high output value. As the pi'npin device is photosensitive and can be wavelength selective by optical bias, then a particular wavelength can be enhanced or quenched. The presence of an input wavelength could be quenched indicating that a high level input value would produce a low level output value. But if there is no wavelength input, which is equivalent to a low value input, it is not possible to produce a high output value. To build a NOT function there had to be another wavelength involved. Another important aspect is the photocurrent output resulting from input signal change. If an input is at a low or high logical state for a long period of time, the input is not considered a signal but a bias setting; there would be no photocurrent change. These two conditions pointed to a solution of two different wavelengths with the signal varying in time when the logic signal maintains its state; two Manchester coded signals in which one is the inverse, complementary, of the other. This is a mimic of Manchester coded in a differential transmission media. This defined the Digital Light Signal; one component of the signal (red) belongs to the 500-700 nm range and the other (blue) to the 400-500 nm wavelength range; with the red component transmitting the digital data and the blue component the inverse of the digital data.

The NOT operation is performed with a digital light signal input to the pi'npin device which is always set with illumination at the back surface, the blue component, the inverse data, is then presented at the output. The NOT is a unary operator, meaning that it has only one input and one output.

With the digital light signal and the NOT operator defined other logical operators where searched for.

The interaction of two digital light signals can be input to the OR, AND, XOR operators. By using the front and back illumination of the pi'npin it was possible to determine the output of these functions. By observation, and due to the Manchester coding inherent of the digital light signal, the OR, AND, XOR operations can be constructed by fixing the bias at the front surface, and then by comparing the output level with a threshold the AND, OR operations were defined. The XOR operation involved two thresholds.

The Boolean Algebra needs only two operators to build any other logical function; the unary operator NOT and a binary operator which can be either the AND or the OR. These two operators can be built with a single pi'npin device.

The XOR binary operator is in fact an expression; A XOR B is equivalent to (A AND NOT B) OR (NOT A AND B). With the pi'npin, a binary operator is built by illuminating the device with two digital light signals. The XOR output is identified by the value that is within two threshold values.

As the pi'npin can be illuminated simultaneously by different wavelengths then the interaction of more than two digital light signals was attempted and studied. The AND, OR and XOR operations still worked and other threshold lines had to be used.

A rather complex function is the majority function MAJ, considered as the voting function because its result is active when there are more than half of its inputs active. Logical operators are commutative.

The pi'npin device also identified the MAJ function with threshold lines.

The results were acceptable for pi'npin logical operations with up to five digital light data input signals.

The AND and OR logical functions are rather easy to build using at most two threshold lines. Even for the maximum number of digital light signals that can be handled by a single pi'npin. Using the 11+12=23 channel distribution, defined previously, and knowing that two wavelengths, one from each long and short range of the visible spectrum, must be used for the digital light signal, then the maximum number of digital light signals is 11.

The adder is a logical function that is commonly used. The adder of n bits is based in the concatenation of n full-adder modules. And a full-adder module can be simplified for two bits into a half-adder.

The half-adder has two inputs and two outputs and is built by a XOR and an AND. The pi'npin can provide both. The full adder has three inputs and two outputs and is built by a MAJ3 and a XOR. These are also provided by a pi'npin device.

Summing up, the pi'npin device can be used as a logical function as long as the input signals are all digital light signals. The digital light signal is composed by a wavelength belonging to the 500-700 nm wavelength range called red component and by a wavelength belonging to the 400-500 nm range; the blue component. The maximum number of digital light signals that can be used simultaneously is eleven. The red component holds the logical data value and the blue component is the inverse of the red component. Both red and blue components are Manchester coded.

The unary NOT is built for any digital light signal.

Two digital light input signals interact and a AND, OR, XOR operators can be built.

Three or more digital input light signals interact and a AND, OR, XOR, MAJ operators can be built.

A half-adder or a full-adder can also be built with two p'inpin devices, each with a specific operation.

Although only 5 digital light input signals were experimented, more experiments must be set to reach the predicted 11 digital light signal limit.

Using the digital light signals as inputs for the multiplexer/demultiplexer results in a more efficient classification because each cluster is tighter reducing the area around the same output. This use would define the maximum data throughput to be 6000*11 = 66000 Baud.

8.3 Memory Function

The pi'npin device has been studied with digital input signals at data rates of 12000 bps in the visible wavelength 400-800 nm and with best results in the 400-700 nm range. Surface illumination with steady ultra-violet light (390, 400 nm) is also used for optical bias. Observation of the experiments indicated a influence in time of one bit over the other. This pointed out a possible memory function due to stored charges from the previous signal. The background illumination of the front and back surfaces are maintained by LED's with a high light flux compared to the input data signal LEDs. This stimulated a question to be researched regarding a volatile memory.

To design a memory with the pi'npin, the front and back illumination had to be used because they produce ant-agonic behaviour in the input signals.

The study involved a single impulse, like a flash, of the front or back surfaces (front control, back control respectively) and the output of a single digital input signal (sense signal) in the 500-700 nm range was observed. Prior to the flash of either surface the output of the sense signal was registered.

A single impulse of the front illumination followed by the output of a 526 nm sense signal was observed. The signal was enhanced compared to its dark reference. The same observation was made with the single impulse flashing the back surface of the device. In this situation the same sense signal produced an output that was quenched in respect to the equivalent dark reference. This concluded that the flash was memorized.

Research followed to understand what would happen if a front flashed before a back flash of the surface and the pi'npin device acted as if the last flash was the one that was stored. Changing the flash order, with the back flash first followed by the front flash produced an output sense signal that indicated a storing of the front flash event. The device stored a state that indicated the last surface in which a flash occurred. This resembled a set-reset (SR) flip-flop. In a SR flip-flop the S input stores a high level value (1) in the flip-flop and the R input stores a low level value (0). Both S and R cannot be active simultaneously without producing undefined results at the output. The front impulse was associated to the S input and the back impulse to the R. This allowed for a modelling of the pi'npin device as a set-reset flip-flop.

Continuing the quest, the data sense signal was modified to a 256 bit sequence and observation of its influence by either flashes showed that the state still held its value. The time during which a sense signal can maintain its output according to the flash used is around 25 ms; this time depends on the flash energy and on the data sense signal energy.

Using a digital light signal as a data sense signal and performing the flashes of the control front or control back the experiment showed that it was possible to produce an output that was equivalent to the front and back signals when a constant optical bias is used. This allowed for the modelling of this experiment as a set-reset flip-flop connected to a multiplexer.

Summing up, it is possible to construct a volatile memory with data sense, front and back control, signals. The control signals work like a single flash that sets the pi'npin device in a state in which the side that was illuminated by the flash will influence the data sense signal as if that same signal was under the influence of a constant steady state illumination by that same flashed side. Resembling a set-reset flip-flop, the pi'npin device can be modelled accordingly.

Further, it was shown that this flashing was able to demultiplex the digital light signal into its components. This predicts the use of this type of strategy to be used for a n-channel multiplexer with a single pi'npin using a 3 ms front flash sequenced by the frame followed by a 3 ms back flash sequenced by the same frame, this would be faster than the 5 plus 15 ms that was suggested before. This is a topic that could be researched in future.

8.4 Future trends

The p'inpin device has proven to be versatile and with several applications in which it was used as a still picture photo scanning device prior to this thesis, and here as a multiplexer, logical gates and a volatile memory.

To build these components it is necessary the inclusion of analogue to digital converters (ADC) and the use of available audio ADCs of 16 bits can be a good choice.

PiscaLed and HexaLed, the software and hardware used; also need some improvement to include 23 data signal LEDS and the two that illuminate the

surfaces. They can also be modified to produce analogue signals besides the digital square wave, fixed like sine and cosine, or random pattern. The amplitude modulation of the LEDs could also be configured for a value different than 100%. The duty cycle of each bit is 50%, and this value could also be changed.

IndicaLed, which classifies the sensor's output, could be improved by connecting directly to the oscilloscope. Building specific hardware that electrically bias the device and produces a 16 bit output would improve the overhaul performance. The IndicaLed would also be responsible for the background illumination of the front and back surfaces, so that the receiver and transmitter ends can be completely separated.

In the continuation of this thesis, the pi'npin device as a receiver for visible light communication (VLC) is being studied within the GIAMOS working group.

As a direct continuation of the study presented here, the demultiplexer and the memory function can both be used to build a low power demultiplexer; one in which the bias is not always active.

By experimental observation the simultaneous incidence of the front and back optical illumination is equivalent to a front bias illumination. This characteristic could be used by having the back surface always illuminated and using the front bias when convenient. Although using higher power this could speed up the demultiplexing function, and simplify the logical functions.

The sensor illumination has always flooded the whole surface. Studying the use of masks to allow only certain parts of the sensor being used by spatially distributing the input wavelengths over the surface can produce curious results.

The memory effect has a strong influence on the sensor's behaviour. This effect should be studied deeply and its result would certainly improve the optoelectronic model.

The photocurrent varies linearly with the flux intensity of the input signals. By using analogue signals a "light transistor" can be built using the background illumination as a constant amplification setting.

Studying the device with analogue signals, sensing the sensor's temperature to avoid its destruction, and verifying avalanche type responses would be a very interesting research topic.

The possibility to change the pi'npin heterostructures by depositing more pins and enabling their junctions to be accessible by ITO contacts will definitely improve the research of this simple photosensitive device. The ideal device would be one that could also emit light; with optical inputs and outputs it would effectively be considered as an optical gate. The demultiplexer would then emit in separate channels, the logical functions would work as gates that could be connected as circuits including the memory component.

Due to the low throughput of 12000 bps of each channel the pi'npin device can be used in audio and signalling applications. The pi'npin device has a very rapid response to a positive derivative of the illumination comparing to the negative derivtive, and this feature could be explored as an advantage. Opto-couplers with several channels could also be an application.

The less input data channels impinge on the front surface of the device the more effective is the selection of the different channels, by the demultiplexing strategy. To build complex optoelectronic systems with this type of device, a more interesting approach would be a parallel optoelectronic system, where the use of multiple sensors with two data channel inputs would, under appropriate connectivity and control, produce complex results as a whole.